Master's thesis

NTNU
Norwegian University of Science and Technology
Faculty of Engineering
Department of Geoscience and Petroleum

Ståle Breimoen

Modeling and Analysis of Liquid Loading Phenomena and Its Impact on Crossflow in Gas Wells Using ROCX and OLGA

Master's thesis in Petroleum Engineering
June 2023

NTNU
Norwegian University of
Science and Technology

Ståle Breimoen

Modeling and Analysis of Liquid Loading Phenomena and Its Impact on Crossflow in Gas Wells Using ROCX and OLGA

Master's thesis in Petroleum Engineering
June 2023

Norwegian University of Science and Technology
Faculty of Engineering
Department of Geoscience and Petroleum

NTNU
Norwegian University of
Science and Technology

Abstract

This thesis investigates the reservoir and well interaction during liquid loading. Crossflow can occur between reservoir zones of different properties, and this study examines whether liquid loading can trigger such a phenomenon. The study is based on numerical simulations, where a reservoir simulator is coupled to a transient multiphase wellbore simulator.

The first part of the study focuses on the flow dynamics that initialize liquid loading. Turner's equation is compared to the gas, droplet, and liquid film velocities generated by the wellbore simulator. In addition, steady-state and transient-flow models are compared, since steady-state descriptions are commonly used but may be inadequate for analysis. The second part of the study addresses liquid-loading-related phenomena in multilayered reservoirs with different properties. Specifically, how liquid loading affects production through fluid redistribution, condensate buildup, and crossflow between reservoir zones.

Supportive software is developed in Python using Conda and Jupyter Notebook to efficiently process, analyze, and generate plots from the output files generated by the wellbore and reservoir simulators. The software also incorporates a critical velocity and rate calculator based on Turner's equation, with the addition of using fluid properties from PVT files and pressure and temperature from the simulations.

Simulations show that the liquid loading starts when the liquid film reverses. If liquid loading occurs, most of the liquid will flow into the most depleted zone, which is typically the high-permeability zone, rather than accumulating at the bottom of the well. However, this depends on the production strategy and reservoir properties such as capillary pressure. Liquid loading can trigger crossflow between adjacent reservoir zones, but the production strategy, reservoir properties, and fluid properties significantly affect the phenomenon. Isolating the reservoir zones and regulating the flow from each zone can increase the total production of gas, without the use of an artificial lift.

It is important to note that the research has not been compared to real-world data. Suggested future work is to make a model based on real-world input and verify whether the key findings in this thesis are plausible. Additionally, liquid loading and the occurrence of crossflow can be studied in inclined or horizontal wells, since orientation strongly affects fluid flow.

Sammendrag

Denne oppgaven undersøker samspillet mellom reservoar og brønn under væske-opphopning (liquid loading). Det kan oppstå kryss-strømninger mellom reservoarsoner med ulike egenskaper, og denne oppgaven undersøker om væske-opphopning i brønnen kan utløse et slikt fenomen. Studiet baseres på numeriske simuleringer der en reservoarsimulator er koblet til en flerfase brønnsimulator.

Den første delen av oppgaven setter søkelys på strømningsdynamikken som fører til væske-opphopning. Turners ligning sammenlignes med gasshastighet, dråpehastighet og væske-filmhastighet frembrakt av brønnsimulatoren. I tillegg sammenlignes modeller for stasjonær og ikke-stasjonær strømning, ettersom stasjonære strømningsbeskrivelser kan være upassende for å beskrive ikke-stasjonære hendelser. Den andre delen av studien tar for seg fenomener relatert til væske-opphopning i flerlagsreservoarer med ulike egenskaper. Spesielt hvordan opphopning påvirker produksjon gjennom omfordeling av væske, kondensatbanking og kryss-strøm mellom reservoarsoner.

Støttende programvare er utviklet i Python ved bruk av Conda og Jupyter Notebook for å behandle, analysere og generere figurer basert på utdatafiler fra brønnsimulatoren og reservoarsimulatoren. Programvaren inkluderer også en kritisk hastighets- og ratekalkulator basert på Turners ligning, som bruker væskeegenskaper fra PVT-filer og trykk- og temperaturverdier fra simuleringene.

Simuleringene viser at væske-opphopning starter når væskefilmen begynner å strømme nedover. Hvis opphopning oppstår, vil det meste av væsken strømme inn i den mest uttømte sonen, som vanligvis er den høypermeable sonen, i stedet for å samle seg i bunnen av brønnen. Denne kryss-strømningen viser seg å avhenge av kapillært trykk. Væske-opphopning kan utløse kryss-strøm mellom reservoarsoner, men produksjonsstrategi, reservoaregenskaper og væskeegenskaper påvirker fenomenet betydelig.

Det er viktig å merke seg at forskningen ikke er sammenlignet med virkelige data. Fremtidig arbeid kan inkludere modellering basert på virkelige inngangsdata og verifisere om de viktigste funnene i denne avhandlingen er mulige. I tillegg kan væske-opphopning og forekomsten av kryss-strøm studeres i inklinerte eller horisontale brønner, ettersom væskestrømning påvirkes av orientering.

Acknowledgements

This project was part of the Master of Science Program, Petroleum Engineering, at the Norwegian University of Science and Technology (NTNU). The author expresses his sincere gratitude and appreciation to Curtis H. Whitson and Milan Stanko for their guidance and expertise. A special thanks to friends, colleagues, and family for their continuous support and encouragement.

Thank you all for your contributions, encouragement, support, challenges, and unforgettable moments throughout this academic journey.

Contents

Figures

Tables

Nomenclature

$\dot{m}$	Mass flow $[kg/s]$
$\dot{Q}_H$	Overburden/underburden heat source $[J]$
γ	Specific weight $[-]$
μ	Viscosity $[Pa \cdot s]$
ϕ	Porosity $[-]$
Ψ	Rate of mass transfer between phases $[kg/s]$
ρ	Density $[kg/m^3]$
$\underline{v}$	Phase velocity $[m/s]$
$\underline{v}^D$	Darcy velocity $[m/s]$
g	Standard gravity $[m/s^2]$
H	Energy source $[J/s]$
h	Specific enthalpy $[J/kg]$
k	Permeability $[md]$
k_r	Relative permeability $[-]$
k_T	Thermal conductivity $[W/J \cdot s]$
m	Mass $[kg]$
n	Moles $[mol]$
p	Pressure $[Pa]$
p_c	Capillary pressure $[Pa]$
q	Flow rate under standard conditions $[Sm^3/s]$
R	Gas constant $[m^2kg/s^2 \cdot K \cdot mol]$

S	Saturation $[-]$
T	Absolute temperature $[K]$
t	time $[s]$
u	Specific internal energy $[J/kg]$
V	Volume $[m^3]$
Z	Gas deviation factor $[-]$

Chapter 1

Introduction

1.1 Introduction

The significance of effective extraction of oil and gas from subsurface reservoirs is heightened due to the increasing global demand for energy and the need for greener solutions. Advanced numerical simulations can be employed to aid in optimizing extraction processes by providing insights into the subsurface behavior of fluids. This thesis focuses on the investigation of liquid loading and potential crossflow in gas wells through the application of sophisticated reservoir and wellbore simulation tools such as ROCX and OLGA.

Liquid loading refers to the accumulation of liquids in the wellbore and is a critical phase in the life of a gas well. The phenomena can significantly hamper gas production by increasing the backpressure on the formation and by reducing the ability of gas to flow through the reservoir. Liquid loading can be predicted, and production strategies can be employed to prolong the productive life of a gas well. Crossflow occurs when fluid from higher-pressure reservoir zones flows into a lower-pressure reservoir zone rather than up the conduit. Understanding these phenomena and how they affect production and recovery requires a detailed examination of the flow dynamics and the interplay of forces between the wellbore and reservoir.

In this thesis, several numerical simulations are used to perform tests and analyze phenomena related to liquid loading and crossflow. The main part of the study investigates liquid loading and crossflow in a two-layered reservoir with different reservoir properties. Each case uses a reservoir simulator and a dynamic multiphase flow simulator to simulate the flow in the reservoir and well. Further analysis is conducted using Python to process and plot relevant data, calculate mass production, and search for anomalies in pressure, temperature, and saturation data.

The first part of the study examines the flow pattern, droplet velocity, liquid film velocity, and Turner's critical rate and compares them to the gas rate as the liquid begins to accumulate to determine which should be used to predict the onset of liquid loading. A comparison of the liquid loading using ROCX and IPR as inflow models to OLGA are conducted to assess whether computationally demanding simulations provide similar rates during steady and transient flow. The second part of the study investigates whether crossflow can be initiated by transient events such as liquid loading and how flow is affected by adjacent reservoir zones with different reservoir properties. The post-loading period is studied to see how production rates are changed due to liquid accumulation and how the relative location of reservoir zones affects metastable production. In addition, supportive software is developed for analysis.

The thesis is organized into chapters detailing the theoretical background, methodology, results, and discussion, which cumulates in a conclusion that summarizes key findings and suggests potential future work.

Chapter 2

Literature Review

2.1 Liquid Loading

The phenomenon of liquid loading in a gas well is characterized by the inability of the gas produced to efficiently lift the liquids produced from the wellbore. As a result, these liquids accumulate in the well, leading to a reduction in production and a shortening of the time until the well becomes unproductive.

If the liquid loading goes unnoticed, the accumulated liquids can cause damage to both the wellbore and the surrounding reservoir, potentially leading to temporary or permanent losses. Therefore, it is crucial to identify the impacts of liquid loading and address them in a timely manner to prevent production losses and potential reservoir damage [1].

Methods for detecting liquid loading can take the form of predictive models or observations of field symptoms. The use of actual field symptoms is considered more reliable, as predictive methods may deviate from reality. However, relying on field symptoms also has limitations as a decrease in production is costly and may be caused by factors such as formation damage, sand accumulation, or scaling, and could be wrongly attributed to liquid loading. Furthermore, field symptoms are an after-the-fact indication, and, ideally, preventive measures are in play before the fact.

To bridge the gap between reliable field symptoms and predictive methods, transient multiphase modeling can be used. However, large amounts of data regarding fluids, reservoirs, and wells are required for such a method to simulate results close to reality, and such data may not be available.

2.1.1 Critical Velocity

The transportation of liquids in gas flow within pipelines has been the subject of extensive research. Turner *et al.* [2] were among the first to investigate the mechanisms by which liquids are lifted as individual particles and/or transported as a liquid film along the tubing wall. Their work evaluated the correlations based on the two transport mechanisms using a large experimental data set.

Droplet Model

Turner *et al.* [2] discovered that the best predictions were made using a droplet model, as illustrated in Figure 2.1. The figure shows the movement of a drop in a gas flow. The drop moves either upward (when the gas flow was above the critical velocity) or downward (when the gas flow was below the critical velocity). The liquid-film model was rejected for many years, since the droplet model appeared to be more accurate and, therefore, an analytical expression is not discussed in detail in this paper.

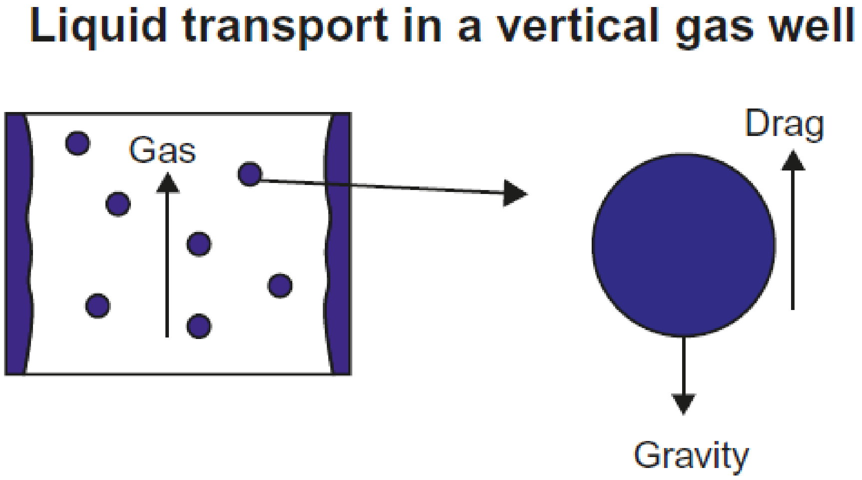

Figure 2.1: Illustration of liquid droplet model (taken from Lea *et al.* [1]).

Turner *et al.* [2] developed a correlation to predict the critical velocity in near-vertical gas wells, assuming the droplet model. Under normal flowing conditions in this model, the weight of the droplets acts downward, and the drag force from the gas acts upward. The critical velocity is defined as the point at which the drag is equal to the weight of the droplets, causing them to be suspended in the gas stream. If the gas velocity is below the critical velocity, droplets move down the well and accumulate in the wellbore (and potentially flow into the reservoir).

In practice, the critical velocity is defined as the minimum gas velocity required to move the droplets upward. Methods to increase gas velocity above critical velocity include the use of a *velocity string* to reduce tubing size, lower surface pressure by compression, and increase velocity with foam. Pumps can also be used to pump liquids up the tubing while allowing gas to flow up the casing. The addition of gas through gas lift can also increase the velocity above the critical value [1] by reducing the hydrostatic pressure.

The critical velocity formulas derived by Turner *et al.* [2] can be applied at any location within a well, given the knowledge of the pressure and temperature at that location. For example, in wells with tapered strings, the bottom of each tapered size would have the lowest production velocity of that given section, making it the first to be loaded with liquids [1]. Liquid loading occurs at the bottom of the well in most low-pressure, low-temperature wells. In contrast, for high-pressure and high-temperature wells, loading may occur close to the surface. Therefore, the critical velocity should be calculated at the locations of interest with the respective temperatures and pressures if downhole data are available.

Calculations of minimum critical velocity are relatively insensitive to temperature, which can be estimated through linear gradients. Downhole pressures must be determined using flowing gradient routines, using a gradient curve, or simulation software such as OLGA. It is important to note that the accuracy of the critical velocity prediction is highly dependent on the accuracy of the predicted flow pressure [1].

The estimation of critical velocity can also be applied to deviated and horizontal wells through the use of correlations; however, this paper will not delve into this topic, as it focuses solely on vertical wells.

Several modifications have been proposed to increase the accuracy of Turner's critical velocity equation, although they are not discussed in detail in this article. Nosseir *et al.* [3] considered other flow regimes by correcting the value of the drag coefficient C_D. Li *et al.* [4] proposed changes to C_D based on droplet shape. Zhou and Yuan [5] found an empirical correlation to account for the liquid holdup. Sutton *et al.* [6] proposed better PVT correlations.

Derivation of the Critical Velocity Equation Using the Droplet Model

The transport of a liquid droplet in a gas stream flowing within a vertical wellbore is depicted in Figure 2.1. The droplet is subject to the effects of gravity, which pulls it downward, and the upward drag force exerted by the gas as it flows around the droplet. The gravitational force is given by

$$F_G = \frac{g}{g_C}(\rho_l - \rho_g)\frac{\pi d^3}{6} \tag{2.1}$$

and the drag force is given by

$$F_D = \frac{1}{2g_C}\rho_g C_D A_d (v_g - v_d)^2 \tag{2.2}$$

where g is the gravitational acceleration, g_C ($= 1\ (kgm)/(Ns^2)$ for SI-units) is a unit conversion factor, d is the droplet diameter, ρ_l and ρ_g are the liquid and gas densities, respectively, C_d is the drag coefficient, A_d is the droplet cross-sectional area, and v_g and v_d are the gas and droplet velocities, respectively (all variables are in consistent units).

The drag force must be greater than the gravitational force to lift the droplet upward. A liquid droplet is kept in suspension when $F_D = F_G$, which means that $v_d = 0$. At this point, $v_g = v_c$, which yields the following equation:

$$v_c = \sqrt{\frac{4g}{3}\frac{(\rho_l - \rho_g)}{\rho_g}\frac{d}{C_D}}. \tag{2.3}$$

The droplet diameter is unknown and depends on the gas velocity. The Weber number, We, compares the inertia of the droplet with the surface tension. Turner *et al.* [2] assumed $We = \frac{v_c^2 \rho_g d}{\sigma g_C} = 30$. Solving the Weber number for the diameter and substituting it into Equation 2.3 yields the following:

$$v_c = \left[\frac{40 g g_C}{C_D}\right]^{\frac{1}{4}} \left[\frac{\rho_l - \rho_g}{\rho_g^2}\sigma\right]^{\frac{1}{4}} \tag{2.4}$$

where σ is the surface tension of the droplet. C_d can be set as 0.44 when the conditions are fully turbulent. To simplify the equation, $k = \left[\frac{40 g g_C}{C_D}\right]^{\frac{1}{4}} = 5.465$ which is consistent with Coleman *et al.* [7], or $k = 6.558$ that Turner *et al.* [2] found after tuning the correlation by 20%. The equation can then be written as

$$v_c = k\left[\frac{\rho_l - \rho_g}{\rho_g^2}\sigma\right]^{\frac{1}{4}} \tag{2.5}$$

The fluid properties applied in Equation (2.5) should be evaluated under relevant conditions using the real gas law and fluid property correlations (see Sutton *et al.* [6] for proposed property correlations) or PVT tables. The critical rate under standard conditions can be evaluated by using

$$q_c = \frac{T_{SC}}{T}\frac{p}{p_{SC}}\frac{Z_{sc}}{Z} v_c A \tag{2.6}$$

where the critical rate, q_c, is a function of the local temperature (T), pressure (p), and gas deviation factor (Z), as well as the cross-sectional area of the tubing (A) and the critical velocity evaluated under local conditions (v_c). The standard condition temperature of 15.56 ^oC, the pressure of 1.01325 $bara$, and the gas deviation factor (≈ 1) are denoted by the subscript $_{SC}$.

Liquid Film Reversal

Most engineering expressions for liquid loading assume that droplet flow reversal is the cause [8] of liquid loading. The Turner criterion states that droplets of a specific size require a certain (critical) gas velocity to balance drag and gravity forces. The maximum droplet size controlled by a Weber number of 30 is 8.2 mm, which is much larger than droplets typically observed in flow loop experiments and actual gas wells, as stated by van't Westende *et al.* [9]. The droplet size required to satisfy $We = 30$ does not exist under most circumstances, and the minimum gas velocity required to carry realistic droplet sizes to the surface is much lower than predicted by Turner. This led to new research on liquid film reversal.

The paper by van 't Westende *et al.* [10] described the multiphase flow phenomena that occur in flow-tube experiments, including the exchange between liquid droplets and film. By measuring the velocity and size of the droplets and the velocity of the film in a flow loop, van't Westende *et al.* [9] concluded that the liquid loading is likely initiated by the reversal of the direction of the liquid-film flow rather than the reversal of the droplet flow. This was supported by other flow loop experiments and simulation models using OLGA [11]. The idea of film-flow reversal appears to be a credible explanation for liquid loading, but it does not dispute the practical effectiveness of the droplet-based Turner criterion, which is based on the same balance between drag and gravitational forces that governs the onset of film-flow reversal [8].

2.1.2 Nodal Analysis

Nodal analysis is a valuable tool for modeling the performance of oil or gas wells during steady state. This method can include flowlines, chokes, perforations, gravel pack, inflow performance, etc., which is important from the perspective of a petroleum engineer. The user can see the impact on well performance by varying factors such as reservoir performance, choke openings/pressures, and flow line properties.

A nodal analysis divides the system into two subsystems:

- Tubing Performance Curve (TPC)
- Inflow Performance Relationship (IPR)

The IPR curve considers the inflow from the reservoir and the TPC considers the outflow through the tubing, valves, and other completion components. The specific location of interest in the system is called the *nodal point*. The nodal point is usually located above the perforations or at the bottom of the well, although other locations are also valid. Both the IPR and TPC subsystems are plotted separately as pressure-rate curves. The point where the two curves intersect is the predicted operating point [1].

Tubing Performance Curve

The tubing performance curve, also known as the outflow curve, combines the surface pressure with the pressure drops caused by friction, hydrostatics, and acceleration (at high rates) to show the total pressure and its relationship to the production rate. The frictional pressure drop is highly correlated with the production rate and the tubing diameter. The hydrostatic pressure drop is the static pressure imposed by a column of water, oil, and gas. And lastly, the acceleration pressure drop is often neglected [1].

The blue curves in Figure 2.2 illustrate the outflow curves. They have a distinct upward concave shape with a minimum point at which neither the hydrostatic nor the friction forces are dominant. The minimum point may be considered as the transition from annular / mist to slug flow [12] or the lowest operating rate and pressure before liquids begin to accumulate. The hydrostatic pressure increases to the left of the minimum because the gas is unable to remove all of the produced liquid, and the liquid starts to accumulate. This is called *unstable production*. As the hydrostatic force gains more dominance towards the left, the flow regime

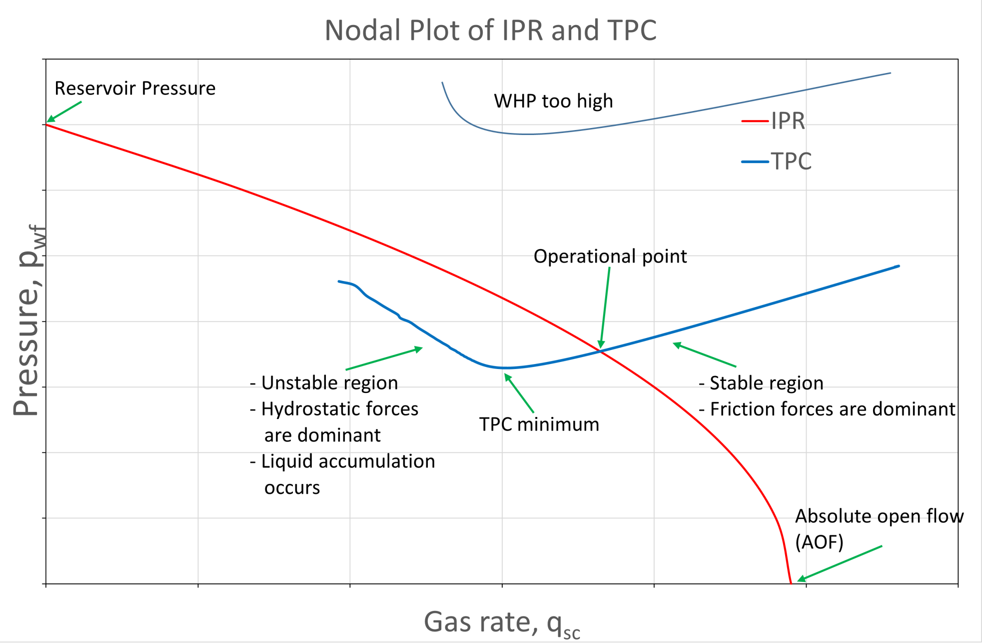

Figure 2.2: Graphic illustration of inflow and outflow curves (taken from S. Breimoen [12])

shifts toward a high liquid holdup regime, such as bubbly flow [1]. This results in a decrease in reservoir production due to reduced drawdown. Frictional pressure drop is dominant to the right side of the minimum. The likely flow regime is annular/mist due to the high gas velocity. Ideally, the operating point is on the right side of the minimum point, where the gas rate is sufficient to transport the liquid to the surface. Production is then referred to as *stable*.

The well does not accumulate liquids when friction forces are dominant. Conversely, the well is prone to accumulate when friction forces become less dominant than hydrostatic. Knowing this and given at least two sets of rate and pressure, the slant of the TPC can be calculated and used to estimate whether the well is experiencing liquid loading or not [1].

Inflow Performance Relationship

The inflow performance relationship (IPR) is the correlation between the rate at which the fluid flows from the reservoir to the well and the pressure difference between the reservoir and the well. It is often represented graphically as a pressure-rate curve, as seen in red in Figure 2.2. When the wellbore pressure is zero, the reservoir produces at the highest rate, known as *absolute open flow* (AOF) [1].

Most IPR expressions are derived from partial differential equations of reservoir flow [13]. The pressure-rate correlation usually contains information about:

- Permeability and porosity

- Drainage area and formation thickness
- Boundary condition
- Formation damage, stimulation, fracturing, perforations, screens, etc.
- Wellbore
- Average pressure
- Convergence effect
- Saturations

These parameters are usually separated based on pressure and geometry and integrated separately. Occasionally, there is no explicit solution to the partial differential equation for flow in a porous medium, and must be solved numerically. Reservoir simulators solve PDEs numerically, and they often use sophisticated methods (e.g., a full compositional approach) to calculate accurate fluid properties [13].

A common equation used to generate an inflow curve of gas rate versus flowing pressure at the nodal point (often bottomhole or point above perforations) is the *backpressure equation*

$$q = C(p_r^2 - p_{wf}^2)^n \tag{2.7}$$

where q is the standard condition flow rate, p_r is the reservoir pressure, p_{wf} is the flowing pressure at the nodal point, n is a turbulence constant (it ranges between 0.5 and 1), and C is a constant that accounts for most items listed above. If sufficient information about the system is known, then C can be calculated without well-test data. If the data are missing, n and C can be determined from at least two test rates. This equation is only good for approximating gas inflow for reservoirs with moderate to high permeability [1].

Fetkovitch [14] derived an approximation for future inflow curves by modifying Equation (2.7)

$$q = C\frac{p_r}{p_{ri}}(p_r^2 - p_{wf}^2)^n \tag{2.8}$$

where p_{ri} is the initial average reservoir pressure, p_r is the current average reservoir pressure, p_{wf} is the current flowing wellbore pressure, q is the current flow rate and C and n are the same as in the backpressure equation (given at initial conditions).

2.1.3 Multiphase Flow Regime

How liquid and gas phases interact under flowing conditions can be represented by multiphase flow regimes. What separates multiphase flow from one-phase flow is that each phase behaves differently according to differences in physical properties such as density, viscosity, compressibility, and interactions between gravity, inertia, and buoyant forces [15]. There are a number of flow regime maps available to describe flow in vertical and deviated wells. They can be used to predict liquid loading; however, superficial velocities should be evaluated at all locations for a complete analysis [1]. In a vertical well, annular / mist flow is the ideal flow regime for gas wells. If it drops out of that flow regime, an artificial lift is required to keep the well from accumulating liquid. Slug / churn flow appears as the superficial gas velocity declines below a threshold given for a specific pipe/well under flowing conditions. A dispersed bubble or bubble flow may occur if the superficial gas velocity becomes even lower.

Flow regime maps, such as in Figure 2.3, are used as tools to predict the appearance of flow patterns as the flow rates change for a given set of properties. Transitions and definitions of flow patterns are qualitatively defined from visual observation and therefore are highly subjective without a universal solution [15].

A gas well with an initial high production rate is normally in the annular / mist flow regime region. Annular flow appears as a turbulent gas core (which may contain liquid bubbles) surrounded by a wavy film of liquid. The thickness of the film depends on the orientation of the pipe and the flow rates of liquid and gas. The film is evenly distributed around the circumference of the pipe if the orientation is vertical. For deviated pipes, the film thickness is greater at the bottom due to gravitational effects. The gas-liquid interface can be stable or unstable. Small-amplitude and high-frequency waves can force the liquid to detach from the film and enter the core of turbulent gas. This is known as liquid entrainment [15]. What separates annular and mist flow is the action of shearing liquid from the liquid film, often seen in high-pressure systems with high heat flux [15].

As the production rate decreases or the liquid-gas ratio changes, the flow regime is prone to change. Slug flow appears as alternating slugs of liquid or gas. The size, frequency, and shape of the slugs depend on the geometry of the pipe / well, the orientation, and the fluid properties. Slug flow may be classed as a subcategory of intermittent flow regime, since the transition from annular flow to more liquid-rich flow is chaotic and hard to define explicitly, except when properly developed slugs appear.

Bubbly flow occurs when the gas rate is relatively low and the liquid rate is high. Bubbly flow can be identified as dispersed bubbly flow since gas bubbles travel in a continuous liquid medium. For vertical orientation, bubbles are normally distributed evenly across the cross-section of the pipe. For deviated orientations, the bubbles are distributed closer to the upper wall.

Flow regimes can change with depth or length along a pipe. A common scenario is annular / mist flow near the surface, but other flow regimes may exist at depth because of a more liquid-rich flow. When slugs appear on the surface, the measured production rate will be erratic and the decline curve will change drastically. Eventually, production will stabilize as gas bubbles travel through a continuous column of liquid. Gas production can in some cases continue for a long time below the critical rate. However, the production rate is severely decreased and the well will die prematurely.

Flow regime maps, critical velocity, and nodal analysis are all predictive methods for estimating the onset or severity of liquid loading. The absolute best indicators of the phenomenon are field symptoms. However, field symptoms are an after-the-fact indicator, and preventive measures should already be in place. Therefore, verified multiphase transient simulators with coupled reservoir and wellbore models should be used to predict the phenomenon and its potential solution before liquid loading occurs.

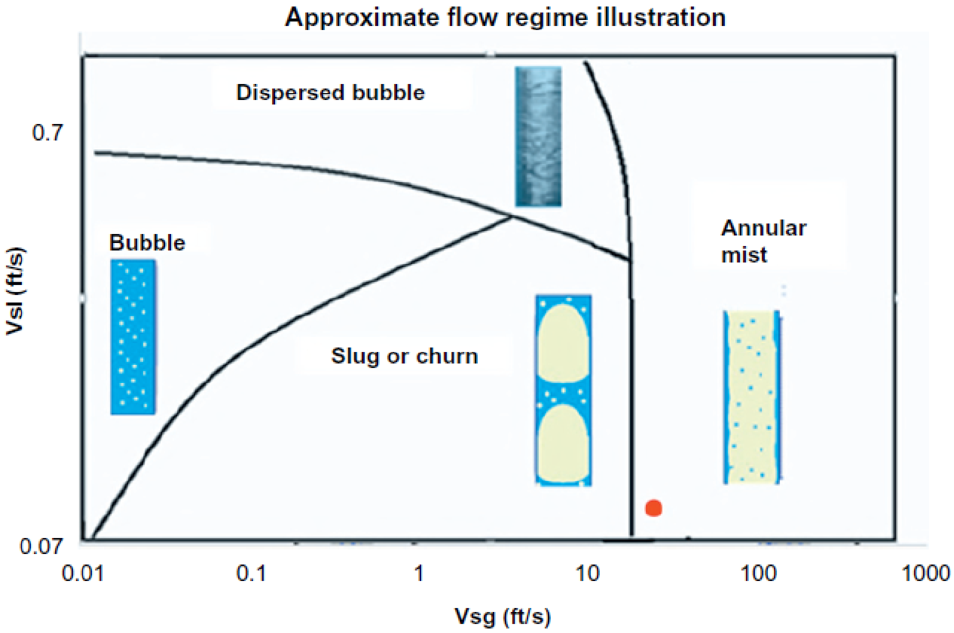

Figure 2.3: Example flow regime map (taken from Lea *et al.* [1]).

2.1.4 Multiphase Transient Simulator

Multiphase transient pipe / wellbore simulators (e.g. OLGA) are traditionally used to estimate transient and steady-state events within pipes, where the source of fluids is defined using predefined fluid rates (from mass nodes) or steady-state / pseudo-steady-state inflow criteria defined using IPRs (pressure nodes). During liquid loading and other time-dependent events, the near-wellbore reservoir region can experience fluid redistribution, backflow, temperature changes, and pressure changes that affect reservoir flow and performance. Traditional reservoir models (IPRs) oversimplify the near-wellbore reservoir and may be inappropriate in estimating transient phenomena. The near-wellbore region is one of the most essential elements in a petroleum production system; however, it is still one of the most underappreciated areas.

To better predict and model the complexity of transient events in the wellbore and near-wellbore region, a tool capable of integrating the reservoir and wellbore is necessary. The pipe / wellbore simulator, OLGA, can be coupled to a near-wellbore reservoir simulator called ROCX. The integrated model has been tested and verified for various transient events:

- Chemical placement (Sagen *et al.* [16])
- Load on sandface during well bean-up (Sagen *et al.* [16])

- Water coning (Chupin *et al.* [17])
- Gas well liquid loading (Veeken *et al.* [11])

See Section 2.3 for a detailed description of OLGA, ROCX, and integration of both models.

2.2 Near Wellbore Region

Near wellbore reservoir properties refer to the properties of the reservoir located in the vicinity of the wellbore. These properties are important to understand the flow of fluids from the reservoir to the well. During production, liquid accumulation may occur in the well and reservoir, leading to a decrease in gas velocity and ultimately reduced production. One way to combat liquid loading is to study the interactions between the near-wellbore reservoir and the wellbore and design the completion and production strategy accordingly.

Liquid loading in gas wells occurs when the reservoir pressure decreases in mature gas fields, restricting or stopping the flow of gas because of the liquid content of the well. The industry has focused on alleviating this problem, but the fundamental understanding of the associated phenomena is weak, especially with regard to the near-wellbore region [18]. Liquid loading can cause flow reversal and phase redistribution in the wellbore and near-wellbore region which changes the flow dynamics over time.

The relevant reservoir properties include permeability (absolute and relative), capillary pressure, porosity, compressibility, volumetric parameters (e.g. radius and pay zone), and phase saturations, pressures, and temperatures. Permeability refers to the ability of a reservoir rock to transmit fluids through interconnected pores and fractures. Capillary pressure is the pressure difference across the interface of two immiscible fluids as a result of surface tension. Porosity is the volume of void space in the reservoir rock, while compressibility refers to the ability of the reservoir to compress under pressure. Saturation refers to the ratio of fluids present in the reservoir rock. Mobility is the ratio of relative permeability to fluid viscosity and represents the ease of fluid flow through the reservoir. During the production of hydrocarbons, there are dynamic changes in pressure, temperature, and fluid composition. Furthermore, the fluid saturation levels of water, oil, and gas can also vary. These changes in fluid saturation levels result in a corresponding shift in the mobility of the different phases present in the reservoir and capillary pressure. The changes are due to the correlation between relative permeability and saturation, the dependence of viscosity on pressure, temperature, and composition, and the correlation between saturation and capillary pressure. *Condensate banking* refers to a relative permeability effect caused by liquid dropout in the near-wellbore region due to a pressure drop [19]. *Condensate buildup* is similar, but caused by condensate backflow from the wellbore instead of condensation in the reservoir.

In a cylindrical reservoir where the well is the only source of energy loss, conventional pressure profiles have the lowest pressure near the well and monotonically increasing pressure towards the outer boundary. Fluid flows from high pressure to low pressure, so the pressure differential drives the flow of fluids toward the well during normal production. Unconventional pressure profiles in reservoir simulation refer to pressure profiles that deviate from conventional patterns. They can occur under certain circumstances. For example, in wells with very low permeability, the pressure drop near the wellbore may be less significant because of the low flow rate. This can lead to a flatter pressure profile near the well. Another example is in fractured reservoirs, where the pressure profile can show a series of spikes and dips due to the presence of fractures, which can create pathways for fluid flow and affect the pressure distribution. Unconventional pressure profiles can also occur in wells where production is affected by transient events such as liquid loading, where the pressure drop near the wellbore is less than expected due to the accumulation of liquids, or if the pressure is greater in the well than in the reservoir. Figure 2.4 shows a conventional, U-shaped, and shifted U-shaped pressure profile. Conventional pressure profiles indicate flow from the reservoir to the well. Conversely, the U-shaped pressure profile indicates backflow. Shifted U-shaped pressure profiles can be caused by transient events and are a result of fluid redistribution within the reservoir and flow to the well.

The conventional pressure profile in the near-wellbore region is not suitable to characterize transient phenomena, since fluid moves from high to low pressure. The U-shaped pressure profile was proposed by Zhang *et al.* [18] and the experimental investigations conducted have verified the occurrence of the phenomena. Phase redistribution in the wellbore under transient-flowing conditions, which leads to downhole pressure fluctuations, can trigger flow from the well to the near wellbore region. Liu *et al.* [20] conducted core-scale experiments to verify the existence of U-shaped pressure profiles during dynamic interactions between the well and the reservoir. They also noticed that the transition from a steady state to a transient state to a new steady state occurs quickly, and the U-shaped profile disappears after a short period of time.

2.2.1 Crossflow

Schlumberger [21] defines crossflow as "A condition that exists when two production zones with dissimilar pressure characteristics are allowed to communicate during production. Reservoir fluid from the high-pressure zone will flow preferentially to the low-pressure zone rather than up the production conduit unless the production parameters are closely controlled." The pressure equalization phenomenon can be divided into two separate terms:

Natural crossflow occurs during no-flow scenarios when the reservoir zones are at a hydrostatic pressure equilibrium. The driving mechanism is the difference in diffusivity, as stated by Jalali *et al.* [22]. The diffusivity is mathematically defined as $D = k/\phi \mu c_t$, where k is the permeability, ϕ is the porosity, μ is the viscosity, and c_t is the total reservoir compressibility. This is not as relevant during

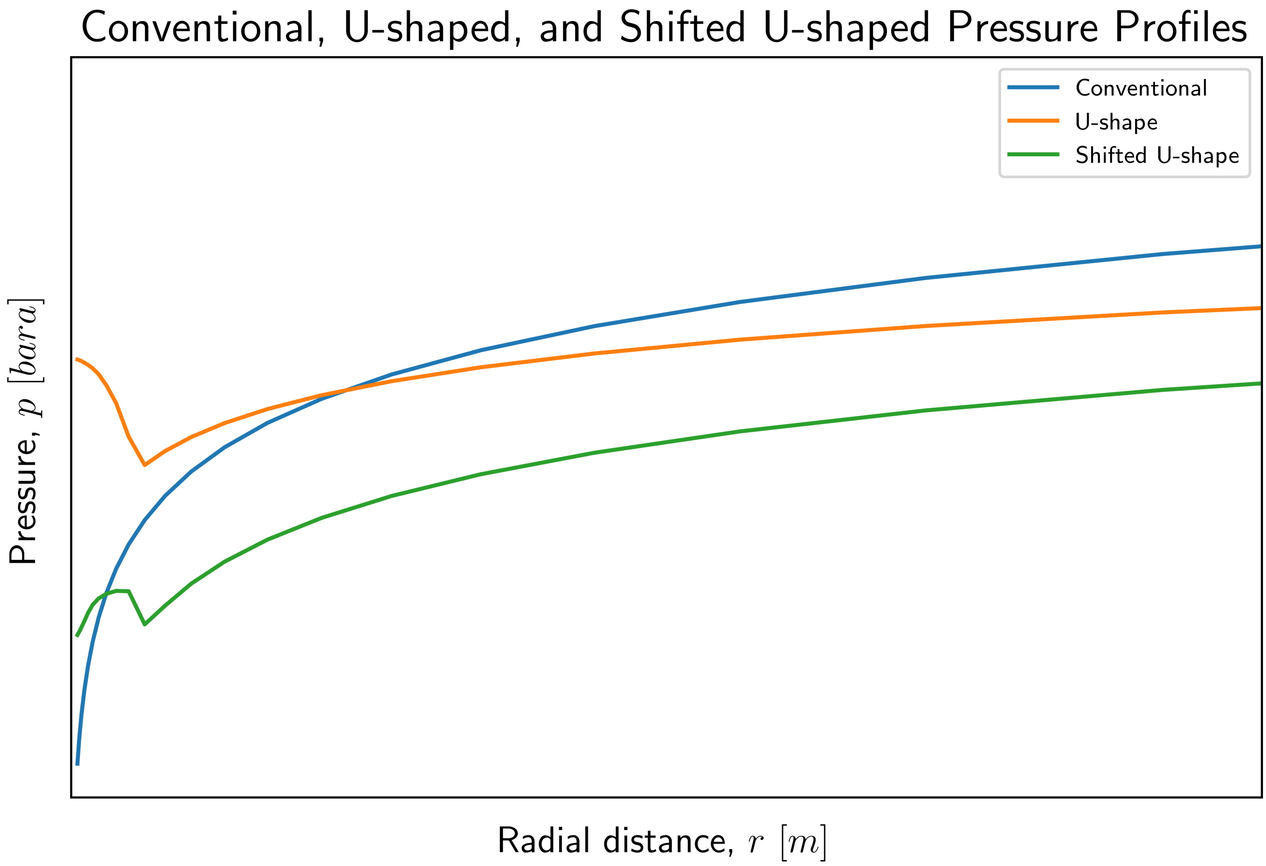

Figure 2.4: A conventional, a U-shaped, and a shifted U-shaped pressure profile. The shape of the pressure profile determines if fluid flows from the well to the reservoir, from the reservoir to the well, redistribution within the reservoir, or a combination. The radial distance is measured from the sandface.

production and injection.

Forced crossflow occurs when the reservoir zones are not in equilibrium with the pressure. Several phenomena can cause this. For example, abnormal pressure gradients can create a pressure difference greater than that of the hydrostatic, and reservoir characteristics can make the zones deplete at different rates during production, increasing the pressure disequilibrium.

2.2.2 Fluid Redistribution

Fluid redistribution in the near-wellbore region is a critical phenomenon that occurs as a response to pressure changes in the reservoir that are related to phase saturations. Changes in reservoir pressure are related to well production events and phase saturation. Fluid redistribution is also influenced by rock and fluid properties, such as permeability, relative permeability, capillary pressure, viscosity, and density, as preferential flow paths can be generated.

2.3 Reservoir and Pipeline Model

2.3.1 OLGA - Pipeline model

OLGA is the industry standard tool for transient simulations of multiphase petroleum production [23]. It is used mainly for engineering, design, estimating operational limits, and establishing operational procedures. Additionally, the software is used in safety analysis to map out the consequences of equipment malfunction and failure. One of the advantages of OLGA over other commercial software used in the industry is its ability to handle both steady-state and transient flow.

Model Basics

OLGA is a simulator that is used to study the behavior of three types of fluid in pipelines and wells: gas, oil or condensate, and water. The model assumes that the gas is lighter than the other fluids and uses separate continuity equations to track the movement of each component. Oil may be heavier than water, although the model has only been verified for fluids where oil is less dense than water. Fluids may interact through mass transfer at their interface [23].

OLGA uses a set of conservation equations to mathematically model fluid behavior and flow. These equations include the mass, momentum, and energy equations for each phase present in the system. In particular, the simulator uses three continuity equations for the liquid phases (oil, water, and oil and water) and one continuity equation for the gas phase. OLGA also uses three momentum equations for the liquid phases and one momentum equation for the combination of gas and liquid droplets. The droplet velocity in the gas phase is determined by using a slip relation. In addition to the momentum and continuity equations, OLGA applies a mixture energy equation, which assumes that all phases are at the same temperature. The energy equation accounts for thermal conduction and convection, as well as phase changes such as condensation or evaporation. This results in seven conservation equations and one equation of state for pressure, which are used to ensure the conservation of mass, momentum, and energy throughout the simulation.

To solve these equations, properties, boundaries, and initial conditions are required. Linearized equations are solved using a sequential scheme, where the current pressure is based on the previous temperature. The semi-implicit time integration method allows for longer time steps than explicit methods, limited by the Courant-Friedrichs-Lewy criterion. Numerical errors are corrected over time as they exist as local errors in fluid volume, as compared to the relevant pipe volume [23].

The transport equations outlined in the OLGA help manual [23] contain underdetermined quantities that depend on the flow regime, for example, friction coefficients and mass transfer between phases. OLGA recognizes four types of flow regimes: stratified, annular, slug, and bubbly flow. There are also defined criteria for how one type of flow transitions to another. Details on transport equations and flow regimes are described in the OLGA help manual [23] in the *Modeling basics* section.

In general, the OLGA fluid model is a complex mathematical representation of fluid behavior and movement in pipelines and wells. When these equations are solved numerically, OLGA is able to predict the behavior and movement of gas, oil/condensate, and water in a system under both transient and steady-state behavior.

Fluid Model

There are four principal techniques utilized in OLGA for describing fluid properties (PVT). See the OLGA help manual for more detailed information [23].

1. Table lookup: Fluid properties are obtained from a PVT-file by reading the tabulated values at specified pressures and temperatures. This is the most computationally efficient method and is appropriate for situations where the fluid composition remains relatively stable throughout the flow paths or over time. Further information can be found in the section on *PVT Lookup Table* in the OLGA help manual.
2. Compositional tracking. Fluid properties are calculated using a comprehensive compositional approach. This method is computationally intensive and should be utilized in instances where significant variations in composition are anticipated. More information can be found in the section on *Compositional Tracking* in the OLGA help manual.
3. Blackoil: The fluid properties are determined using black-oil correlations. This method is useful when information about the production fluid is scarce. Further details can be found in the section on *Blackoil* in the manual.
4. Single component: This technique is designed to handle single-component fluids that cross the saturation line. Additional information can be obtained from the section on *Single Components* in the manual.

When fluid flows back and forth between models (OLGA and ROCX), it is important to ensure the same properties under the same pressure and temperature conditions. Otherwise, the simulation may experience discontinuous fluid behavior and the simulator may crash. There are only two fluid options available in ROCX: table lookup and black-oil tracking. Table lookup is generally preferred to the black-oil model since tabulated data is often generated using comprehensive compositional tracking software (e.g. Multiflash or PVTsim), and the method ensures consistent fluid properties for any given pressure and temperature.

The black-oil model is often used when the description of the fluid is poor, as it requires little input. The only required data are the specific gravity of gas and oil (and water if present) and the gas-oil ratio under standard conditions. The black-oil correlations available are defined by Standing [24], Lasater [25], Vasquez & Beggs [26], and Glasø [27]. See the OLGA Help manual [23] for a detailed description of the black-oil model (tuning, enthalpy, conductivity, specific heat, surface tension, etc.).

2.3.2 ROCX - Reservoir Model

ROCX is a three-dimensional near-wellbore simulator capable of simulating three-phase flow in porous media. It can be used in integrated wellbore-reservoir transient simulations by being coupled to OLGA, see Section 2.3.3. The flow model is built on the mass-conservation equations for water, oil, and gas flowing in a porous medium and energy conservation. The flow and energy equations are solved using a fully implicit method to achieve numerical robustness; refer to the paper by Sagen *et al.* [28] and the ROCX documentation [29] for details. The model manages both positive and negative flows through the sand face and throughout the reservoir, which may be the case during transient events. The simulator handles both radial and rectangular grid types, which is beneficial for near-wellbore simulation, but not ideal for full-fledged reservoir simulation due to the complexity of the geometry.

Inputs to the reservoir model are rock properties such as permeabilities, capillary pressures, saturations, and porosities in the directions x, y, and z relative to the well, fluid properties (tabulated values or black oil model), thermal properties for fluids and rock and rock compressibility. Furthermore, time-dependent boundary conditions in the well and in the reservoir define the flow direction (radial, angular, or z), temperature, and pressure or phase flow rates. The boundary at the well defines skin and well index factors for each phase. Well index factors are multiplied by the sand face transmissibility, which directly impacts phase rates [29]. However, when the reservoir model is coupled to a pipeline model, the well boundary is replaced by the pipeline model. Regarding the outer boundary condition, if it is not defined, then the boundary is assumed closed and has zero flow going through. Setting the pressure at the boundary as zero means that there is no flow at the boundary, except for heat transfer, which can be used to simulate heat transfer at the outer boundaries [28].

ROCX calculates phase densities, pressures, temperatures, and saturations in every grid cell, based on the input to the model, the time-dependent boundary conditions, and the coupling level. Grid cell data can be saved in user-defined intervals at the cost of simulator performance. A script to parse the simulation data into arrays working with Python is included in Appendix A.3.2.

Conservation of water, oil, and gas flow in a porous medium is presented by the following equations:

$$\frac{\delta}{\delta t}(\rho_w \phi S_w) + \nabla \cdot (\rho_w \underline{v}_w^D) = \dot{m}_w + \Psi_{w \leftarrow g} \tag{2.9}$$

$$\frac{\delta}{\delta t}(\rho_o \phi S_o) + \nabla \cdot (\rho_o \underline{v}_o^D) = \dot{m}_o + \Psi_{o \leftarrow g} \tag{2.10}$$

$$\frac{\delta}{\delta t}(\rho_g \phi S_g) + \nabla \cdot (\rho_g \underline{v}_g^D) = \dot{m}_g + \Psi_{g<-o} + \Psi_{g\leftarrow w} \tag{2.11}$$

where subscripts w, o, g refer to water, oil, and gas, respectively. ρ is density, ϕ is porosity, S is saturation, $\underline{v}^D$ is Darcy velocity, $\dot{m}$ is the source mass rate and Ψ is the rate of mass transfer between phases.

The Darcy velocity is given by

$$\underline{v}_{w,o,g}^D = -k \frac{k_{r-w,o,g}}{\mu_{w,o,g}} (\nabla p_{w,o,g} - \rho_{w,o,g} g) \tag{2.12}$$

where k is the absolute permeability, k_r is the relative permeability, μ is the viscosity, p is the pressure, and g is the gravitational acceleration.

Volume balance for the phases and mass balance for the flash terms (Ψ) is given by

$$S_w + S_o + S_g = 1 \tag{2.13}$$

$$\Psi_{o\leftarrow g} + \Psi_{g\leftarrow o} = 0 \tag{2.14}$$

$$\Psi_{w\leftarrow g} + \Psi_{g\leftarrow w} = 0 \tag{2.15}$$

The capillary pressures between oil/water and gas/oil are given by

$$p_{cow}(S_w) = p_o - p_w \tag{2.16}$$

$$p_{cgo}(S_g) = p_g - p_o \tag{2.17}$$

The energy equation used in ROCX is given by

$$\begin{aligned} &\frac{\delta}{\delta t}(\rho_w \phi S_w \mu_w + \rho_o \phi S_o \mu_o + \rho_g \phi S_g \mu_g + (1-\phi)\rho_s \mu_s) + \nabla \cdot (\rho_w h_w \\ &\underline{\mu}_w + \rho_o h_o \underline{\mu}_o + \rho_g h_g \underline{\mu}_g) + \nabla \cdot (k_T \nabla T) = \dot{Q}_{H\ overburden} + \dot{Q}_{H\ underburden} + H_S \end{aligned} \tag{2.18}$$

where the subscript s refers to solid (rock), k_T is thermal conductivity, H_S is energy source, and $\dot{Q}_H$ is the overburden/underburden heat source.

If the black oil approach is used, the conservation equation for water, oil, and gas flow in a porous medium is

$$\frac{\delta m_{l,c}}{\delta t} + \nabla(m_{l,c} \underline{v}_l = Q_{l,c} + \sum \Psi_{l,c\leftarrow k,c} \tag{2.19}$$

where the velocity is given by

$$\underline{v}_l = -\frac{k}{\phi S_l} \frac{k_{rl}}{\mu_l} (\nabla p_l - \rho_l g) \tag{2.20}$$

where the subscipts l, k are phase indexes and c is component index.

Refer to the ROCX manual [29] and the paper by Sagen *et al.* [28] for more information.

2.3.3 Pipe and Reservoir Model Coupling

Traditionally, models of production systems to receiving facilities are steady-state models where timesteps are on the scale of days to a month. It is helpful in estimating depletion, field layout, and production planning. However, it does not account for dynamic interactions between the reservoir and the well, which is useful for predicting flow assurance and production issues. The OLGA-ROCX coupling is designed to be numerically stable by solving the energy and conservation equations iteratively at small timesteps, using Newton-Rhapson's method. This is a necessity, as the timesteps involved in reservoir/wellbore simulations are only a fraction of full-fledged reservoir simulations to account for the dynamic interactions that occur [28]. The OLGA-ROCX coupling is designed for the following scenarios:

- Fluctuations in bottomhole pressure caused by slugging in pipelines and wells change the inflow to the well from the reservoir. Due to changes in inflow, feedback can aggravate the slugging.
- Liquid build-up in low-rate wells where either liquid is lifted out as a slug or kills the well.
- During well shut-in, pressure builds up slowly, while the flow gradually decreases. The liquid will be redistributed in the well as the flow stops. Peak pressure and liquid distribution are important parameters in the design of the well and are highly affected by the characteristics of the reservoir and well.
- Restarting production after a shut-in period takes time. The time it takes to reach normal production should be as short as possible. However, the redistribution of fluids can take time.
- Capturing well inflow details during water breakthrough and coning of gas and water.
- Simulate crossflow between reservoir zones with different properties.
- Other transient phenomena (e.g. backflow, chemical placement, and well cycling).

The reservoir model is a plug-in to the wellbore model. Fluid flow and temperature from the reservoir to the well are defined by matching the grid defined in ROCX with the grid in OLGA. OLGA provides the pressure boundary at the well for ROCX. ROCX in return generates flow and temperature into the pipeline.

Assuming that the simulation has reached timestep n, the coupling between OLGA and ROCX is outlined in three steps:

1. OLGA requests the reservoir model to calculate the coefficients in Equation (2.21)
$$Q_i^{n+1} = a_i p_i^{n+1} + b_i \tag{2.21}$$
where p_i^{n+1} is the pressure in the control volume and Q_i^{n+1} is the mass flow of the phases.
2. OLGA uses Equation (2.21) as a boundary condition and solves the flow

network. Then the pressure and phase mass rates are transmitted back to ROCX.

3. ROCX uses the pressure and phase mass rates to complete the timestep integration.

Since the coefficients are unknown, they are solved in the previous timestep, where the pressure and mass rates are known. The only exception is for the first integration, where $a = 0$ and b = the flow rate from ROCX. More details are described by Sagen *et al.* [28].

If using the coupled simulators in conjunction with full-scale reservoir simulation, a proposed workflow is as follows [17]:

- Identify the location of interest (wellbore and location within the reservoir). Information from the wellbore should not reach the boundary of the grid defined in ROCX.
- Snapshots of interest provide properties that should be used as initial conditions for the coupled simulation.
- Grid information, rock properties, fluid properties, and phase saturations should be defined in the coupled simulator. The grid definition should be revised as it is likely too coarse for an accurate simulation of transient events.

2.3.4 Numerical Considerations

Several numerical considerations should be taken into account when using coupled simulators such as ROCX and OLGA.

Grid resolution plays a critical role in capturing detailed behavior of the reservoir and wellbore system. Using a coarse resolution makes the simulator unable to accurately predict the pressure gradients, saturations, fluid behavior, crossflow between layers, etc. A fine grid consists of a large number of grid cells which makes it possible to simulate in more detail at the cost of computational load and simulation time.

Time step size influences the precision and computational efficiency of the simulations. Small timesteps can capture rapid changes in the system at the cost of computational time. On the contrary, a long timestep requires fewer computations but might fail to capture transient events.

Boundary and initial conditions can affect the simulation results. It is therefore important that they are based on reasonable assumptions.

A grid sensitivity analysis can be performed to determine the ideal number of grid cells. This is done by gradually increasing the number of grids until satisfactory accuracy is reached without excessively increasing the computational time. Satisfactory accuracy refers to the change in performance indicators (i.e. pressure, rate, etc.) not being significant with further grid refinement. However, the "ideal" number of grid cells and timestep size can vary depending on the specific problem.

Chapter 3

Model Setup and Analysis Strategy

The objective of this study is to improve the understanding of fluid flow in both the well and the reservoir during liquid loading, which is an important issue in oil and gas production. Traditionally, most research has focused on the wellbore, but it is increasingly apparent that the behavior and movement of fluids in the reservoir are equally important.

In this study, ROCX is used to simulate reservoir flow, as it has significant advantages over traditional inflow performance relationships (IPRs) due to its ability to handle transient events such as backflow and crossflow of separate phases that can occur during liquid loading. By coupling ROCX with OLGA, the fluid moved in the wellbore and reservoir can be tracked under both steady-state and transient conditions.

Two different models are considered: a single, continuous reservoir layer and two layers separated by a non-permeable zone:

- In the first part of the study consists of **Case 1.1 - IPR** and **Case 1.1 - ROCX**. OLGA is coupled to an IPR and to ROCX in two separate models to compare the results. Identical wellbore and fluid properties are used, and the reservoir properties are tuned to be similar. This is done to compare the techniques for estimating the onset of liquid loading and the behavior post-loading. However, because of the simplicity of the IPR expressions, a significant deviation from the ROCX case is expected during liquid loading due to the lack of transient capabilities. Similar data from the wellbore domain are expected prior to liquid loading for the setup using ROCX and IPR since liquid loading is initiated in the wellbore. This part of the study places additional emphasis on the wellbore domain with respect to the critical rate. The occurrences of conventional and unconventional pressure profiles and fluid redistribution within the reservoir are also discussed.
- For the second part of the study, three models, **Case 1.2a**, **Case 1.2b**, and **Case 1.2c**, are designed with two separate zones. In the first model, the per-

meability of both zones is identical. In the second model, the permeability of the top zone is ten times greater than that of the bottom zone, while in the third model, the permeability of the bottom zone is ten times greater than that of the top zone. Several tests are conducted on these models. The base case for each of the models is to run the setup until liquid loading starts and production stabilizes. The second case is a shut-in during loading. The third case is to reduce the wellhead pressure to see whether it makes a difference to crossflow between zones. Capillary pressure is turned off in one of the tests to see whether it affects liquid loading. The final case is with another fluid model. These tests are conducted to study fluid flow through the sandface, crossflow between reservoir zones, fluid redistribution, and overall how performance is affected by liquid loading.

Overall, this study is expected to provide valuable information on fluid movement in both the wellbore and reservoir before and during liquid loading, which can help optimize production strategies and improve oil and gas recovery.

3.1 Simulation Setup

3.1.1 Fluid Models

Fluid 1 - Wet Gas

The wet gas fluid file used in cases 1.1 - IPR, 1.1 - ROCX, 1.2a, 1.2b, and 1.2c is generated using Multiflash. Multiflash is a software package commonly used in the oil and gas industry to calculate fluid properties such as density, viscosity, and phase behavior. The gas-oil ratio (GOR) is 20111 Sm^3/Sm^3, and the relative gas density is 0.63. The relative oil density is 0.723.

Both the reservoir and wellbore models use the same precalculated fluid properties as a function of pressure and temperature. During the simulation, interpolation is used to obtain the required values for the simulation. This approach ensures consistency and accuracy in the fluid properties used in both the reservoir and wellbore models. The main drawback is that the fluid model may not be adequate if the fluid composition has a significant change at a particular place in time. Compositional tracking is not available in the 2020 version of ROCX.

The fluid composition is tabulated in Table 3.1. Figure 3.1 shows the phase envelope of the fluid. Based on the figure, a reservoir temperature of 110^oC prevents gas condensation for every defined pressure. Therefore, the gas may only condense in the wellbore.

Fluid 2 - Gas Condensate

The gas condensate fluid file is also generated using Multiflash. It is used in cases *1.2b Gas Condensate as Fluid Model* and *1.2c Gas Condensate as Fluid Model* to check whether the fluid composition affects crossflow and other events related to

Table 3.1: Wet gas fluid composition.

COMPONENT	FRACTION
NITROGEN	0.0025
CO2	0.0141
METHANE	0.9246
ETHANE	0.0318
PROPANE	0.0101
ISOBUTANE	0.0028
N-BUTANE	0.0024
ISOPENTANE	0.0013
N-PENTANE	0.0008
C6	0.0014
C7+	0.0082

liquid loading. The GOR is 1294 Sm^3/Sm^3, with a relative gas density of 1.08 and a relative oil density of 0.700. The fluid composition is shown in Table 3.2. The phase envelope is included in Figure 3.2, where the blue line marks the dew points and the orange line marks the bubble points.

Table 3.2: Gas condensate fluid composition.

COMPONENT	FRACTION
METHANE	0.45
ETHANE	0.20
PROPANE	0.10
BUTANE	0.10
HEXANE	0.10
DECANE	0.05

3.1.2 Wellbore Model in OLGA

The wellbore model, sketched in Figure 3.3, is defined in OLGA (version 2020). The model consists of a vertical well with 3,000 m tubing, an outer diameter of 2 3/8 in, and an inner diameter of 2 1/4 in. The roughness of the pipe is 2.286E-05 m. The tubing is discretized into 150 sections. The discretization is not optimized with respect to performance and accuracy; however, it is evenly spaced to match the grid in ROCX and to get evenly spread data output, which can be used in the analysis. It also has a fluid source defined by ROCX or IPR. The heat transfer coefficient, which measures the ability of a fluid to transfer heat through a material, is normally known to change with depth due to the different types of completion components and cement used. However, in this case, it is assumed that it is constant at 31 $W/m^2 \cdot^o C$.

The default minimum and maximum timesteps are set as 0.001 and 100 s,

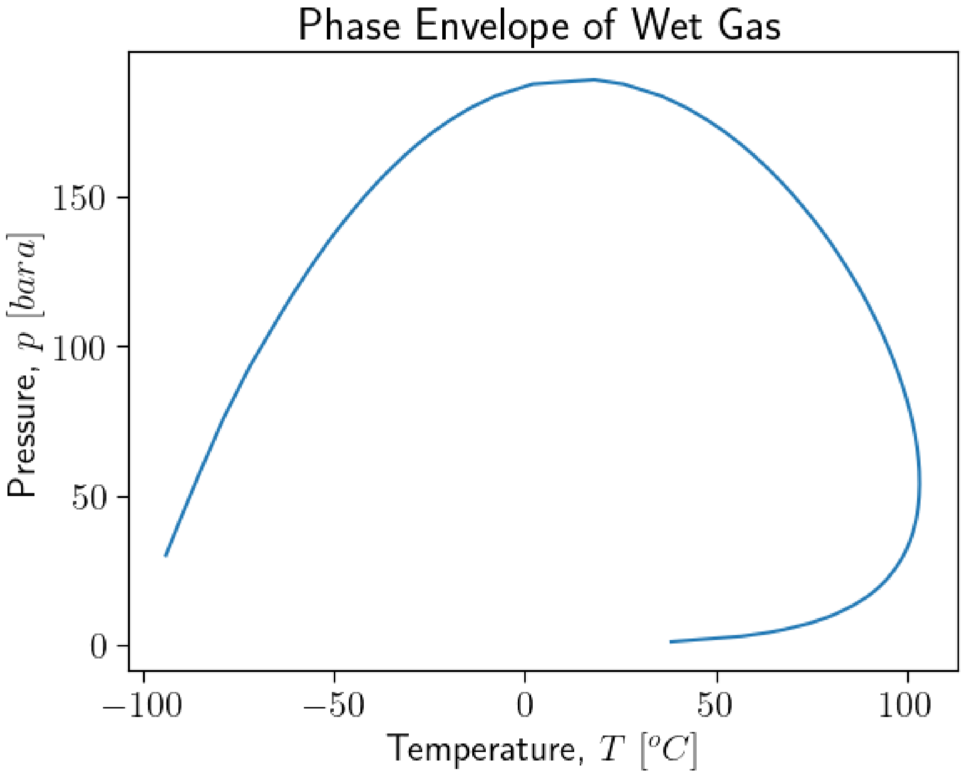

Figure 3.1: Wet gas phase envelope.

respectively, for fast-occurring transient events. The minimum timestep can be readjusted by OLGA if convergence is not met. Transient event timesteps are much shorter than those of traditional reservoir simulation, which may be on the scale of days or months. This slows down the simulation but increases the accuracy of the results and makes it possible to capture rapid transient events.

The variables of trend data (referring to measurements made in a single location over time) include the surface rates of gas, oil, and water, bottomhole pressure, and the liquid fraction of the wellbore volume. Profile data variables (referring to variables where measurements are saved for every section over time) include pressure, temperature, liquid holdup, gas velocity, droplet velocity, liquid film velocity, and flow regime identifier. Data are stored at intervals of 200 or 600 seconds, depending on the case.

Case 1.1 and 1.2 Wet Gas Specific Model Inputs

The wet gas fluid model defined in Section 3.1.1 is used in the simulations. The ambient temperature at the bottom of the well is 110^oC, while it is 20^oC at the wellhead. The steep temperature gradient is defined to ensure that the gas condenses in the well. This yields a producing OGR of approximately 5E-05 Sm^3/Sm^3.

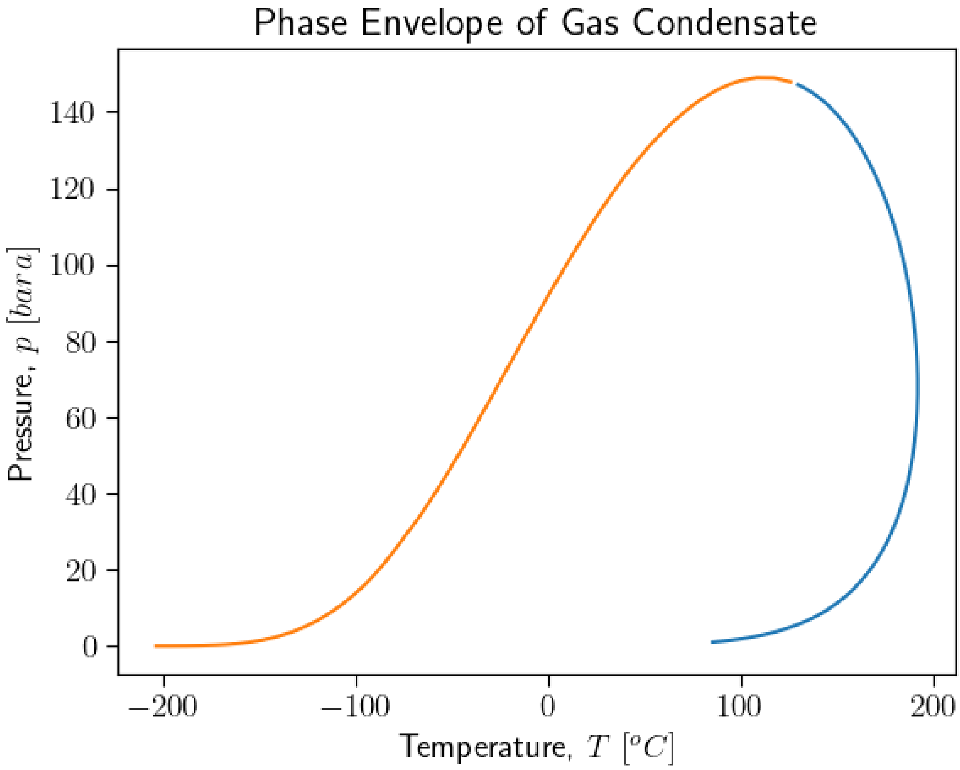

Figure 3.2: Gas condensate phase envelope.

For cases 1.1 and 1.2a, 1.2b and 1.2c, the wellhead pressure is set at 60 $bara$. The initial temperature and pressure in the wellbore are set identically to the reservoir because of the fluid definition. The tubing is gas-filled (no liquid), with a pressure of 80 bara (identical to the reservoir pressure) and a temperature of 110^oC (reservoir temperature).

In cases 1.2b and 1.2c with a reduced P_{wh}, the wellhead pressure is reduced to 40 $bara$. In addition, the reservoir pressure is reduced to 55 $bara$. The depletion time is extended

Case 1.2 Gas Condensate Specific Model Inputs

The gas condensate fluid model defined in Section 3.1.1 is used. The initial pressure and temperature in the reservoir and well are 100 $bara$ and 200^oC, respectively. The ambient temperature at the bottom of the well is constantly 200^oC and 160^oC at the top.

3.1.3 Reservoir Model in ROCX

The 2020 version of ROCX is used. Several sets of conditions are tested to check the limitations and capabilities of the simulator. Three key findings are included in

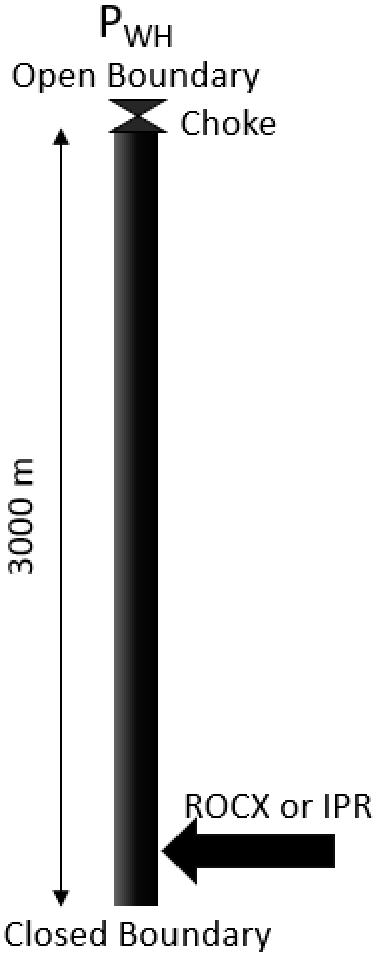

Figure 3.3: A wellbore sketch showing the inflow zone (IPR or ROCX), boundaries, and the tubing

all simulation cases to obtain proper results. A test case included in Appendix A.1 shows that the reservoir should be depleted numerically instead of by defining time-dependent boundary pressures. Furthermore, the grid in the z-direction is increased from 3 to 10 numerical layers to better capture fluid movement and increase the accuracy of the results. The simulator is also sensitive to the fluid definition, which means that it crashes if the pressure and temperature values are outside the tabulated values.

The ROCX input file used in **Case 1.1 ROCX** (Section 4.1.2) is included in Appendix A.2.2. It contains all relevant reservoir data and coupling parameters to the well. To generate the two-zone models, the z-grid is changed from 10 to 11 numerical layers, an additional boundary condition is defined for layer 11, and the permeability in the principle directions is defined below. The rest of the setup is identical. Layers 6-11 are referred to as the *top zone* and layers 1-5 are referred to as the *bottom zone*.

The near-wellbore radius is set to 100 m. The radial extension of the reservoir is discretized using an irregular (logarithmic spacing) grid. This choice is made because of the logarithmic grid's ability to more accurately capture the behavior of fluids and hydrocarbons within the reservoir, particularly in the vicinity of the wellbore. The grid is defined using cylindrical coordinates, with 20 radial grid layers, 1 angular layer, and 10 or 11 vertical layers depending on the case. The pay zone has a thickness of 100 m, and in the cases with 11 layers in the z-direction, the 6th layer has zero permeability to cut off communication between the top and bottom zone of the reservoir. Each layer is coupled to the wellbore grid, as defined in the wellbore model. The study assumes isotropic porosity throughout the reservoir and ignores the compressibility of the rock. The reservoir is also defined to be isothermal.

The residual saturations for gas (S_{gr}) and water (S_{wc}) are set to 0, while the residual saturation for oil (S_{or}) is set to 0.1. The reservoir is initially filled with gas ($S_g = 1$). The relative permeability of gas and water is generated using the Corey correlation [30], with the exponent set to 2 and the relative permeabilities of phases at saturation of 1.0 is unity. The relative permeability of oil is a function of the saturation of gas (and water), and is defined using the *Stone II* model [31]. The oil-water and gas-oil capillary pressures are defined as a linear relationship between the lightest and the densest phase. When $S_g = 0$, $P_{cgo} = 0$. When $S_g =$ 1-$S_o r$), $P_c go = 1\ bara$. Water is not included in the simulation, but P_{cow} is defined identically to the gas-oil capillary pressure.

The outer boundary of the reservoir is defined as a no-flow boundary, including the outer radial boundary and the top and bottom of the reservoir. The inner boundary is defined by OGLA, and all energy losses are through the well. This means that any pressure drop or change in energy within the reservoir is due solely to the production or injection of fluids through the well, and not through any potential losses that can occur at other places, as in real reservoirs.

The study considers four different reservoir models, as seen in Figure 3.4. In Case 1.1, the reservoir is divided into 10 identical vertical layers, all with a permeability of 10 md. Case 1.2a consists of 11 vertical layers, with layers 1-5 and 7-11 having a permeability of 10 md, and layer 6 having a permeability of 0 md. In Case 1.2b, the reservoir is divided into 11 vertical layers, with layers 1-5 having a permeability of 10 md, layer 6 having a permeability of 0 md, and layers 7-11 having a permeability of 100 md. In Case 1.2c, the reservoir is divided into 11 vertical layers, with layers 1-5 having a permeability of 100 md, layer 6 having a permeability of 0 md, and layers 7-11 having a permeability of 10 md.

The reservoir pressure and temperature are defined in such a way that condensate does not drop out of the vapor phase in the reservoir. Fluid definitions and initial pressures and temperatures of the reservoir are defined identically to those of the well, as described in Section 3.1.2.

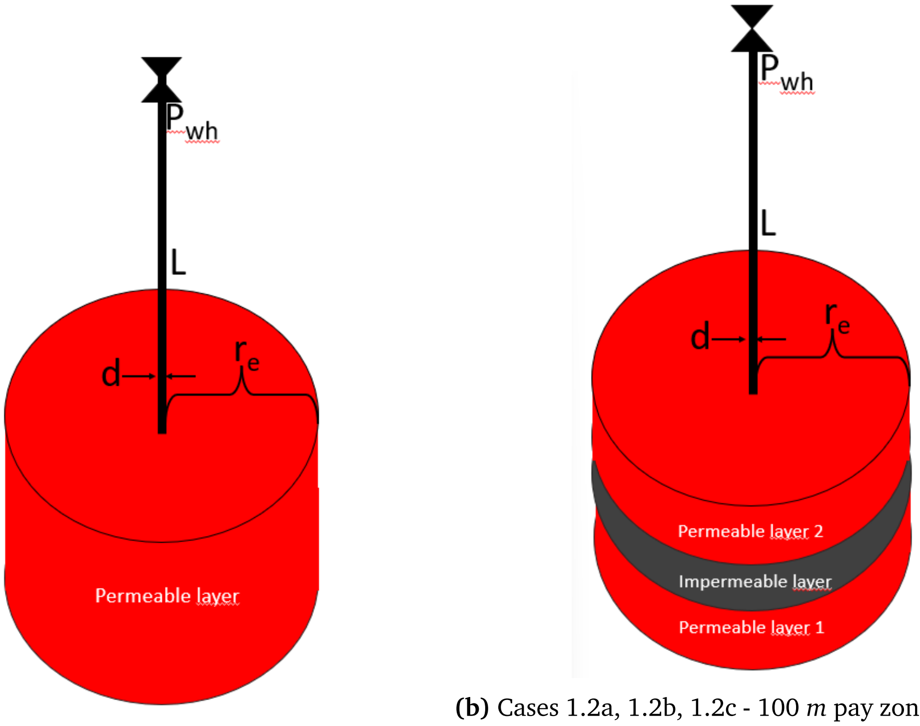

(a) Case 1.1 - IPR and 1.1 - ROCX - 100 m continuous payzone

(b) Cases 1.2a, 1.2b, 1.2c - 100 m pay zone, no direct communication between the top and bottom reservoir zones.

Figure 3.4: Sketchings of the wellbore and reservoir models.

3.1.4 Reservoir Model using IPR

A *reservoir contact* is defined, instead of the *nearwell* nodes that can be coupled to ROCX, in the bottom 100 m of the wellbore model. An IPR defines both the flow from the reservoir to the well and the flow from the well to the reservoir. The backpressure equation 2.7 is selected since it is suitable for both gas and oil reservoirs. The model is designed to describe inflow performance in the pre-depleted state of the reservoir. Based on the definition in OLGA, the backflow rates are calculated in the same way as the inflow rates are calculated.

To obtain the constants C and n for the backpressure equation, five test rates and bottomhole pressures are taken from a standalone simulation with ROCX and OGLA coupled. Identical properties are used in the ROCX model as in the model in Section 3.1.3. Test rates are taken as the surface choke is gradually closed in and after the production stabilizes. The following choke openings are used: 144/64, 72/64, 36/64, 16/64, and 8/64 in. A best-fitting line on a log-log plot of the production rates and pressures yields $C = 286.86 Sm^3/d \cdot bara^2$ and $n = 0.9687$.

The model is set to isothermal because the temperature changes are turned off in the ROCX model. Additionally, the reservoir pressure drop is defined using a gradient similar to that observed in the coupled case.

The rest of the wellbore model is identical to the model described in Section 3.1.2.

3.2 Analysis Strategy

OLGA produces extensive datasets consisting of five trend data variables, namely liquid fraction, bottomhole pressure, and surface rates of gas, oil, and water, which are stored every 200 or 600 seconds during simulation time. Additionally, profile data variables are saved along the 150 sections of the wellbore, including total liquid holdup, oil holdup, water holdup, flow regime identification, pressure, temperature, droplet velocity, gas velocity, liquid film velocity, superficial gas velocity, superficial droplet velocity, and superficial liquid film velocity, all of which are also recorded every 200 or 600 seconds. Regarding ROCX, the temperature, saturations, and pressures are stored for every grid cell. In addition, the phase production rates through the sandface of each horizontal layer are saved at intervals of 200 or 600 seconds. Due to the large amounts of data, Python is a convenient tool for analysis. However, to use Python, the datasets must be processed and converted to arrays or dictionaries. The following sections briefly identify the contents of the software developed for this study, which significantly speeds up the analyzing process. Some code snippets are available in Appendix A.3.

The analysis is divided into two domains:

- Wellbore
- Near-wellbore Reservoir

The wellbore domain was discussed by Breimoen [12] in his project report. Critical rate and velocity were determined from analytical calculations and simulations. Production rates were compared before and after loading to characterize the severity of the liquid loading. This study examines whether the droplet velocity or the liquid film velocity is the first indication of liquid loading. In addition, the simulated velocities are compared to Turner's velocity. How fluid flow and pressure drop in the wellbore are related to the flow in the reservoir and the potential crossflow between reservoir zones is also examined.

The near-wellbore domain, often where the least effort is put in, is analyzed using phase saturations and pressure data, and mass rates through the sandface. Typical abnormal events may be fluid redistribution between adjacent interconnected layers, crossflow between different zones, and production losses due to condensate banking or buildup. These events are studied to see if and how they correlate with liquid loading and how reservoir performance is affected.

3.2.1 Liquid Loading in the Wellbore

The critical rate and velocity are estimated using analytical expressions and simulations. The droplet model first introduced by Turner *et al.* [2] is used to calculate the critical velocity. See Section 2.1.1 for the derivation of Equation (2.5). The critical rate and velocity are also determined using OLGA, where the velocity of the gas, droplets, and liquid film is determined. Flow regimes are identified along the wellbore in time using OLGA. Production rates, pressures, holdups, and pressure drops are simulated to give insight into when liquid loading occurs, the direction of flow, and how much production is inhibited by the phenomenon.

Velocity

The Turner critical velocities are calculated using Equation (2.5) and translated to critical rates using the real gas law in Equation (2.6). OLGA does not compute Turner's critical rate and it is therefore done using Python, but with pressure and temperature data from the simulator. The critical rate is also calculated from the critical velocity using the tabulated density through $q_c = v_c A/B_g = v_c A\rho/\rho_{sc}$ Code snippets are available in Appendix A.3.2. Fluid densities and surface tension are evaluated in each numerical section along the wellbore using table interpolation with local pressures and temperatures. Because pressure and temperature are not constant over time, the properties are evaluated at every timestep.

OLGA generates gas, liquid film, and droplet velocities along the wellbore in time. These velocities are compared in time to verify whether liquid film reversal or reversal of the bubble flow is the initiation of liquid loading. The simulated gas velocities are also compared with the critical velocities determined using Turner's equation.

An important difference between the calculated and simulated rates is that the calculated rates are based on simplified assumptions and equations that may not capture the complexity of real-world fluid flow as accurately as the industry standard flow simulator. The calculations are limited to simplified physics, assuming turbulent flow and only basic interactions between phases.

Plots are generated in Python showing the velocity of the gas, droplets, and liquid film along the wellbore in time. In addition, the calculated critical velocity is plotted. This visualizes what initiates the liquid loading, the depth at which it happens, and how it compares with the Turner velocity. In the software developed, indexes of when the velocities change from positive to negative are stored, and the corresponding surface rates of gas are returned to the user.

Decline Curve

As the reservoir depletes, the rate of gas production declines. If there is a change in the global trend of the decline, it is an indication of a flow restriction due to liquid buildup, sand production, damaged tubing, or damage to the reservoir. Sand production and tubing damage have not been modeled in this study. The only driving factors for rate decline are pressure depletion of the reservoir, formation damage, and liquid loading in the well.

Sudden changes to the decline curve indicate liquid loading in this study. A gradient search approach is used to identify the flow rate and time at which abnormal events occur. The interior points of the production rates and time use second-order central differences to compute the gradient, while the boundaries use first-order or second-order one-sided differences (either forward or backward), as stated in the Numpy reference manual [32]. If the gradient changes more than a user-defined value, the index is returned and used to identify the rates and pressures.

Flow Regime

OLGA has a built-in flow regime identifier capable of tracking slugs and identifying stratified, annular, slug, and bubbly flow. The data are manipulated to show the length of the slug flow regime over time rather than time-series plots of the type of flow regime along the wellbore. Tracking slug development can provide valuable insight into production. For example, if there is a sudden change in the production rate during liquid loading, it may be due to slugs or other changes in the flow regime.

3.2.2 Reservoir Indications

ROCX computes the phase temperatures, pressures, and saturations in every cell of the grid defined in the model. Phase flow rates through the sandface of each layer are also calculated.

Flow Rate Through the Sandface

The phase flow rates are plotted in time for layers 1-10 (11). Positive flow is defined as the flow from the reservoir to the well. Negative flow is defined as the opposite. The mass rate through the sandface of the reservoir is plotted to see how parts of the reservoir experience positive or negative flow at different times or magnitudes.

The accumulated mass of oil and the produced mass of gas are found by integrating the mass rates over time. The trapezoidal method, Equation (3.1), is used to approximate the cumulative mass. However, without a continuous function, the error of the integrated dataset cannot be explicitly found. However, it is assumed to be accurate enough for this study. The error related to numerical integration increases drastically if there is a lot of oscillation in the data.

$$\int_a^b f(x)dx \approx \sum_{k=1}^{N} \frac{f(x_{k-1}) + f(x_k)}{2} \Delta x_k \tag{3.1}$$

Gas and oil may flow back during liquid loading. If there is gas backflow, the plots or the integrated mass rates can be used to check whether the inflow is correlated to an additional outflow of the same reservoir zone. If the amount of inflow approximately equals the amount of outflow or less, then it is likely related to sudden changes in pressure caused by transient events, rather than crossflow between reservoir zones.

Saturation

Saturation profiles are key components of reservoir modeling, as they provide information on the relative amounts and distributions of fluids in the subsurface. Normally, it is used to estimate recoverable reserves, but in this case, it is used to study fluid redistribution and condensate buildup because of liquid loading. Since saturation has a massive impact on relative permeability and capillary pressure, phase rates are expected to be highly affected by changes in saturation because of how relative permeabilities and capillary pressure are defined in the reservoir model.

Pressure

Pressure profile plots are used to identify areas of the reservoir with abnormal pressure gradients. Potential abnormal gradients can then be used in conjunction with mass rates and saturations to study the movement of fluids in the reservoir and through the sandface. ROCX makes calculates the movement of individual phases given the phase pressures, saturations, and temperature data in each grid cell.

In addition, the average reservoir pressure in each zone is calculated. It is used to compare the overall depletion rate of the reservoir zones, which may be interesting when the zones have different properties. How the pressures from different phases affect the total pressure is assumed to be directly correlated with the saturations. Furthermore, due to the irregular grid, a weighted average given by Equation (3.2) is used to compute the average reservoir pressure for each numerical layer z_i. Then, the zone pressures are found by calculating the average of layers 1-5 and 6-11.

$$p_{avg,z_i} = \frac{\sum_{j=0}^{j=N-1} \Delta r_j [p_{w,j} S_{w,j} + p_{o,j} S_{o,j} + p_{g,j} S_{g,j}]}{\sum_{j=0}^{j=N-1} \Delta r_j} \tag{3.2}$$

where z_i refers to the horizontal layers, w, o, g are at phases, Δr is the difference in radial extension, and subscript $_j$ denotes the index of the radial grid cell.

Crossflow, Backflow, and Fluid Redistribution

Crossflow refers to the migration of fluids between different reservoir zones. This can occur when there are zones that have different reservoir properties or fractures connecting them. Forced crossflow, as defined in Section 2.2.1, is caused by a difference in pressure between the reservoir zones. This can be studied using pressure data (or pressure derivative data) to check whether depletion from one zone corresponds to increased pressure in the other zone. This, in conjunction with mass rates through the sandface, is used to determine if crossflow occurs and how it affects total production. Crossflow can greatly affect reservoir performance, particularly if oil or water flows into a gas-saturated reservoir due to changes in mobility and capillary pressure, as discussed previously.

Crossflow can also be checked using wellbore data such as pressure data and flow rate data between and above the reservoir zones. For example, if the pressure above the top zone is greater than below the top zone, then fluid flows down and into the bottom zone.

3.3 Limitations, Errors, and Variability

This study does not account for stochastic variability in any parameter used to define the reservoir, fluid, or well model. In reservoir simulations, there are typically numerous properties that are not certain, and a common way to account for the uncertainty is to perform sensitivity studies. A sensitivity study is normally conducted by discretizing uncertain parameters and running several simulations with different combinations of the uncertain parameters (e.g. Monte-Carlo simulation). After this, the outcome is sorted using percentiles (or a clustering technique) on the properties of interest. Then, probable and improbable cases are run on a full-scaled, full-fledged reservoir simulator. Similar simulations can be run on the wellbore simulator as well. However, it is not commonly done, as there are fewer uncertainties. Since this is a synthetic study, it does not rely on field data. Therefore, ignoring stochastic variability is okay.

Since a general understanding of liquid loading in the wellbore and the near-wellbore reservoir is the target knowledge, synthetic setups such as in this study are fine given that the simulators provide realistic data. As this study is not compared to real cases, the mathematics and physics of the simulators are assumed to generate close to real data, based on the work of others (see Section 2.3). However, since liquid loading is a complex and transient phenomenon, the results should be verified through experimental data, as few studies on transient events have been conducted with a coupled reservoir and well simulator. This study does not compare simulation data to experiments!

Every computation has errors related to timesteps, grid definition, and definitions. Smaller time steps and a finer grid definition make for more accurate computations at the cost of simulation time. The OLGA documentation [23] states that *the number of arithmetic operations per time step increases proportionally to* *the number of sections. The accuracy of the solution increases with smaller steps, but in a complex manner that is difficult to estimate quantitatively. The numerical solution should approach the analytical one as Δt and Δz approach zero.* Here, the grid definition is discretized into smaller pieces until satisfactory precision is achieved, as explained in Section 2.3.4.

Another source of deviation from reality are the temperature calculations utilized by ROCX and OLGA. The near-wellbore reservoir region is assumed to be isothermal, which is likely not the case, as changes in pressure through the sandface and cooled fluid flowing back from the well can cause temperature changes. In OLGA, the heat transfer coefficient is assumed to be constant, although it changes in reality as different types of completion are used at different locations. Heat storage in the pipe walls is simplified to a single layer because it is not considered important for the objective. The OLGA documentation [23] states that if heat storage in pipe walls is important, then *thin layers, such as paint, should be included in a neighboring layer*. Although it is not important in this case, it is still a source of deviance from the real world.

The total mass production through the reservoir zones is approximated using a numerical integration technique of the mass rates. The trapezoidal method is used because of its simplicity to implement. However, the accuracy of the results is affected by discretization, curvature, step size, and round-off errors. If oscillations are present, the approximation can be severely affected.

Increasing the radius and/or decreasing the permeability would make the time it takes to reach the outer boundary increase. This could be done to better study de-liquefication techniques such as shutting down the well (or parts of it) to let the near wellbore reservoir regain pressure, etc.

The flow regime identifier is limited by a set of assumptions and simplifications based on generalized fluid flow and the process of slug formation/dissipation. Transitions between flow regimes are also based on correlations that may not be 100% accurate for every scenario. In complex flow scenarios (i.e. several slugs), the slug tracker might generate different slug lengths, volumes, and frequencies compared to real flow.

The initial pressure is assumed to be identical in each numerical layer. In reality, at least a pressure gradient should be defined to account for the difference in hydrostatic pressure in the vertical direction. The start of every simulation is affected by the identical pressure in the zones. However, since liquid loading is typically initiated later in production, the initial transient flow does not significantly affect the study.

Chapter 4

Results & Discussion

4.1 Comparison of a Reservoir Model and IPR as Inflow

This part of the study is to verify whether the liquid film reverses before the droplets begin to move downward and to see how it correlates with Turner's equation. Furthermore, a comparison of the liquid loading using ROCX and IPR as input to OLGA is conducted to assess whether computationally demanding simulations are required to estimate the changes related to the liquid loading. Fluid redistribution within the reservoir is also discussed.

4.1.1 Case 1.1 - IPR

This case is used as a comparison to **Case 1.1 - ROCX**. The IPR is based on steady-state inflow, whereas ROCX is capable of handling transient events. Therefore, when transient events, such as liquid loading, are initiated, the models are expected to generate different results. Liquid loading is expected to begin at the same critical rate and bottomhole pressure as in the ROCX case because the completion remains identical. What happens after loading is expected to vary between the cases, as the IPR does not compute transient behavior such as backflow and saturation changes in the same way as the reservoir simulator.

Wellbore Domain

The onset of liquid loading is after 157 hrs. The simulation transitions naturally from an unloaded to a loaded condition. Table 4.1 shows the critical rates and the corresponding bottom hole pressures. The gradient search method identifies the surface rate of gas as 33,712 Sm^3/d and the liquid film reversal method finds a surface rate of 35,393 Sm^3/d. Slug flow and droplet reversal are observed at similar rates of 19,905 and 20,331 Sm^3/d, respectively.

Figure 4.1 shows the surface rates of oil and gas. As seen in the figure, the gas and oil rates start at 43,265 and 2.15 Sm^3/d, respectively. The rates decrease linearly until the onset of liquid loading since the reservoir pressure is defined to decline over time. The gas production rate stabilizes at a rate of 22,146 Sm^3/d, and the oil rate drops below zero (because of backflow) until production stops (see Appendix A.2 for a longer simulation). From the onset to stabilization, approximately 4 hrs pass. Figure 4.2 shows the liquid fraction, bottomhole pressure, and length of slug flow regime in time. Simultaneously, as the surface rates drop, the bottomhole pressure increases as a result of the increased liquid fraction. The slug flow is also initiated at the same time, although only the bottom section is affected by slugging after the surface rates stabilize.

Figures 4.3, 4.4, and 4.5 show the liquid holdup in conjunction with phase velocities and Turner's critical velocity before and early and late during liquid loading. The gas and droplet velocities are correlated through a slip relation, which explains why they are similar. The velocity of the liquid film is calculated using another mathematical model that accounts for the various forces that act on the film. For numerical reasons, in areas that do not contain liquid, the velocity of the liquid film is defined identically to the velocity of the gas. Based on this, it is clear that the gas begins to condense 350 m from the bottom of the well. As the liquid loading progresses, Figure 4.4 shows that the liquid holdup begins to increase further down the tubing compared to Figure 4.3. Notice how similar the calculated critical velocity is to the droplet velocity both during and after liquid loading is initiated. Lastly, Figure 4.5 shows that the liquid accumulates in the bottom of the well late during liquid loading.

The rate gradient search and liquid film reversal methods find similar critical rates, although not identical. Liquid film reversal is likely the best option in acquiring critical rates from simulation data since it consistently returns the first index where the film velocity is less than zero with the corresponding surface rates, bottomhole pressures, and time, without relying on user-defined input. The gradient search method takes both the rate and the time into the gradient approach and finds the index, rate, pressure, and time based on when a user-defined criterion is met. However, both estimated rates are within the vicinity of the steep rate drop in Figure 4.1. The liquid film reversal rate can be calculated, whereas the gradient search rate is applied to production data.

The slug initiation rate and droplet reversal rate are slightly lower than the stabilized rate after loading. This has to do with the transient flow behavior in the wellbore as the liquid film reverses, which increases the liquid fraction toward the bottom of the well. Additionally, when the production rate is abruptly reduced, the pressure propagates down the well, causing the bottomhole pressure to increase for a short period of time. During this short period, slug flow and droplet reversal are initiated, which is why the slug flow rate and droplet reversal rate are lower than the stabilized production rate after the onset of liquid loading.

The phase velocity and liquid holdup plots, Figures 4.3, 4.4, and 4.5 show that before liquid loading, the liquid holdup is highest close to the surface. This is due to the fluid composition, where more gas condenses at lower temperatures. The liquid film initially reverses close to the surface. As the liquid film reverses down the tubing, the holdup of the liquid increases further down the tubing.

The turner critical velocity calculations along the wellbore are similar to the droplet velocity at the onset of liquid loading. A potential improvement to critical velocity calculation is to include a slip-relation, similar to that of OLGA. Although the liquid film appears to better estimate the onset of liquid loading, similar to the findings of Veeken *et al.* [8].

Table 4.1: Case 1.1-IRP: Comparison of critical rates.

Method	q_g $[Sm^3/d]$	p_{wf} $[bara]$
Rate gradient search	33,712	78.84
Slug index	19,905	79.39
Droplet reversal	20,331	79.60
Liquid film reversal	35,393	78.79
Turner critical rate	23,606	

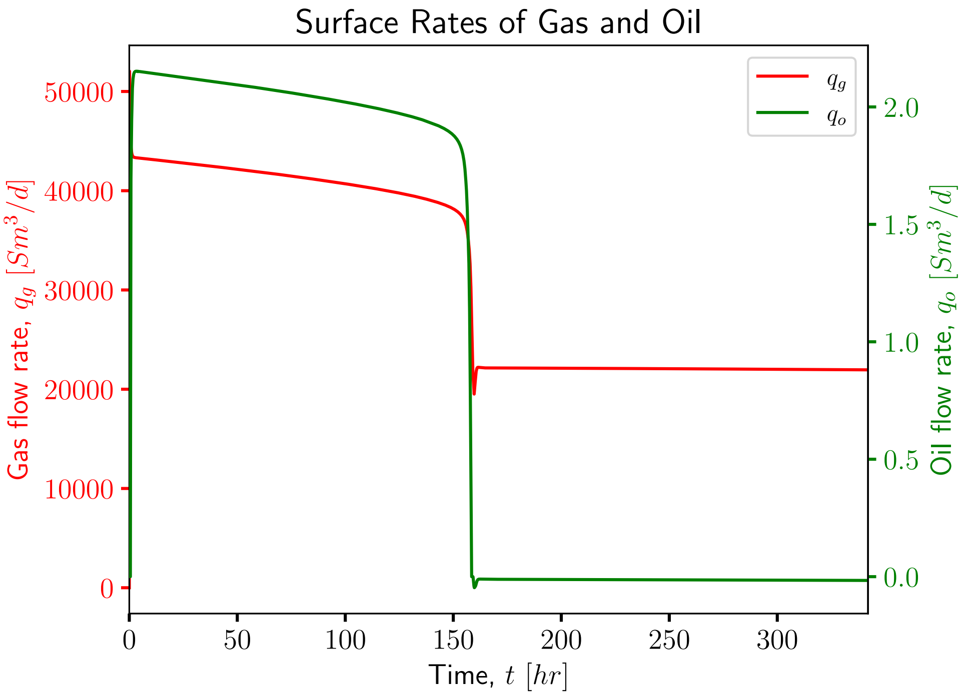

Figure 4.1: Case 1.1 - IPR: Surface rates of oil and gas.

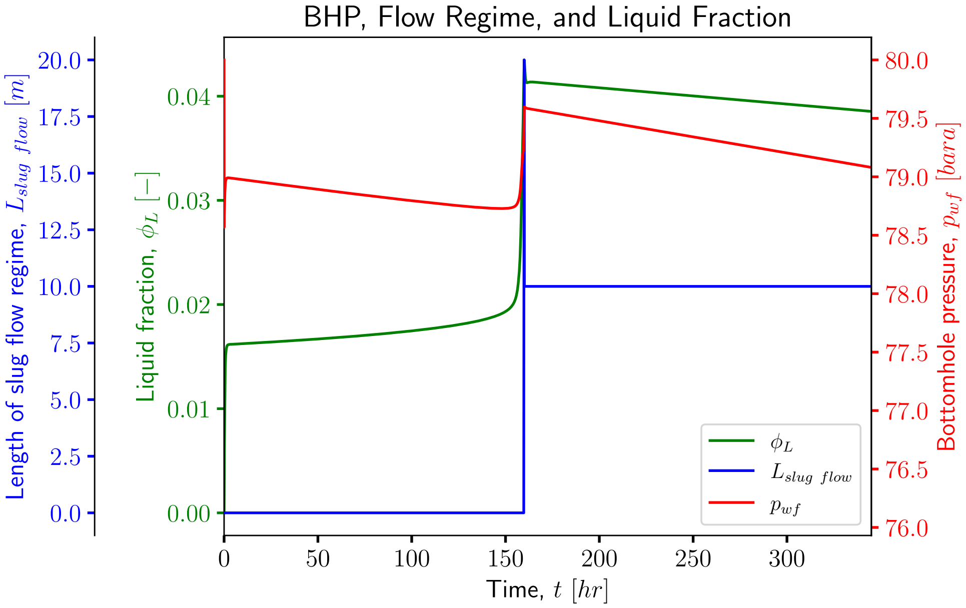

Figure 4.2: Case 1.1 - IPR: Volume fraction of liquid in the tubing, length of slug flow regime, and bottomhole pressure.

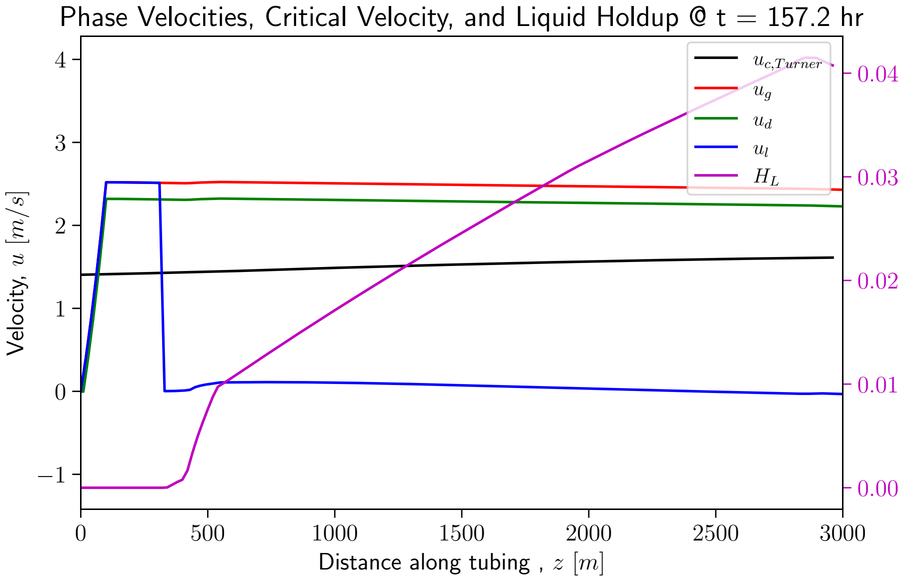

Figure 4.3: Case 1.1 - IPR: Gas, liquid film, droplet, and critical velocity along the branch before liquid loading. In addition, the liquid holdup shows the area of the oil along the wellbore at the given phase velocities.

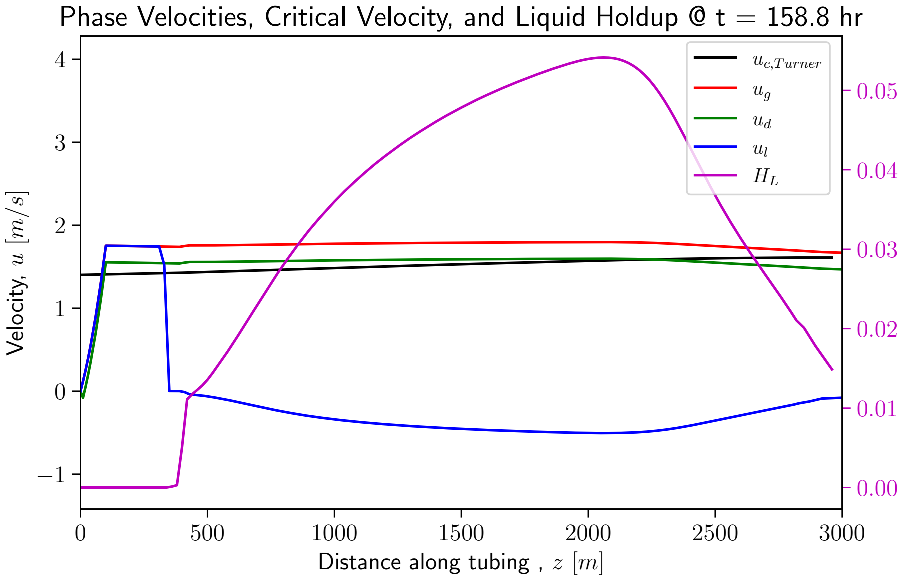

Figure 4.4: Case 1.1 - IPR: Gas, liquid film, droplet, and critical velocity along the branch early during liquid loading. In addition, the liquid holdup shows the area of the oil along the wellbore at the given phase velocities.

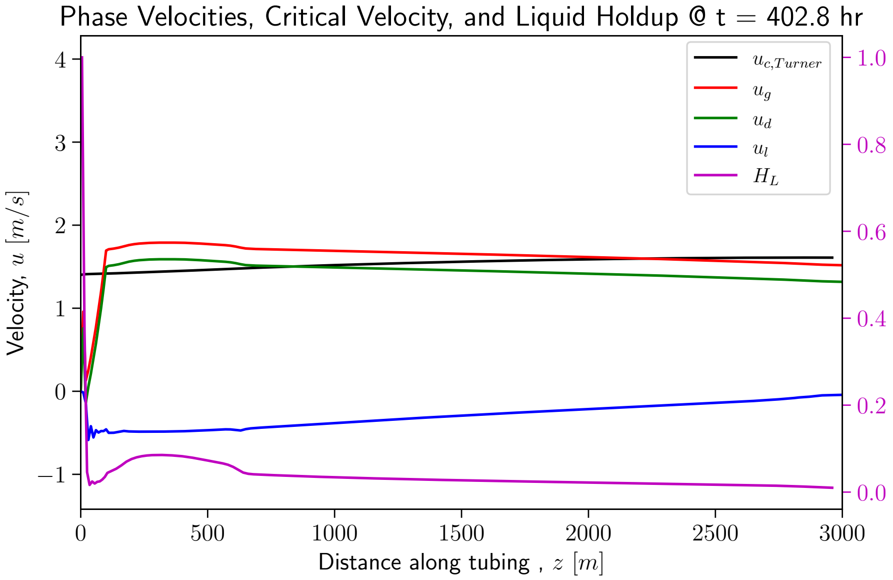

Figure 4.5: Case 1.1 - IPR: Gas, liquid film, droplet, and critical velocity along the branch late during liquid loading. In addition, the liquid holdup shows the area of the oil along the wellbore at the given phase velocities.

4.1.2 Case 1.1 - ROCX

The reservoir model comprises 200 grid cells, including 20 radial, 1 angular, and 10 vertical cells. Each horizontal layer has a permeability of 10 md. Increasing the number of grid cells allows the simulation to better capture the complex flow dynamics near the wellbore, resulting in more accurate results and a better representation of the behavior of a real-world reservoir, as described in Section 2.3.4. The outer boundary is a closed boundary with an initial pressure of 80 $bara$, based on observations from the previous case where loading occurred below 80 $bara$. The reservoir is numerically depleted, the well being the only source of energy loss, making this approach more reliable than the approach described in Appendix A.1, where the reservoir pressure was decreased by changing the boundary pressure. However, it is time consuming because of the increased number of numerical grid cells and the depletion strategy. The radius of the near-wellbore region has been reduced from 500 to 100 m to accelerate the pressure depletion rate. Since the simulation runs standalone (not as an addition to a full-scale reservoir simulation), the information from the well is allowed to reach the boundary of the near-wellbore region.

Wellbore Domain

The well initially produces gas at a rate of 42,273 Sm^3/d, resulting in an initial oil production rate of approximately 2.10 Sm^3/d, with a producing OGR of 4.96$E-5$ Sm^3/Sm^3. Figure 4.6 displays the production rates during the first 300 hrs of depletion. After around 63 hrs, the gas production rate is halved and stabilizes at 21,700 Sm^3/d, while the oil production rate drops below zero (because of backflow), marking the onset of liquid loading. This reduced stable rate during liquid loading is termed *metastable* by Dousi *et al.* [33]. They also found that gas production can reach a stabilized rate below the critical rate, where the liquid column reaches an equilibrium height. Oil continues to condense in the wellbore, but the gas velocity is insufficient to carry the liquid out of the well to the surface. Some of the liquid accumulates at the bottom of the well and some enters the reservoir. Figure 4.7 presents the flowing bottomhole pressure, length of slug flow regime, and the liquid fraction in the tubing, illustrating that liquid accumulation begins about 63 hrs. Additionally, the liquid fraction fluctuates, increasing, decreasing, increasing again, and finally stabilizing a few hours after the initiation of liquid loading. During this transient event, the flow regime undergoes a transition from annular flow to slug flow. This transient interval is examined in more detail in Section 4.1.2, which focuses on the reservoir domain.

Another observation is the transient behavior observed during the first few hours of the simulation. This can be attributed to the initial condition, where the tubing is initially filled with gas and the pressure and temperature are 80 $bara$ and 110^oC, respectively. As production begins, the oil condenses out of the gas stream when pressure and temperature cross the dewpoint line of the fluid mixture, which occurs at a depth of approximately 2650 m relative to the wellhead.

Since production remains stable for more than two days before the occurrence of liquid loading, the effects of the transient behavior during start-up are mitigated and do not significantly impact the liquid loading phenomenon.

Table 4.2 presents the critical rates determined from the simulation and calculated using Turner's equation. The rate gradient search and liquid film reversal method yield rates of 33,909 and 35,402 Sm^3/d, respectively. Almost identical to the rates found in Case 1.1 - IPR. This simulation also reveals that the slug flow and liquid droplet reversal appear at a lower rate than the reversal of the liquid film. Droplets start traveling downward at a rate of 27,337 Sm^3/d, approximately 2 hrs after the liquid film reversal. Slug flow appears after 87 hrs, about 22 hrs later, at a rate of 21,973 Sm^3/d.

Table 4.2: Case 1.1 - ROCX: Comparison of rates.

Method	q_g $[Sm^3/d]$	p_{wf} $[bara]$	**time** $[hr]$
Rate gradient search	33,909	78.81	63.2
Slug index	21,973	78.74	87.1
Droplet reversal	27,337	78.96	65.0
Liquid film reversal	35,402	78.77	62.8
Turner critical rate	23,599		

Another observation is that the liquid fraction does not exceed 4.5% at most. Following the initiation of liquid loading, it takes approximately 50 hrs for the liquid fraction to increase from less than 2% to 4.5%. Remarkably, even when a small fraction of the wellbore contains liquid, production rates are severely reduced. This suggests that the near-wellbore region can have a significant impact on the deliverability of the well.

The phase velocity and liquid holdup plots are included in Appendix A.4.1. The same conclusion is drawn from the velocity plots in this case and **Case 1.1 - IPR** in Section 4.1.1.

The liquid film reversal rate is almost identical in both this case and in **Case 1.1 - IPR**. Since the wellbore and fluid properties are identical in both cases, these rates are expected to be similar. The time it takes for liquid loading to begin is 65 hrs, approximately 90 hrs less than in the previous case, even though the pressure gradient is defined similarly to the pressure gradient of this simulation. The two reasons for this are that the average pressure gradient is not identical to the pressure gradient prior to liquid loading (the gradient is much higher before liquid loading) and that the IPR is an approximation to the physics that occur in the reservoir.

The appearance of slugs was expected to occur at about the same rate as the droplet reversal rate. An explanation for the delay in transitioning to a flow regime with reduced gas production could be attributed to the short transient period that follows the onset of liquid loading. During this period, the gas production rate is reduced as a result of the increased liquid fraction in the well and the backflow

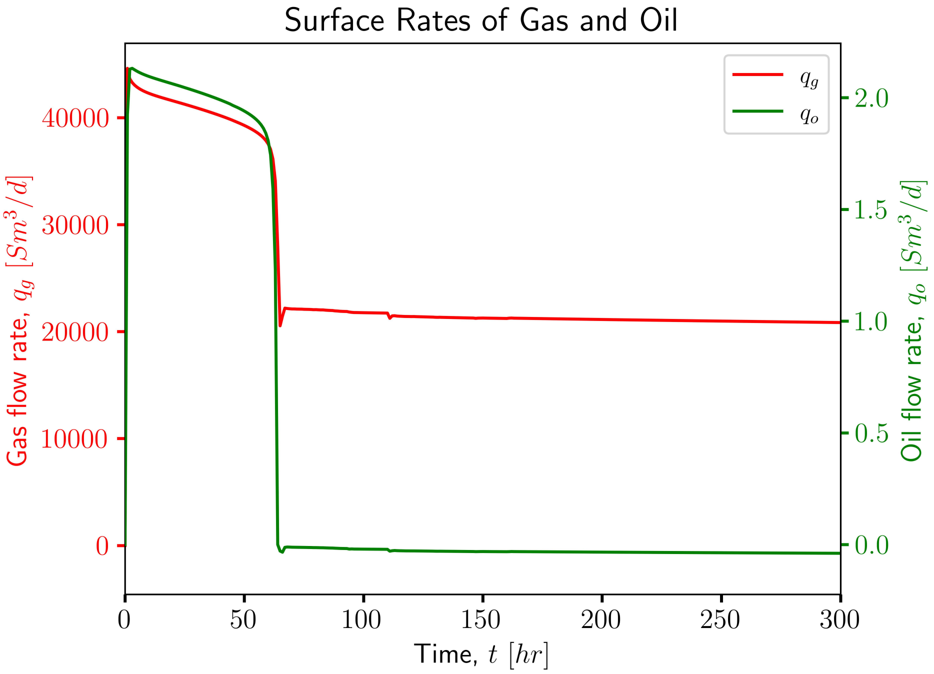

Figure 4.6: Case 1.1 - ROCX: Surface rates of oil and gas.

of oil into the reservoir. The liquid-gas ratio in the wellbore remains low while oil progressively flows back through each numerical reservoir layer. This delays the time it takes for the liquid to accumulate in the well and create slugs.

The calculated critical rate is 23,599 Sm^3/d, which is close to the slug initiation rate and the droplet reversal rate, being only 15% greater than the latter. Based on this result, it appears that Turner's equation generates a value similar to that of the liquid droplet reversal rate when it is provided with fluid properties, pressures, and temperatures identical to those of the simulator.

The question arises as to whether droplet reversal should be considered as the initiation of liquid loading. Liquid film reversal rate, being closely related to the rate gradient search, better predicts the onset of liquid loading. This observation aligns with the findings of Veeken et al. [8] and the findings in **Case 1.1 - IPR** (Section 4.1.1). On the other hand, the droplet reversal rate appears to be closely associated with the rate at which the flow regime transitions from annular to slug. Understanding the rate at which annular flow transitions to slug flow is valuable. However, it is essential to prepare a well for liquid loading before the phenomenon occurs to mitigate the production losses and formation damage that may occur as a result of liquid loading.

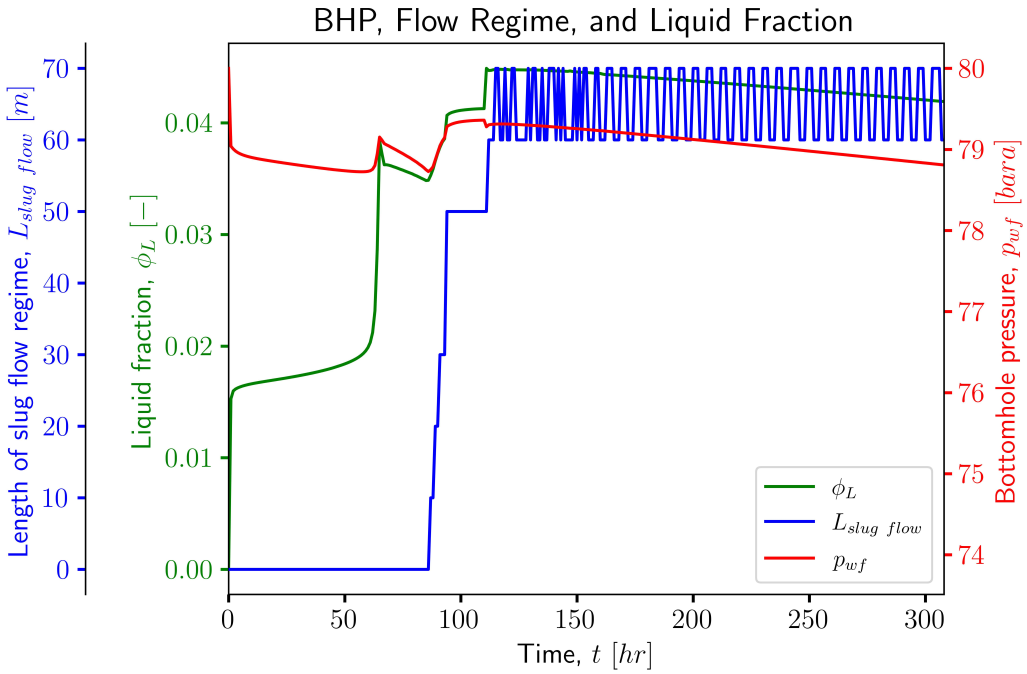

Figure 4.7: Case 1.1 - ROCX: Bottomhole pressure, liquid fraction, and length of slug flow regime.

Reservoir Domain

The reservoir is initially filled with gas and kept at a constant temperature of 110^oC to prevent gas condensation. Any change in gas or oil saturation in the reservoir is attributed to the liquid that forms in the wellbore and flows through the sandface into the reservoir.

Figure 4.8 illustrates the gas mass rates through the sandface of the ten numeric layers that are coupled to the well. Prior to the reversal of the liquid film in the wellbore, which occurs after approximately 63 hrs of simulation time, all layers produce gas at similar rates. Figure 4.9 shows the mass rates of oil through the sandface, with the backflow of oil occurring after 65 hrs, 2 hrs after the reversal of the liquid film.

Table 4.4 tabulates the oil rate through the sandface just before liquid loading and when production stabilizes. Clearly, the lower layers account for most of the oil inflow to the reservoir, and some low-mass rates of oil are produced to the wellbore from the upper layers. Figure 4.9 shows that the oil starts to flow back through the top layer, gradually flowing back through the lower layers during the transient period. Eventually, the lowermost layers receive most of the backflow and the three uppermost layers produce small amounts of oil. Another trend is observed in Figure 4.8 with respect to the gas. As the layers receive backflow from oil, the gas flow rate is reduced, and a new steady rate appears after the transient period. Layer 10 (the top layer) takes backflow first, and the lower layers receive backflow in descending order. Production from every layer restabilizes almost simultaneously, however, at different rates where the bottommost layers have almost zero gas production while the topmost layers actually produce more gas than prior to the transient event.

The mass rates of oil and gas are clearly dependent on each other, but the cause of the rapidly changing mass rates cannot be deduced from the mass rate data alone. Neither do the data explain the flow of gas and oil during and after liquid loading, they only show the result of what is happening. The pressure profiles generated from the simulation data provide insight into the flow behavior and are discussed below.

Figure 4.10 presents the pressure and saturation profiles of gas and oil shortly after the liquid film reversal. The first 10 m of the reservoir are plotted to visualize the changes in pressure and saturation near the well. Based on Figures 4.10a and 4.10b, it is evident that the reservoir is fully saturated with gas until 65 hrs have passed and that the initial backflow occurs in layer 10 (the upper layer). Figures 4.11, 4.12, and 4.13 show the pressure and saturation profiles during liquid loading and after production has stabilized.

Table 4.3: Case 1.1 - ROCX: Mass rates of gas through the sandface:

Mass rate of gas through the sandface, $[m_g]$			
	Pre Loading $[kg/s]$	Post Fluid Redistribution $[kg/s]$	Ratio (Post/Pre) [%]
Layer 1	0.03441	0.001157	3.34
Layer 2	0.03433	0.001417	4.12
Layer 3	0.03433	0.004669	13.6
Layer 4	0.03431	0.01290	37.6
Layer 5	0.03431	0.01983	57.8
Layer 6	0.03432	0.02525	73.6
Layer 7	0.03436	0.02945	85.7
Layer 8	0.03443	0.03293	95.6
Layer 9	0.03452	0.03529	102
Layer 10	0.03457	0.03670	106

The flow from the reservoir to the well is affected by variations in the phase pressures and saturations in the layers. Initially, the backflow begins in layer 10, as it has the greatest pressure difference from the well to the reservoir. When the liquid film is reversed, the liquid holdup increases quickly toward the lower sections of the well. Layer 10 is first affected by the increase in liquid hold and pressure. The combination of both effects causes the initial backflow to occur in that layer. Gradually continuing down in the lower layers, the pressure in the well is greater than in the reservoir layers, which encourages backflow. In this setup, only oil flows back and the main reason is that the oil phase pressure in the reservoir is much lower than the gas pressure because the saturation is zero,

Table 4.4: Case 1.1 - ROCX: Mass rates of oil through the sandface:

Mass rate of oil through the sandface, $[m_o]$		
	Pre Loading $[kg/s]$	Post Fluid Redistribution $[kg/s]$
Layer 1	0	-0.00573
Layer 2	0	-0.00541
Layer 3	0	-0.00278
Layer 4	0	-0.000861
Layer 5	0	-0.000326
Layer 6	0	-0.000134
Layer 7	0	-1.12E-05
Layer 8	0	9.84E-06
Layer 9	0	1.34E-05
Layer 10	0	1.14E-05

which makes the capillary pressure difference 1 $bara$.

As the pressure increases in the near-wellbore region of layer 10 due to an increasing amount of oil that restricts the flow of gas, the near-wellbore pressure in the layer increases higher than the pressure in the next layer (layer 9). This, in combination with an increase in wellbore pressure as the liquid holdup increases in the well, results in flow from the well and layer 10 to layer 9. Fluid redistribution occurs in the near-wellbore region due to variations in phase pressures between layers, as illustrated by the difference in Figures 4.10, 4.11, 4.12, and 4.13. The process of fluid redistribution continues down in the lower layers in a similar way until approximately 95 hrs have passed (33 hrs after the onset of liquid loading), with the oil tending to be redistributed in the lower layers due to gravity. Simultaneously, gas is displaced and forced to the upper layers. When production is stabilized, layers 9 and 10 produce gas at a higher rate than before the onset of liquid loading, although the presence of oil decreases the relative permeability of gas. And as discussed previously, the stabilized gas rate in layers 1-8 is reduced, seemingly dependent on oil saturation.

Figures 4.8 and 4.9, along with Figures 4.10, 4.11, 4.12, and 4.13, show that a higher saturation of oil near the well causes a greater reduction in gas production, partially consistent with changes in phase mobility due to changes in relative permeability, reduced capillary pressure and how the pressure differential from the well to the reservoir changes during production. After the transient period of fluid redistribution ends and production stabilizes, the mass rate of the gas has increased by 6% in layer 10, and 2% in layer 9. The mass rate of gas is reduced by 4.4% in layer 8, 14.3% in layer 7, 26.4% in layer 6, 42.2% in layer 5, 62.4% in layer 4, 86.4% in layer 3, 95.9% in layer 2, and 96.7% in layer 1. At this time, the average oil saturation in the first 0.7 m is 0.18 in layer 10, 0.19 in layer 9, 0.20 in layer 8, 0.22 in layer 7, 0.25 in layer 6, 0.29 in layer 5, 0.37 in layer 4, 0.51 in layer 3, 0.62 in layer 2, and 0.64 in layer 1. The condensate reaches a radial depth of approximately 0.95 m in layers 10-5 and gradually increases to 2.5 m in the bottom layer. The oil penetrates deeper into the reservoir production continues. However, the total gas production rate does not appear to be affected by it.

The reduction in rate caused by pressure depletion is negligible, as the reservoir has an average depletion rate of approximately 0.07 $bara/d$. The bottomhole pressure increases by approximately 0.6 $bara$ due to liquid buildup, which negatively affects production. Another contributor to the reduction in gas production is the decreased gas mobility and pressure as a function of oil saturation. After the top layers have distributed liquid to the lower layers and steady gas production is restored, the remaining oil saturation remains higher than in the initial state, indicating that all parts of the reservoir with liquid backflow are permanently affected. Oil blocks the path of the gas in the lower layers, which restricts the gas flow. And as more oil accumulates in the reservoir, the gas is displaced and migrates to the upper layers, causing a slightly increased gas mass rate in layers 9 and 10.

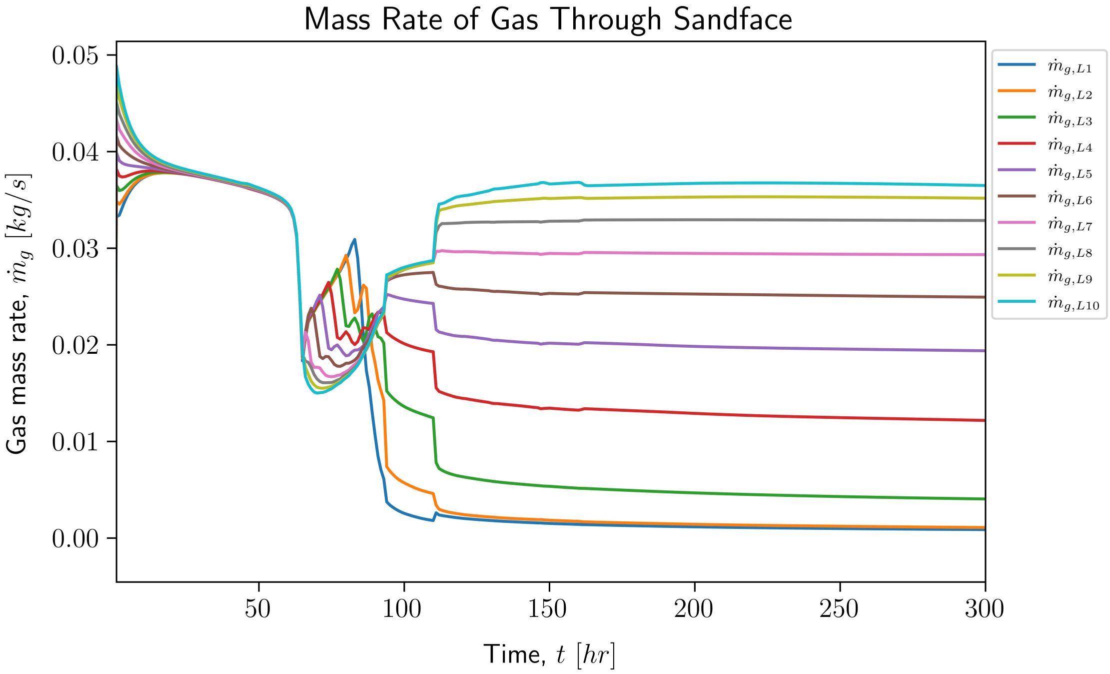

Figure 4.8: Case 1.1 - ROCX: Mass rates of gas through the sandface.

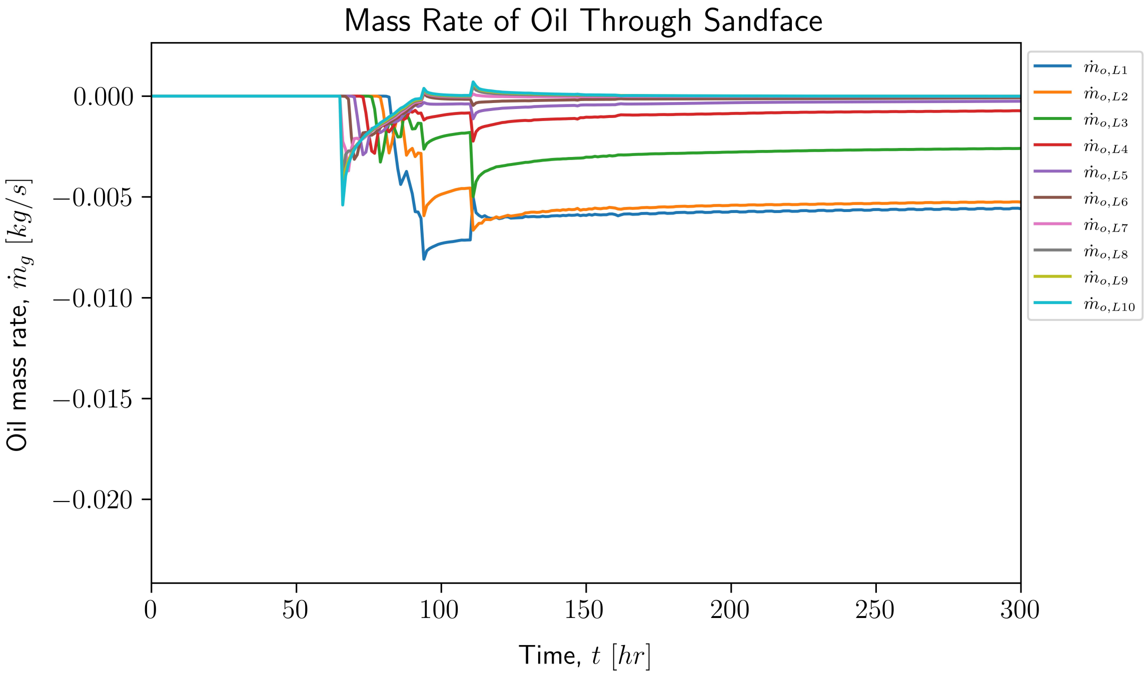

Figure 4.9: Case 1.1 - ROCX: Mass rates of oil through the sandface.

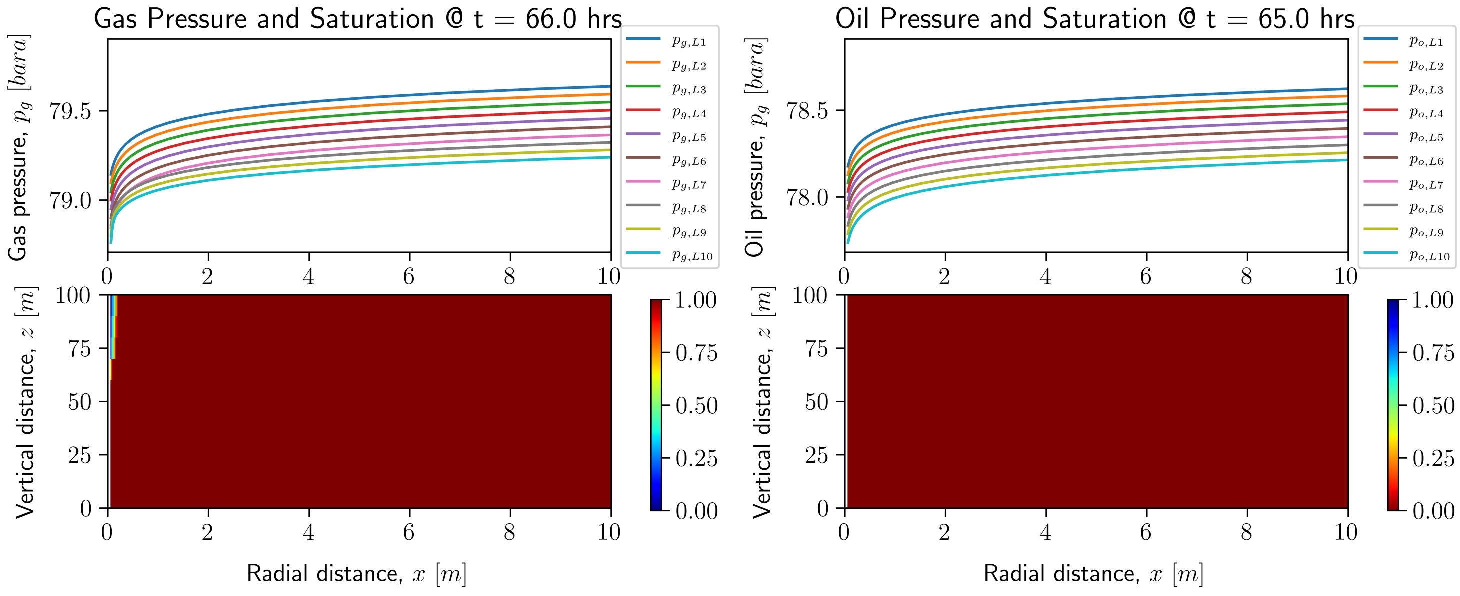

(a) Gas plot

(b) Oil plot

Figure 4.10: Case 1.1 - ROCX: Saturation and pressure plots of gas during liquid loading and oil before the onset of liquid loading.

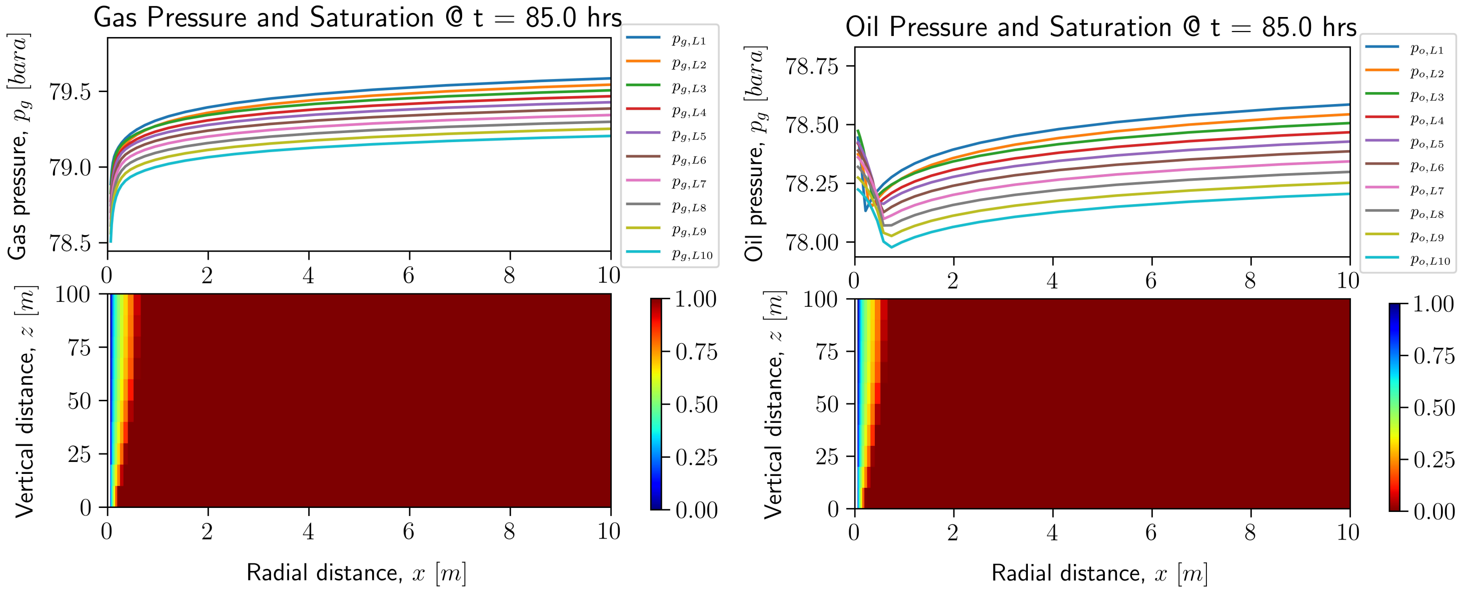

(a) Gas plot

(b) Oil plot

Figure 4.11: Case 1.1 - ROCX: Saturation and pressure plots of gas and oil in the early during liquid loading.

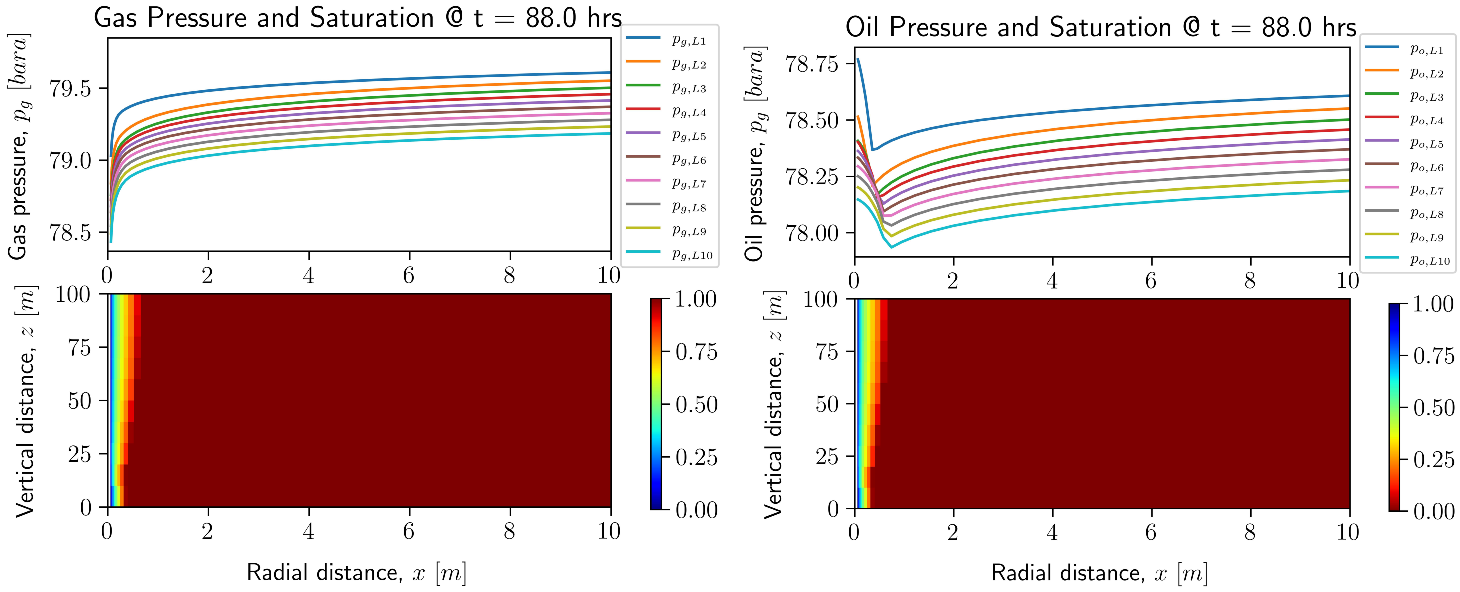

(a) Gas plot

(b) Oil plot

Figure 4.12: Case 1.1 - ROCX: Saturation and pressure plots of gas and oil before stabilization.

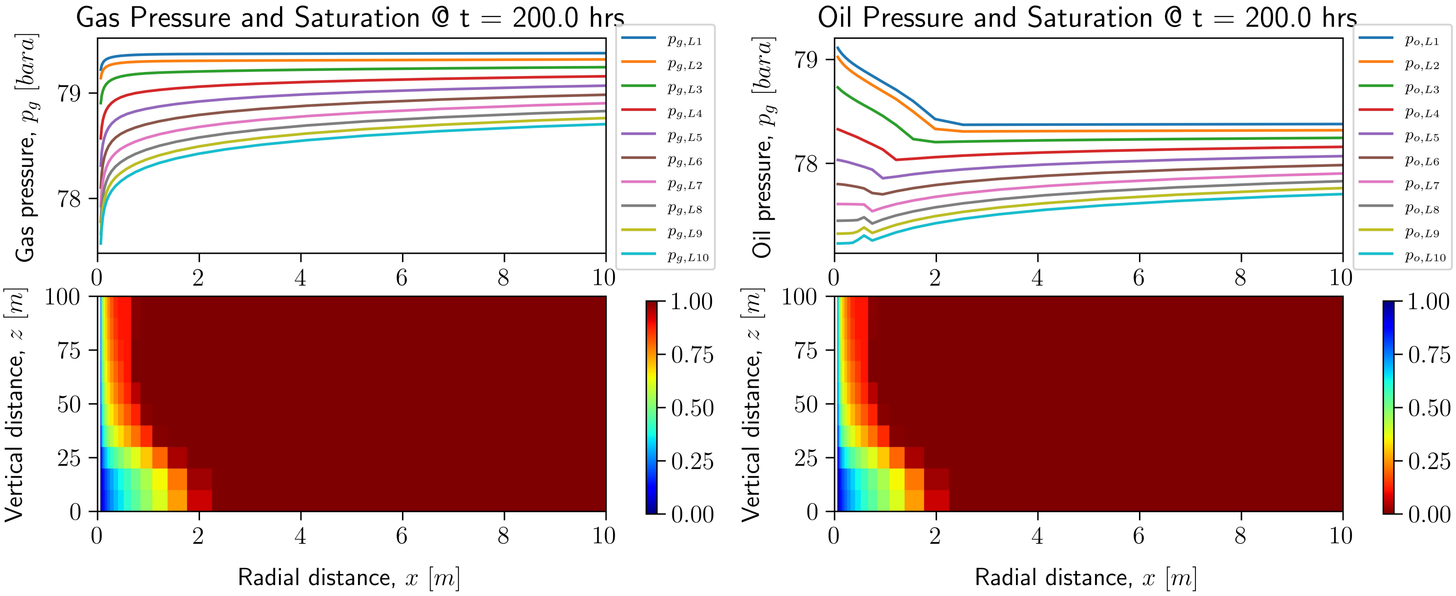

(a) Gas plot **(b)** Oil plot

Figure 4.13: Case 1.1 - ROCX: Saturation and pressure plots of gas and oil after stabilization.

4.1.3 Comparison & Summary

Case 1.1 - IPR does not give any information on where which parts of the reservoir take backflow, which layers produce, at which rate, or the fluid redistribution in the reservoir. Using ROCX, these data are provided and may be valuable for the design of completion and production strategies, especially in multilayered reservoirs. How the reservoir depletes must be explicitly defined when using the IPR. With ROCX, the depletion rate can be computed based on the reservoir properties, initial conditions, and boundary conditions. This gives ROCX an advantage over the IPR when multiple zones or layers have different properties, which causes them to deplete at different rates. The ROCX coupling is slower than the IPR, depending on the complexity of the model. In this study, ROCX used approximately 40% more time, but the simulation speed is significantly reduced after loading starts due to the transient flow. Surprisingly, both ROCX and IPR delivered similar inflow rates to OGLA during steady (and metastable) production.

The initial production rate and the stabilized rate after liquid loading are approximately 2% less in **Case 1.1 - ROCX** compared to **Case 1.1 - IPR**. This indicates that both reservoir models, ROCX and IPR, generate similar results when transient events do not occur. A small difference of 2% can have a significant impact on the overall production of the well, depending on the time it takes for the well to be decommissioned and other events during production. Another key difference between the two cases is the time it takes for the production to stabilize. In **Case 1.1 - IPR**, approximately 4 hrs pass from the onset of liquid loading to the stabilized rate. In **Case 1.1 - ROCX**, the production rate is not fully stabilized until approximately 57 hrs have passed since the liquid film reversal. This indicates that transient events related to the reservoir are not taken into account when using an IPR to represent the reservoir.

In the ROCX case, it is estimated that a 60 m section has a slug flow after liquid loading. In the IPR case, only 10 m has slug flow. This is probably attributed to the way inflow and outflow from the reservoirs are defined. The IPR defines uniform flow in the bottom 100 m, but ROCX defines different flows to and from each numerical layer.

The reversal of the velocity of the liquid film appears to be the best indication of when the liquid loading begins, similar to the observations made by Veeken *et al.* [8]. The critical droplet velocity appears to be similar to the calculated Turner velocity. However, a slip relation would make the Turner velocity more similar to the critical gas velocity computed by OLGA.

During liquid loading, the reservoir layers that are in contact with the liquid in the wellbore have a backflow of oil. The backflow rate and how the fluid is redistributed in the reservoir depend on the phase pressures that change due to depletion and saturation. ROCX accounts for these transients, but an IPR will not.

4.2 Analysis of Liquid Loading and Crossflow Dynamics in Reservoirs with Varied Zone Properties

This part of the study investigates whether crossflow can be initiated by transient events such as liquid loading and how flow is affected by adjacent reservoir zones with different reservoir properties during liquid loading. Several tests are conducted:

- Two reservoir zones with identical properties (Case 1.2a)
- High permeable reservoir zone on top of a low permeable zone (Case 1.2b):
    - Base case
    - Shut-in before liquid loading
    - Shut-in during liquid loading
    - Reduced wellhead pressure
    - Gas condensate as a fluid model instead of wet gas
    - Reduced capillary pressure
- Low permeable reservoir zone on top of a high permeable zone (Case 1.2c):
    - Base case
    - Shut-in before liquid loading
    - Shut-in during liquid loading
    - Reduced wellhead pressure
    - Gas condensate as a fluid model instead of wet gas
    - Reduced capillary pressure

4.2.1 Case 1.2a

This model is similar to **Case 1.1 - ROCX**, except for an additional numerical layer in the z-direction. The bottom and top zones consist of numerical layers 1-5 and 7-11, respectively. Numerical layer 6 has a permeability of 0 md and the other layers have a permeability of 10 md. This setup is designed to be comparable to **Cases 1.2b** and **1.2c**, where the upper and lower reservoir zones have different permeabilities.

This case is not expected to have any crossflow between the upper and lower zones since they should deplete at similar rates. When the well starts to accumulate liquid, the flow and fluid redistribution should be similar to **Case 1.1 - ROCX**, except for the discontinuity of layer 6.

The reservoir is the domain of interest. Therefore, the wellbore domain results are not discussed in detail here, but are included in Appendix A.4.2 unless significant differences or new findings are observed.

Base case

Table 4.5 shows the cumulative mass production of gas and oil through the sandface of the top and bottom zones of the reservoir before the onset of liquid loading, during fluid redistribution, and from the production stabilizes until 200 hrs have passed. Figures 4.14 and 4.14 show how mass rates change over time. The gas mass rate plot shows that the top layer contributes more to total production than the bottom layer prior to liquid loading, with a cumulative production of 49,510 kg compared to 40,517 kg in the bottom zone. The backflow of oil and fluid redistribution in the near-wellbore region changes the flow dynamics of both phases for approximately 40 hrs. During this period, 30,529 kg of gas have been produced and the top layer accounts for 54% of it. Cumulative oil production is -1,820 kg, where 44% of the backflow flows through the top layer. The lower zone is more affected by the accumulation of liquids in the well after the transient event. The cumulative production of gas from stabilization until 200 hrs have passed is 67,314 kg, where the top layer accounts for 66% of it. The production of oil sums up to -4,571 kg, where 6.3% of the backflow goes through the top zone.

Figures 4.16, 4.17, 4.18, and 4.19 provide a time series of the saturation and pressure profiles of gas and oil. Prior to liquid loading, the pressure profile of both phases is conventional, which means that backflow does not occur. Although the oil saturation at this point is zero, the pressure profiles are still defined for numerical reasons in ROCX. At this point in time, the reservoir depletes almost uniformly, as seen by the pressure profile curves being almost identical except for the pressure difference caused by gravity. 2.5 hrs after the liquid film reversal, the oil begins to flow back through layer 11 (top of the top zone). Within the next half hour, the backflow has progressively reached numeric layer 7 (bottom of the top zone). The bottom 5 numerical layers exhibit backflow in a similar order as the liquid holdup increases toward the bottom. The gas pressure profile in the lower layers becomes more linear over time, which means that the pressure in the bottom of the well and the reservoir gas pressure approach similar values. This results in reduced gas rates. On the contrary, the difference between the oil pressure profiles in the lower layers increase. This indicates that as time progresses, more liquid flows back through the lower layers. The pressure profiles of gas in the top zone remain conventional throughout the simulation; however, they are affected by depletion and changes in saturation. The oil pressure profiles in the top zone remain U-shaped; however, the characteristic shape becomes less distinct as time progresses, since the saturation reaches an equilibrium with the flowing conditions.

Since both reservoir zones are identical, except for the relative placement in the z-direction, they are expected to deplete similarly. This remains true until liquid loading is initiated. The main reason that the top zone initially accumulates liquid is that liquid is first introduced to this layer through the well. During the first hours, the top zone is able to accumulate large volumes of condensate. The backflow rate through the top zone decreases as the liquid holdup increases further down the well. The bottom zone gradually overtakes most of the backflow, and the flow stabilizes, as explained above. However, even with the difference in reservoir performance caused by liquid loading, there is no indication of crossflow between the upper and lower zone.

Fluid redistribution within each zone is shown by the time series of the saturation and pressure profile. Redistribution only lasts for a short period of time. The difference in pressure between the numerical layers in each zone and the drawdown drives the flow between the numerical layers and the backflow through the sandface. For example, as seen in Figure 4.17, the oil pressure in layer 11 ($p_{o,L11}$) is higher than the pressure in the neighboring layer, which drives the migration of the liquid from layer 11 to layer 10. Eventually, as seen in Figure 4.19, a state of equilibrium is reached for saturation. This is seen by a similar curvature on the pressure profiles, and the saturation plots also show almost identical saturations from one timestep to another. The bottom zone clearly does not reach such an equilibrium state as in the top layer, probably because the liquid accumulates at the bottom of the well.

Table 4.5: Case 1.2a: Cumulative production of gas and oil before the onset of liquid loading, during fluid redistribution, and after production restabilizes.

Cumulative production of gas and oil					
	Time interval $[hours]$	m_g $[kg]$ Top layer	m_g $[kg]$ Bottom layer	m_o $[kg]$ Top layer	m_o $[kg]$ Bottom layer
Before liquid loading	0, 67	49,510	40,517	0	0
During fluid redistribution	68, 108	16,503	14,026	-794	-1,026
After stabilization	108, 200	44,315	22,999	286	-4,285

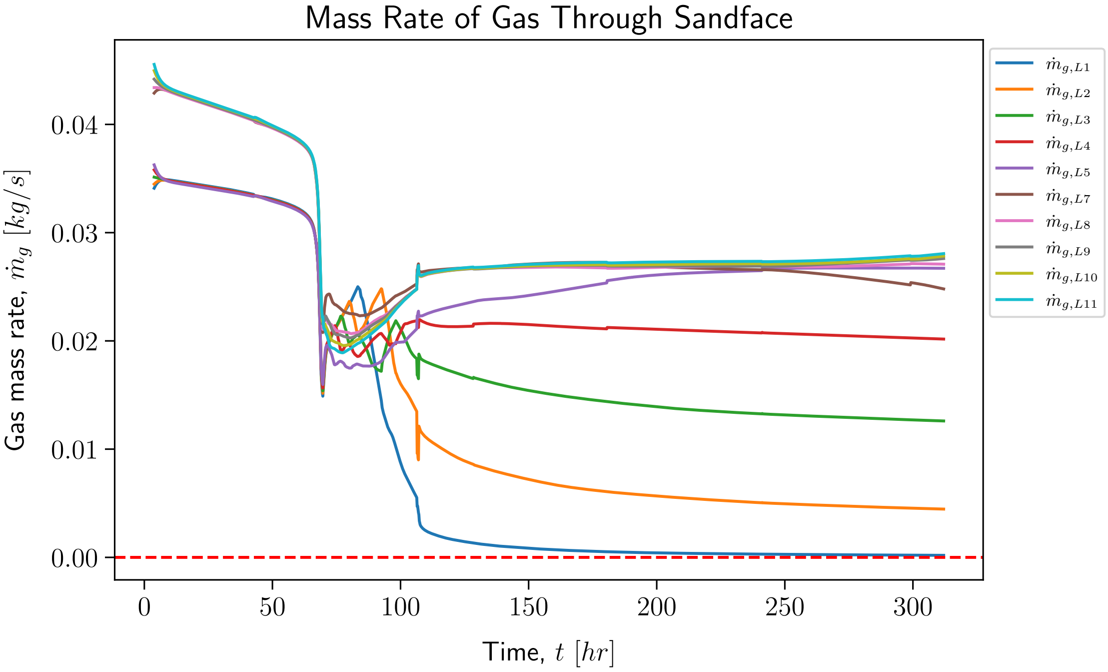

Figure 4.14: Case 1.2a: Mass rates of gas through the sandface of each reservoir layer.

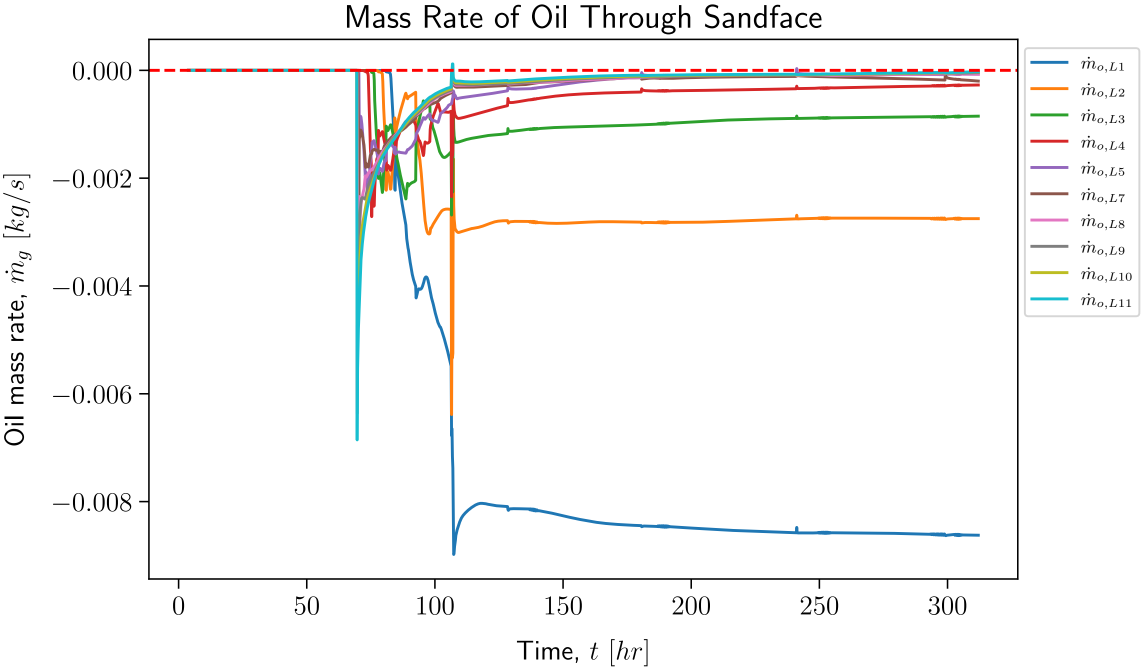

Figure 4.15: Case 1.2a: Mass rates of oil through the sandface of each reservoir zone layer.

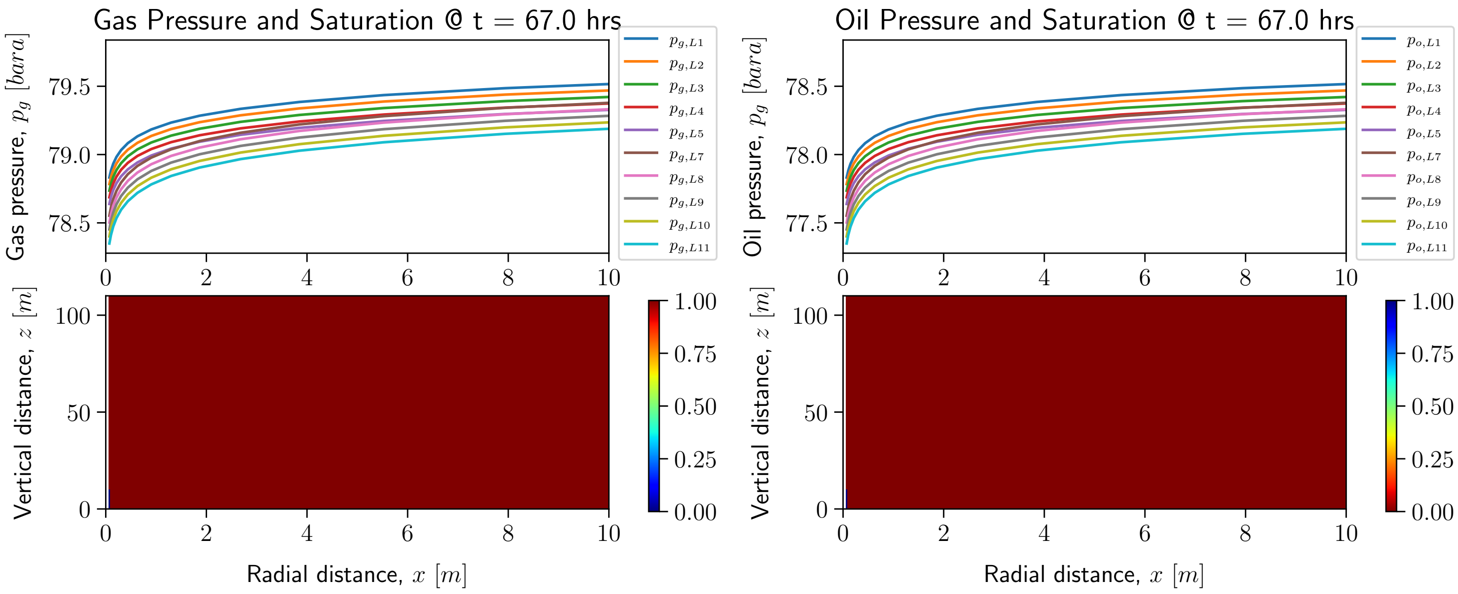

(a) Gas plot

(b) Oil plot

Figure 4.16: Case 1.2a: Saturation and pressure plots of gas and oil before the onset of liquid loading.

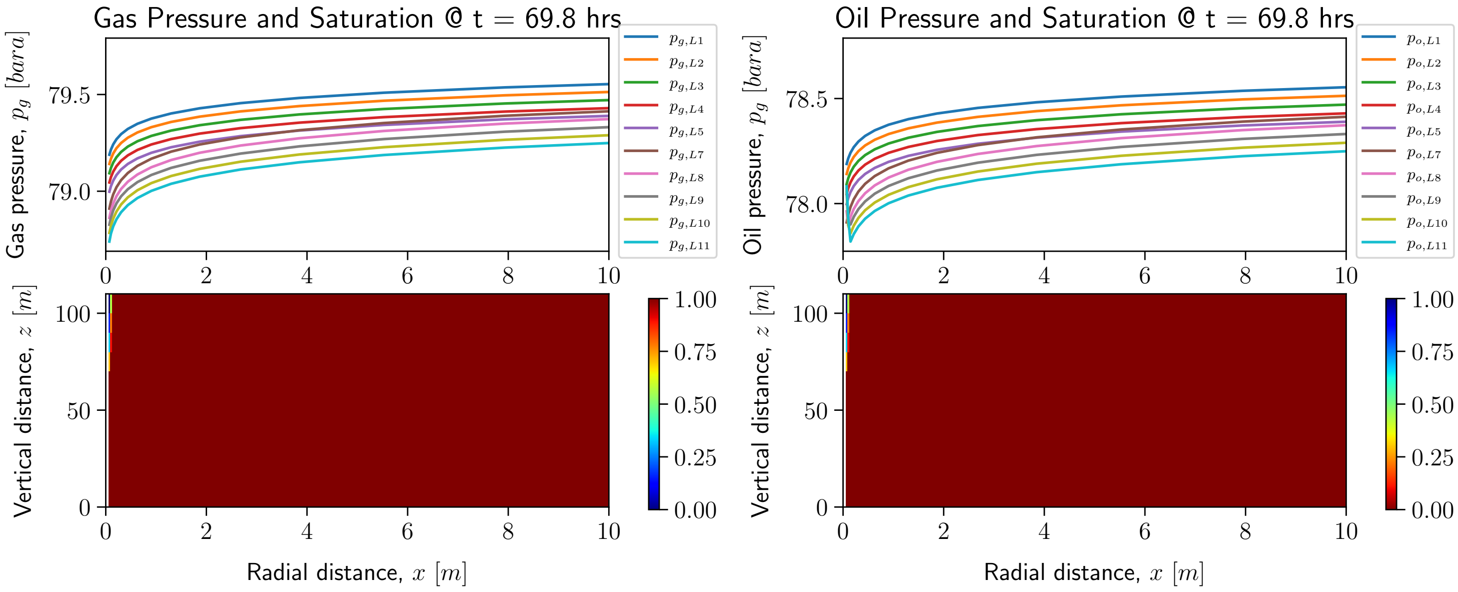

(a) Gas plot

(b) Oil plot

Figure 4.17: Case 1.2a: Saturation and pressure plots of gas and oil after initial backflow.

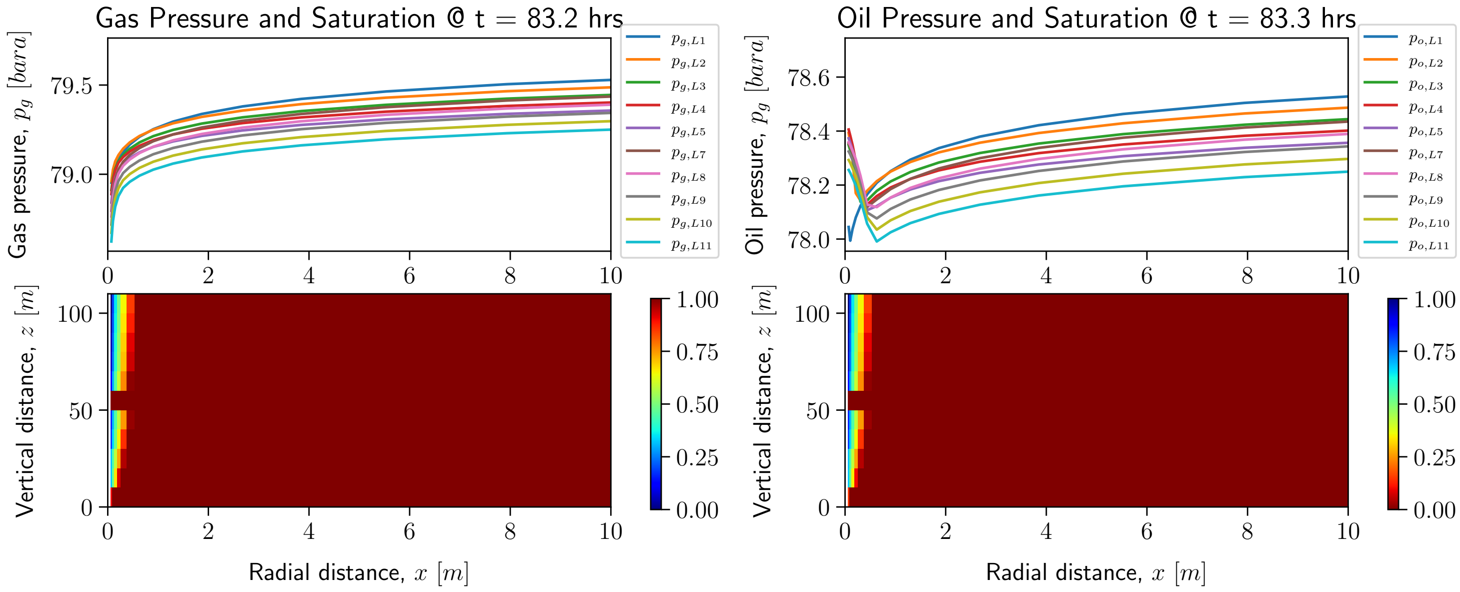

(a) Gas plot **(b)** Oil plot

Figure 4.18: Case 1.2a: Saturation and pressure plots of gas and oil before stabilization.

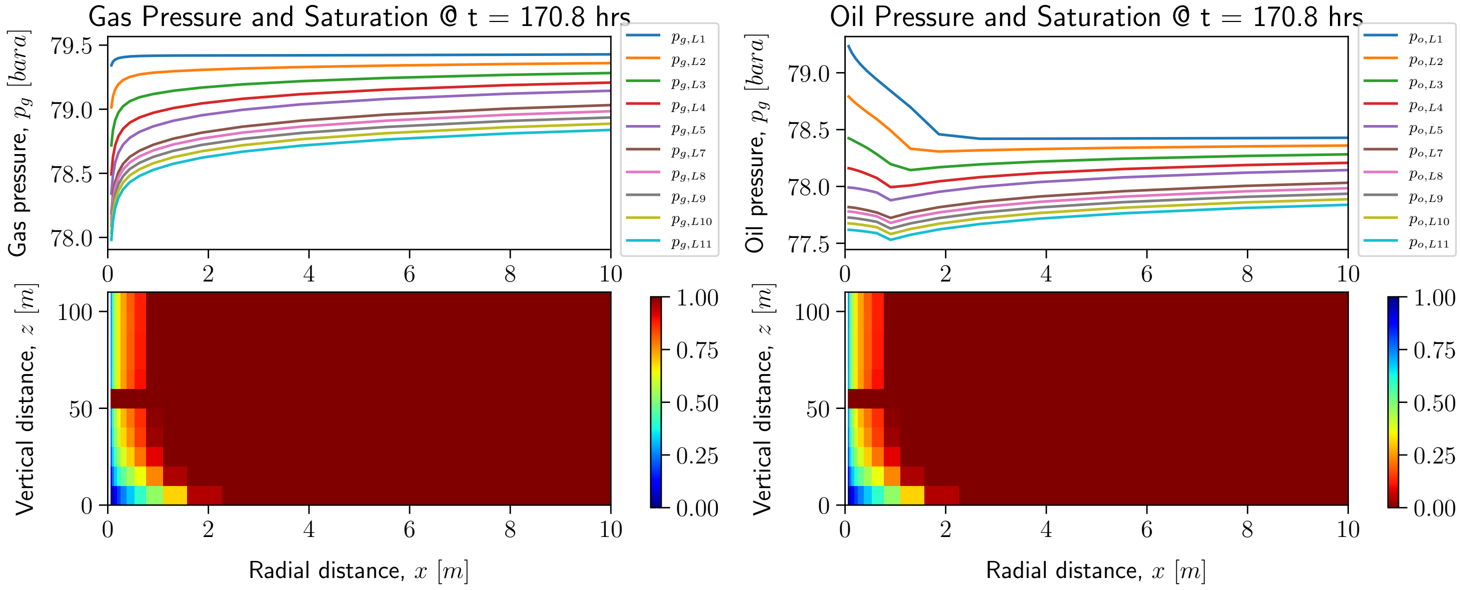

(a) Gas plot **(b)** Oil plot

Figure 4.19: Case 1.2a: Saturation and pressure plots of gas and oil after stabilization

4.2.2 Case 1.2b

The two-layer model used in this study shares the same fluid properties and wellbore characteristics (including wellhead pressure, thermal properties, discretization, and initial conditions) as the model in **Case 1.2a**. The reservoir properties are also comparable between the two cases. The notable difference is that the permeability in the top zone (numerical layers 7-11) increases to 100 md. The bottom zone (layers 1-5) has a permeability of 10 md and layer 6 has a permeability of 0 md, similar to the previous case. This design allows for evaluating the impact of non-communicating zones on reservoir performance during liquid loading, specifically how the increased permeability and pressure depletion in layers 7 to 11 affect the reservoir's susceptibility to liquid accumulation and potential crossflow between the zones.

Based on inflow performance relationships, payzone thickness nand permeability normally exhibit a linear correlation with production. Consequently, the surface gas production rate is expected to be higher in this case compared to **Case 1.2a**. Although the wellbore and fluid properties remain unchanged, the initiation time for liquid loading is expected to be later than that in the previous case since one of the reservoir zones is more productive. The factors that influence liquid loading are complex and may be impacted by changes in permeability and pressure depletion in the reservoir layers.

Base case

The production starts with rates greater than 50,000 Sm^3/d for gas and 2.5 Sm^3/d for oil, maintaining a steady oil-to-gas ratio, as seen in Figure 4.20. The onset of liquid loading is around 33,000 Sm^3/d, slightly lower than in previous cases. In the initial 150 hrs, rates decrease with reservoir depletion until liquid loading is initiated, leading to a metastable gas production rate of around 11,700 Sm^3/d and a negligible oil rate.

The critical rates and corresponding bottomhole pressures are determined by various methods, all of which provide similar results to the previous cases due to analogous flow conditions and identical fluid properties. The liquid film reversal reverses at a surface gas rate of approximately 33,000 Sm^3/d.

Slug flow and droplet reversal begin approximately 2 hrs after the onset of liquid loading at a rate of 16,489 Sm^3/d. The maximum length of the slug flow regime is reached quickly, as seen in Figure 4.56. The calculated Turner critical rate is 23,668 Sm^3/d. Liquid droplets deposited at the tubing wall are transported back down the tubing and into the reservoir, initiating slug flow around the same time as droplet reversal.

Stable surface production rates occur about 15 hrs after the onset of liquid loading, probably facilitated by the high permeability in the top zone. Slug flow appears above the top zone, which significantly affects the sandface mass rates of oil and gas.

The reservoir is initially filled with gas and kept at a constant temperature of

Table 4.6: Case 1.2b: Cumulative production of gas and oil before the onset of liquid loading and the following 349 hrs.

Cumulative production of gas and oil					
	Time interval $[hours]$	m_g $[kg]$ Top zone	m_g $[kg]$ Bottom zone	m_o $[kg]$ Top zone	m_o $[kg]$ Bottom zone
Before liquid loading	0, 151	173,828	52,434	0	0
After liquid loading	152, 500	54,987	102,058	-33,976	0

110^oC to prevent gas condensation. Any changes in gas or oil saturation in the reservoir are attributed to liquid that forms in the wellbore and flows through the sandface into the reservoir. Table 4.6 shows the cumulative production of gas and oil in the top and bottom zone before and after liquid loading. Clearly, after liquid loading begins, the well becomes less productive, and the top zone is the most affected by the phenomenon.

Figure 4.22 shows the gas mass rates through the sandface of every numerical layer in the top and bottom zone. Similar to previous cases, all layers of the same permeability produce at similar rates prior to the reversal of the liquid film, which initiates liquid loading in the wellbore. Figure 4.23 shows the oil mass rates through the sandface of every numerical layer in the top and bottom zone. Before the liquid loading, there is zero flow of oil since oil condenses further up the conduit and is transported to the surface. Numerical layer 11 has an oil backflow after 153.6 hrs, about 2 hrs after the liquid film reversal. Unlike previous cases, almost all liquid flows back to the reservoir through layer 11, a negligible amount through layer 10, and zero flow through the other layers.

The mass rates through the sandface of gas and oil and liquid holdup in the well before liquid loading are presented in Figure 4.25. The holdup is zero since the gas condenses further up in the well, and all of it is transported to the surface while the gas rate is greater than the critical rate. The mass rate of oil through every numerical layer is zero since the reservoir only contains gas. The top zone (layers 6-11) produces similar mass rates that vary between 0.047 and 0.052 kg/s. The bottom zone produces at rates varying between 0.028 and 0.027 kg/s. This shows that the high permeable zone produces gas more efficiently than the bottom zone, and therefore depletes faster, before liquid loading, as seen in Figure 4.24.

The top zone is greatly affected by the liquid loading, as seen by looking at the mass rates and liquid holdup in Figure 4.26. Oil flows from the well to layer 11 at a rate of 0.027 kg/s. A small amount of gas also flows back into the reservoir through layer 11. Layers 7-10 are barely producing gas at rates varying between 0.001 and 0.003 kg/s. The liquid holdup shows that oil is not in contact with layers 1-10, which is contrary to the anticipated results. Two explanations can be used to explain the holdup at this snapshot in time; the liquid is still moving down the well, and the snapshot is taken before it reaches further down, or the top zone is able to accumulate all of the oil and gas rate from below is sufficient to keep oil in suspension. Looking at the saturations and pressures in Figure 4.27a, the gas pressure profiles in the bottom zone remain conventional and the profiles in the top zone flatten out. This also indicates that the top zone barely produces gas and that the bottom zone is still productive. The oil pressure profiles in the top zone indicate backflow through layer 11 (and 10, but very little), which is consistent with the mass rates discussed above. The pressure profiles in the bottom zone remain conventional even though there is no contact with oil, and the reason is that each phase is defined in the system (related through capillary pressure) even though the saturation is zero.

During liquid loading, gas production through the top zone increases while it decreases in the bottom zone, as seen in Figure 4.28. Layer 11 has an oil backflow. It also produces gas but at a limited rate compared to the rest of the zone. It appears that the liquid holdup remains zero below layer 10, similar to the observation in the previous snapshot. This indicates that most of the gas that condenses in the wellbore flows back into the reservoir through layers 11 and 10 (small amount) and some is kept in suspension. Pressure and saturation profiles are shown in Figure 4.29. Gas pressure profiles are conventional for both zones. The oil pressure profiles show the greatest pressure differential in layer 11, which explains the backflow of oil. The pressure profile in layer 10 indicates a small pressure difference between the well and the near-wellbore region, but the main contributor to the oil saturation in layer 10 is the pressure difference between layers 11 and 10.

Crossflow between the two reservoir zones is not evident in this case, although the depletion rates are different. The upper zone depletes faster because of increased permeability. Therefore, if crossflow is to occur, it will be from the bottom zone to the top zone. Looking at Figure 4.23, there is no oil flow from the reservoir to the wellbore, only an inflow through the upper layer of the top zone. The backflow of oil is not considered crossflow, as condensation occurs further up the tubing and there is no inflow of oil to the well. Figure A.13 (in the Appendix) shows the gas mass rates from each numerical reservoir layer, but zoomed in around the loading point. The up-and-down spiking mass rates are from the same reservoir zone, which means that the backflow is attributed to the pressure changes in the wellbore as loading is initiated, and not to crossflow from the bottom zone. The positive and negative spikes approximately cancel out the total mass rate, although slightly positive. The bottom zone is barely affected by the liquid loading, as it is only affected by a slightly increased backpressure.

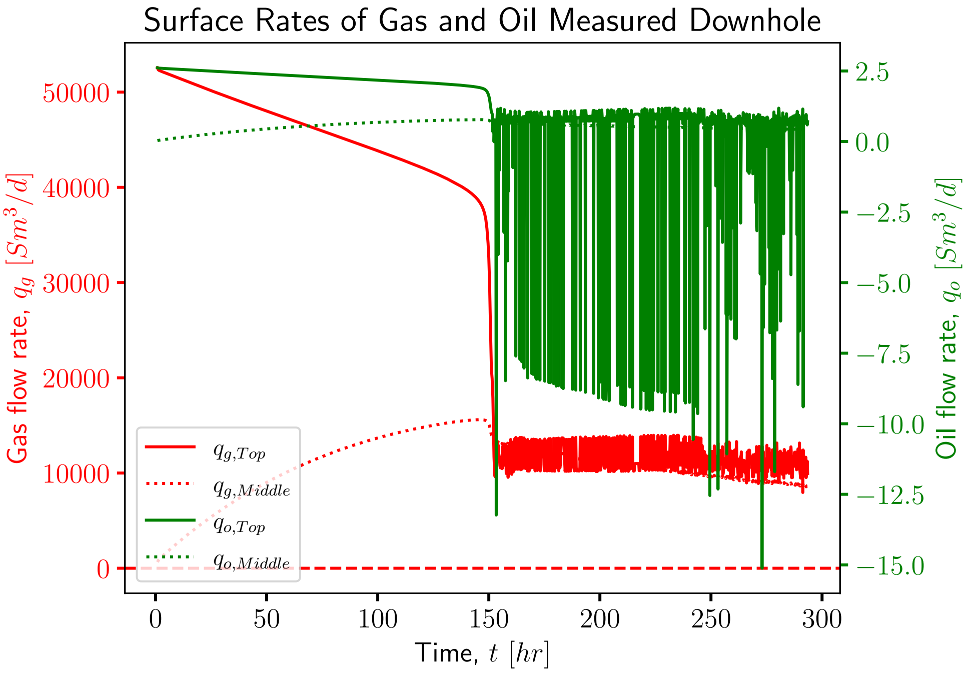

Figure 4.20: Case 1.2b: Surface rates of oil and gas.

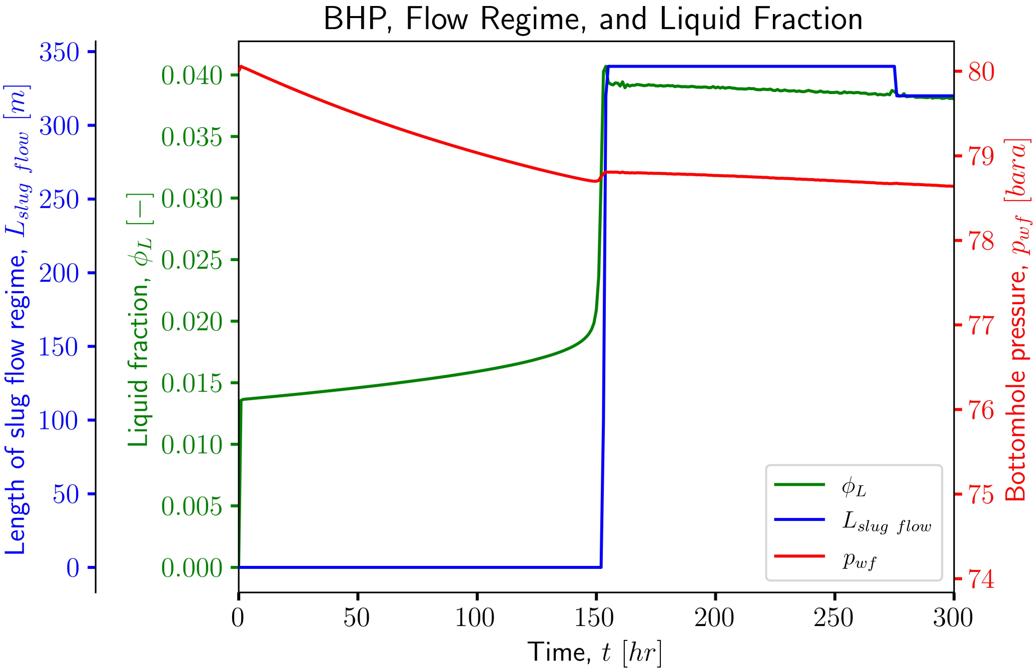

Figure 4.21: Case 1.2b: Liquid fraction, bottomhole pressure, and length of slug flow regime.

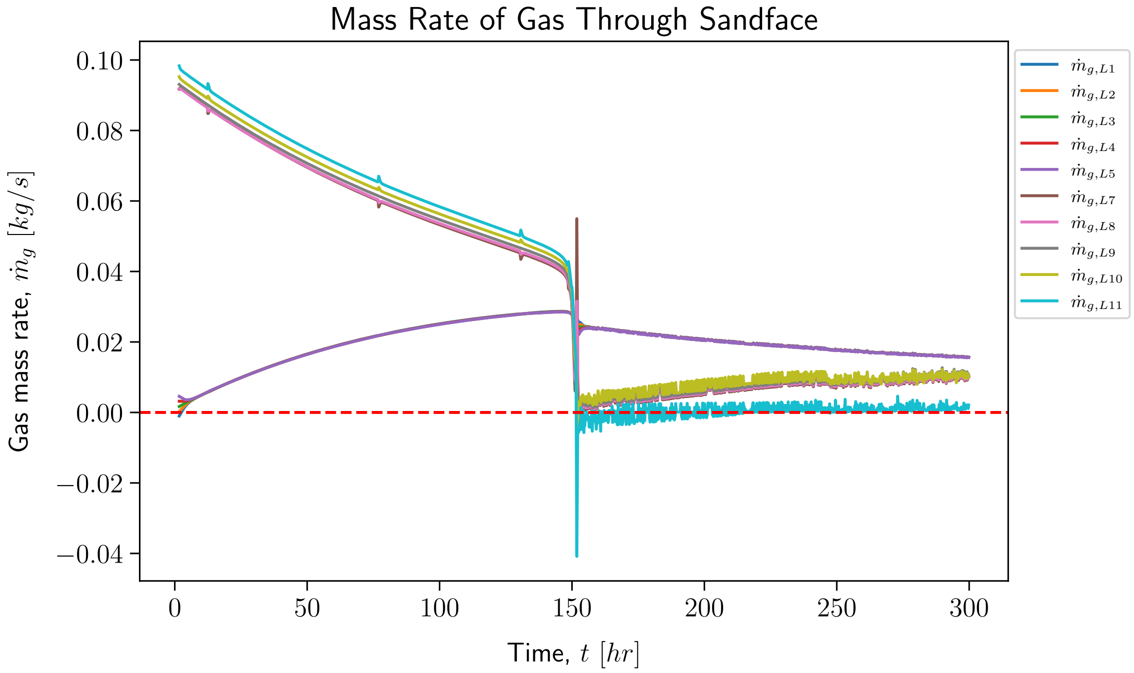

Figure 4.22: Case 1.2b: Mass rates of gas through each numerical layer of the sandface.

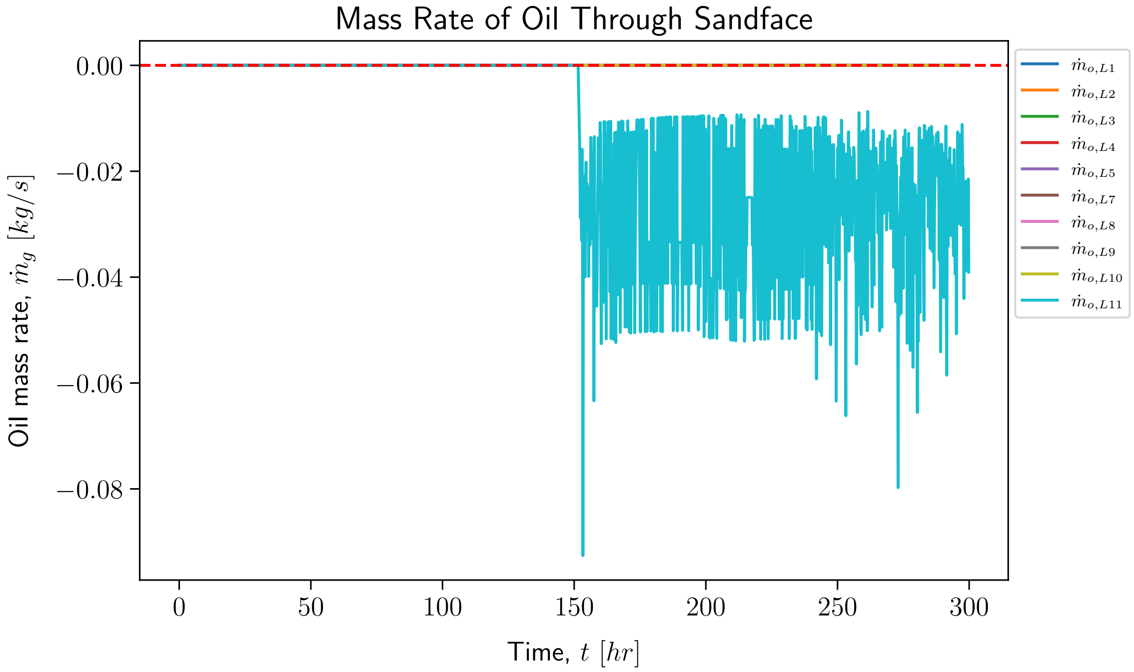

Figure 4.23: Case 1.2b: Mass rates of oil through each numerical layer of the sandface.

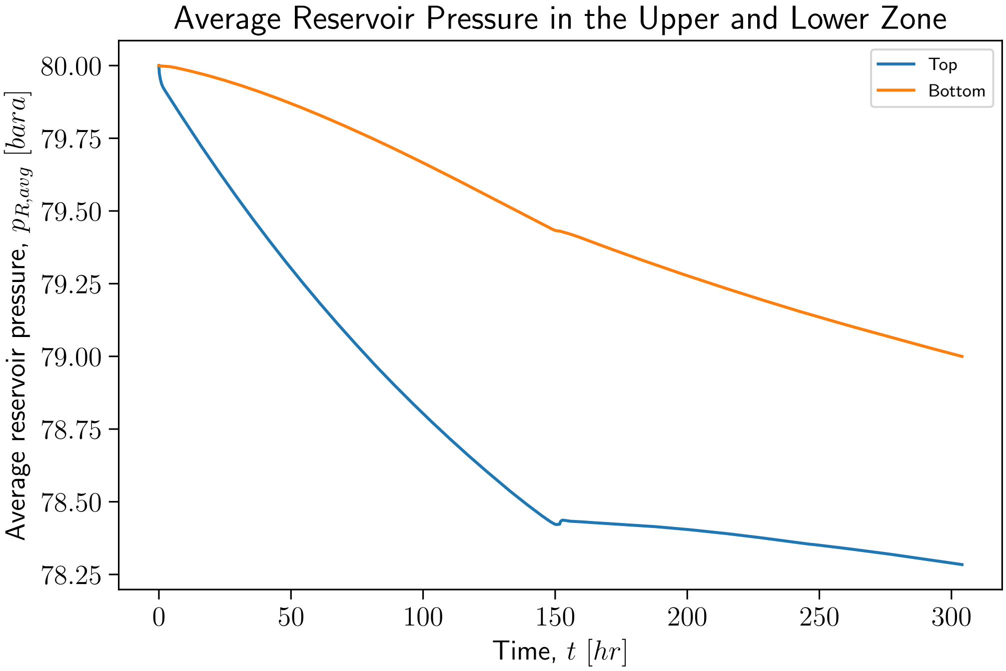

Figure 4.24: Case 1.2b: Average reservoir pressure in the top and bottom zone.

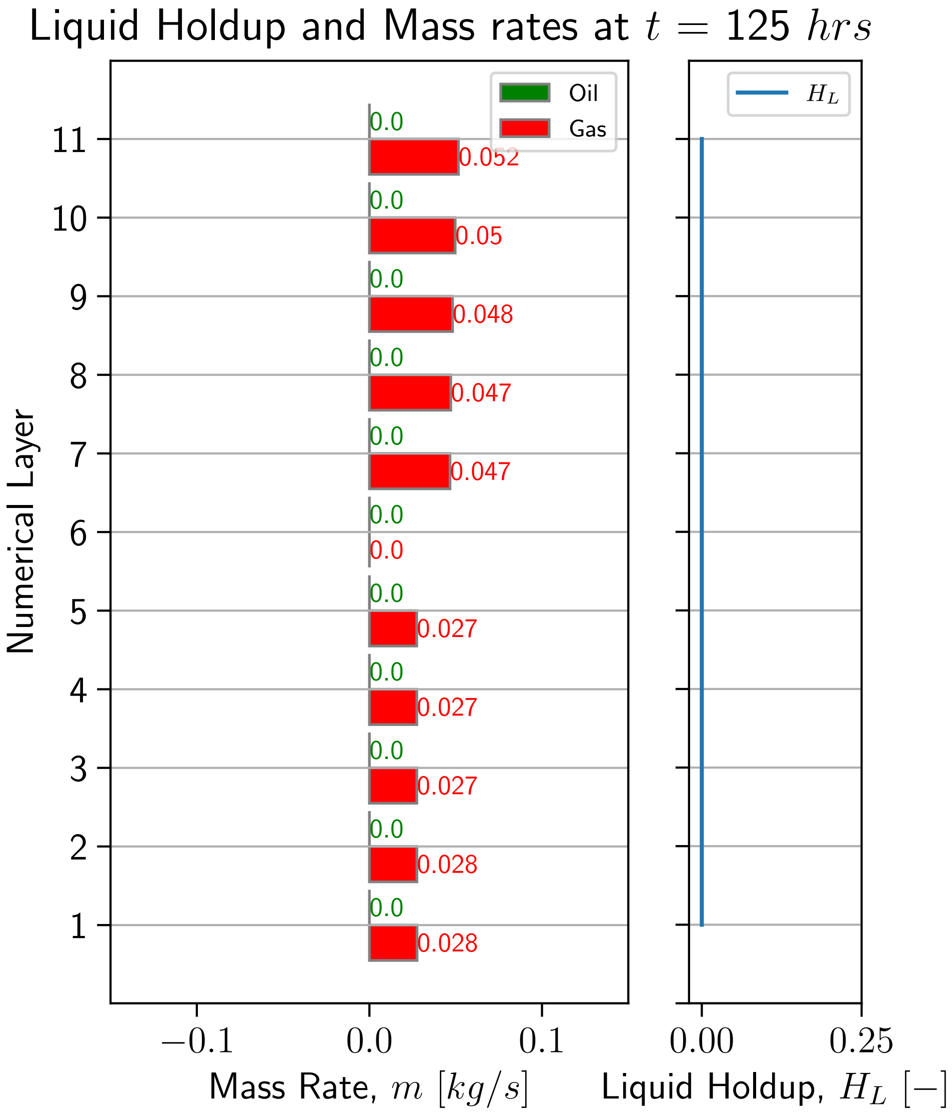

Figure 4.25: Case 1.2b: Snapshot of mass rates of oil and gas, and liquid holdup before liquid loading.

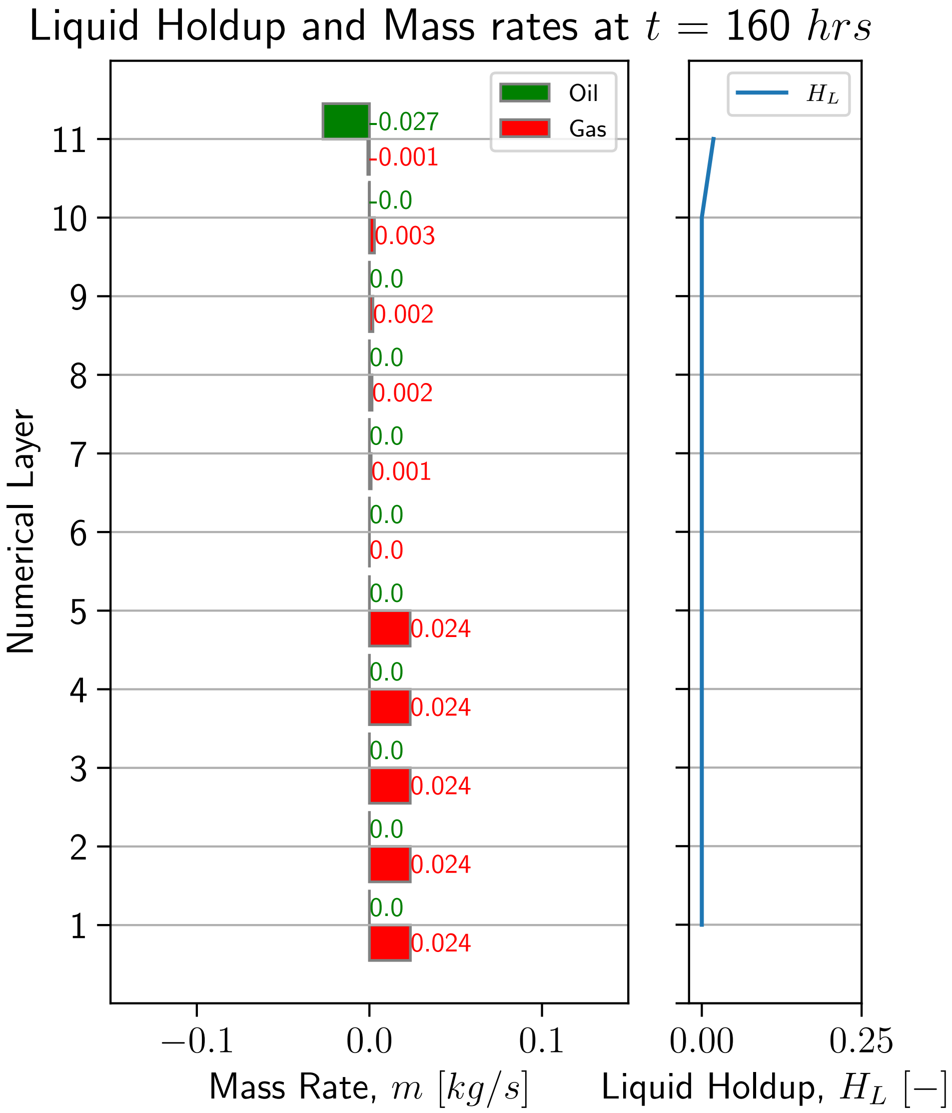

Figure 4.26: Case 2.2b: Snapshot of mass rates of oil and gas, and liquid holdup early during liquid loading.

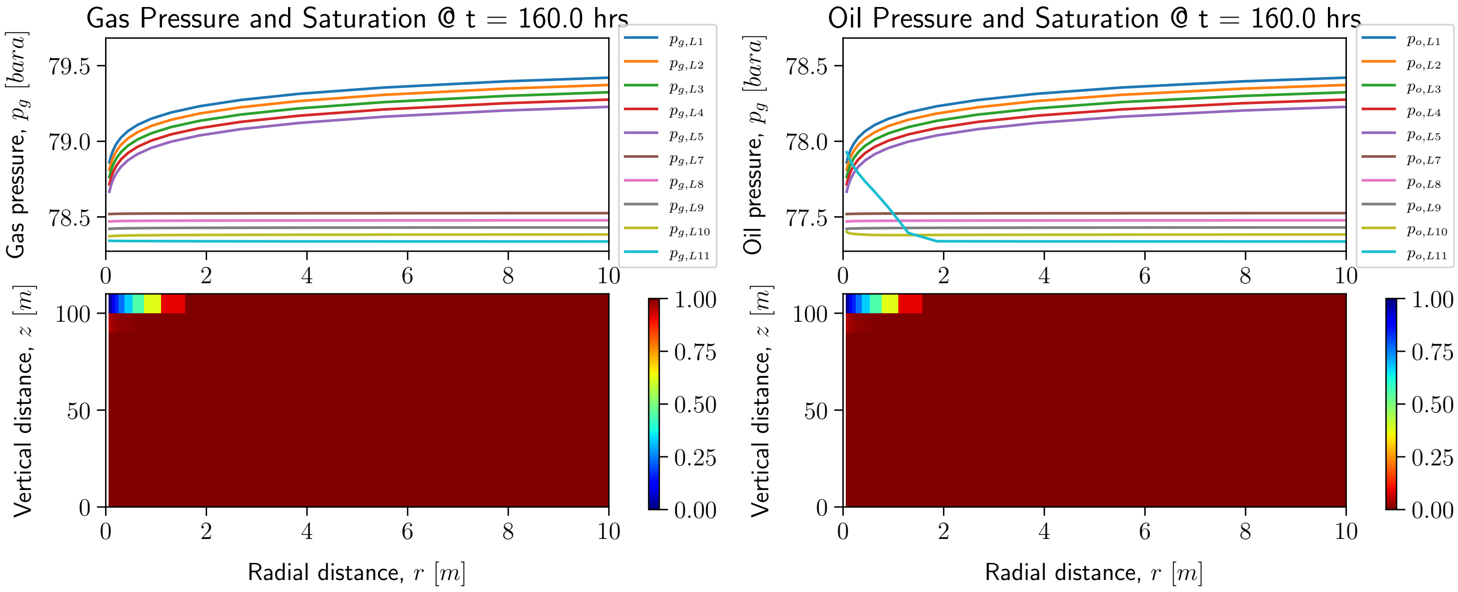

(a) Gas plot

(b) Oil plot

Figure 4.27: Case 1.2b: Saturation and pressure plots of gas and oil after stabilization.

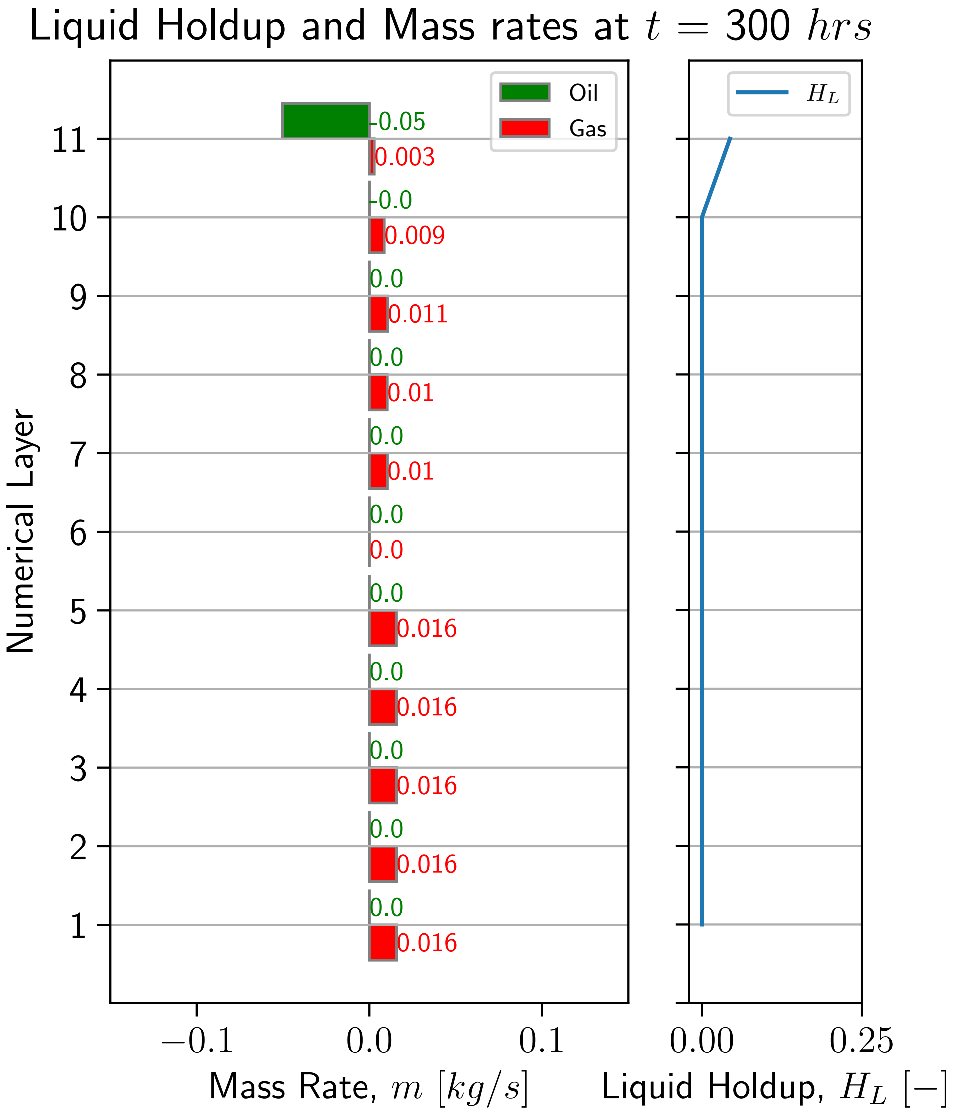

Figure 4.28: Case 1.2b: Snapshot of mass rates of oil and gas, and liquid holdup late during liquid loading.

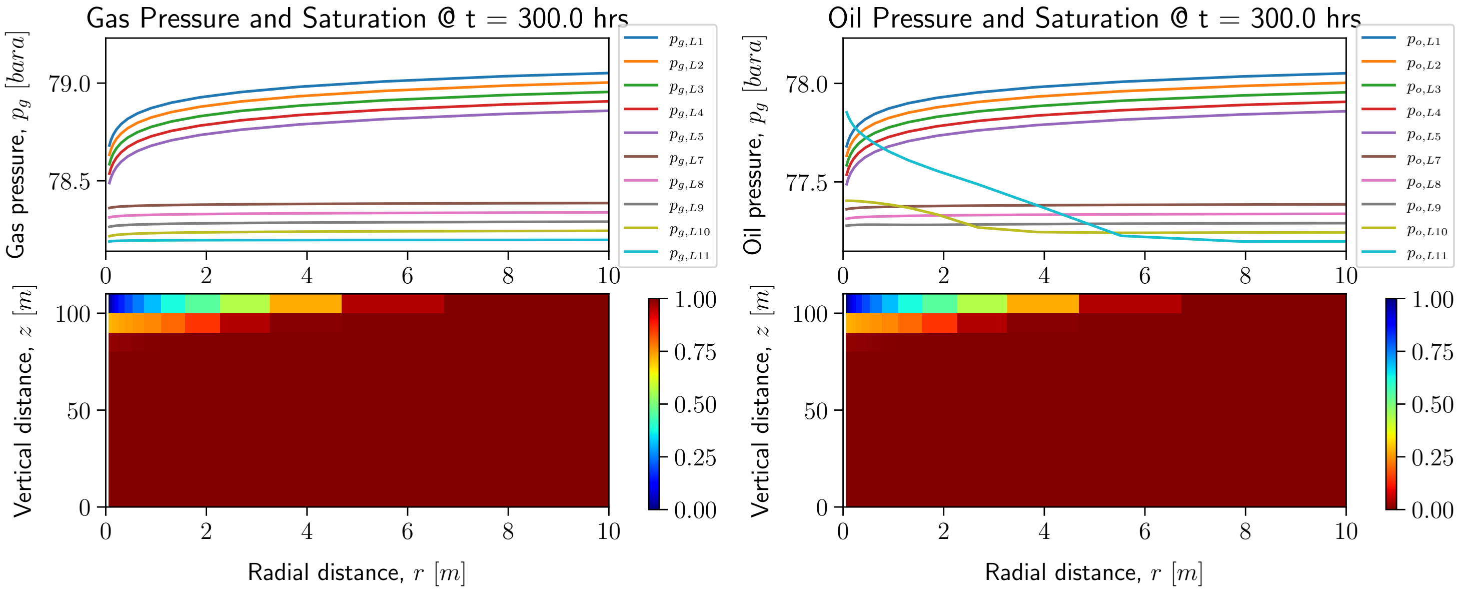

(a) Gas plot

(b) Oil plot

Figure 4.29: Case 1.2b: Saturation and pressure plots of gas and oil late in production

Shut-In Before Loading

The well is closed after 120 hrs using a valve located at the wellhead. Pressure propagates quickly down the well and changes the fluid dynamics in the system. The average pressures at the shut-in in the upper and lower zones are 78.68 and 79.58 $bara$, respectively. During shut-in, the pressure difference causes a gas crossflow from the lower zone to the upper zone, as seen in Figure 4.30 by the total mass rates being almost symmetric around $\dot{m}_g = 0$. Crossflow of oil is not evident. Figure 4.31 shows an initial backflow of oil when the well is shut in; however, the backflow is due to the sudden increase in pressure as the well closes. As the gas flows from the bottom to the top zone, the average reservoir pressure in each respective zone approaches an equilibrium where the difference in pressure is the difference in hydrostatic pressure, as seen in Figure 4.32.

After opening the well, gas production from the top layer is increased, as pressure has been regained from the bottom zone.

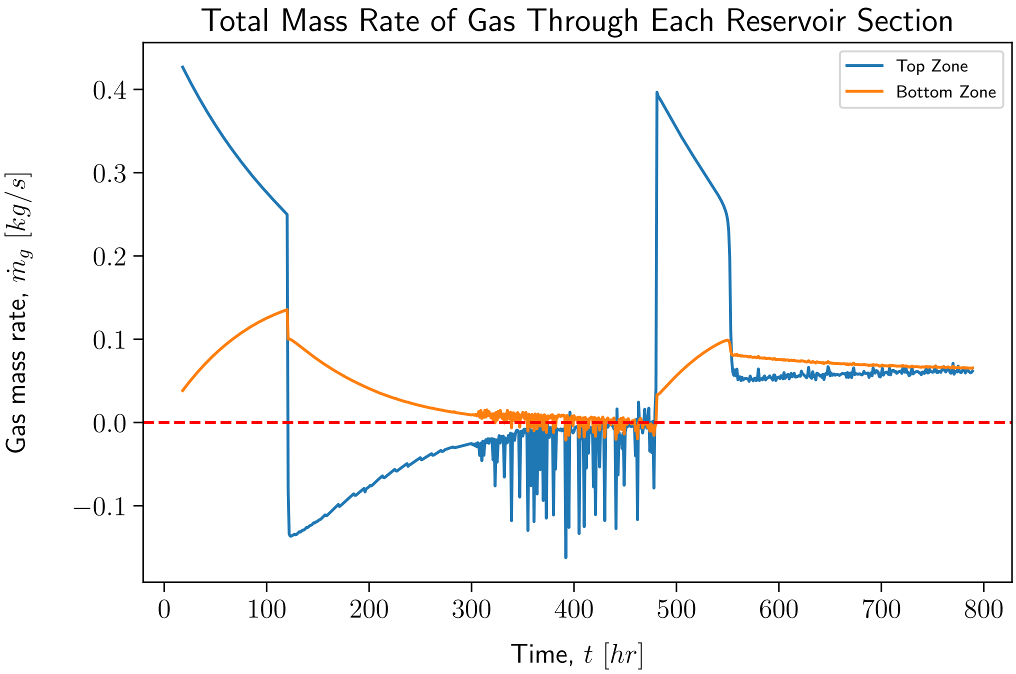

Figure 4.30: Case 1.2b Shut-In 1: Total mass rate of gas through the upper and lower reservoir zones during shut-in before liquid loading.

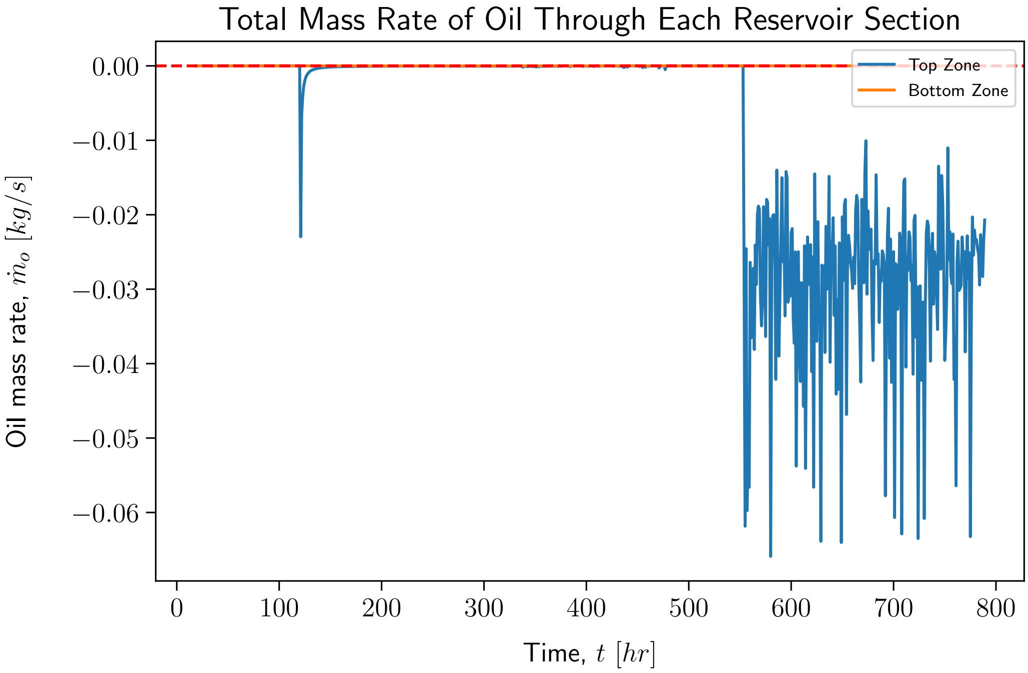

Figure 4.31: Case 1.2b Shut-In 1: Total mass rate of oil through the upper and lower reservoir zones during shut-in before liquid loading.

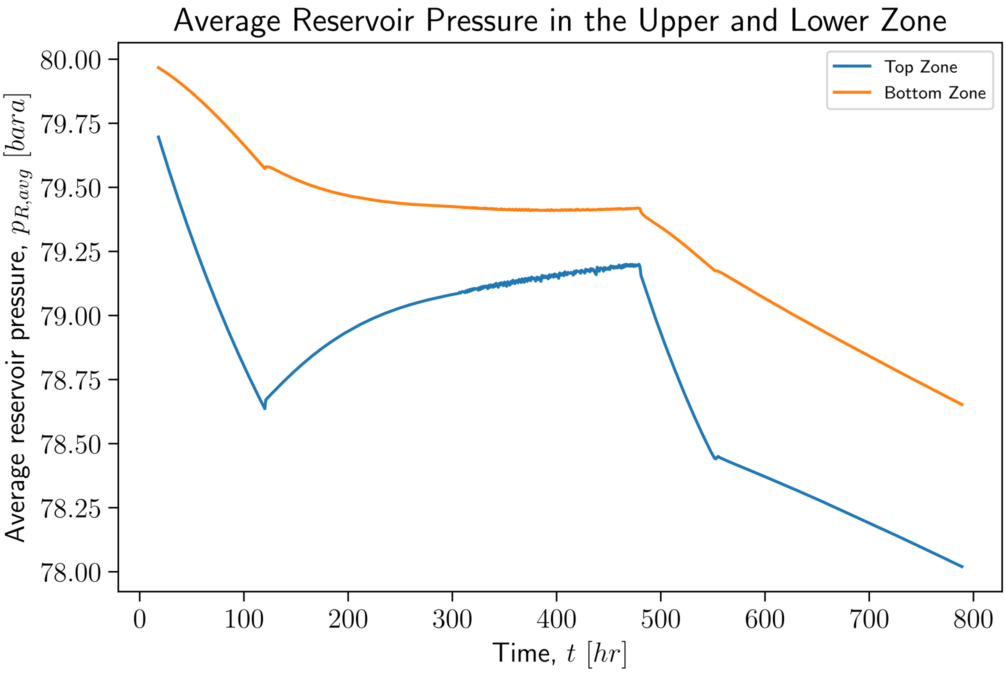

Figure 4.32: Case 1.2b Shut-In 1: Average reservoir pressure in the top and bottom zones.

Shut-In During Liquid Loading

When the well is shut in a while after the liquids have started to accumulate (288 hrs after the simulation is started), the bottom zone continues to produce gas while the top zone has a backflow of gas and condensate. The cumulative backflow of gas through the top zone is 60,111 kg. Through the bottom zone, only 7,050 kg of gas is produced during shut-in. The mass of gas in the wellbore is not the remaining 53,000 kg to make the math go up; however, looking at Figure 4.33, the bottom zone initially produces gas and then gradually starts to have backflow as well. In the same period, 147 kg of oil flows back through the top zone (through layer 11), and the bottom zone is not in contact with the oil, as seen in Figure 4.34. It should also be noted that when the well is shut in and the condensate falls down the well, some of it vaporizes into gas. This contributes to the asymmetric gas flow seen in the gas mass plot.

The liquid holdup and mass rates of gas and oil early during shut-in are shown in Figure 4.36. At this point, there is no liquid remaining in the well, since the top zone absorbs the condensate with ease, similar to the base case. The backflow rate of gas in the top zone varies between 0.007 kg/s in layer 7 and 0.044 kgs/s in layer 11. In the bottom zone, the backflow rate is 0.01 kg/s through every layer. This means that more gas flows into the top zone than is being produced from the bottom zone. An explanation is that as gas flows down the well as pressure propagates down after the shut-in until the pressure at the wellhead equals the reservoir pressure minus the hydrostatic pressure of the gas. Figure 4.37 shows the mass rates and liquid holdup late in the shut-in. At this point, the well is almost static. However, there is still some additional backflow into layers 11 and 10. Layers 7-9 produce small amounts of gas, and the bottom zone accumulates small amounts of gas. The slight crossflow between the top zone and the bottom zone is attributed to the pressure difference between the reservoir zones that approaches the hydrostatic pressure difference.

After the well is reopened, liquid loading begins immediately. However, the top zone is more productive than the bottom zone, contrary to what was seen in the base case during liquid loading. The explanation is that the top zone has regained pressure at the cost of the bottom zone, as seen in Figure 4.24. Similarly to the base case, layer 11 is the only layer with a backflow of oil (negligible rate through layer 10).

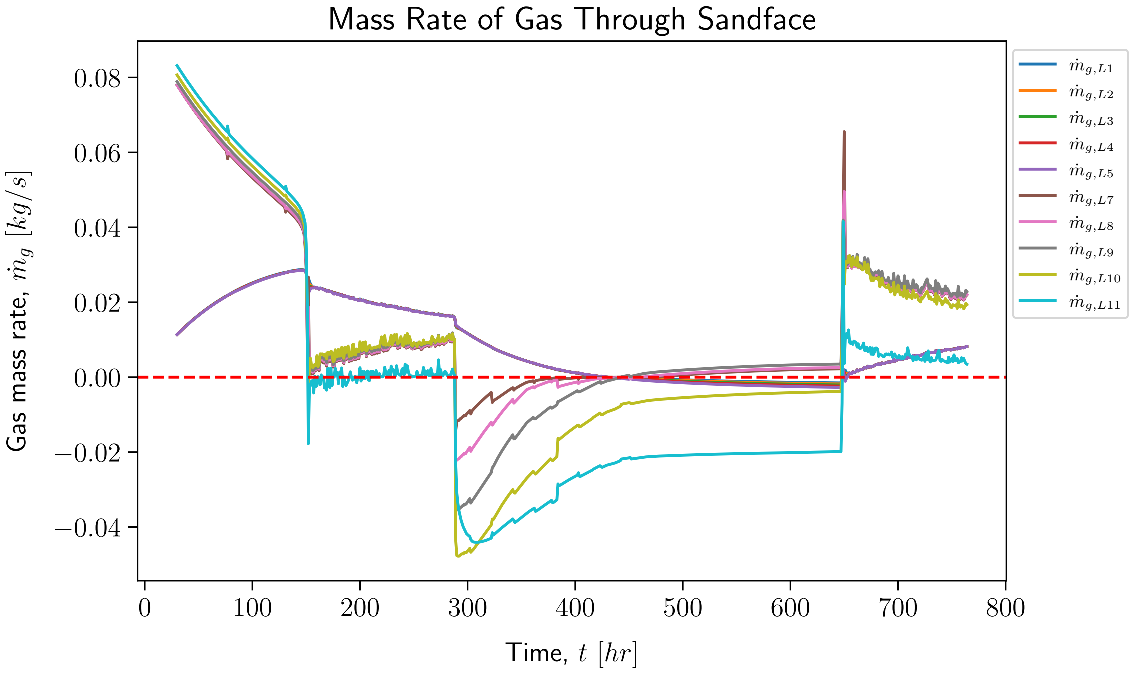

Figure 4.33: Case 1.2b Shut-In 2: Mass rate of gas through every numerical reservoir layer during shut-in.

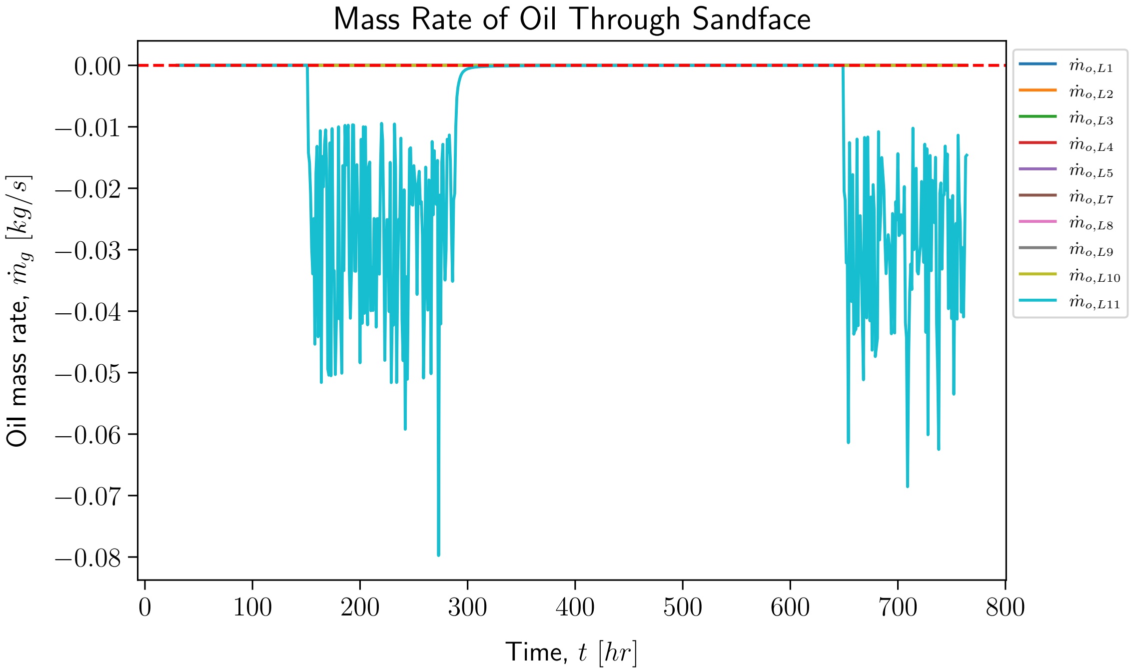

Figure 4.34: Case 1.2b Shut-In 2: Mass rate of oil through every numerical reservoir layer during shut-in.

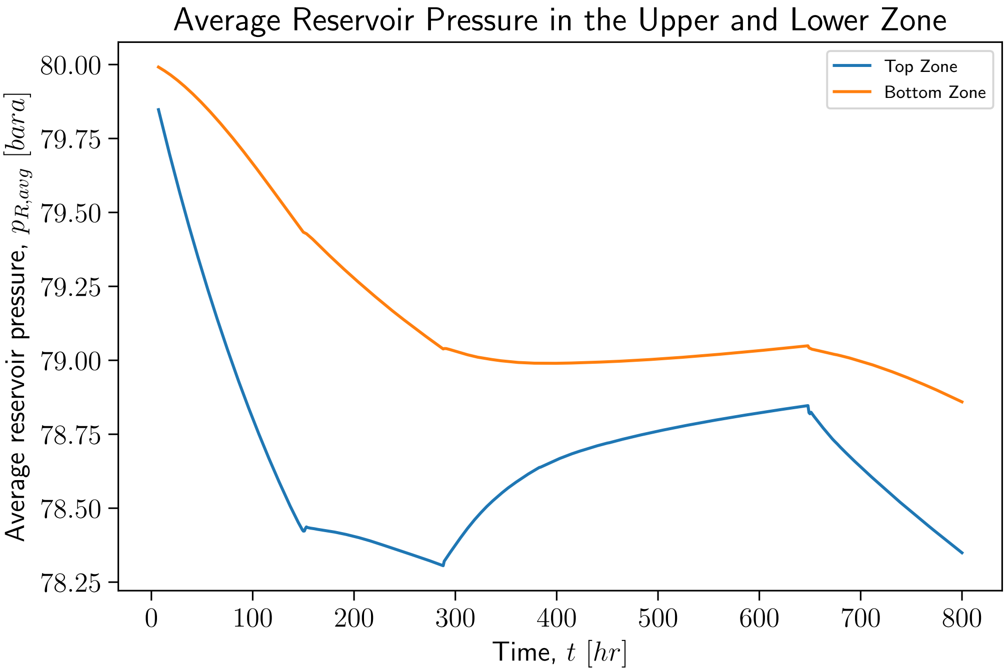

Figure 4.35: Case 1.2b Shut-In 2: Average reservoir pressure in the top and bottom zones.

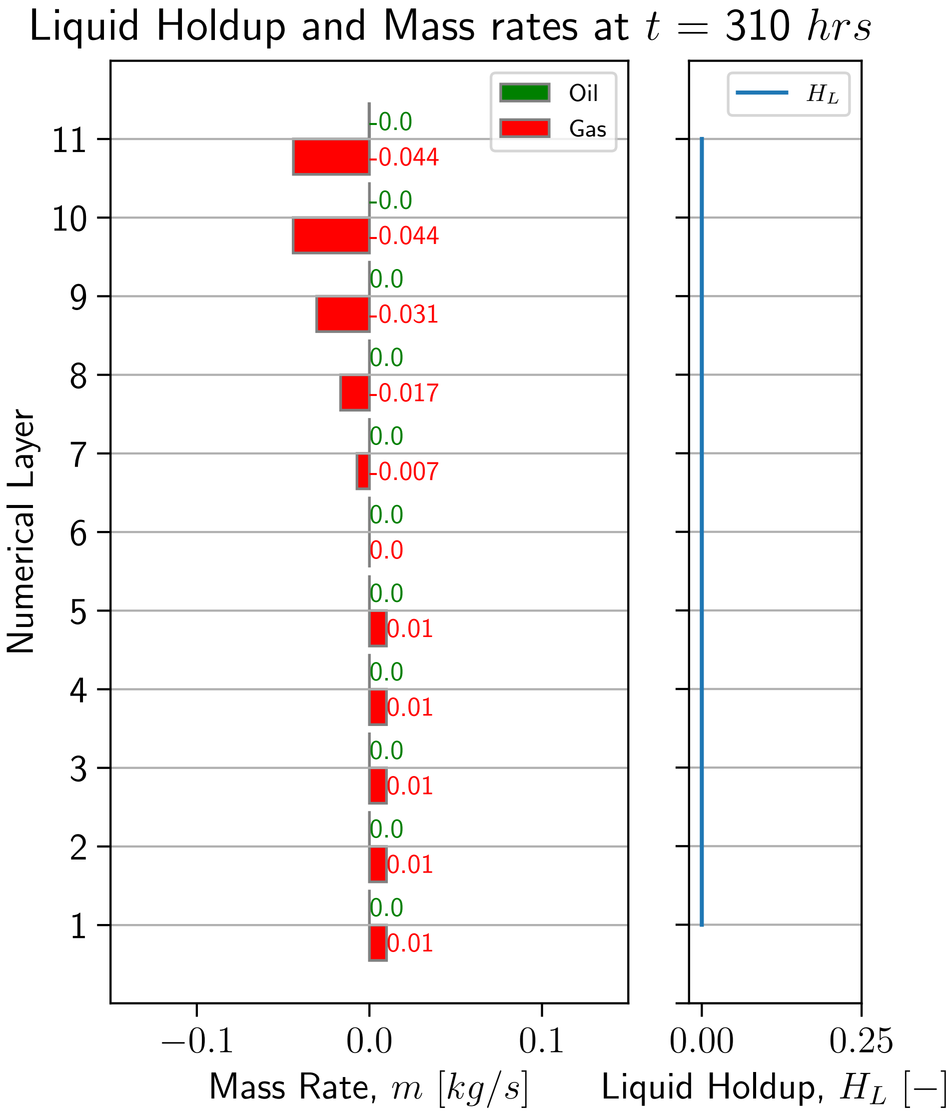

Figure 4.36: Case 1.2b Shut-In 2: Snapshot of mass rates of oil and gas, and liquid holdup early during the shut-in.

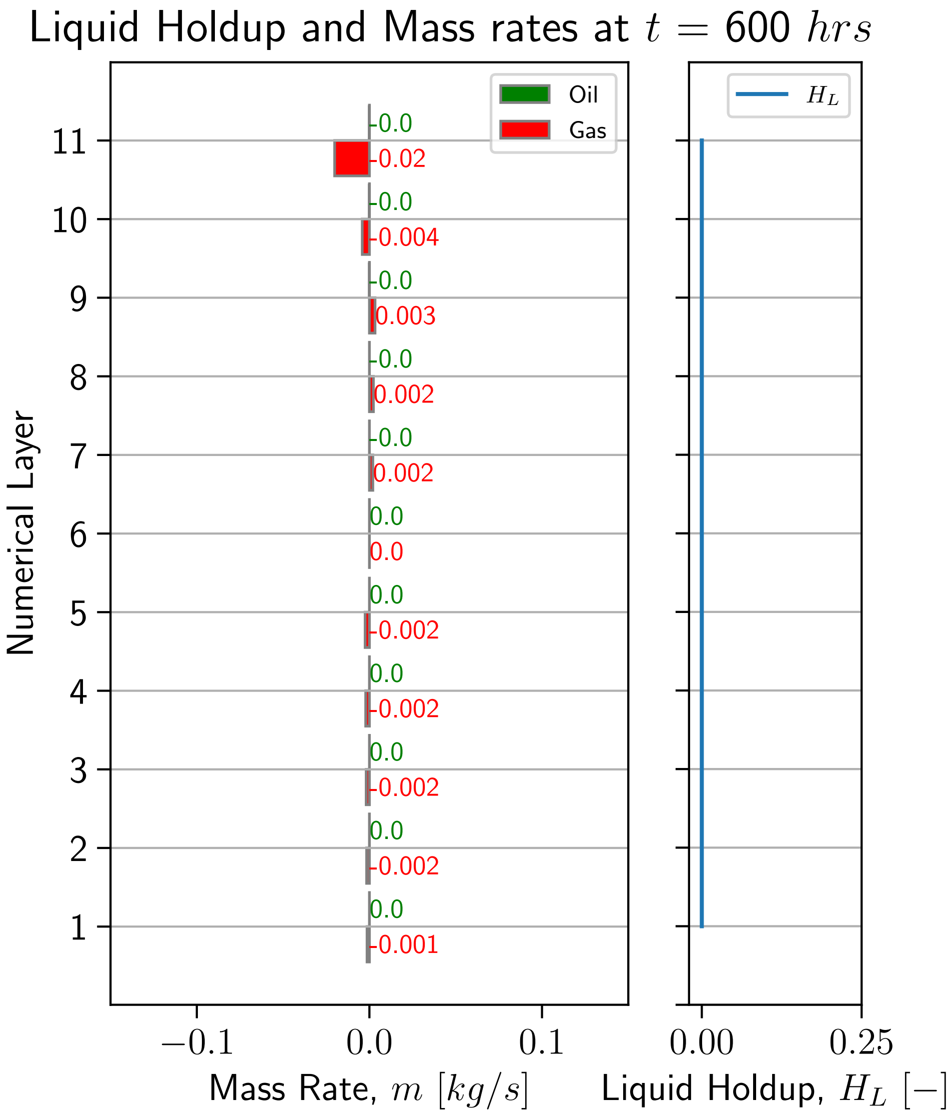

Figure 4.37: Case 1.2b Shut-In 2: Snapshot of mass rates of oil and gas, and liquid holdup late during the shut-in.

Reduced Wellhead Pressure

Wellhead pressure is reduced to 40 $bara$ to check whether a production strategy with less flow restriction affects the flow behavior and potential crossflow between zones.

Because the wellhead pressure is decreased, liquid loading is initiated at a lower rate than observed in the other cases, similar to the observations by Breimoen [12]. The liquid film reversal rate is 28,555 Sm^3/d, which is 5,000-7,000 Sm^3/d less than that observed when the wellhead pressure is 60 $bara$. This reduced critical rate is consistent with the results from the liquid loading project by Breimoen [12]. Furthermore, the droplet reversal rate and Turner rate are 19,055 and 19,839 Sm^3/d, respectively. This suggests that the equation better predicts liquid loading when the wellhead pressure is not "very high". Breimoen [12] found the opposite to be true; however, the author operated only with wellhead pressures up to 15 $bara$. Perhaps the accuracy of the Turner equation best predicts the onset of liquid loading between high and low pressures.

Figure 4.39 shows that the top zone depletes slightly faster than the bottom zone, similar to the base case. This happens since the permeability is 10 times greater in the top zone. As liquid loading is initiated, the depletion rates change. The average reservoir pressure in the top zone increases approximately 0.15 $bara$ over a period of 40 hrs before it starts to decrease again. During this period, Figure 4.71 shows that gas is flowing into the top layer. In addition, Figure 4.38 shows that the gas rate in the tubing above the reservoir zones is less than between the zones. This indicates crossflow from the bottom zone to the top zone.

The oil mass rates for each numeric layer are plotted in Figure 4.72. Similar to previous findings, the oil flows only back through the top layer of the top zone (layer 11) due to the increased permeability (and hence depletion). This is confirmed by the mass rates and liquid holdup in Figure 4.42. Saturation and pressure profile plots are left out because they provide similar information to the base case but with other numbers.

Since the initiation of liquid loading is primarily dependent on the completion characteristics, a reduced wellhead pressure can influence whether crossflow occurs during liquid loading or not. Reducing the wellhead pressure makes both reservoir zones deplete more before the liquid film is reversed. The increased pressure difference between the zones makes crossflow more likely to occur. Also, since the wellhead pressure and reservoir pressure are lower, the hydrostatic pressure difference and frictional pressure drop are lower. This contributes to the bottom zone being able to produce gas, which ultimately can flow into the top zone or continue to the surface.

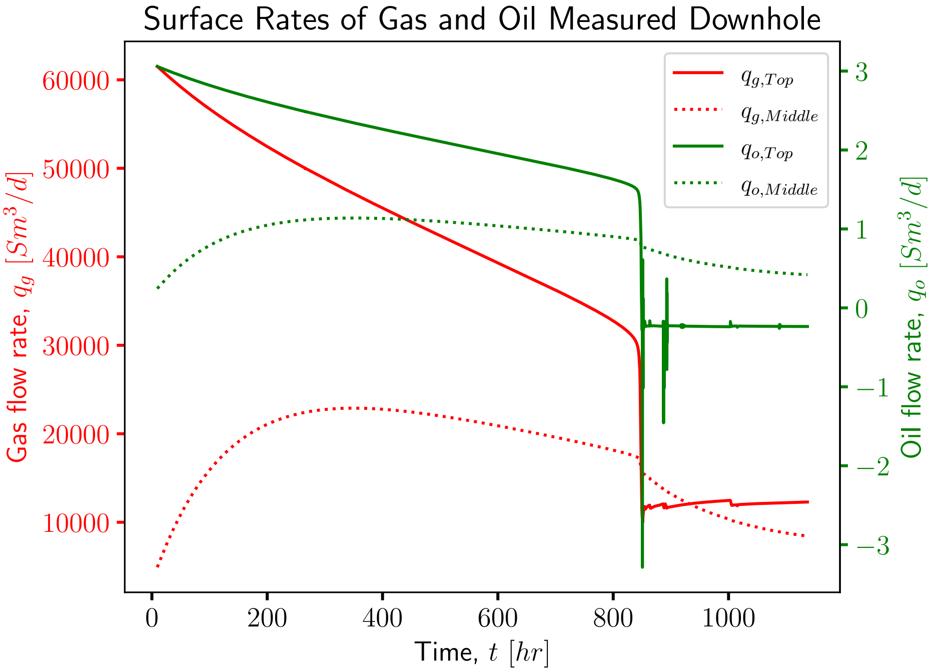

Figure 4.38: Case 1.2b reduced p_{wh}: Production rates in the tubing converted to standard conditions. The measuring probes are placed above the top zone and between the zones.

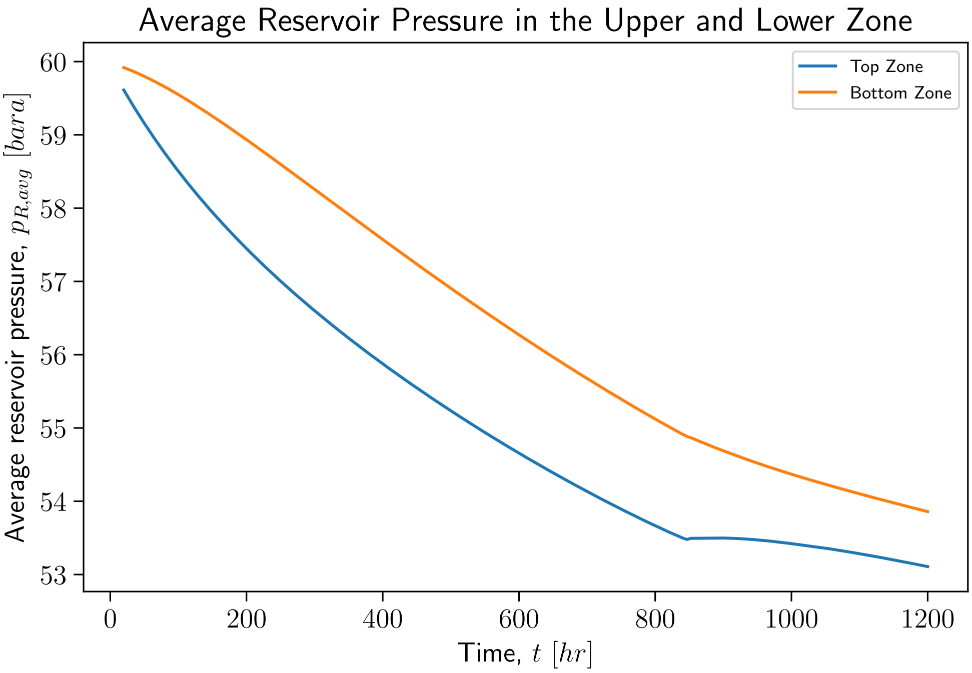

Figure 4.39: Case 1.2b reduced p_{wh}: Average reservoir pressure in the top and bottom zones.

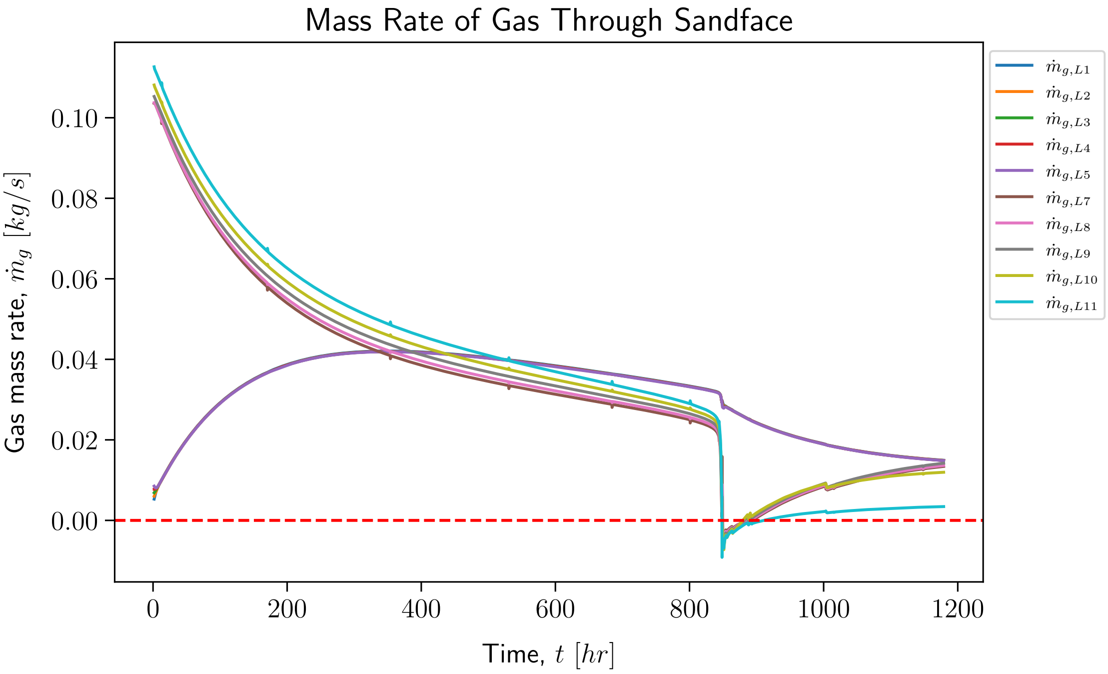

Figure 4.40: Case 1.2b reduced p_{wh}: Mass rate of gas through each numeric layer.

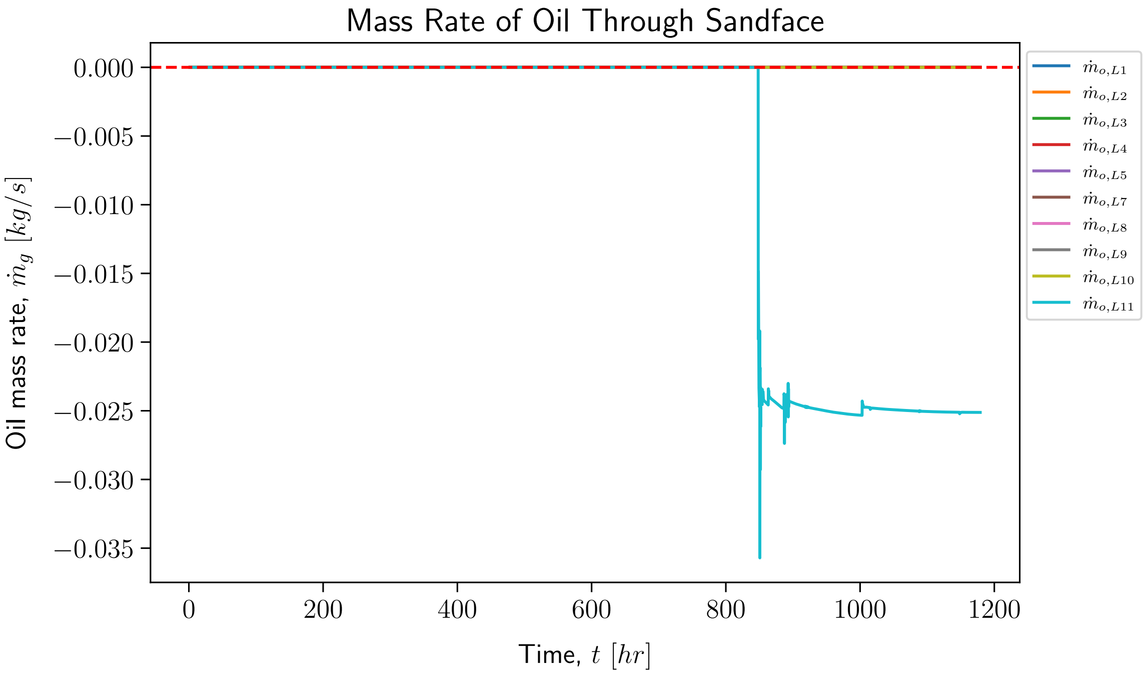

Figure 4.41: Case 1.2b reduced p_{wh}: Mass rate of oil through each numeric layer.

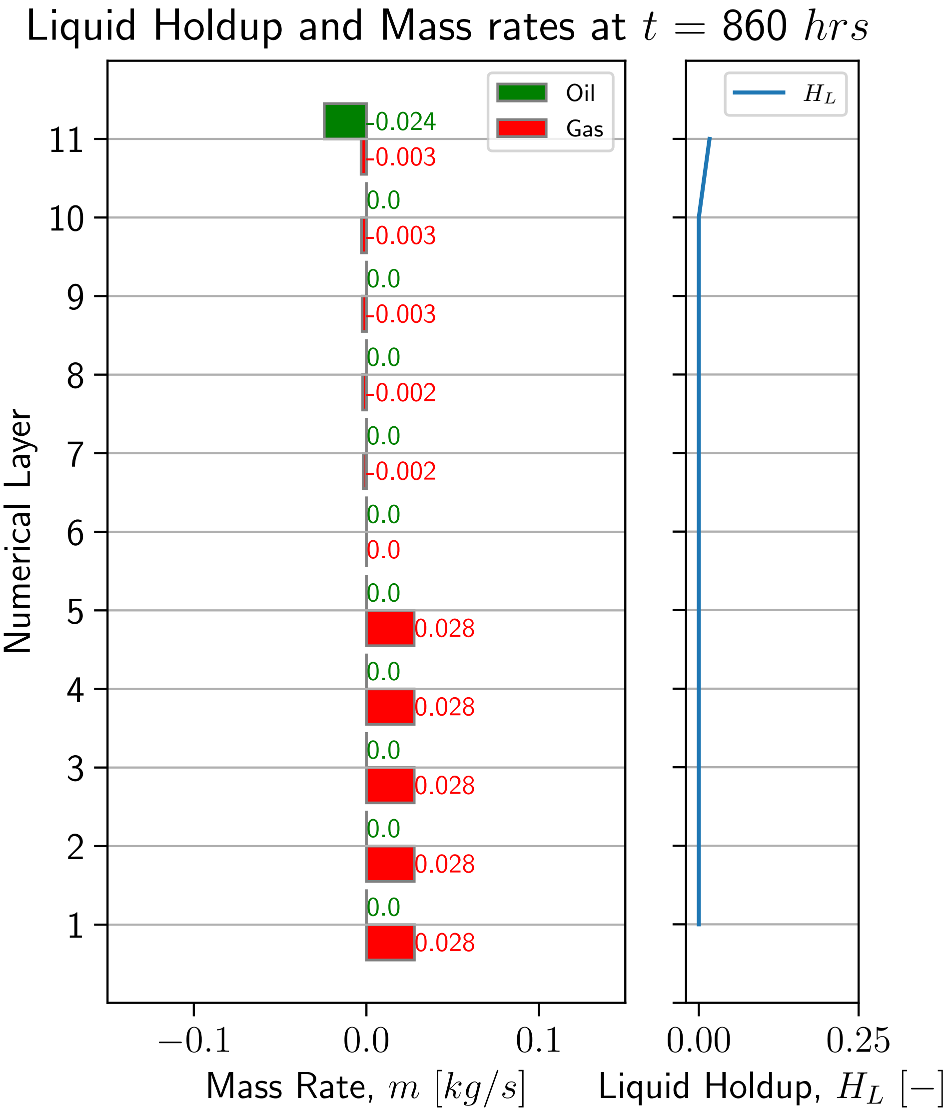

Figure 4.42: Case 1.2b reduced p_{wh}: Snapshot of mass rates of oil and gas, and liquid holdup early during liquid loading which indicates crossflow.

Gas Condensate as Fluid Model

This setup is similar to that of the *base case*. The differences are an updated fluid model with a higher-producing OGR (approximately 0.00077 Sm^3/Sm^3 before liquid loading) and corresponding changes in temperatures and pressures to prevent condensation within the reservoir, as described in Section 3.1.2.

The objective is to see whether the fluid composition makes a difference in crossflow and liquid loading-related events in the reservoir. Liquid loading in the wellbore domain is not discussed in detail for two reasons; The analysis and discussion are similar to the previous findings (different numbers), and the reservoir domain is the focus of this thesis.

Surface rates of gas and oil measured above and between the reservoir zones are shown in Figure 4.43. The bottom zone is initially unproductive. When liquid loading starts, gas and oil appear to flow from the bottom zone to the top zone. However, there is no oil at this location, but the calculated volumetric rate manifests itself in the gas, which will condense further up the well. General observations are that the bottom zone is more productive than the top zone early after loading, but is the first zone to stop producing. The surface rates of gas before and after liquid loading are 22800 and 2105 Sm^3/d, respectively.

Production starts similarly to what was expected, with each numerical layer in the bottom zone (1 to 5) being less productive than the numerical layers in the upper zone (6-11) due to differences in permeability, as seen in Figure 4.45. Initially, during production, the mass rate of gas is negative in the bottom zone, indicating backflow. This happens because the initial pressure in both reservoir zones is defined identically, but the pressure that acts on the bottom zone is greater due to the additional hydrostatic pressure. The total production from each zone approaches the same rate of approximately 0.2 kg/s before liquid loading begins. Figure 4.48 shows a snapshot of the mass rates through the sandface and the liquid holdup in the wellbore. Similar to every other case, the liquid holdup near the reservoir is zero, and the production zones produce at similar rates before liquid loading.

The liquid loading begins after 273 hrs as the liquid film reverses. The average reservoir pressure in the top and bottom zones are 98.1 and 99.4 $bara$, respectively. The liquid fraction in the well continues to increase with time along with the bottomhole pressure, as seen in Figure 4.44. Table 4.7 shows the cumulative mass production of each zone before the start of liquid loading, while the production of each zone stabilizes during liquid loading and during the stabilized period after loading. Between 270 and 565 hrs of production, 36146 kg of gas flows into the upper reservoir zone, and 66,284 kg of gas is produced from the bottom zone. The difference in the average reservoir pressure is approximately 1.3 $bara$ at the beginning of the liquid loading and approximately 0.72 $bara$ when the bottom layer becomes unproductive, as found by subtracting the top curve from the bottom curve in Figure 4.47. Approximately 0.72 $bara$ is the total pressure drop in the well between the center of the top and bottom zone at this point in time. This indicates that the bottom layer is productive while the average reservoir pressure is greater than the average pressure in the top zone plus the total pressure drop (friction, gravity, and acceleration). For approximately 30 hrs, both zones have net positive gas production, as seen in Figure 4.45. A snapshot of the mass rates through the sandface and the liquid holdup in the wellbore is shown in Figure 4.49. As seen in the figure, the oil flows with ease into the high-permeable zone, which makes the holdup below layer 11 zero. The saturation and pressure plots are not included since they are almost identical to those of the *base case*. These data clearly indicate a crossflow from the bottom zone to the top zone. However, since the fluid model is changed, so are the pressure and temperature used in the simulation; this makes liquid loading happen later than in the base case, which also appears to increase the chance of crossflow (as seen in the *reduced wellhead pressure* case).

After 595 hrs, the bottom zone becomes unproductive and has gas backflow because the difference in the mean pressures between the lower and upper reservoir zones decreases more than the total pressure drop between the center of each zone. At this point, the fluid dynamics in the reservoir are severely altered by the condensate backflow (Figure 4.46. The condensate enters the top zone (specifically layer 11) and is redistributed further down, similar to *base case*. As it moves down, the gas is displaced, and the mobility of the gas is reduced as a function of saturation. Eventually, the bottom zone becomes unproductive while the top zone keeps producing at a reduced rate. This happens because crossflow drains the bottom zone, and the backpressure imposes an identical pressure as the reservoir pressure on the bottom zone.

Table 4.7: Case 1.2b Gas Condensate: Cumulative production of gas and oil before the onset of liquid loading, during fluid redistribution, and after production restabilizes.

Cumulative production of gas and oil					
	Time interval $[hours]$	m_g $[kg]$ Top layer	m_g $[kg]$ Bottom layer	m_o $[kg]$ Top layer	m_o $[kg]$ Bottom layer
Before liquid loading	0, 270	439,930	122,152	0	0
During fluid redistribution	270, 565	-36,146	66,284	-153,656	0
After slug initiation	565, 865	20,871	-6,576	-124,429	0

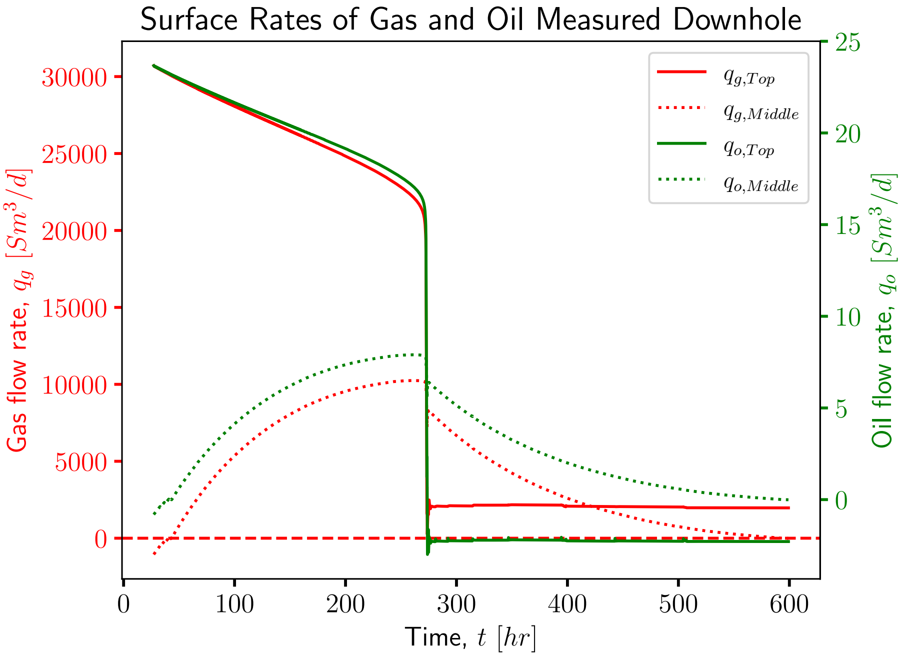

Figure 4.43: Case 1.2b Gas Condensate: Gas and oil rates measured between the reservoir zones and above the top zone, converted to standard condition volumetric rates.

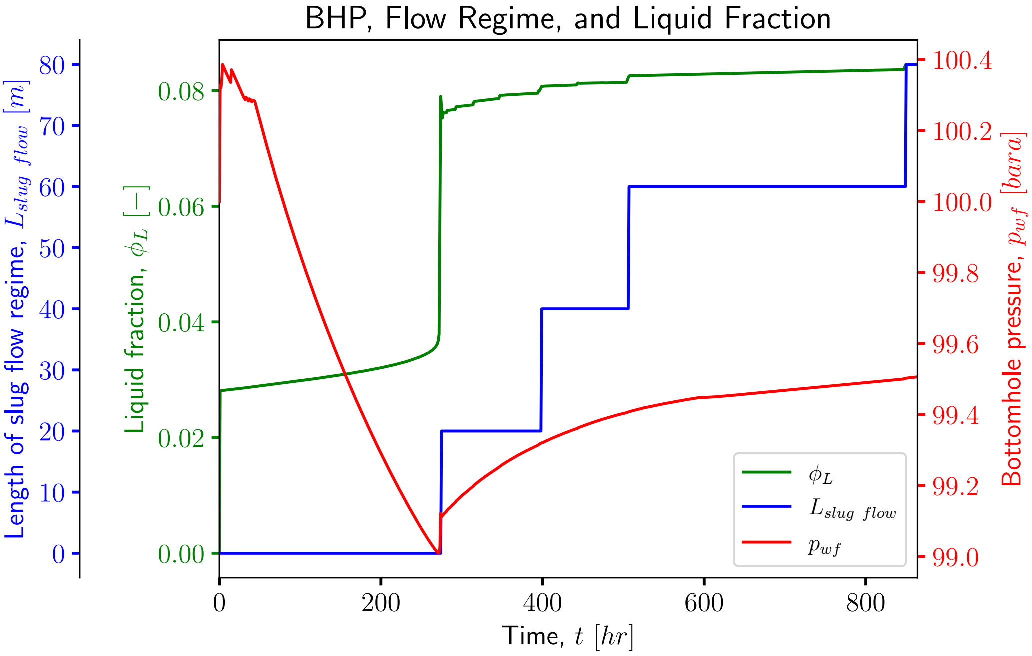

Figure 4.44: Case 1.2b Gas Condensate: Liquid fraction, bottomhole pressure, and length of slug flow regime.

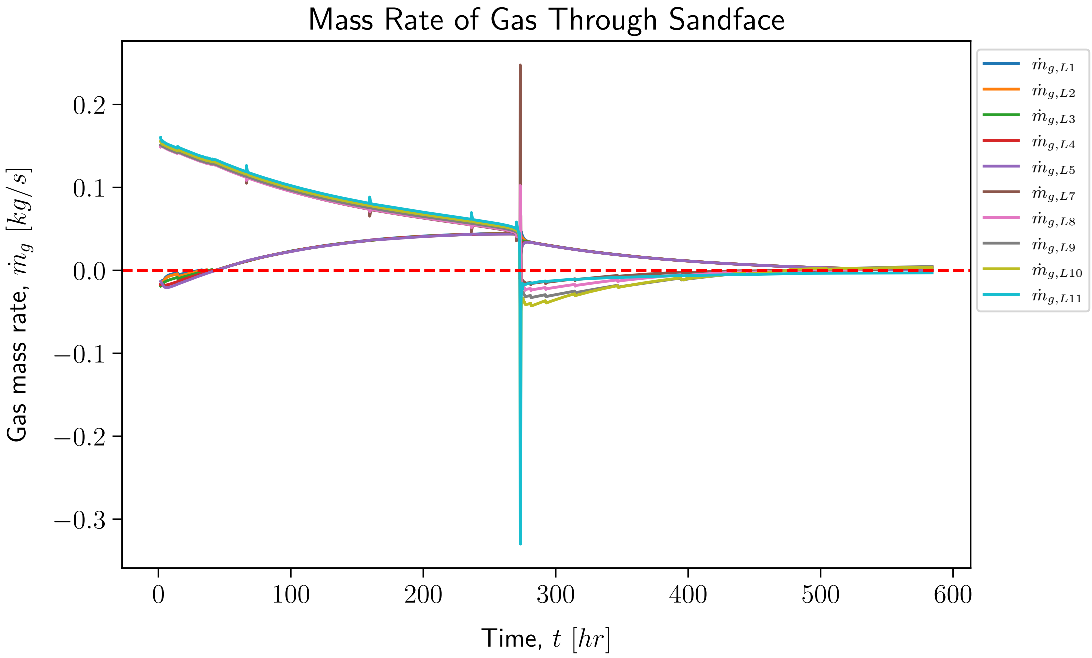

Figure 4.45: Case 1.2b Gas Condensate: Mass rates of gas through the sandface of each numerical reservoir layer.

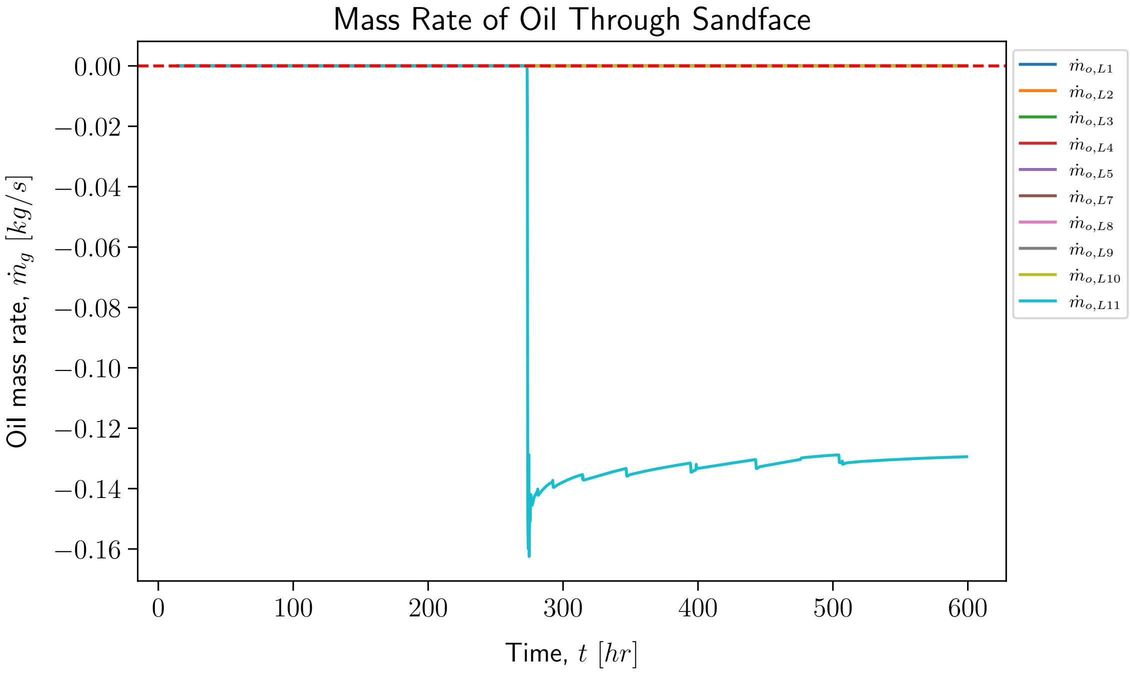

Figure 4.46: Case 1.2b Gas Condensate: Mass rates of gas through the sandface of each numerical reservoir layer.

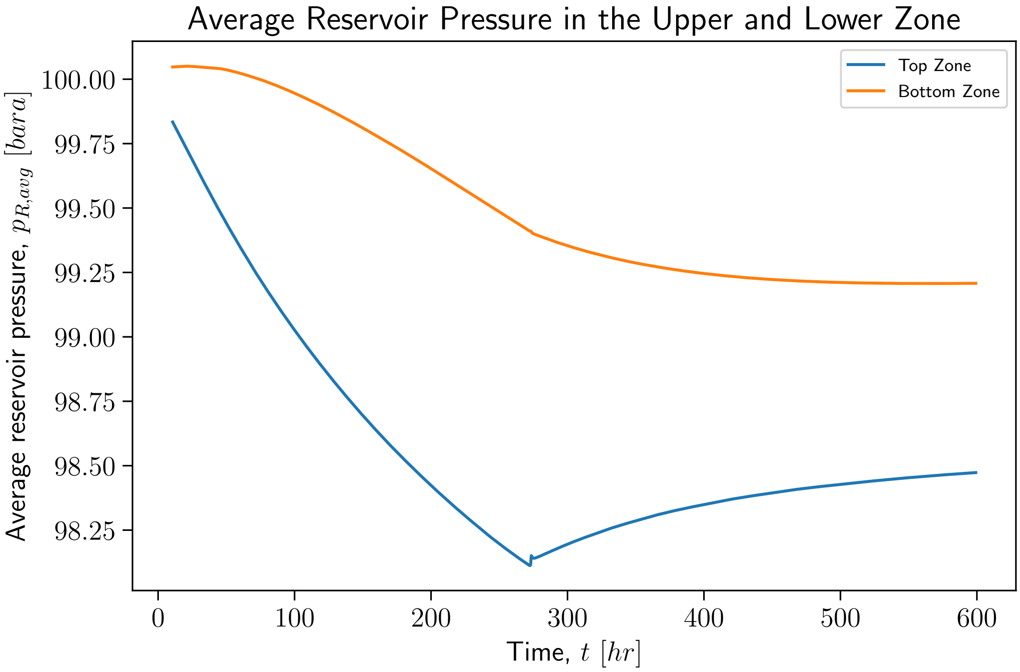

Figure 4.47: Case 1.2b Gas Condensate: Average reservoir pressure in the top and bottom zones.

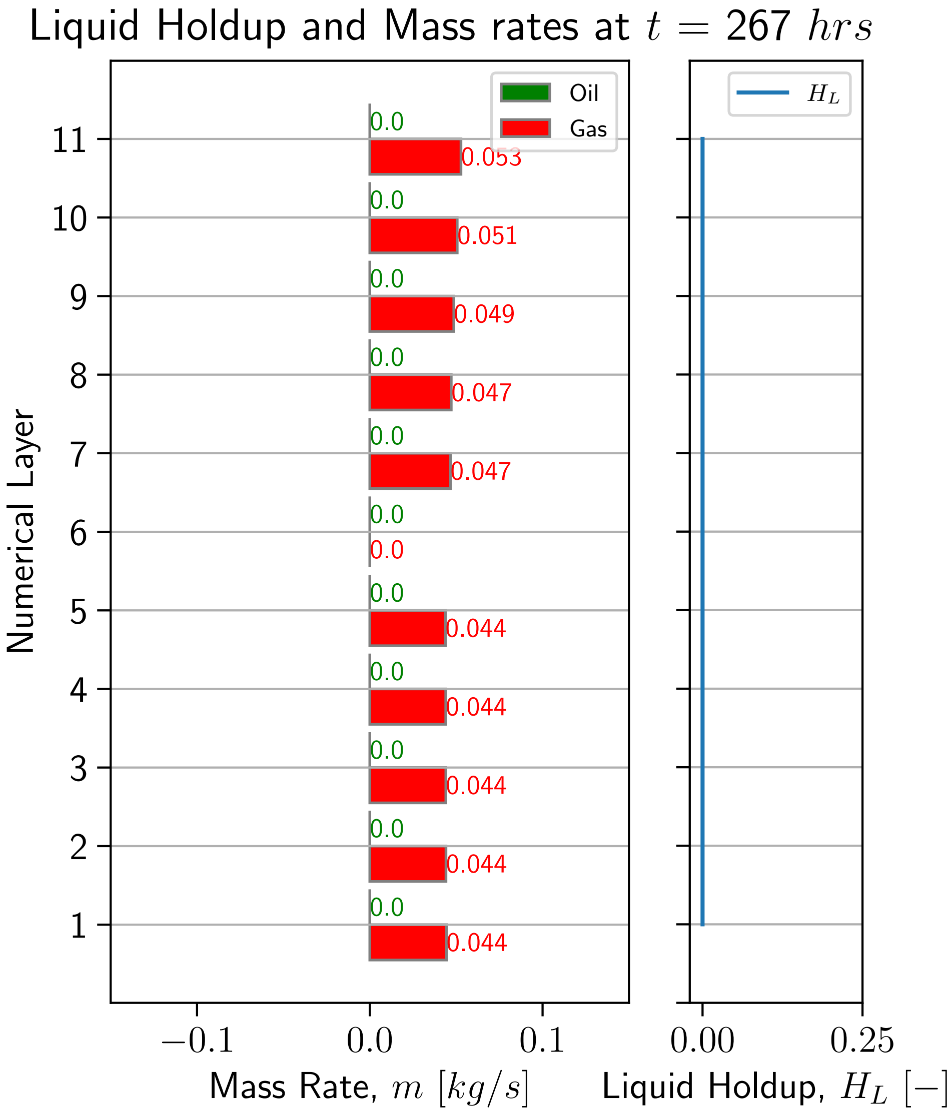

Figure 4.48: Case 1.2b Gas Condensate: Snapshot of mass rates of oil and gas, and liquid holdup before liquid loading.

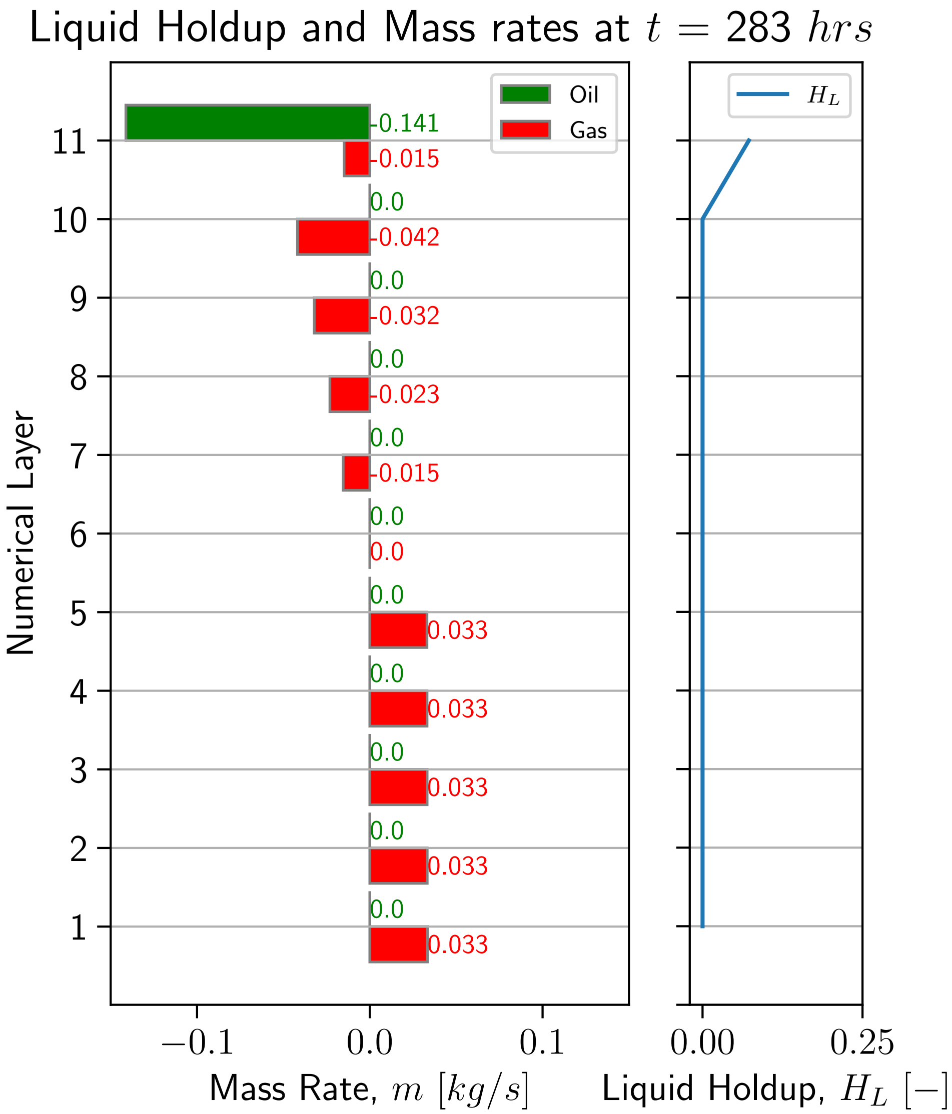

Figure 4.49: Case 1.2b Gas Condensate: Snapshot of mass rates of oil and gas, and liquid holdup early during liquid loading.

Reduced Capillary Pressure

This model is identical to the base case, except for the capillary pressure defined as $P_c(S_g) = 0\ bara$ instead of a linear function from 1 to 0 $bara$. The gas and oil mass rates are shown in Figures 4.50 and 4.51, respectively. The mass rates before loading begin are similar to those of the base case because capillary pressure effects are not present. Figure 4.52 shows that the top zone accounts for approximately 33% more gas than the top zone after 150 hrs. As seen previously, the liquid holdup is zero before loading starts.

The top zone is more productive than the bottom zone for the duration of the simulation, although liquid loading affects both zones. Slug flow exists between layers 3 and 8 from the beginning of liquid loading until the end of the simulation. Figure 4.53 shows that the liquid holdup is approaching 100% in the bottom layer of the well. Layer 1 accounts for all of the backflow of oil and gas is unable to flow. Later during liquid loading, Figure 4.28 shows that gas and liquid flows into the bottom of the top zone (layer 7), in addition to the backflow of oil in layer 1. This indicates a crossflow of gas from the bottom zone to the top zone.

This case shows that when capillary pressure is reduced (or removed), oil flows into the reservoir zones through the bottom layer of each zone. Liquid builds up at the bottom of the well and forces a backflow of oil due to the hydrostatic pressure imposed by the dense column of liquid. Since liquid enters at the bottom of each zone, fluid redistribution effects in the near-wellbore region, such as those seen in previous tests and cases, do not occur. The well quickly transitions to steady (non-oscillating) production, similar to that of **Case 1.1 - ROCX** in Section 4.1.2.

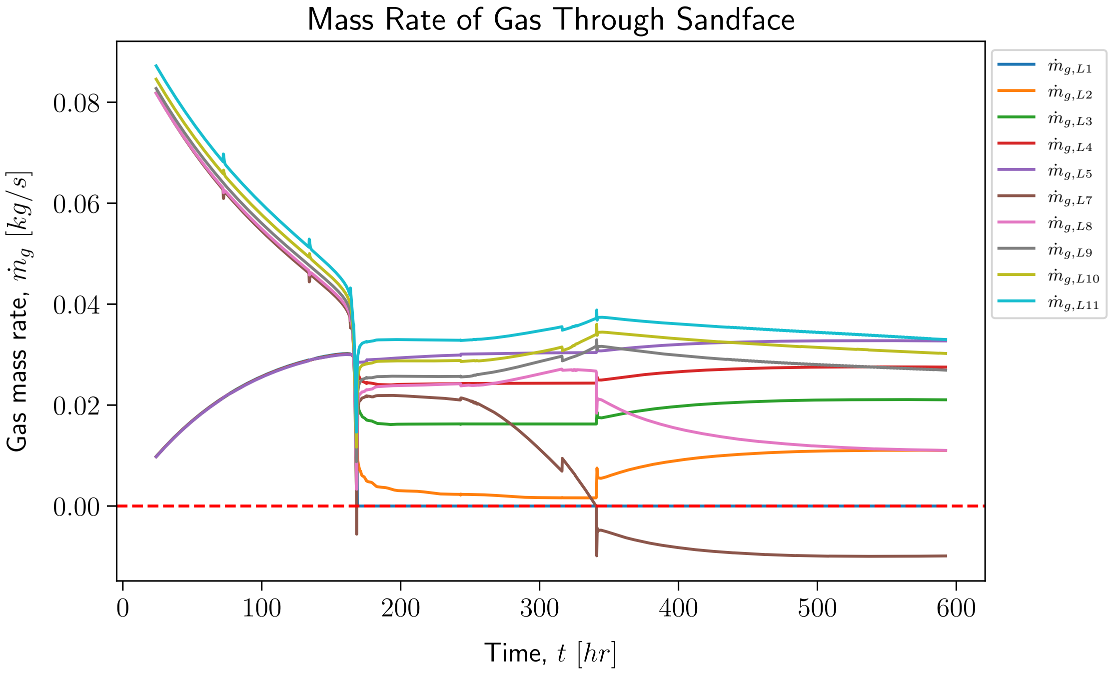

Figure 4.50: Case 1.2b reduced capillary pressure: Mass rates of gas through each numerical layer.

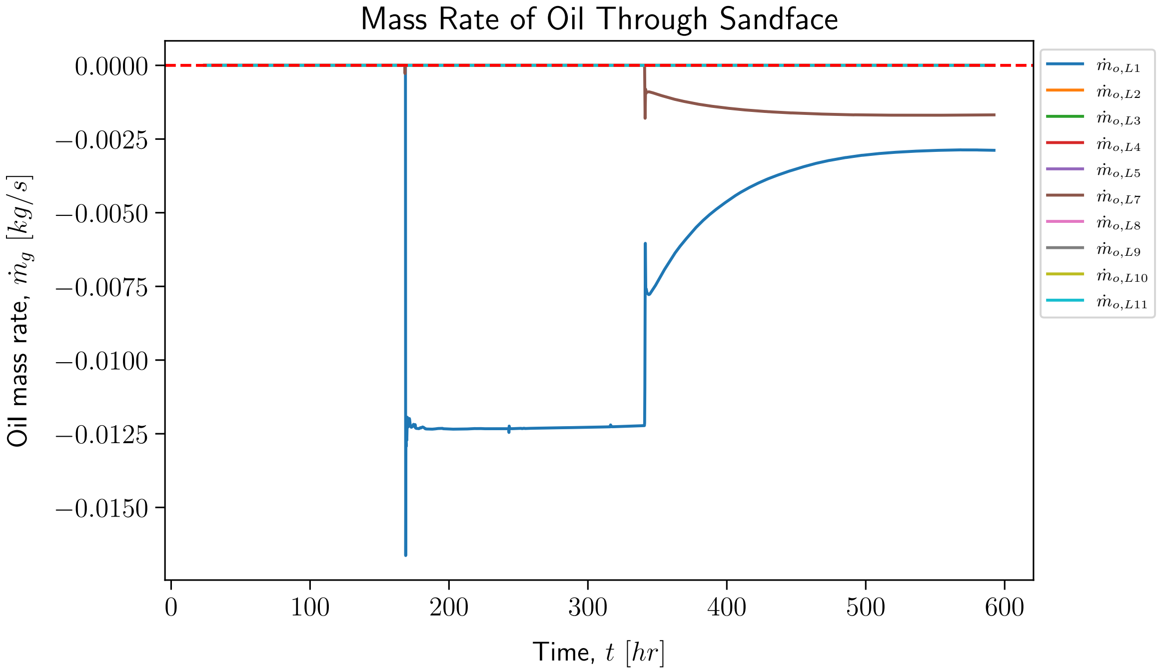

Figure 4.51: Case 1.2b reduced capillary pressure: Mass rates of oil through each numerical layer.

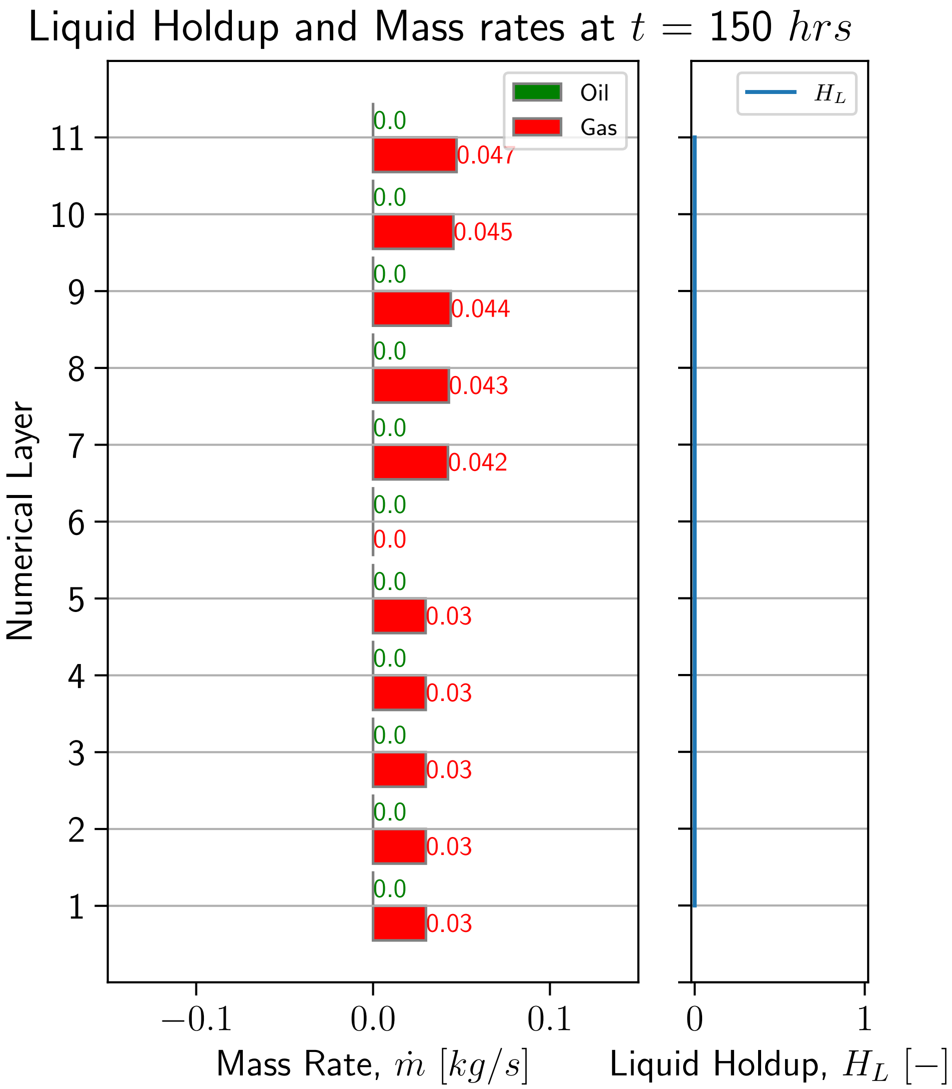

Figure 4.52: Case 1.2b reduced capillary pressure: Snapshot of mass rates of oil and gas, and liquid holdup before liquid loading.

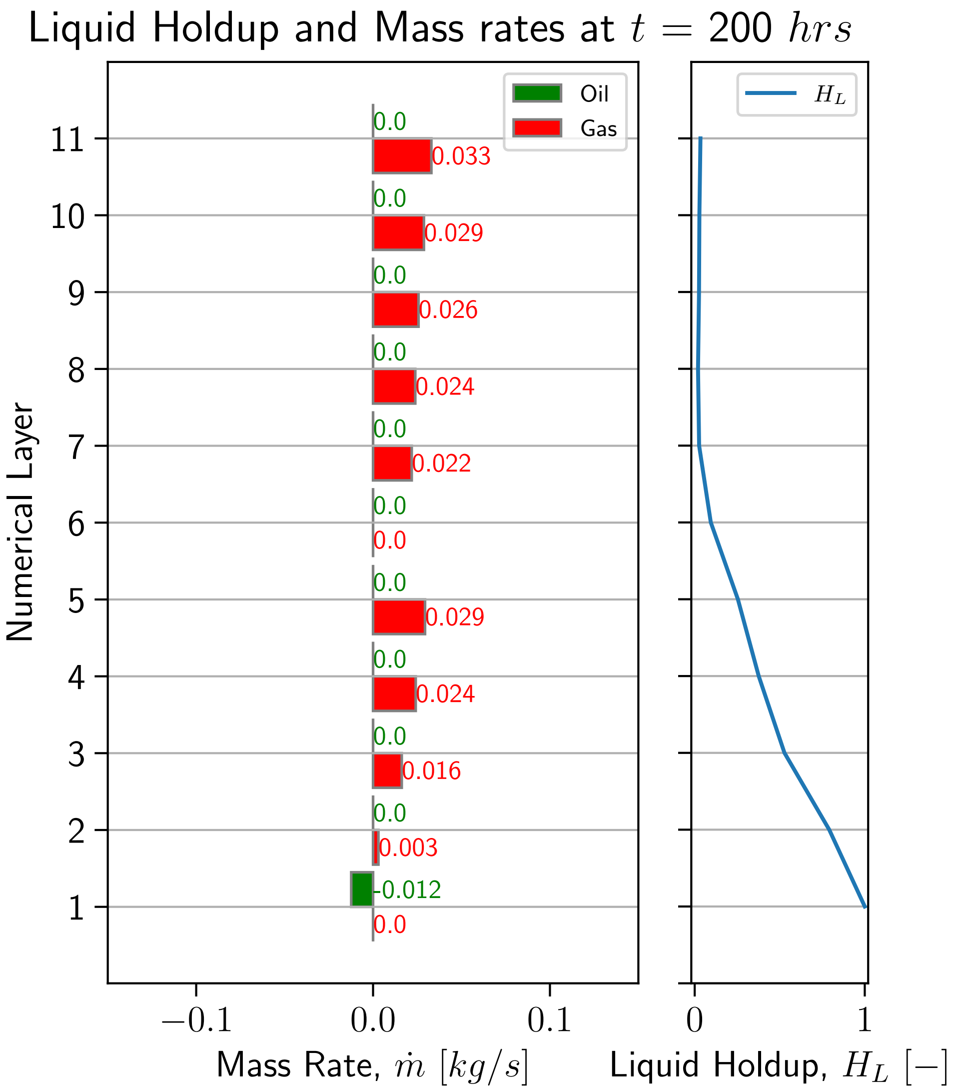

Figure 4.53: Case 1.2b reduced capillary pressure: Snapshot of mass rates of oil and gas, and liquid holdup early during liquid loading.

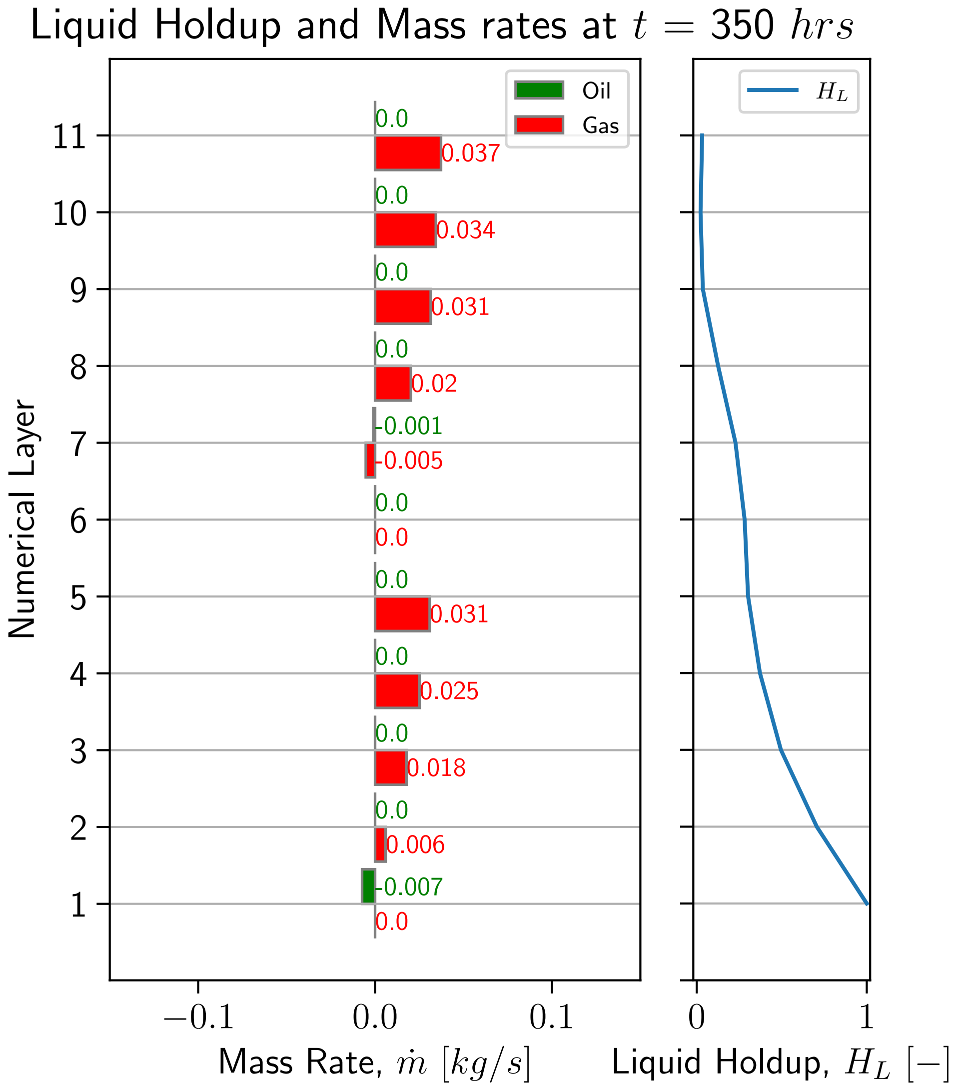

Figure 4.54: Case 1.2b reduced capillary pressure: Snapshot of mass rates of oil and gas, and liquid holdup late during liquid loading.

4.2.3 Case 1.2c

This setup is identical to Case 1.2b, except that the permeability of the bottom zone (layers 1-5) is 100 md and that of the top zone (layers 7-11) is 10 md. Identical tests are also conducted.

Base case

The surface rates of oil and gas are shown in Figure 4.55. The most notable difference in this case compared to **Case 1.2b** (Section 4.2.2) is the stabilized post-loading (metastable) rate between 146-300 hrs, which is 21,905 Sm^3/d in this case and 11,700 Sm^3/d in **Case 1.2b**. Another key difference is the development of slug flow, which in this case is less prominent than in the previous case. Figure 4.56 shows that the slug flow starts after 300 hrs (154 hrs after the beginning of liquid loading) and grows to a maximum length of 130 m over the course of 140 hrs. In **Case 1.2b**, the slug flow length reaches 350 m within hours of the onset of liquid loading.

Table 4.8: Case 1.2c: Cumulative production of gas and oil before the onset of liquid loading, between the initiation of liquid loading slug flow, and the following 203 hrs.

Cumulative production of gas and oil					
	Time interval $[hours]$	m_g $[kg]$ Top layer	m_g $[kg]$ Bottom layer	m_o $[kg]$ Top layer	m_o $[kg]$ Bottom layer
Before liquid loading	0, 147	72,331	145,918	0	0
During fluid redistribution	148, 297	51,191	58,589	-2,079	-5,615
After slug initiation	298, 500	87,895	66,299	-426	-23,340

Figures 4.57 and 4.58 show the mass rates of gas and oil through the upper (low permeability) and lower (high permeability) reservoir zones. Initially, the bottom zone produces approximately 3.7 times as much gas as the upper zone due to the permeability difference. By integrating the gas mass rate from the beginning of the simulation to the beginning of liquid loading, the cumulative gas mass produced from the bottom zone is 146,716 kg and 73,406 kg from the top zone. This means that the bottom zone accounts for 66.7% of the gas production.

After the liquid film reverses (146 hrs), it takes 2 hrs for the liquid to build up in the well and flow into the upper reservoir zone through layer 11. Oil backflow occurs less than 0.5 hrs later in the bottom zone, which is a key difference to that of **Case 1.2b** where most of the backflow went through layer 11.

During the first 150 hrs of liquid loading, the total oil mass accumulated in the reservoir is 2,079 kg in the top zone and 5,615 kg in the bottom zone, which means that 73.1% of the accumulation is in the highly permeable zone. The cumulative production of gas is 50,147 and 57,987 kg from the top and bottom zones, respectively. This means that 53.6% of the gas flow comes from the bottom zone. Figure 4.60 shows that the liquid holdup is low while the oil flows back into the top and bottom zones. Gas production is almost uniformly distributed. The pressure and saturation profiles in Figure 4.61 confirm a nearly uniform gas flow from the top and bottom zones, and backflow of oil distributed across the top zone (represented by U-shaped curves) and layer 5. What marks the end of this semi-stabilized period is that the top zone is saturated to an equilibrium and slug flow is initiated as oil comes out of the reservoir. At this point, Figure 4.62 shows that the oil flows out of the top zone and into the bottom zone, both zones produce gas, and the liquid is distributed in the well from layers 11 to 5. As seen previously, the high-permeable zone is capable of absorbing all of the oil with which it is in contact. The saturation profiles in Figure 4.63 show a near-uniform saturation distribution in the top zone. The steep change in gas pressure near the well is caused by condensate, which reduced the phase pressure of gas because the relative permeability is reduced. The bumps in the oil pressure profiles cause the oil to accumulate within the first 1.5 m of the reservoir and essentially prevent the oil from flowing further into the reservoir. This marks the start of the "saturation equilibrium" where approximately the same amount of oil flows in and out of the zone.

The next 200 hrs after the slug flow is initiated, the bottom zone accounts for 98% of the liquid accumulation, where 455 kg of oil has accumulated in the top zone and 24,092 kg have accumulated in the bottom zone. Only 43.1% of the total gas production comes from the bottom zone. The total gas production is 152,213 kg. The interplay of increased permeability and depletion allows the bottom zone to take in most of the accumulated oil through layer 5. Fluid is redistributed down in the other layers; however, it appears that the amount of gas that condensates in the wellbore is not enough to saturate the bottom part of the reservoir to a state of equilibrium similar to that seen in the top zone for the duration of the simulation.

Before the onset of liquid loading, there is no backflow of oil or gas into any of the zones. During liquid loading, the gas flow from each numeric layer is strictly positive, with one exception: After 297 hrs, the production from layers 4 and 5 is slightly negative, but layers 1 and 2 counter the backflow with an increased flow to the well. Furthermore, Figure 4.59 shows that neither zone is gaining pressure from the other. Based on the flow of each numeric layer and the absence of a clear correlation between pressure changes in the reservoir zones, it is hard to determine whether crossflow occurs. However, since there is a small mass rate of oil out of the top zone and a large mass rate into the bottom zone while the slug flow exists, crossflow may be present. A key difference from that of **Case 1.2b** is that gas crossflow does not occur and oil crossflow appears to occur. Both cases share that the liquid holdup is zero below the upper layer of the high-permeable zone.

As liquid loading is initiated, oil starts to flow back through the top zone, and the bottom zone follows shortly after. On average, during this period, 73% of the oil backflow and 53.6% of the total gas production comes from the bottom zone. The top zone reaches a uniform oil distribution with similar amounts of oil flowing in and out of the reservoir, and the bottom zone has less pressure because it has depleted more before liquid loading. Before slugging starts, the saturation and pressure plots show unconventional (U-shaped) pressure profiles for the oil phase and conventional pressure profiles for the gas, as expected. After slugging is initiated, the upper reservoir pressure profiles show conventional-looking profiles close to the well and unconventional further out. This indicates an outflow of oil from the top zone. The pressure profiles in the lower zone remain unconventional and at a lower pressure than in the upper zone, indicating backflow. Another point to note is that the bottom zone accounts for 98% of the backflow of oil and only 43% of the gas production, which means that most of the backflow in the lower zone originates from the upper zone.

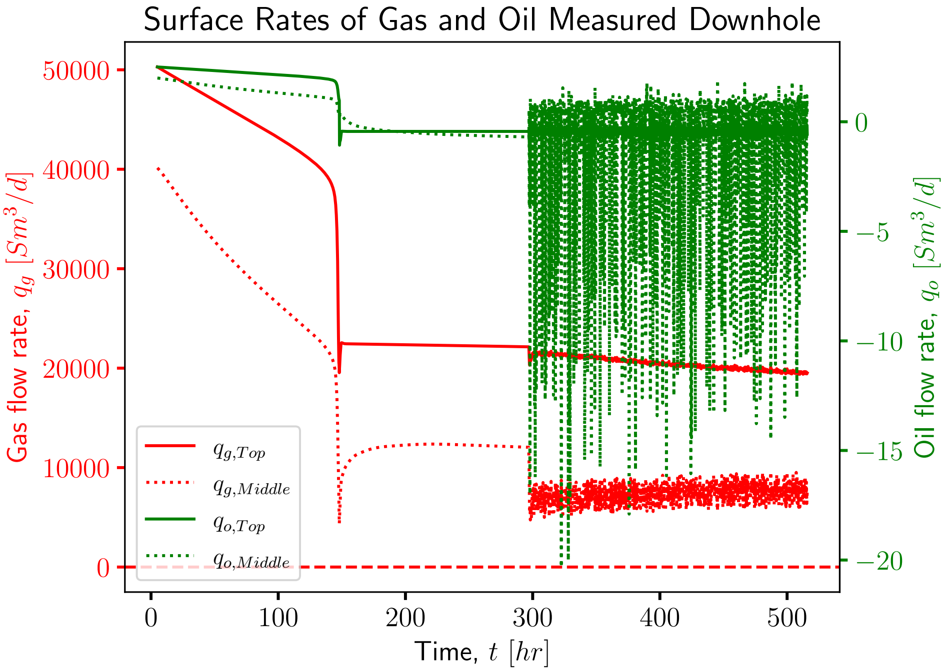

Figure 4.55: Case 1.2c: Surface rates of oil and gas measured above and between the reservoir zones

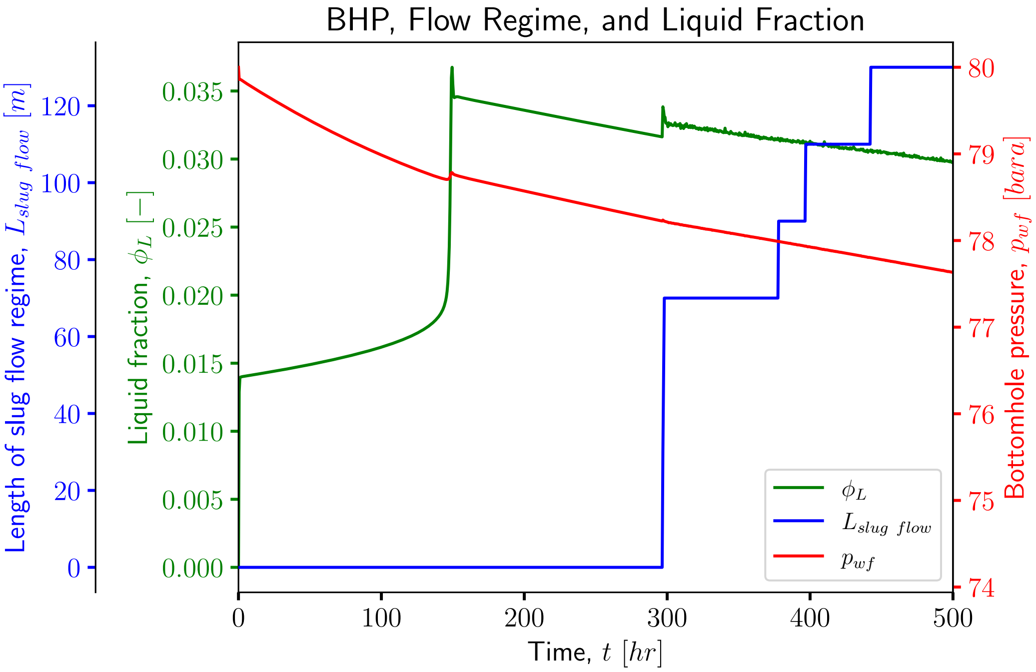

Figure 4.56: Case 1.2c: Liquid fraction, bottomhole pressure, and length of slug flow regime.

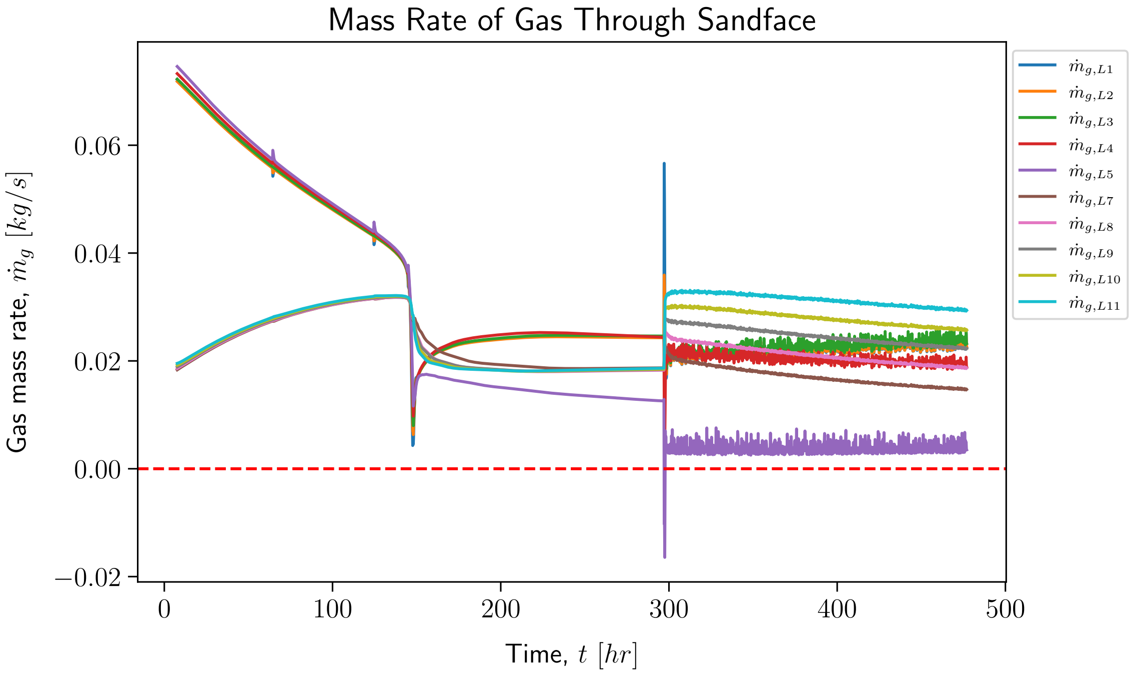

Figure 4.57: Case 1.2c: Mass rates of gas through the sandface of every numerical reservoir layer.

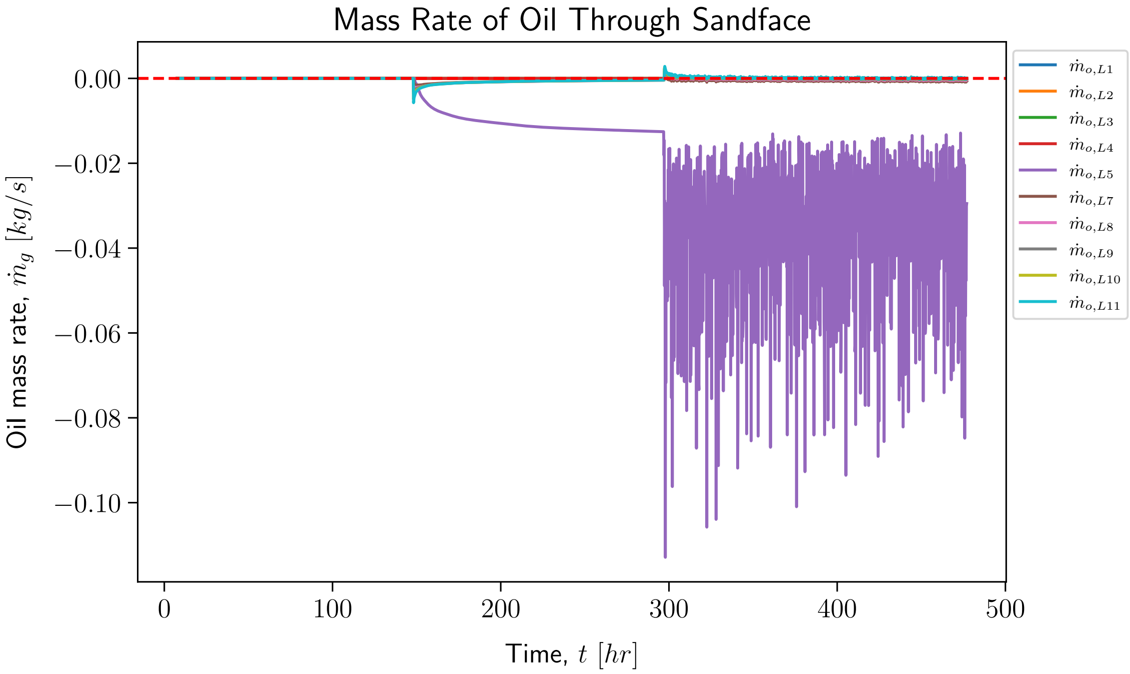

Figure 4.58: Case 1.2c: Mass rates of oil through the sandface of every numerical reservoir layer.

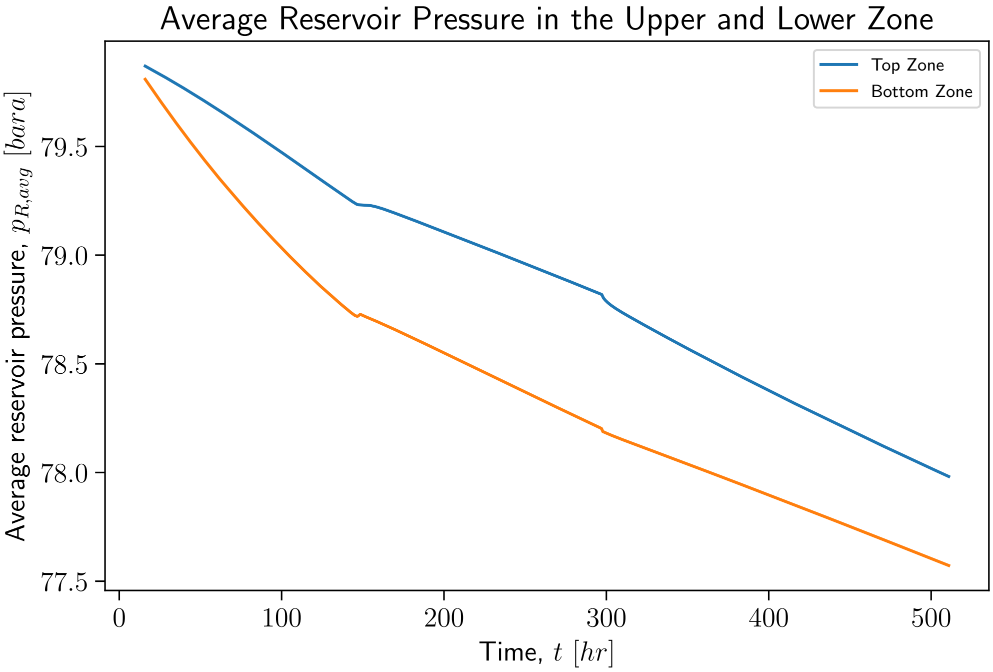

Figure 4.59: Case 1.2c: Average reservoir pressure in the top and bottom zone.

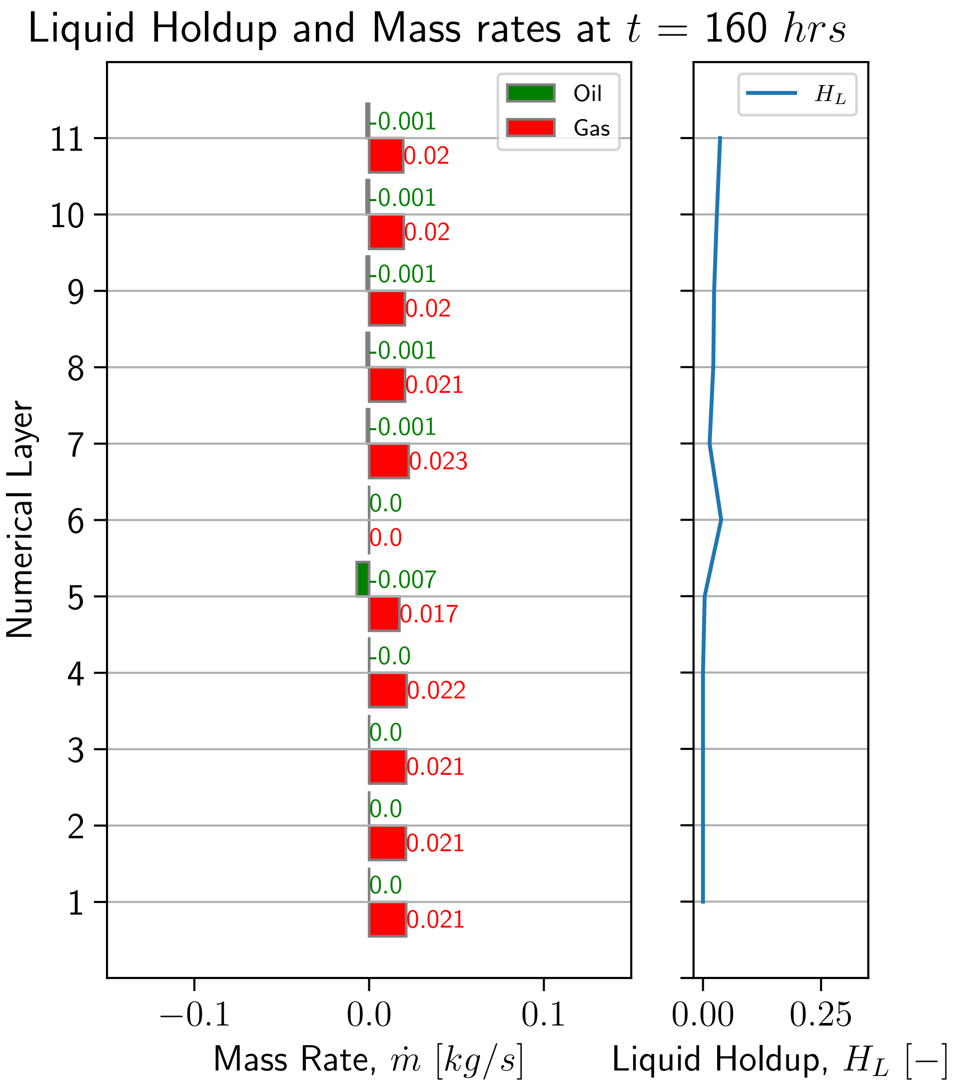

Figure 4.60: Case 2.2c: Snapshot of mass rates of oil and gas, and liquid holdup early during liquid loading.

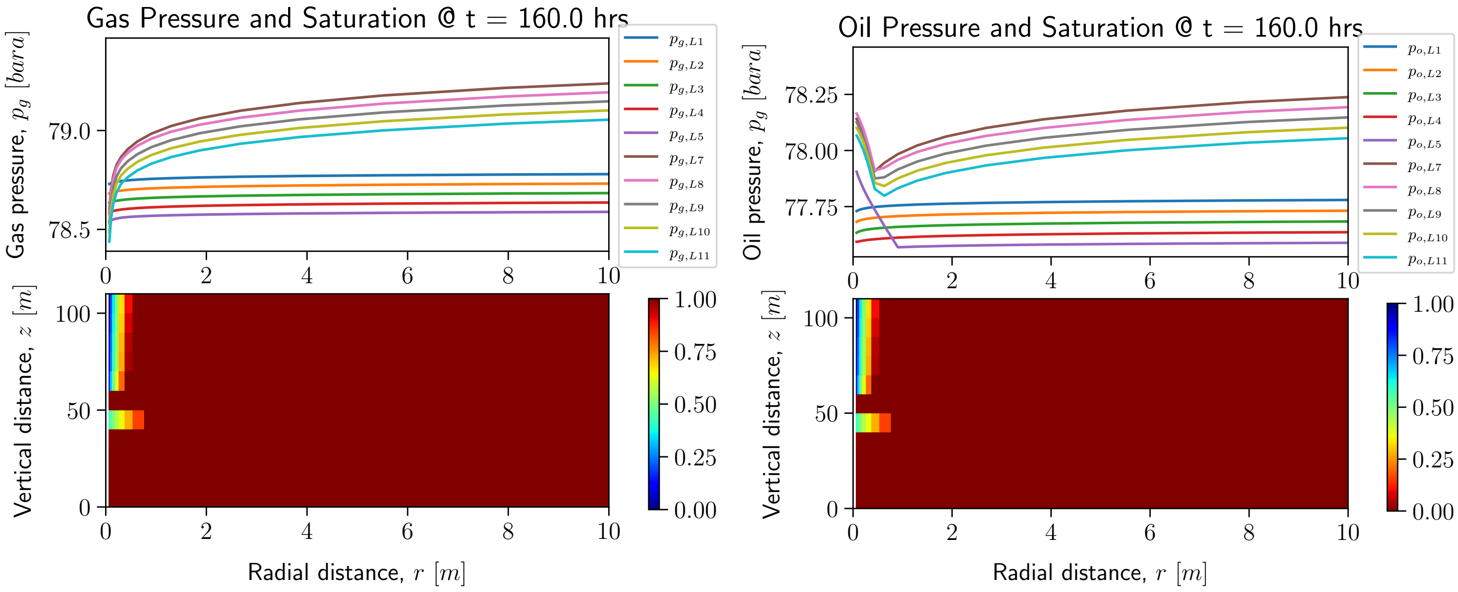

(a) Gas plot

(b) Oil plot

Figure 4.61: Case 1.2c: Saturation and pressure plots of gas and oil early during liquid loading.

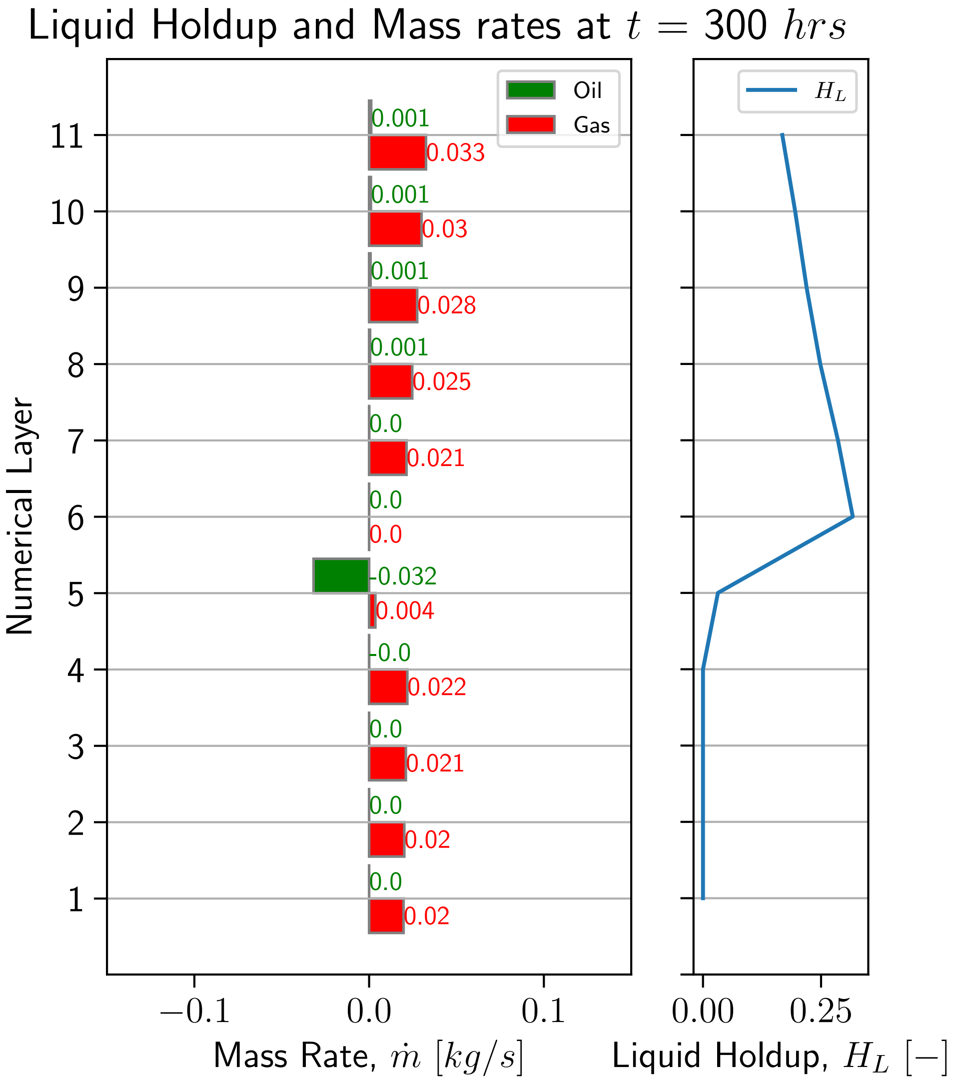

Figure 4.62: Case 1.2c: Snapshot of mass rates of oil and gas, and liquid holdup late during liquid loading.

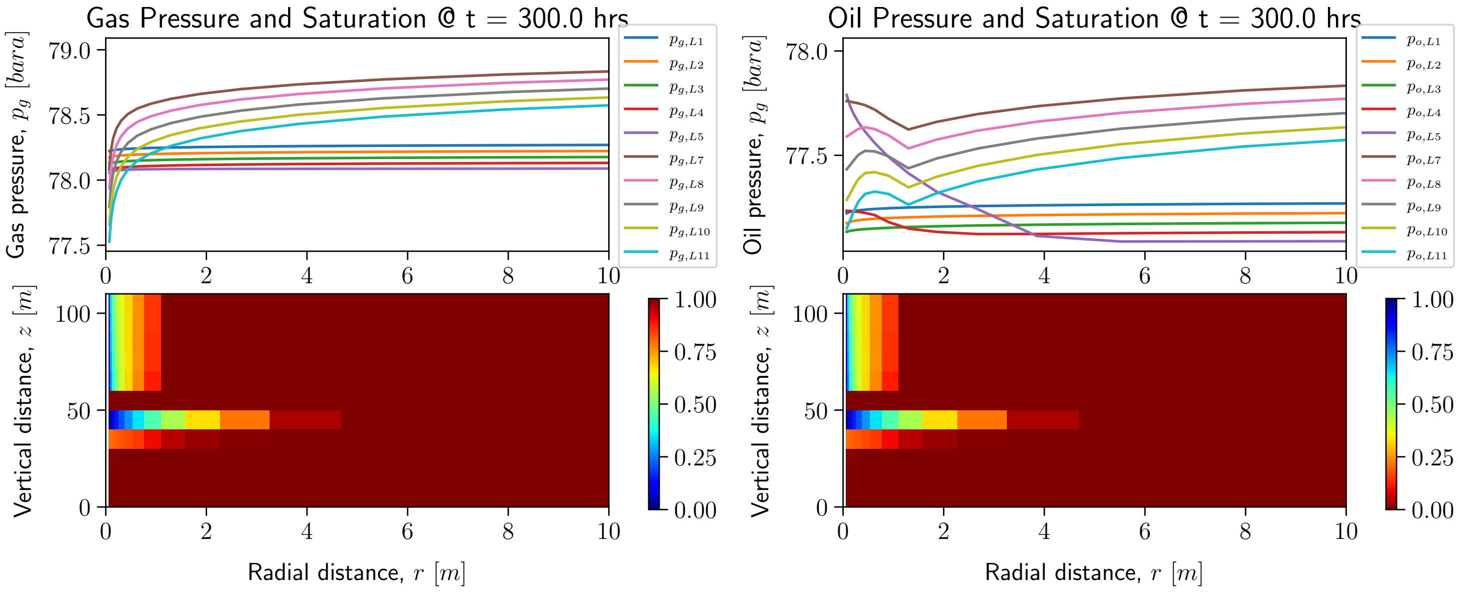

(a) Gas plot

(b) Oil plot

Figure 4.63: Case 1.2c: Saturation and pressure plots of gas and oil late during liquid loading.

Shut-In Before Loading

The first shut-in test is performed prior to liquid loading. Looking at Figure 4.64, the total mass rates from the top and bottom zones are close to symmetric around $\dot{m}_g = 0$ until the end of the shut-in, which identifies crossflow. The cumulative production of gas from the upper zone is 38,400 kg and the backflow into the lower zone is 51,463. The additional backflow is attributed to the gas in the wellbore or to a numerical error due to the oscillating measurement. The oil flows back into both zones, as seen in Figure 4.65, where 70.7 kg is through the top zone and 34.5 kg is through the bottom zone. Figure 4.66 shows that the bottom zone depletes faster than the top zone. During shut-in, the bottom zone builds up pressure and approaches a stabilized pressure approximately 0.2 $bara$ higher than the top zone, which is consistent with the difference in hydrostatic pressure between the zones.

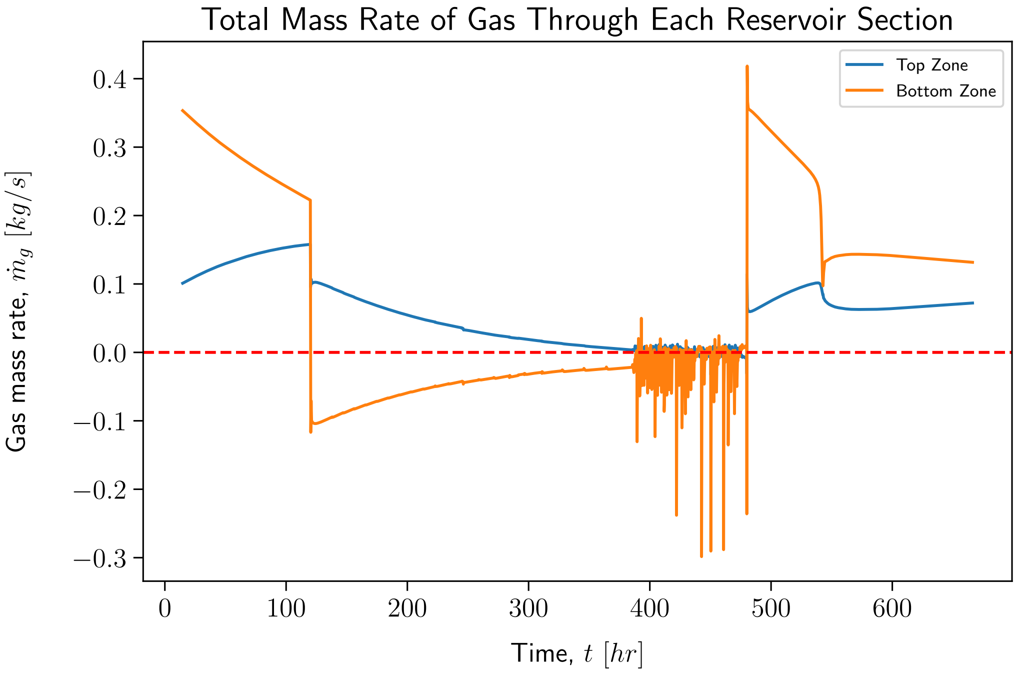

Figure 4.64: Case 1.2c Shut-In 1: Total mass rate of gas through the upper and lower reservoir layers during shut-in before liquid loading.

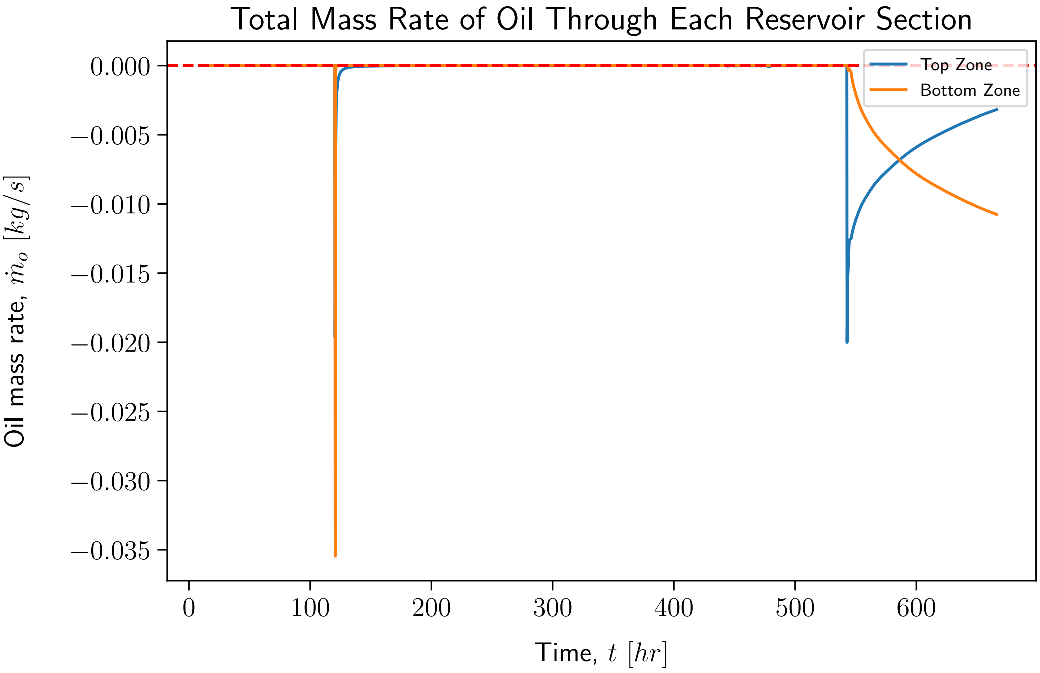

Figure 4.65: Case 1.2c Shut-In 1: Total mass rate of oil through the upper and lower reservoir layers during shut-in before liquid loading.

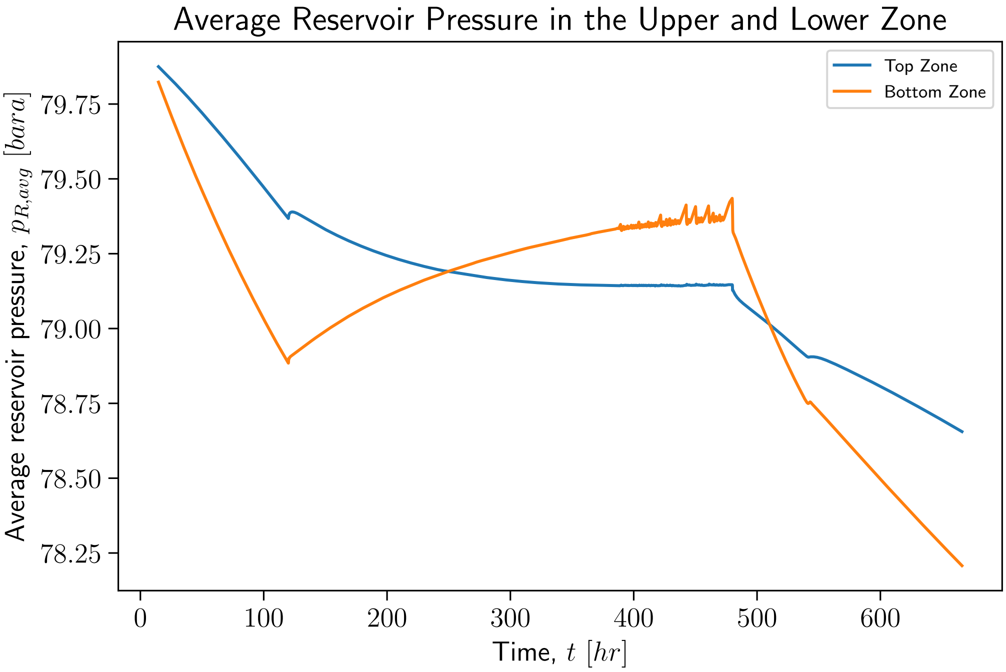

Figure 4.66: Case 1.2c Shut-In 1: Average reservoir pressure in the top and bottom zones.

Shut-In After Loading

Shutting in the well during liquid loading causes the gas flow to the bottom zone from the top zone, as seen in Figure 4.67. Near the end of the shut-in, gas flows into the top zone as well, which makes the cumulative production less than anticipated. The cumulative production of gas through the top zone is 36,497 kg and the backflow through the bottom zone is 60,142 kg. Figure 4.68 shows a slight backflow of oil through the top and bottom zones, which adds up to 65 and 222 kg, respectively. Figure 4.69 shows that the average reservoir pressure in the bottom zone generally increases. In the top zone, the pressure decreases initially and then increases slightly as the well approaches a static condition.

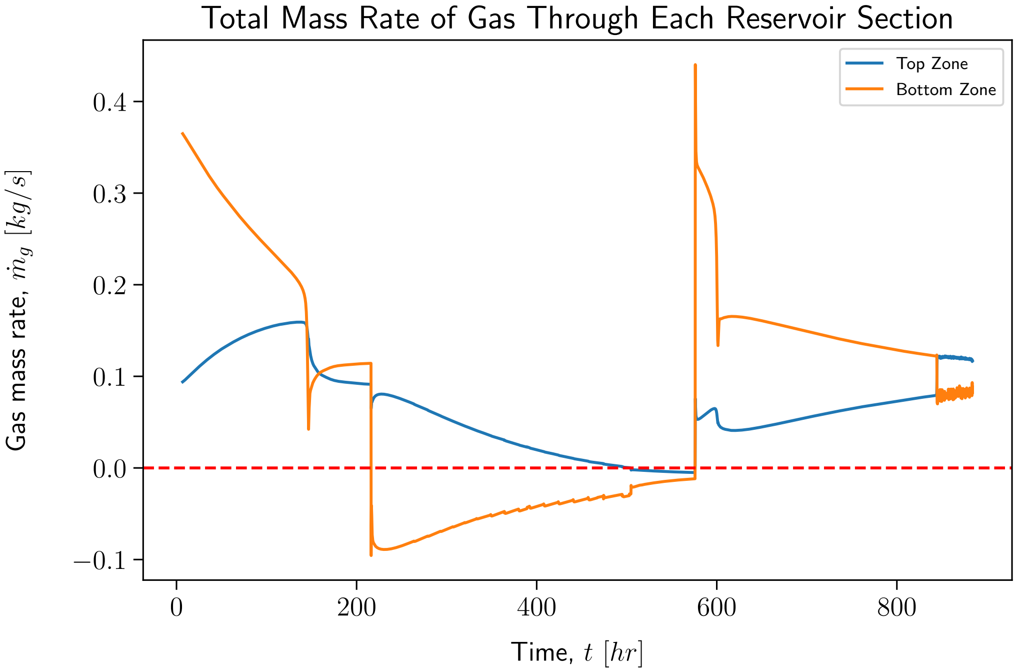

Figure 4.67: Case 1.2c: Total mass rate of gas through the upper and lower reservoir layers during shut-in 2.

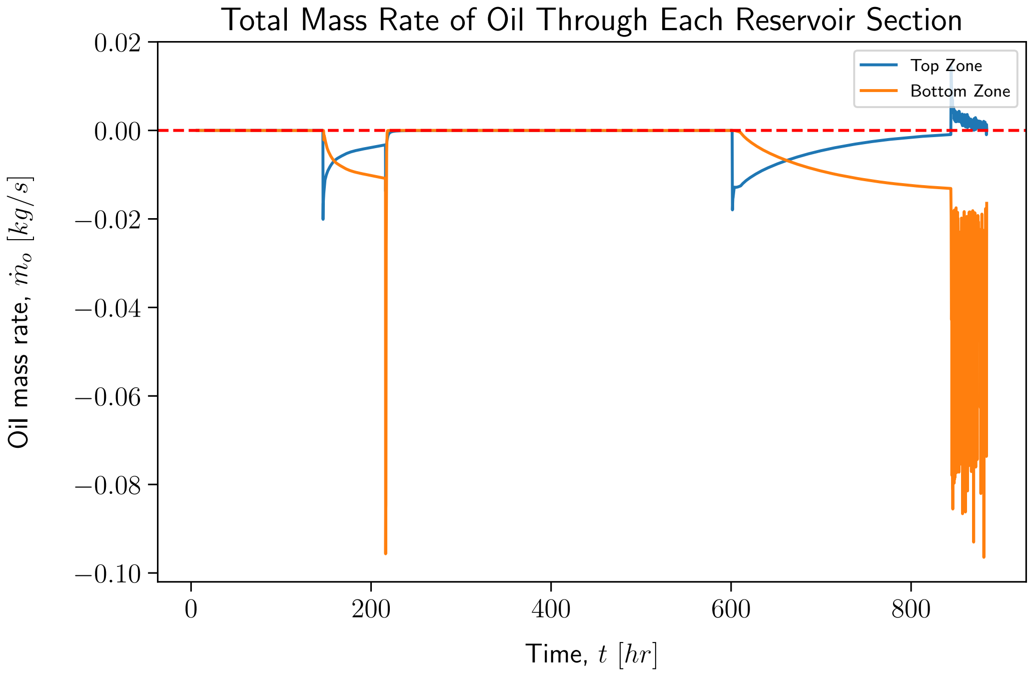

Figure 4.68: Case 1.2c: Total mass rate of oil through the upper and lower reservoir layers during shut-in 2.

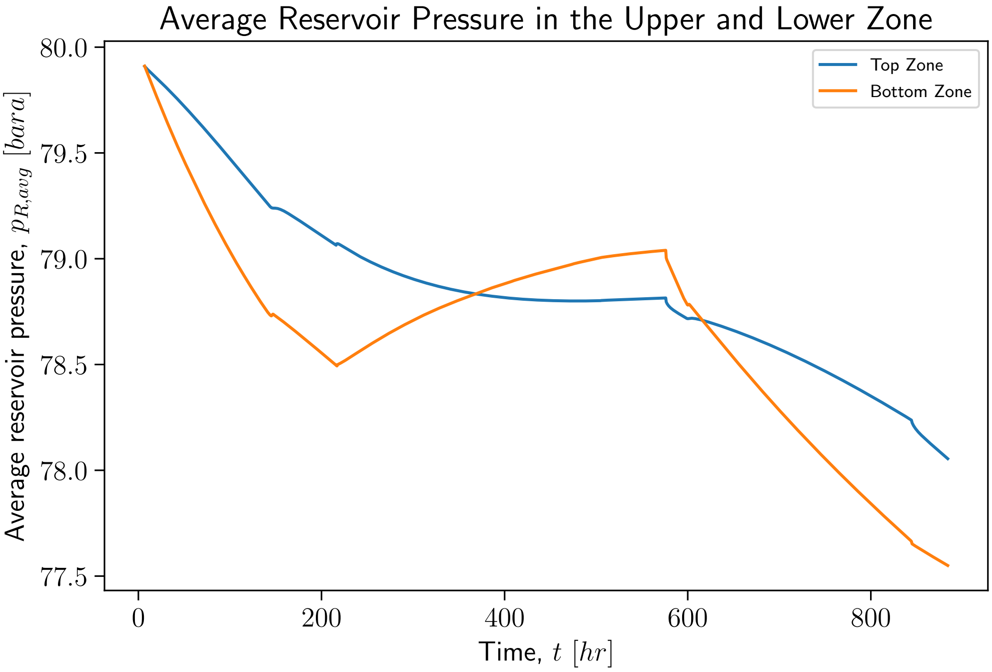

Figure 4.69: Case 1.2c: Average reservoir pressure in the top and bottom zone.

Reduced Wellhead Pressure

The wellhead pressure is reduced to 40 $bara$ to check whether a production strategy with less flow restriction affects the flow behavior and potential crossflow between zones.

Similarly to the reduced wellhead pressure case under **Case 1.2b**, the critical rate is 28,568 Sm^3/d. This is because the cases are identical except for the inflow in the bottom.

Figure 4.70 shows that the bottom zone depletes slightly faster than the top zone initially. Liquid loading starts when the liquid film reverses. The mass rates of gas and oil for each numeric layer are plotted in Figures 4.71 and 4.72, respectively. The gas mass plot shows that every layer has a positive contribution to production, even after liquid loading. The oil plot only shows backflow, except for a small positive spike from numeric layer 11 (the top layer in the top zone).

The liquid holdup and mass rates exhibit similar behavior as in the base case before and after loading, but with different numbers. The mass rates of gas through the top and bottom zones are similar, and most of the oil flows into layer 5 as the top zone reaches equilibrium with the oil saturation. Hence, the holdup below layer 5 is zero.

In conclusion, changing the production strategy when the high-permeable zone is at the bottom does not create crossflow. The reason is that the production from the bottom zone is quickly restricted by the above zone, which maintains a higher pressure. Thus, the pressure difference between the top and bottom zones is not great enough to cause crossflow. An interesting observation is that the stabilized rate post-loading is only 2000 Sm^3/d less than in the base case, but the critical rate is approximately 5000 Sm^3/d less.

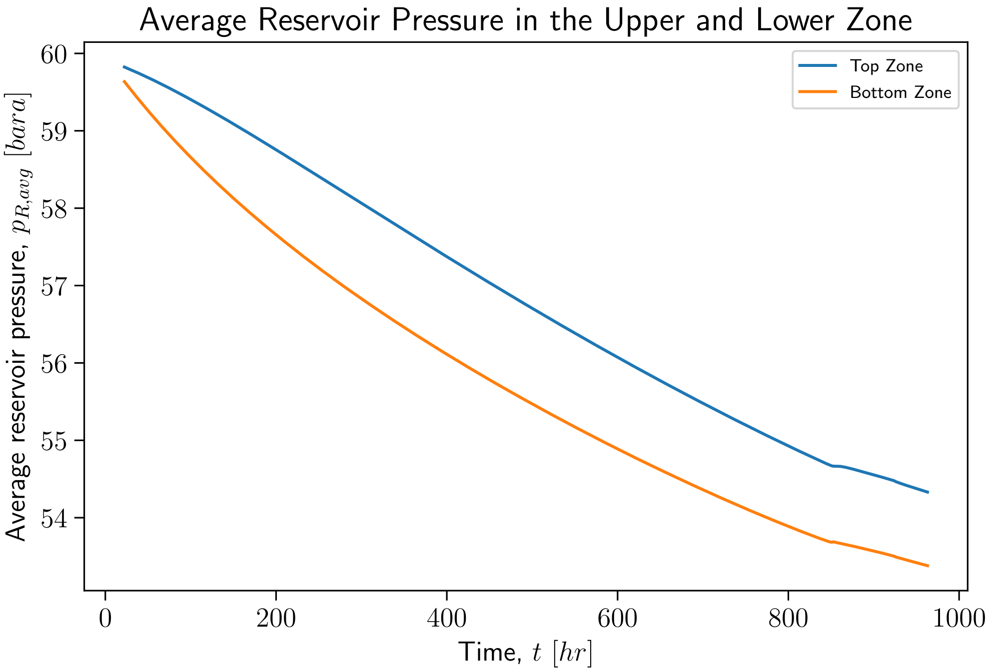

Figure 4.70: Case 1.2c reduced p_{wh}: Average reservoir pressure in the top and bottom zones.

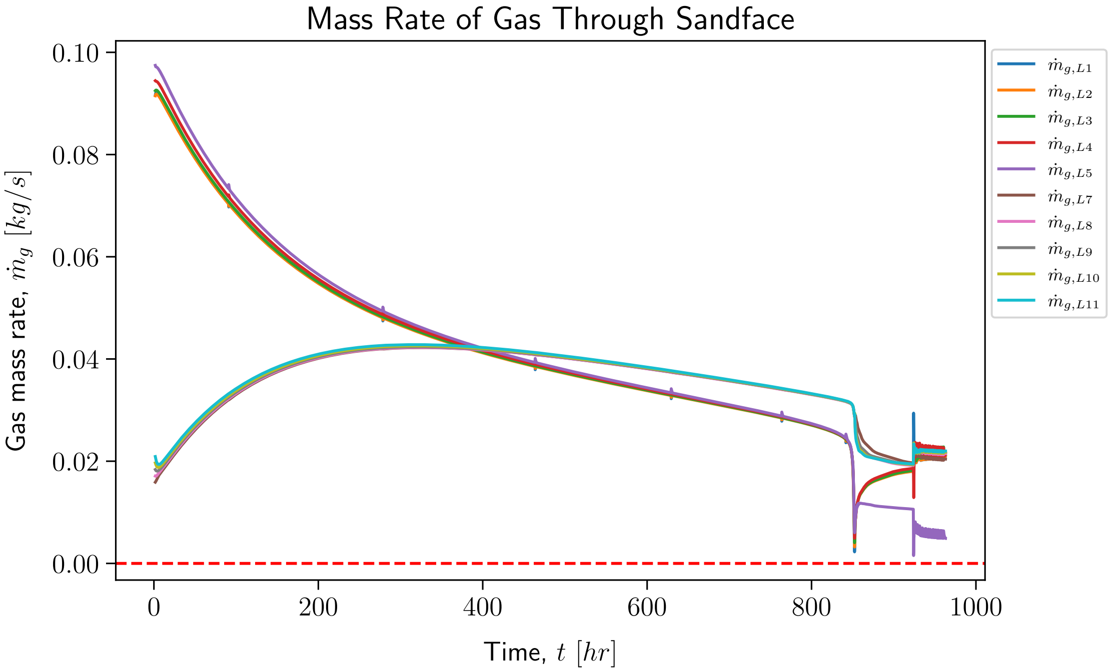

Figure 4.71: Case 1.2c reduced p_{wh}: Mass rates of gas through each numerical layer.

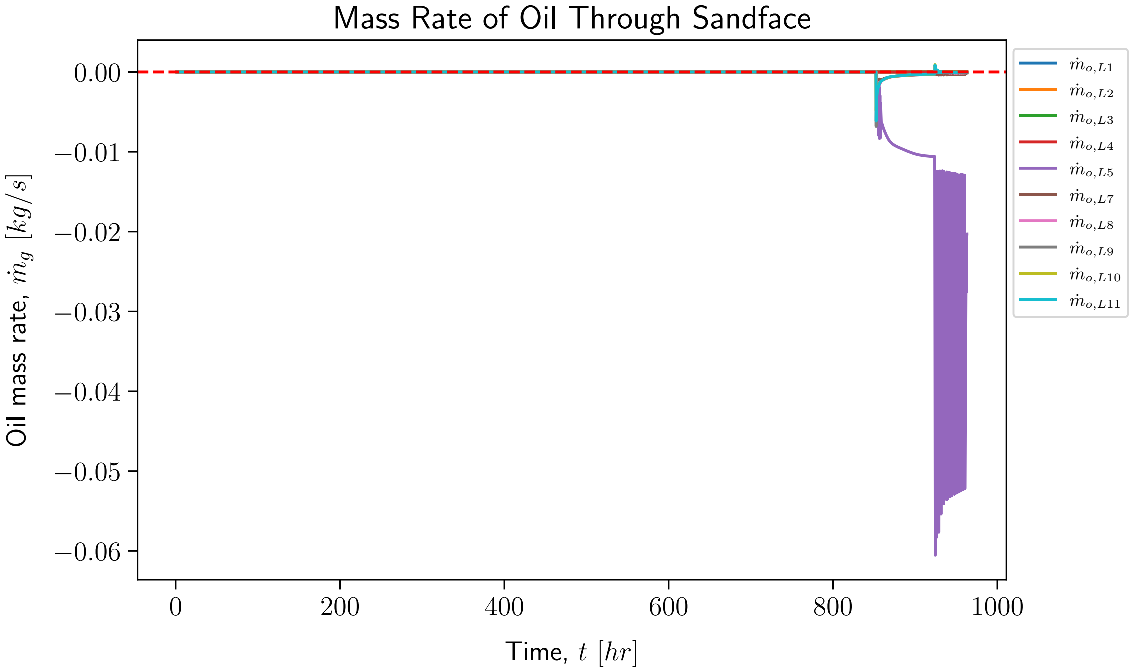

Figure 4.72: Case 1.2c reduced p_{wh}: Mass rates of oil through each numerical layer.

Gas Condensate as Fluid Model

This setup is similar to that in the **base case**. The differences are an updated fluid model with a higher-producing OGR and corresponding changes in temperatures and pressures to prevent condensation within the reservoir, as outlined in Section 3.1.2. This case is also comparable to **Case 1.2b Gas Condensate as Fluid Model** as the only difference from the model is that the upper zone has an isotropic permeability of 10 md and the bottom zone has a permeability of 100 md.

Gas production starts at a higher rate in the bottom zone than in the top zone, as seen in Figures 4.75 and 4.73. The depletion rates are similar, as seen in Figure 4.77; however, the bottom zone depletes slightly more quickly than the top zone during the first 180 hrs. The cumulative mass of gas and oil during different production events is tabulated in Table 4.9.

When the liquid film reverses, the liquid loading is initiated. During the first 9 hrs of liquid loading, the net production of gas from the top zone is 2,610 kg and -8,226 kg from the bottom zone. Figure 4.73 shows negative flow between the reservoir zones and positive flow above the upper zone. This indicates crossflow from the upper zone to the lower zone. A troubling observation is that the mass flow of gas from the bottom zone after the production stabilizes is positive, as seen in Figures 4.75. An explanation for this is that the gas condenses quickly after entering the well, while the well is in a liquid loading state. This makes sense by comparing the mass rates of gas and oil in Figures 4.75 and 4.76. However, a point of confusion is that the temperature increases near the top of the bottom zone, as seen in Figure 4.78. The increase in heat is only observed during slug flow (the temperature increase is not seen when the *advanced particle flow including deposition and entrainment* option is turned off in OLGA); however, the increased temperature should prevent gas condensation. This may indicate that the PVT-table approach is not suitable when the composition at a specific place in time changes significantly during the simulation, as it can do because of condensation and different phase velocities during liquid loading. The temperature increase can also be attributed to latent heat as the gas condenses. This is reasonable since the gas flows through slightly cooled-down oil and condensation releases heat.

The saturation in each numeric layer in the top zone approaches an equilibrium after approximately 9 hrs. After this, the oil backflow rate stabilizes at 0.02 and 0.10 kg/s in the upper and lower zones, respectively. The gas production rate in the top zone decreases monotonically from 0.11 to 0.06 kg/s, while in the lower zone, it increases monotonically from 0.02 to 0.07 kg/s. The pressure in the bottom zone depletes at a slower rate. The reason is that the bottom zone is more affected by the pressure drop in the tubing and has more backflow of oil, even after the gas rates are similar.

Based on the mass rate and pressure data generated by ROCX, the crossflow of gas occurs between the upper and lower zones, but only for approximately 9 hrs. The zones deplete at similar rates. However, when liquid loading is initiated, the backpressure imposed on the reservoir increases. The top zone is first affected by this. The average pressure increases slightly when the backflow of oil occurs. Some of the produced gas travels down and into the bottom zone until a pressure equilibrium with respect to the reservoir pressures and flowing conditions is reached. After this transient period, the surface production rate of gas stabilizes at a rate of 1,780 Sm^3/d, which is approximately 21,000 Sm^3/d less than before liquid loading.

A snapshot of the flow between the reservoir and the well and liquid holdup after liquid loading is shown in Figure 4.79. As seen previously, the top zone (low permeable) has a uniformly distributed inflow of oil and an outflow of gas. Most of the oil flows into the bottom zone through layer 5, which keeps the liquid holdup at zero in the lower layers. The main difference here compared to the base case is that gas continues to flow back through layer 5 for the remaining duration of the simulation.

Table 4.9: Case 2.2c: Cumulative production of gas and oil before the onset of liquid loading, during fluid redistribution, and after production restabilizes.

Cumulative production of gas and oil					
	Time interval $[hours]$	m_g $[kg]$ Top layer	m_g $[kg]$ Bottom layer	m_o $[kg]$ Top layer	m_o $[kg]$ Bottom layer
Before liquid loading	0, 276	263,476	292,669	0	0
During fluid redistribution	276, 285	2,610	-8,226	-941	-1,118
After slug initiation	285, 500	56,556	35,947	-12,091	-75,346

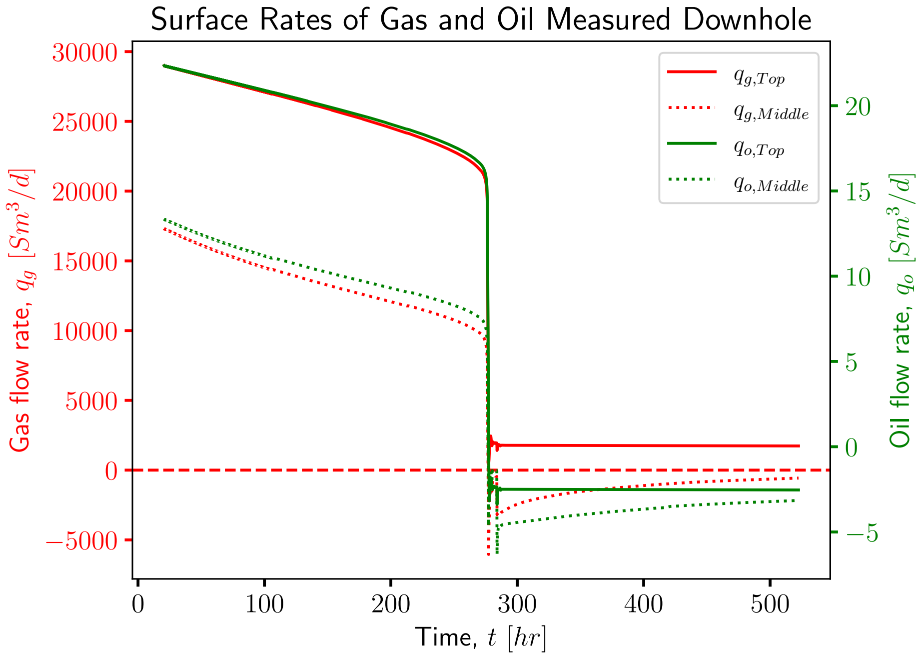

Figure 4.73: Case 1.2c Gas Condensate: Gas and oil rates measured between the reservoir zones and above the top zone, converted to standard condition volumetric rates.

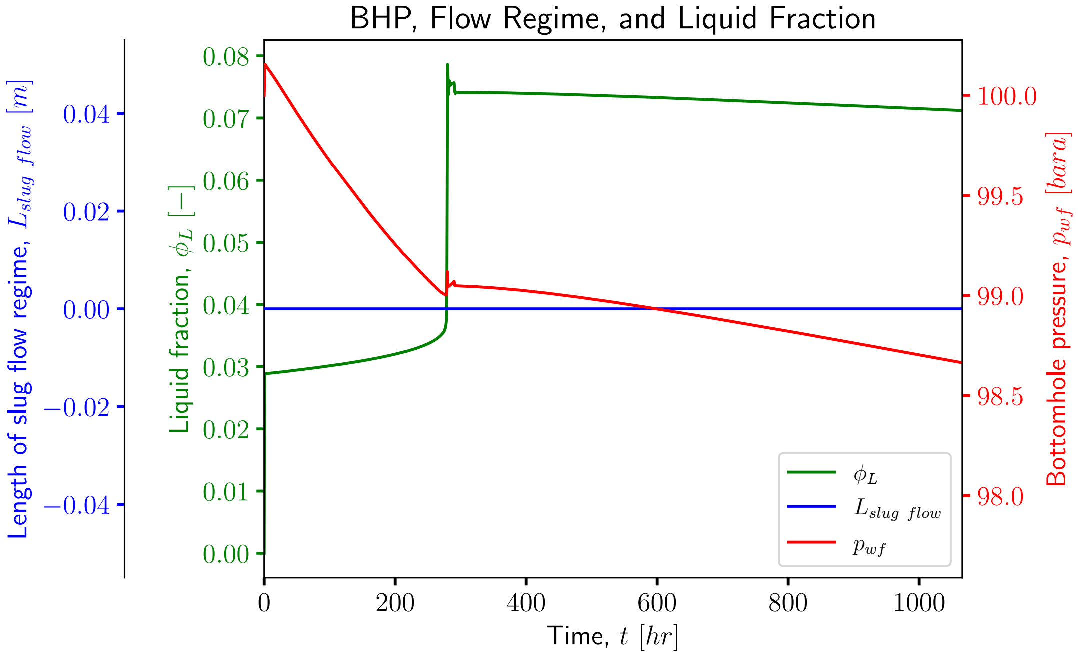

Figure 4.74: Case 1.2c Gas Condensate: Liquid fraction, bottomhole pressure, and length of slug flow regime.

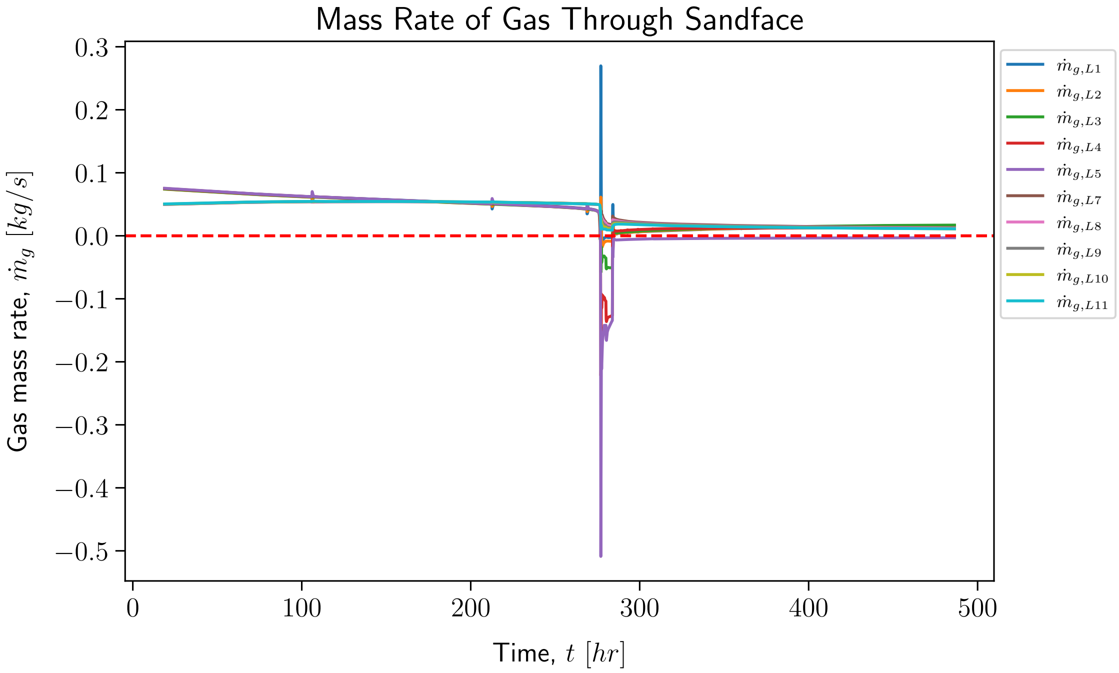

Figure 4.75: Case 1.2c Gas Condensate: Mass rates of gas through every numerical reservoir layer.

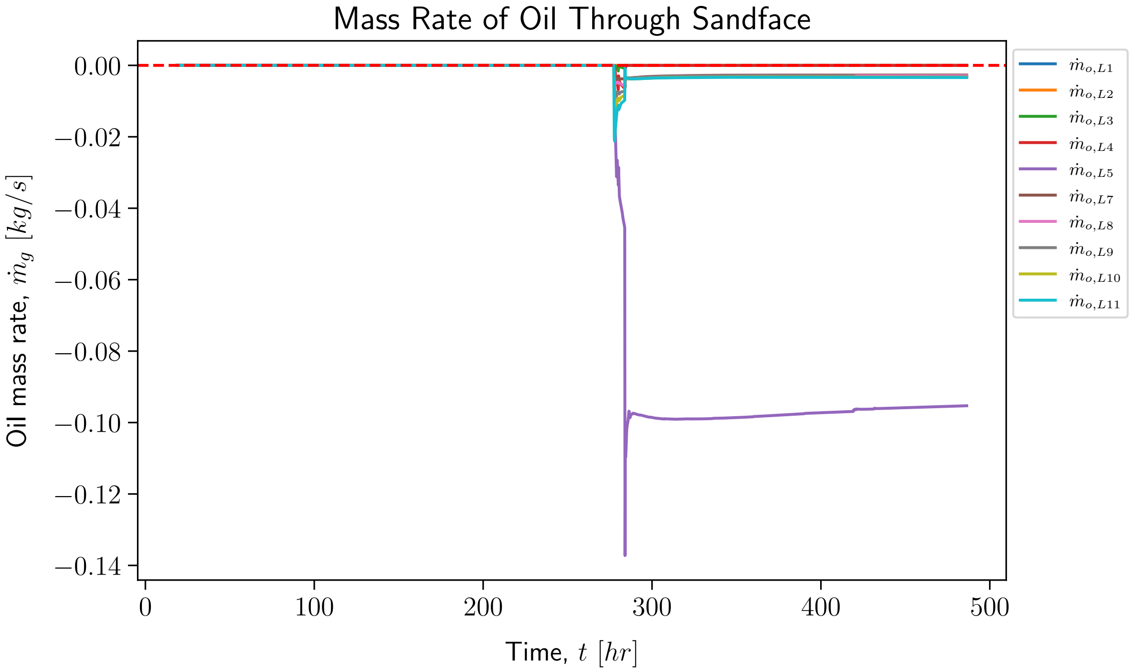

Figure 4.76: Case 1.2c Gas Condensate: Mass rated of oil through every numerical reservoir layer.

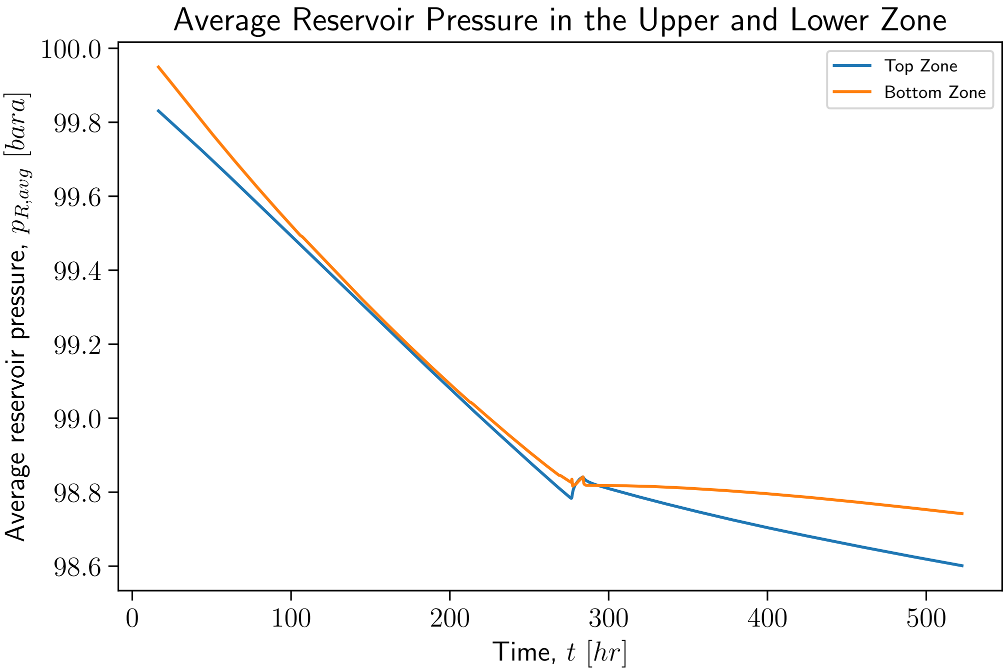

Figure 4.77: Case 1.2c Gas Condensate: Average reservoir pressure in the top and bottom zones.

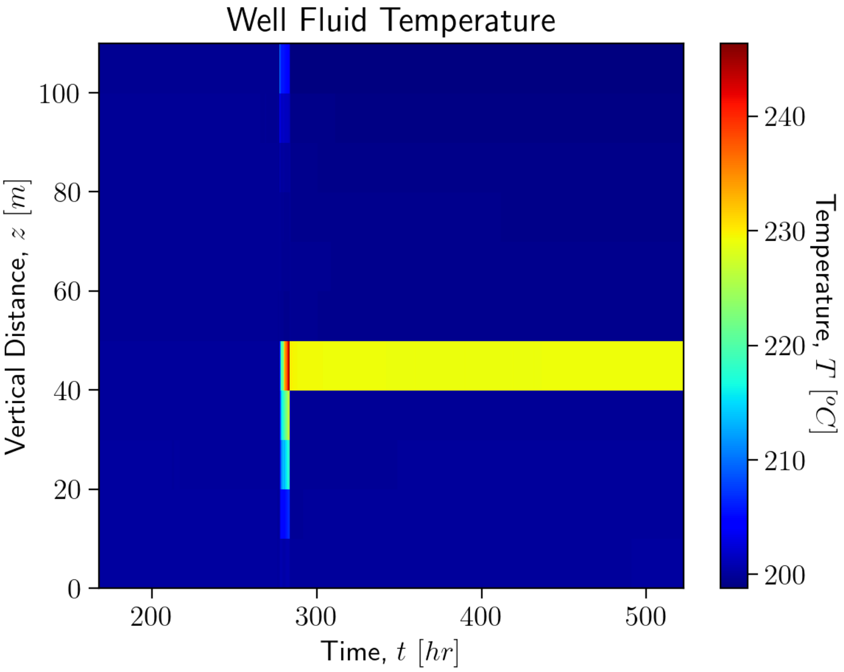

Figure 4.78: Case 1.2c Gas Condensate: Colormap of fluid temperature in the bottom 110 *m* of the well.

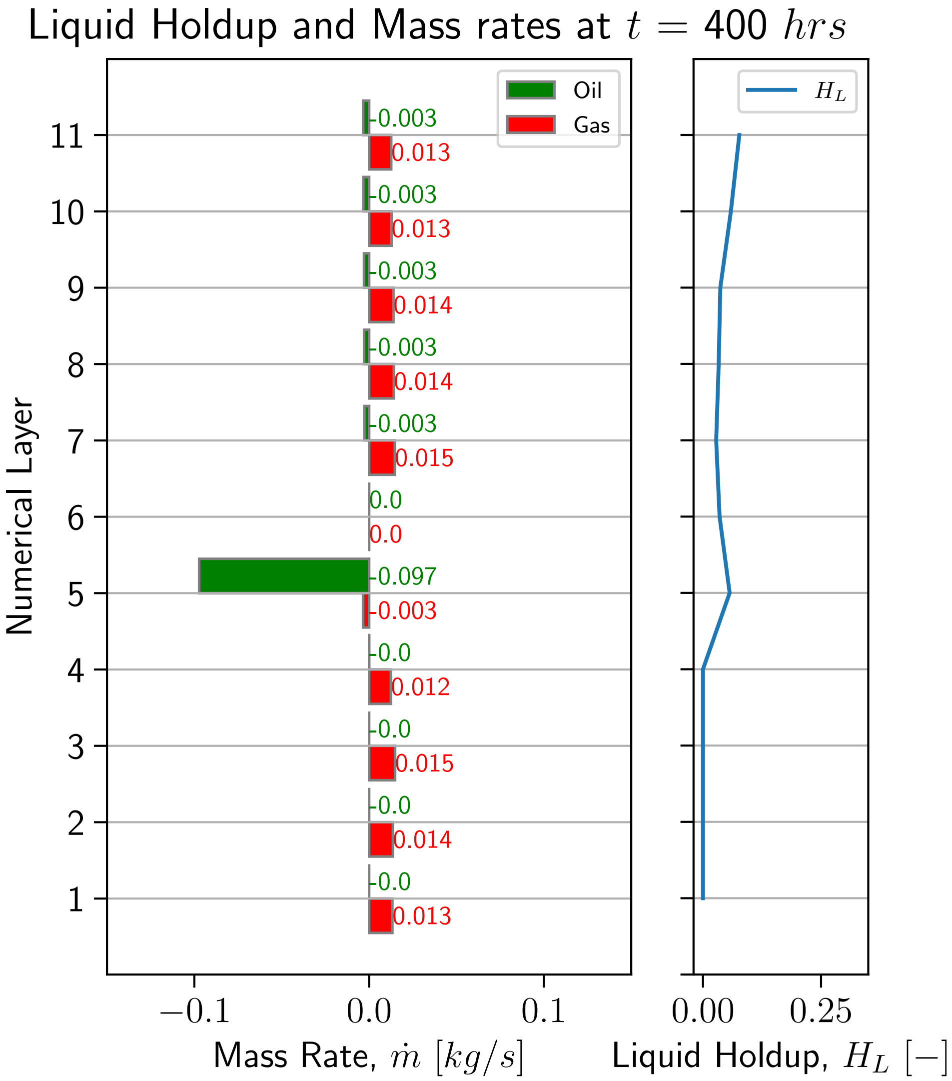

Figure 4.79: Case 1.2c Gas Condensate: Snapshot of mass rates of oil and gas, and liquid holdup during liquid loading.

Reduced Capillary Pressure

This model is identical to the base case, except for the capillary pressure defined as $P_c(S_g) = 0\ bara$ instead of a linear function from 1 to 0 $bara$. The gas and oil mass rates are shown in Figures 4.80 and 4.81, respectively. The plots are similar to those in the base case before liquid loading starts. This is because there are no changes in capillary pressure while the gas saturation is 100%. Figure 4.82 shows that the bottom zone accounts for approximately 20% more gas than the top zone after 150 hrs. In addition, the liquid holdup is zero near the bottom of the well, as seen in every case before liquid loading starts.

After liquid loading starts, the top zone is more productive than the lower zone for approximately 150 hrs. Slug flow does not occur, which is contrary to the expectation, since the oil is not flowing into layers 2-11. Figure 4.83 shows that the liquid holdup is approaching 100% in the bottom layer of the well. Layer 1 accounts for all of the backflow of oil and it has a slight backflow of gas.

This case shows that when capillary pressure is reduced (or removed), oil flow into the reservoir becomes more unlikely. Therefore, the liquid builds up at the bottom of the well and increases the backpressure that acts on the bottom layer of the reservoir. Since the liquid enters at the bottom of the bottom zone, fluid redistribution effects, such as those seen in previous tests and cases, do not occur. The well quickly transitions into steady (non-oscillating) production, similar to that of **Case 1.1 - IPR** in Section 4.1.1.

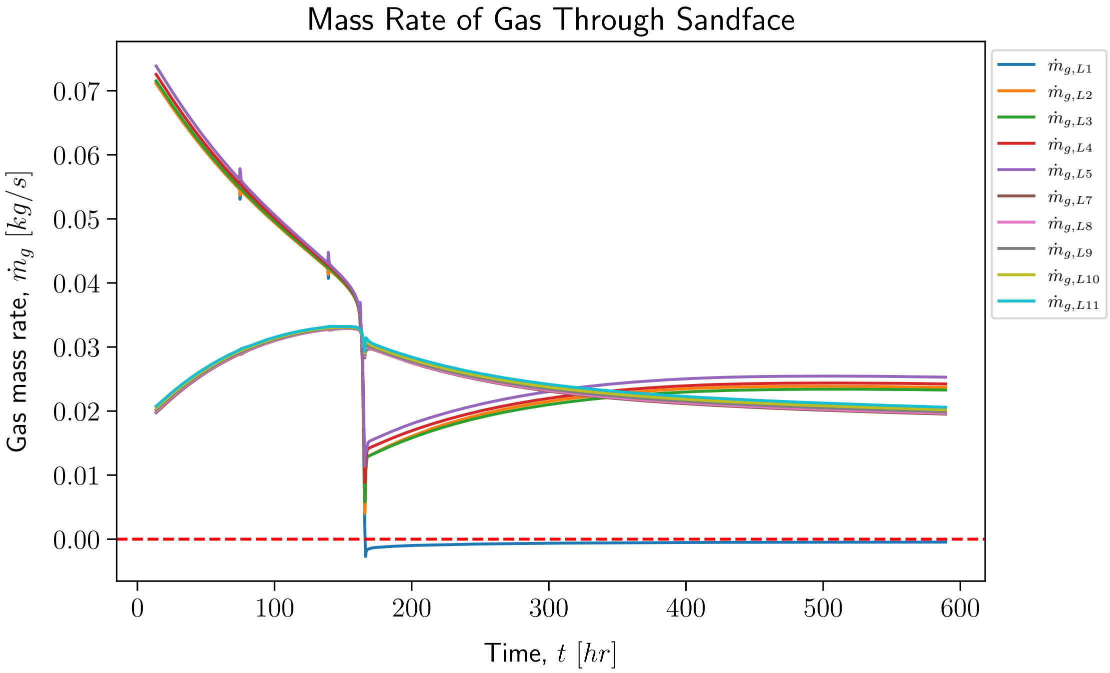

Figure 4.80: Case 1.2c reduced capillary pressure: Mass rates of gas through each numerical layer.

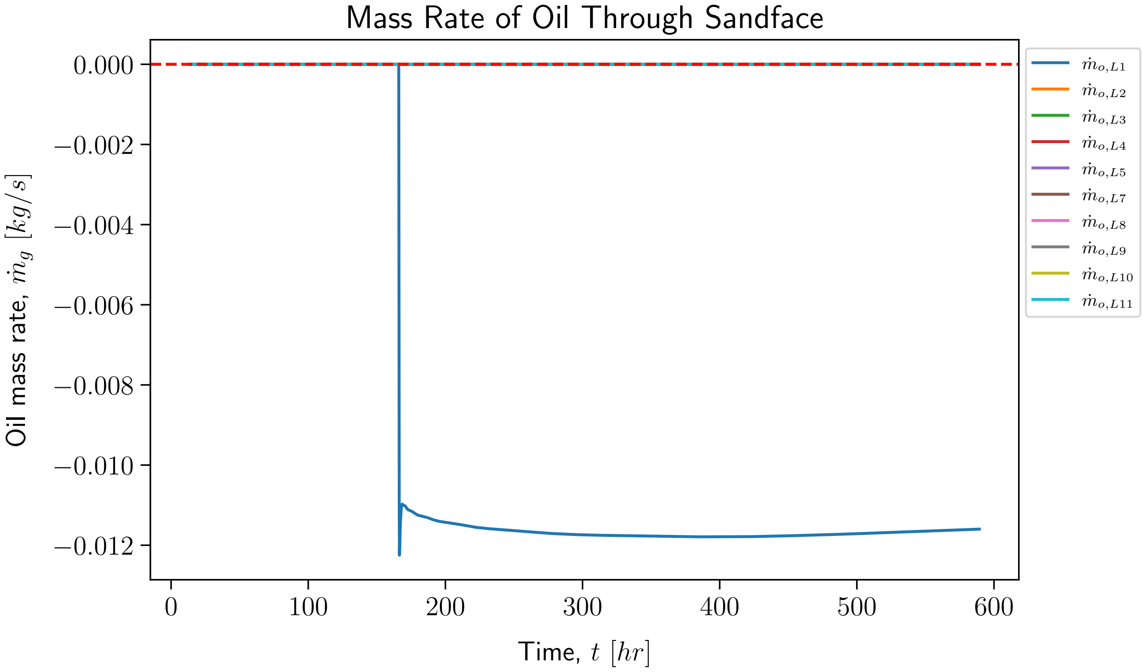

Figure 4.81: Case 1.2c reduced capillary pressure: Mass rates of oil through each numerical layer.

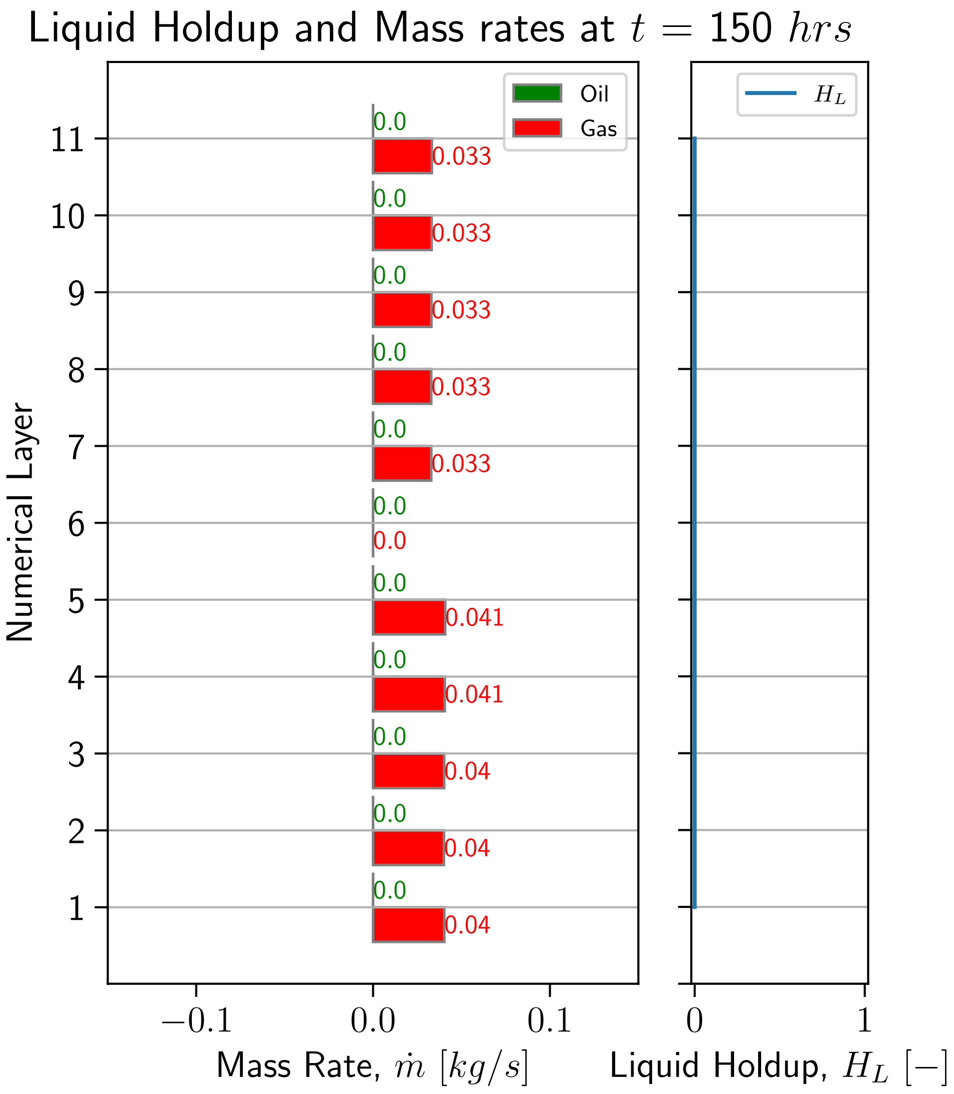

Figure 4.82: Case 1.2c reduced capillary pressure: Snapshot of mass rates of oil and gas, and liquid holdup before liquid loading.

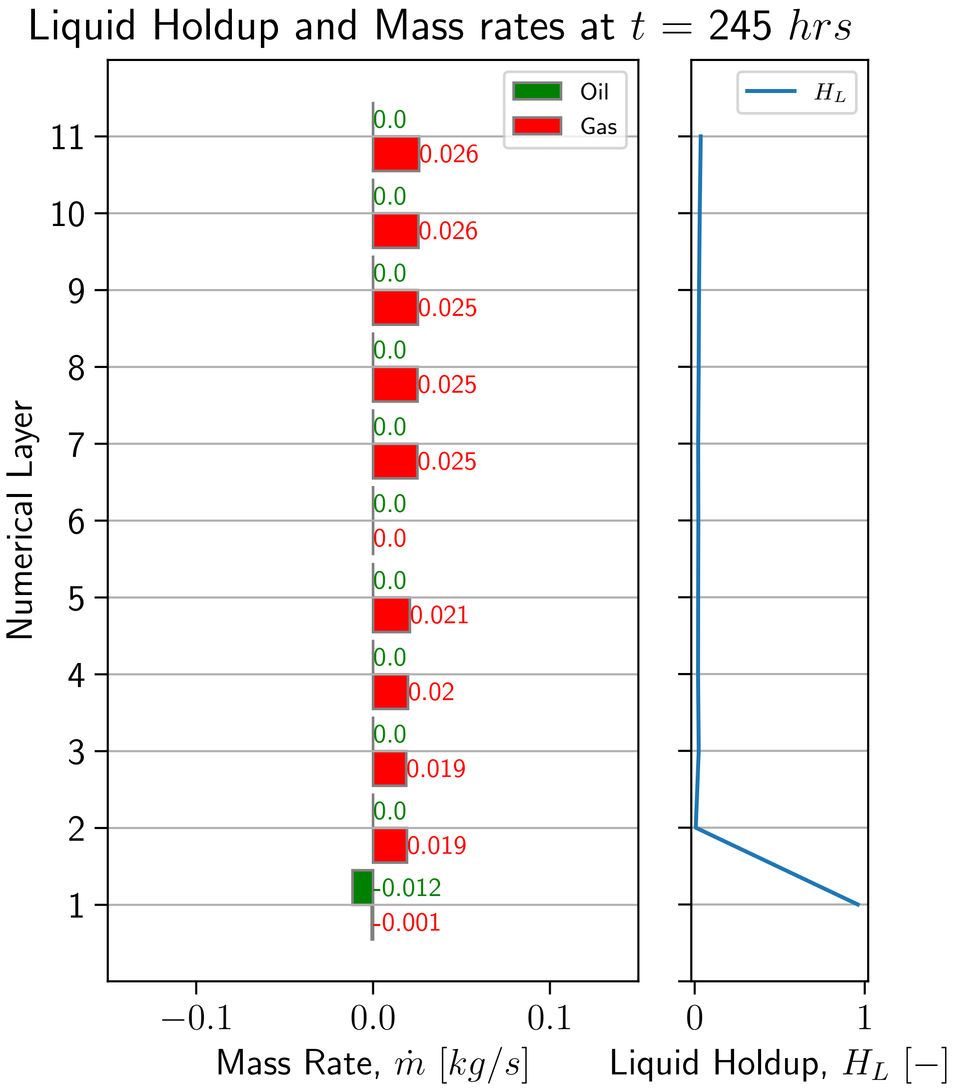

Figure 4.83: Case 1.2c reduced capillary pressure: Snapshot of mass rates of oil and gas, and liquid holdup during liquid loading.

4.2.4 Comparison & Summary

For all cases, the liquid film reversal was the first certain indication that liquid began to accumulate in the well. In addition, the reversal rate was approximately the same for every case with identical completion characteristics. The reservoir did not significantly affect the critical rate, as it is mainly affected by the forces that act on the fluids in the tubing. However, what happens after the liquid starts to accumulate depends greatly on the reservoir and the interplay between the reservoir and the well.

In **Case 1.2a**, there are no signs of natural or forced crossflow between the reservoir zones before or during liquid loading. Only one study was conducted on this model since the top and bottom zones have identical properties, which makes crossflow unlikely, based on the crossflow analysis by Jalali *et al.* [22]. Production in this case, before and after liquid starts to accumulate, resembles **Case 1.1 - ROCX** more than it resembles the other two-zone cases because every layer has a permeability of 10 md. Due to the low permeability defined in the model, liquid accumulates at the bottom of the well and flows into the reservoir mainly through the lowest numerical layers.

In **Case 1.2b**, the top and bottom zones have isotropic permeabilities of 100 md and 10 md, respectively. The base case in Section 4.2.2 shows that the high permeable zone initially produces gas at a much higher rate than the low permeable zone. As liquid loading starts, the low-permeable zone becomes the most productive zone. This is because it is less depleted and is not affected by condensate build-up near the well. Shutting in the well causes gas flow from the bottom zone to the top zone until pressure equilibrium is reached, as seen in Section 4.2.2. When the well is shut in, the liquid flows almost instantly into the high-permeability zone. Reducing the wellhead pressure increases the pressure difference between the zones, as it takes longer for the liquid loading to begin. This makes crossflow more likely to occur, as seen in Section 4.2.2. Changing the fluid model to a more liquid-rich fluid appears to make crossflow more likely, as seen in Section 4.2.2. However, in this case, the crossflow can also be a result of increased depletion. Reducing the capillary pressure caused by gas and oil reduces the injectivity of the reservoir. Oil flows back into the reservoir, but tends to accumulate more in the wellbore than in the other cases. In addition, gas from the bottom zone flows into the top zone late during liquid loading. An interesting observation for every test, except for the reduced capillary pressure test, is that the bottom zone is never in contact with oil, as oil easily flows into the top zone (more specifically layers 11 and 10) because of the high permeability and capillary pressure.

Case 1.2c has the highest permeability in the bottom zone. Crossflow of gas is not observed in the base case in Section 4.2.3. Contrary to **Case 1.2b**, a small oil crossflow is observed that flows from the top to the bottom zone after the top zone is saturated to an equilibrium. When the well is shut in, pressure will equilibrate, causing flow from the top zone to the bottom zone, as seen in Section 4.2.3.

When the wellhead pressure is reduced, crossflow is not observed, as seen in Section 4.2.3. For this to occur, a greater pressure differential between the reservoir zones is needed. A more liquid-rich gas stream, as in Section 4.2.3, appears to increase the chance of crossflow. Reducing the capillary pressure tends to make the reservoir less susceptible to oil backflow. This makes the liquid accumulate at the bottom of the well. Crossflow is not observed in this case. An intriguing observation for all of the test cases, except for the case of reduced capillary pressure, is that the liquid holdup below layer 5 is zero since the oil flows into the high permeable zone rather than further down the well. Another observation is that the bottom zone (high permeability) depletes at a rate similar to the top zone (low permeability), which is contrary to **Case 1.2b**.

In all cases, the gas condenses above the reservoir zones in the tubing, making the top layer the first layer to experience additional backpressure and contact with liquid; hence liquid backflow. The main difference between **Case 1.2b** and **Case 1.2c**, when liquid loading begins, is how production from the two zones is affected by fluid redistribution and the interplay between zones and well. In cases where the top zone has the greatest permeability, the bottom zone is not in contact with liquid since the top zone is capable of storing all of the backflow (unless capillary pressure is reduced). When the top zone has the lowest permeability, the liquid flows progressively through each numerical layer until it reaches a high-permeability layer, which delays the onset of slug flow. In addition, the liquid redistributes to an equilibrium in the low-permeability zone. After this, the bottom zone accounts for most of the liquid backflow, since oil flows more easily into the high-permeability reservoir zone than down the well while there is gas flow from below. In the simulations conducted, the high-permeable zone does not reach equilibrium with respect to the liquid saturation, probably because not enough time is given or an insufficient volume of condensate is produced.

Another notable difference between **Case 1.2b** and **Case 1.2c** is how liquid loading affects production differently. The onset occurs approximately at the same rate, but the metastable rates while loading are 11,700 and 21,905 Sm^3/d for cases 1.2b and 1.2c, respectively. This indicates that when a high-permeable zone is above a low-permeable zone, the liquid loading reduces the total production more than if the low-permeable zone is on top. Since oil readily flows into the high-permeable zone when capillary pressure is defined, the bottom zone remains unaffected by condensate buildup. This means that if deliquefication techniques are deployed to stop the well from accumulating liquid (and remove the liquid), the bottom zone (if low-permeable) will produce as if the well had never experienced liquid loading (no formation damage).

The onset of liquid loading occurs after 150 and 146 hrs for **Case 1.2b** and **Case 1.2c**, respectively. As discussed above, what happens after the liquid starts to accumulate is also different. Without any optimization, **Case 1.2b** produces 384,383 kg of gas in 500 hrs. **Case 1.2c** produces 482,990 kg of gas in 500 hrs. This indicates that production can be optimized, at least for the case where the top zone is the high-permeability zone, without the use of artificial lift. A suggested method is to isolate the zones and regulate a valve such that they deplete at more similar rates.

During normal production, the reservoir pressure is higher than the well pressure for both gas and oil, as seen by conventional pressure profiles. When liquid loading starts and oil is in contact with the reservoir, the pressure profile quickly changes to a U-shaped curve where the wellbore pressure is greater than the near-wellbore reservoir pressure (highly related to capillary pressure), similar to the observations of Zhang *et al.* [18]. This promotes the backflow of oil (condensate). The flow of gas in the vicinity of the well is restricted by the changes in mobility and capillary pressure caused by oil saturation. It appears that the reservoir zones in contact with oil will always be affected by changes in saturation because some condensate gets trapped. Some zones (low permeability in the top zone) reach equilibrium with the oil flowing in and out of the reservoir. This is seen by the shifted U-shaped curves.

In summary, if two reservoir zones have different properties, liquid loading affects each zone differently and the surface production rate can be greatly affected by this. If the high-permeable zone is at the bottom, the production of each zone appears to self-regulate more than in the opposite case. When liquid loading starts, both reservoir zones will be permanently affected by condensate in the vicinity of the wellbore. Ideally, liquid loading should be prevented before it starts, but if it goes unnoticed, the well will continue to produce at a moderate rate. If the high-permeable zone is on top, then the top zone will deplete faster than the bottom zone. If liquid loading starts, production rates are severely reduced, but condensate does not necessarily flow to the low-permeable zone.

4.3 Optimized Production from Two Reservoir Zones

Observations show that the reservoir zones deplete at different rates when they have different properties. During liquid loading, the metastable gas production rate is almost 50% lower in the case where the high permeability zone is the top zone, as compared to the high permeability in the bottom zone. This indicates that production can be optimized without the use of artificial lift by zonal isolation and valves regulating the flow from each zone. Flow from the bottom zone can be restricted using a downhole valve, but this might only increase the overall production of gas if the high-permeable zone is at the bottom.

4.3.1 Optimization of Case 1.2b by Zonal Isolation

The top and bottom zones are isolated by installing two separate tubing strings with valves to regulate the flow of each zone. The tubing strings are connected to the main production tubing. The valve on the tubing that controls the flow from the high-permeability zone is regulated by a PID controller that keeps the gas rate slightly higher than the critical rate. The valve in the low-permeability zone is kept fully open. When the PID controller is unable to maintain steady production above the setpoint value, it opens the valve fully.

Figure 4.84 shows the mass rates through each numerical layer. The valve regulating the high-permeability zone fully opens after approximately 100 hrs, as seen by the increase in gas rate. Liquid loading starts after 154 hrs, similar to the onset time in the base case in Section 4.2.2. In 500 hrs of production, the total mass of gas produced is 489,714 kg. This is similar to the total mass production of **Case 1.2c** in Section 4.2.3 which was 482,990 kg. It is also significantly higher than in **Case 1.2b**, which was only 384,383 kg. By isolating the zones and regulating the flow, the high-permeable top zone is restricted from flowing freely, similar to when the high-permeable zone is at the bottom. Therefore, production increases while the well is in a loaded state, compared to **Case 1.2b**.

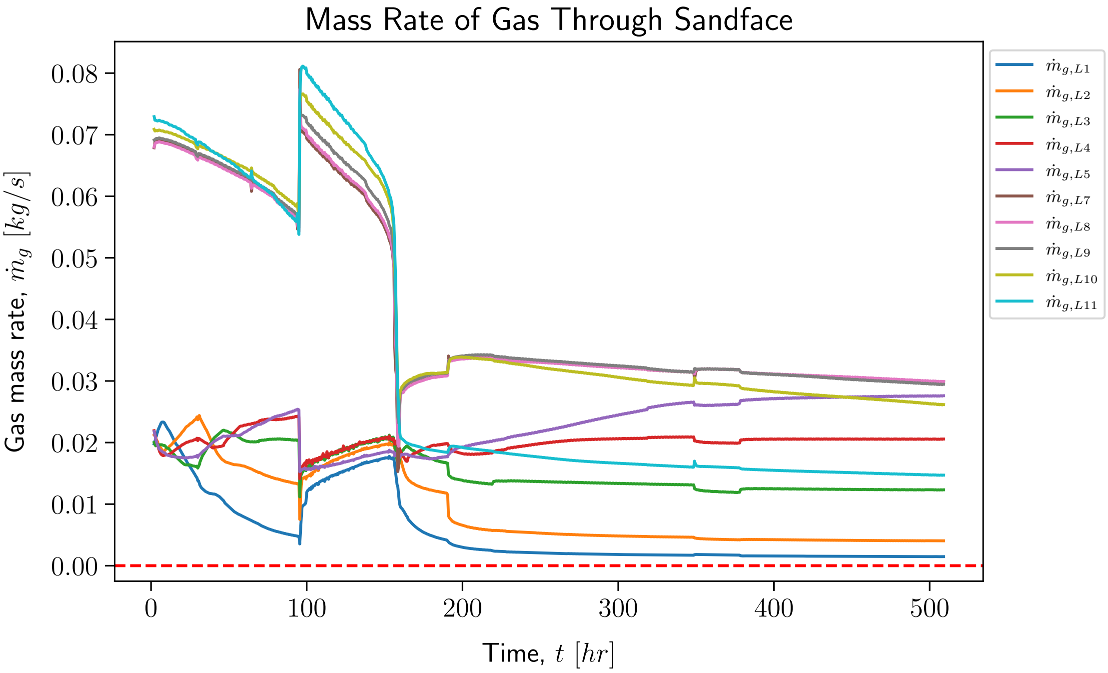

Figure 4.84: Case 1.2b by Zonal Isolation: Mass rates of gas through each numerical layer.

4.3.2 Optimization of Case 1.2c by Zonal Isolation

This setup is similar to the previous case. The only difference is that the bottom zone has the highest permeability and thus is regulated by the controller.

Figure 4.85 shows the mass rates through each numerical layer. Oscillations early in production are caused by the valve, which is constantly regulated by the PID to produce gas slightly at a rate higher than the critical rate. The valve regulating the high-permeability zone fully opens after approximately 182 hrs. The total gas production during 500 *hrs* of production is 481,269 *kg*. This is 0.4% less than in the base case in Section 4.2.3. This indicates that when the bottom zone is more permeable than the top zone, the production from each zone is naturally optimized. This result might be affected by the PID controller not maintaining steady flow during the first 50 *hrs* of production.

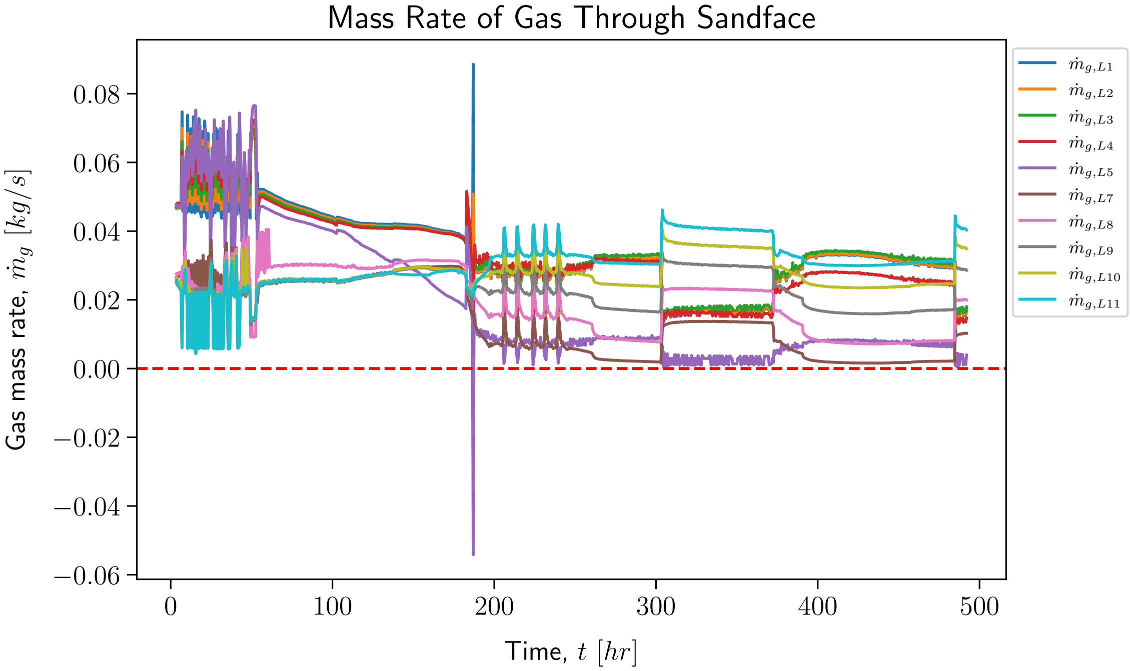

Figure 4.85: Case 1.2c by Zonal Isolation: Mass rates of gas through each numerical layer.

4.3.3 Optimization of Case 1.2c by Downhole Valve

The setup is identical to the base case in Section 4.2.3, except for a downhole valve installed between the reservoir zones. The valve is regulated by a PID controller to produce the same rate of gas from each reservoir zone. When this becomes impossible, the valve opens completely.

Figure 4.86 shows the mass rates of gas. The valve opens fully after approximately 80 *hrs* as the PID controller is not perfectly tuned. The total gas production during the first 500 *hrs* is 486,504 *kg*, which is only 0.7% more than in the base case. The slight increase can be attributed to a slight increase in production from the top zone, as liquid loading starts after 160 *hrs*.

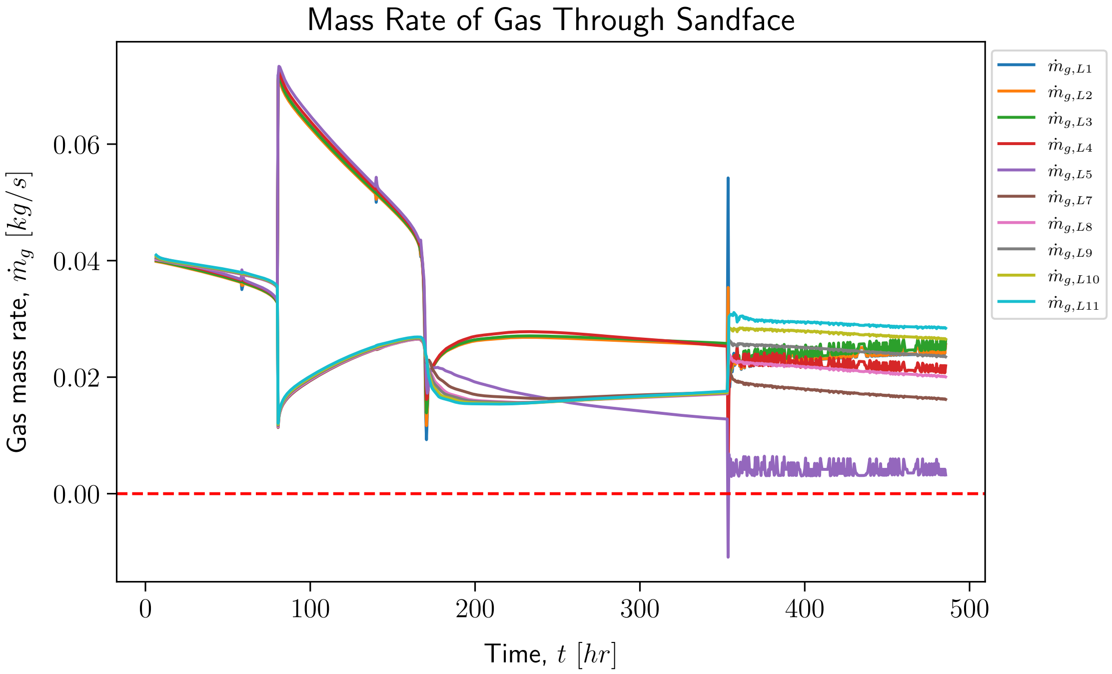

Figure 4.86: Case 1.2b Downhole Valve: Mass rates of gas through each numerical layer.

4.3.4 Comparison & Summary

Without the use of an artificial lift, the suggestion was to deplete the reservoir zones at similar rates using downhole equipment. The downhole valve is set to regulate in such a way that the gas flow rate is greater than the critical rate. Without the use of zonal isolation, a downhole valve was installed between the reservoir zones when the bottom zone is the high-permeability zone. This made only a slight difference to the total production. Zonal isolation affects total production by 0.7% when the high-permeable zone is at the bottom. The case with a high-permeable top zone is greatly affected by zonal isolation as total production increases by 27%.

Chapter 5

Conclusion

The objective of the study was to clarify the concept of liquid loading and how the interaction between the reservoir and the well affects production during the phenomenon. Additional emphasis is placed on multilayered reservoirs with different properties to study the interplay between liquid loading, crossflow, and overall production. The study also assesses the pros and cons of using steady-state or transient reservoir descriptions.

The key findings on the use of ROCX and IPR as inflow are listed below.

- Reversal of the liquid film is the first definite indication of liquid loading.
- The use of ROCX and IPR to model reservoir flow provides similar results in predicting the onset of liquid loading. However, ROCX is superior when modeling multilayered reservoirs that include heterogeneities and transient state events such as liquid loading and crossflow. The IPR model is easier to define, but is incapable of accounting for transient flow and does not provide reservoir data such as pressures, temperatures, and saturations.
- ROCX can be used to estimate the depletion rate, which can be crucial in estimating recovery and production from multilayered reservoirs.
- ROCX can be used to study fluid redistribution, backflow, and crossflow. This can help address the location of damaged zones due to condensate buildup (or banking) and how it affects flow through the sandface.
- The Turner critical rate is similar to the droplet reversal rate generated by OLGA when liquid loading begins. To estimate the critical gas velocity, the equation should be modified by a slip relation.
- The IPR-defined inflow is normally more computationally efficient than ROCX.

Reservoir zones with different properties affect total production differently, especially during transient events. Some of the key findings are listed below:

- Reservoir zones with a permeability of 100 *md* and 10 *md* affect the total production of gas and oil differently. The high-permeability zone tends to deplete faster, especially if it is located above the low-permeability zone. If it is located below the low-permeability zone, production is slightly restricted and the zones deplete at more similar rates.

- Crossflow is driven by a difference in pressure between adjacent reservoir zones. The likelihood of crossflow increases when the high-permeability zone is above the low-permeability zone because of different depletion rates.
- Reducing the wellhead pressure increases the chance of crossflow since the reservoir zones are more depleted at the onset of liquid loading.
- Denser and wetter fluid compositions increase the chance of crossflow.
- The critical rate appears to be unaffected by the relative location (top or bottom) of reservoir zones with different properties. The time it takes to reach the critical rate is slightly affected by the location.
- When the capillary pressure is defined, the oil tends to flow back through the upper layers and progressively makes its way down the reservoir as the phase pressures in the numerical layers change due to changes in saturation. The low-permeability layers reach equilibrium with saturation within a couple of days of simulation time. Oil flows easily into the high-permeable layers and prevents liquid buildup at the bottom of the well. When capillary pressure is removed, oil flows less efficiently into the reservoir and builds up at the bottom of the well.
- How total production is affected by liquid loading depends on the location of the reservoir zones with different properties. When the high-permeable zone is at the top, the bottom zone is not in contact with oil, as it flows readily into the top zone. The metastable production rate post-loading is approximately 50% lower in the case with the high permeability on top as opposed to on the bottom.
- If an artificial lift is unavailable, gas production may still be optimized by isolating the reservoir zones and tuning the rate at which they produce. This only works when the high-permeability zone is above the low-permeability zone. This mainly affects the metastable rate during liquid loading.

In conclusion, this study sheds light on liquid loading and the interactions between the reservoir and the well during transient events. Suggested future work is listed below:

- Use real-world reservoir or experiment data to check whether the key findings are plausible.
- Test the impact on liquid loading using different reservoir properties. A sensitivity study is suggested, where relative permeabilities, capillary pressures, porosity, thermal properties, rock compressibility, initial saturations, etc. are systematically changed.
- Conduct a study with different fluid models, e.g. gas/water or gas/oil/water.
- Use BO-model instead of PVT file (or compositional tracking if available in an updated version of ROCX).
- Simulate liquid loading but include deliquefication techniques such as gas lift, tapered tubing, etc.
- Will the flow dynamics in a gas/water system cause water build-up from the

bottom of the well instead of flowing into the high permeable zone?

- Model the reservoir zones with heterogeneity (variation in properties within the reservoir zones).
- Make an inclined well and study the liquid loading. Is crossflow possible between different zones within the same lateral? Is it possible for two separate laterals connected through the well?
- Reducing the capillary pressure of gas and oil increases the pressure required to force oil from the well to the reservoir; How does it affect the flow in the well? Is there a limit to the use of surfactants (through injection, etc.) where the recovery gained from the reservoir decreases production since the gas becomes unable to lift liquid (because of less interfacial tension)?

Bibliography

[1] L. R. James Lea Jr., *Gas Well Deliquification 3rd Edition*. Gulf Professional Publishing, 2019.

[2] R. Turner, M. Hubbard, and A. Dukler, "Analysis and Prediction of Minimum Flow Rate for the Continuous Removal of Liquids from Gas Wells," *Journal of Petroleum Technology*, vol. 21, no. 11, pp. 1475–1482, Nov. 1969, ISSN: 0149-2136. DOI: `10.2118/2198-PA`. eprint: `https://onepetro.org/JPT/article-pdf/21/11/1475/2221983/spe-2198-pa.pdf`. [Online]. Available: `https://doi.org/10.2118/2198-PA`.

[3] *A New Approach for Accurate Prediction of Loading in Gas Wells Under Different Flowing Conditions*, vol. All Days, SPE Oklahoma City Oil and Gas Symposium / Production and Operations Symposium, SPE-37408-MS, Mar. 1997. DOI: `10.2118/37408-MS`. eprint: `https://onepetro.org/SPEOKOG/proceedings-pdf/97POS/All-97POS/SPE-37408-MS/1938697/spe-37408-ms.pdf`. [Online]. Available: `https://doi.org/10.2118/37408-MS`.

[4] *New View on Continuous-Removal Liquids from Gas Wells*, vol. All Days, SPE Permian Basin Oil and Gas Recovery Conference, SPE-70016-MS, May 2001. DOI: `10.2118/70016-MS`. eprint: `https://onepetro.org/SPEPBOGR/proceedings-pdf/01OGR/All-01OGR/SPE-70016-MS/2951680/spe-70016-ms.pdf`. [Online]. Available: `https://doi.org/10.2118/70016-MS`.

[5] D. Zhou and H. Yuan, "A New Model for Predicting Gas-Well Liquid Loading," *SPE Production & Operations*, vol. 25, no. 02, pp. 172–181, Apr. 2010, ISSN: 1930-1855. DOI: `10.2118/120580-PA`. eprint: `https://onepetro.org/PO/article-pdf/25/02/172/2119134/spe-120580-pa.pdf`. [Online]. Available: `https://doi.org/10.2118/120580-PA`.

[6] R. P. Sutton, S. A. Cox, J. F. Lea, and O. L. Rowlan, "Guidelines for the Proper Application of Critical Velocity Calculations," *SPE Production & Operations*, vol. 25, no. 02, pp. 182–194, Apr. 2010, ISSN: 1930-1855. DOI: `10.2118/120625-PA`. eprint: `https://onepetro.org/PO/article-pdf/25/02/182/2119408/spe-120625-pa.pdf`. [Online]. Available: `https://doi.org/10.2118/120625-PA`.

[7] S. B. Coleman, H. B. Clay, D. G. McCurdy, and I. Norris Lee H., “A New Look at Predicting Gas-Well Load-Up,” *Journal of Petroleum Technology*, vol. 43, no. 03, pp. 329–333, Mar. 1991, ISSN: 0149-2136. DOI: `10.2118/20280-PA`. eprint: `https://onepetro.org/JPT/article-pdf/43/03/329/2223107/spe-20280-pa.pdf`. [Online]. Available: `https://doi.org/10.2118/20280-PA`.

[8] C. A. Veeken and S. P. Belfroid, “New Perspective on Gas-Well Liquid Loading and Unloading,” *SPE Production & Operations*, vol. 26, no. 04, pp. 343–356, Jun. 2011, ISSN: 1930-1855. DOI: `10.2118/134483-PA`. eprint: `https://onepetro.org/PO/article-pdf/26/04/343/2121022/spe-134483-pa.pdf`. [Online]. Available: `https://doi.org/10.2118/134483-PA`.

[9] J. van ’t Westende, H. Kemp, R. Belt, L. Portela, R. Mudde, and R. Oliemans, “On the role of droplets in cocurrent annular and churn-annular pipe flow,” *International Journal of Multiphase Flow*, vol. 33, no. 6, pp. 595–615, 2007, ISSN: 0301-9322. DOI: `https://doi.org/10.1016/j.ijmultiphaseflow.2006.12.006`. [Online]. Available: `https://www.sciencedirect.com/science/article/pii/S0301932206001996`.

[10] J. M. C. Van’t Westende, “Droplets in annular-dispersed gas-liquid pipe-flows,” 2008.

[11] K. Veeken, B. Hu, and W. Schiferli, “Gas-Well Liquid-Loading-Field-Data Analysis and Multiphase-Flow Modeling,” *SPE Production & Operations*, vol. 25, no. 03, pp. 275–284, May 2010, ISSN: 1930-1855. DOI: `10.2118/123657-PA`. eprint: `https://onepetro.org/PO/article-pdf/25/03/275/2119278/spe-123657-pa.pdf`. [Online]. Available: `https://doi.org/10.2118/123657-PA`.

[12] S. Breimoen, “Liquid loading of gas wells,” 2022.

[13] *Petroleum Production Systems*, Oct. 2022.

[14] F. MJ, “The isochronal testing of oil wells,” vol. SPE paper No. 4529, 1973.

[15] A. J. Ghajar, “Flow patterns, flow pattern maps, and flow pattern transition models,” in *Single- and Two-Phase Flow Pressure Drop and Heat Transfer in Tubes*. Cham: Springer International Publishing, 2022, pp. 141–165, ISBN: 978-3-030-87281-6. DOI: `10.1007/978-3-030-87281-6_14`. [Online]. Available: `https://doi.org/10.1007/978-3-030-87281-6_14`.

[16] *A Dynamic Model for Simulation of Integrated Reservoir, Well and Pipeline System*, vol. All Days, SPE Annual Technical Conference and Exhibition, SPE-147053-MS, Oct. 2011. DOI: `10.2118/147053-MS`. eprint: `https://onepetro.org/SPEATCE/proceedings-pdf/11ATCE/All-11ATCE/SPE-147053-MS/1659190/spe-147053-ms.pdf`. [Online]. Available: `https://doi.org/10.2118/147053-MS`.

[17] *Integrated Wellbore/Reservoir Model Predicts Flow Transients in Liquid-Loaded Gas Wells*, vol. All Days, SPE Annual Technical Conference and Exhibition, SPE-110461-MS, Nov. 2007. DOI: `10.2118/110461-MS`. eprint: `https://onepetro.org/SPEATCE/proceedings-pdf/07ATCE/All-07ATCE/SPE-110461-MS/2764257/spe-110461-ms.pdf`. [Online]. Available: `https://doi.org/10.2118/110461-MS`.

[18] H. Zhang, G. Falcone, and C. Teodoriu, "Modeling fully transient two-phase flow in the near-wellbore region during liquid loading in gas wells," *Journal of Natural Gas Science and Engineering*, vol. 2, no. 2, pp. 122–131, 2010, ISSN: 1875-5100. DOI: `https://doi.org/10.1016/j.jngse.2010.04.005`. [Online]. Available: `https://www.sciencedirect.com/science/article/pii/S1875510010000314`.

[19] PetroWiki. "Condensate banking." (), [Online]. Available: `https://petrowiki.spe.org/Glossary:Condensate_banking` (visited on 05/05/2023).

[20] *Liquid Loading in Gas Wells: from Core-Scale Transient Measurements to Coupled Field-Scale Simulations*, Journal of Petroleum Science and Engineering, Aug. 2017. DOI: `10.1016/j.petrol.2017.08.025`.

[21] 2. S. Limited. "Crossflow." (), [Online]. Available: `https://glossary.slb.com/en/terms/c/crossflow` (visited on 05/01/2023).

[22] M. Jalali, J.-M. Embry, F. Sanfilippo, F. J. Santarelli, and M. B. Dusseault, "Cross-flow analysis of injection wells in a multilayered reservoir," *Petroleum*, vol. 2, no. 3, pp. 273–281, 2016, ISSN: 2405-6561. DOI: `https://doi.org/10.1016/j.petlm.2016.05.005`. [Online]. Available: `https://www.sciencedirect.com/science/article/pii/S2405656116300013`.

[23] *Olga help*, Schlumberger, 2020.

[24] W. McCain, *The Properties of Petroleum Fluids*. PennWell Books, 1990, ISBN: 9780878143351. [Online]. Available: `https://books.google.no/books?id=EWxUFzW61wkC`.

[25] J. Lasater, "Bubble Point Pressure Correlation," *Journal of Petroleum Technology*, vol. 10, no. 05, pp. 65–67, May 1958, ISSN: 0149-2136. DOI: `10.2118/957-G`. eprint: `https://onepetro.org/JPT/article-pdf/10/05/65/2238926/spe-957-g.pdf`. [Online]. Available: `https://doi.org/10.2118/957-G`.

[26] M. Vasquez and H. Beggs, "Correlations for Fluid Physical Property Prediction," *Journal of Petroleum Technology*, vol. 32, no. 06, pp. 968–970, Jun. 1980, ISSN: 0149-2136. DOI: `10.2118/6719-PA`. eprint: `https://onepetro.org/JPT/article-pdf/32/06/968/2226793/spe-6719-pa.pdf`. [Online]. Available: `https://doi.org/10.2118/6719-PA`.

[27] O. Glaso, “Generalized Pressure-Volume-Temperature Correlations,” *Journal of Petroleum Technology*, vol. 32, no. 05, pp. 785–795, May 1980, ISSN: 0149-2136. DOI: `10.2118/8016-PA`. eprint: `https://onepetro.org/JPT/article-pdf/32/05/785/2227185/spe-8016-pa.pdf`. [Online]. Available: `https://doi.org/10.2118/8016-PA`.

[28] *A Coupled Dynamic Reservoir and Pipeline Model – Development and Initial Experience*, vol. All Days, International Conference on Multiphase Production Technology, BHR-2007-G1, Jun. 2007. eprint: `https://onepetro.org/BHRICMPT/proceedings-pdf/BHR07/All-BHR07/BHR-2007-G1/1801438/bhr-2007-g1.pdf`.

[29] *Rocx help*, Schlumberger, 2020.

[30] *Relative permeability models*. [Online]. Available: `https://petrowiki.spe.org/Relative_permeability_models` (visited on 03/01/2023).

[31] *Probability Model for Estimating Three-Phase Relative Permeability*, Journal of Petroleum Technology, SPE-2116-PA, Feb. 1970. DOI: `10.2118/2116-PA`. [Online]. Available: `https://doi.org/10.2118/2116-PA`.

[32] C. R. Harris, K. J. Millman, S. J. van der Walt, R. Gommers, P. Virtanen, D. Cournapeau, E. Wieser, J. Taylor, S. Berg, N. J. Smith, R. Kern, M. Picus, S. Hoyer, M. H. van Kerkwijk, M. Brett, A. Haldane, J. F. del Río, M. Wiebe, P. Peterson, P. Gérard-Marchant, K. Sheppard, T. Reddy, W. Weckesser, H. Abbasi, C. Gohlke, and T. E. Oliphant, “Array programming with NumPy,” *Nature*, vol. 585, no. 7825, pp. 357–362, Sep. 2020. DOI: `10.1038/s41586-020-2649-2`. [Online]. Available: `https://doi.org/10.1038/s41586-020-2649-2`.

[33] *Numerical and Analytical Modeling of the Gas- Well Liquid Loading Process*, SPE-95282-PA, Nov. 2006. DOI: `10.2118/95282-PA`. [Online]. Available: `https://doi.org/10.2118/95282-PA`.

Appendix A

Additional Material

A.1 Case 1.1 - One Layer Model

The near-wellbore reservoir model is initially discretized into 50 grid cells; 10 radial, 1 angular, and 5 vertical. The outer boundary is set to decrease linearly from the initial pressure of 110 $bara$ to the final pressure of 60 $bara$ in 125 days. A decrease in reservoir pressure at the boundary of 0.4 $bara/day$ was selected since Breimoen [12] used this value in his study of liquid loading in the wellbore using an IPR model as inflow.

125 days of simulation where saturation, pressure, and temperature are saved every 100 seconds resulting in several gigabytes of data. Using tools developed in Python (see Appendix A.3) to parse and plot reservoir simulation data, unnatural pressure profiles were observed. Figure A.1 shows the gas pressure profiles in the vertical layers and saturation profiles. It is clear from the plot that ROCX changes the pressure at the boundary as defined. However, the other grid cells are only affected by neighboring grid cells and the governing physical laws on which the model is built on. To prevent the reservoir from depleting faster at the outer boundary than at the inner boundary, a revised model is designed, where the pressure of the reservoir is only reduced through energy losses at the wellbore.

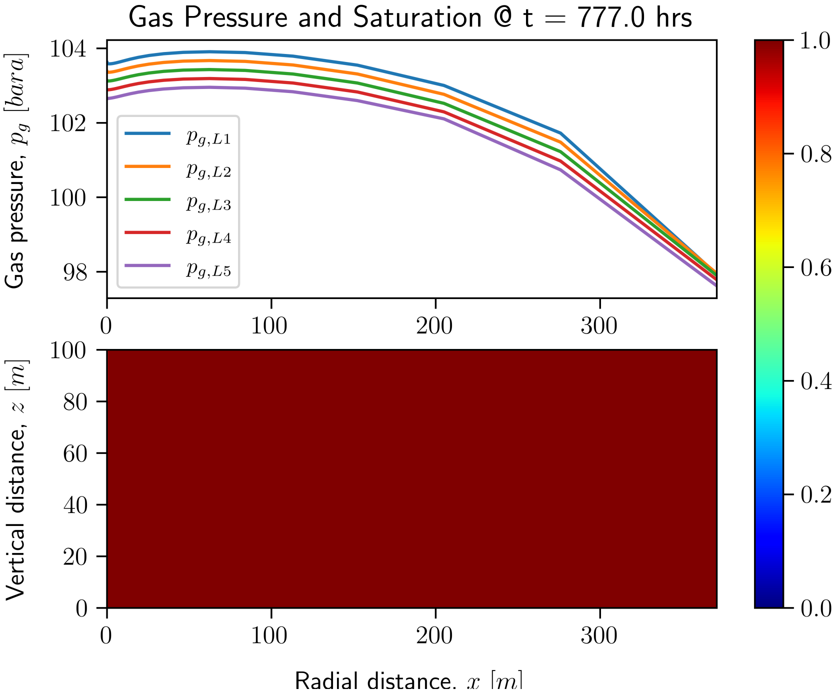

Figure A.1: Case 1.1 - One Layer Model: Gas saturation and pressure late during production.

A.2 Setup Report

A.2.1 Wellbore Model

1. Introduction

Project	Liquid Loading
Case description	Liquid Loading Well
Date	05/09/2022
Author	Staale Breimoen
PVT File	./wet gas.tab
Restart File	./ROCX-PVT-WG-2L.rsw

2. Simulation Options

Overall setting	Flow model	OLGAHD
	Mass eq scheme	2NDORDER
	Compositional model	OFF
	Debug	OFF
	Drilling	OFF
	Phase	THREE
	Elastic walls	OFF
	Void in slug	SINTEF
	Steady state	OFF
	User defined plug-in	OFF
	Temp. calc.	UGIVEN
	Wax deposition	OFF
	Restart	OFF
Integration	Simulation starttime	0 s
	Simulation stoptime	100 d
	Minimum time step	0.001 s
	Maximum time step	100 s

3. System Layout - Graphics

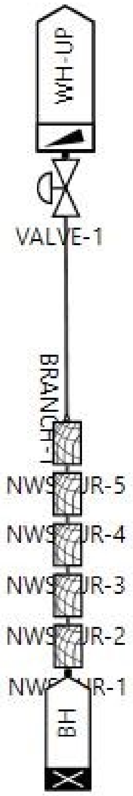

Layout filter On

4. System Layout - Table

4.1 Summary

4.1.1 Overall

No. of Branches	No. of Pipes	No. of Sections
1	1	150

4.1.2 Flows

Branches	No. of Pipes	No. of Sections	Min. Section Length	At	Max. Section Length	At
BRANCH-1	1	150	20 m	PIPE-WELL	20 m	PIPE-WELL

4.2 Layout

Pipe no.	Branch	Label	Diameter	Roughness	XEnd	YEND
1 - 1	BRANCH-1	PIPE-WELL	2.25 in	2.286E-05 M	0 m	3000 m

5. Boundary Conditions

5. 1 Nodes

Label	Type	Pressure	Temperature	GMF
BH	CLOSED			-1
WH-UP	PRESSURE	(60, 60) bara	(20, 20) C	-1

5. 2 Heattransfer

Branch	Pipe	Interpolation	Houteroption.
BRANCH-1	ALL	VERTICAL	HGIVEN

5. 3 Initial Conditions

Branch	Pipe	Mass Flow	Temperatur	VoidFraction	WaterCut
BRANCH-1	ALL	0	110 C	1 -	0 -

6. Equipment

6. 1 Valves

Label	Branch	Pipe	Section	Diameter	Opening	CD
VALVE-1	BRANCH-1	PIPE-WELL	150	2.25 in	1	0.84

6. 2 Position

Label	Branch	Pipe	Section
POS-1	BRANCH-1	PIPE-WELL	1
POS-2	BRANCH-1	PIPE-WELL	5

A.2.2 Reservoir Model

```
   *GEOMETRY RADIAL_LOG

#  Number of grid blocks in horizontal and vertical direction
#  ----------------------------------------------------------
#  nx   ny   nz
   30   1   10

#  Dx and Dy and Dz
#  ----------------
   rw   0.05
   R   100
   dy   const  360
   dz   k   10   10   10   10   10   10   10   10   10   10

#  Direction vector for gravity
#  ----------------------------
#  gx   gy   gz
   0   0   -1

*FLUID_PARAMETERS

#  Table input
#  -----------
   PVT_FILE "wet gas.tab"

*RESERVOIR_PARAMETERS

#  Permeability (mDarcy) in principal directions
#  ---------------------------------------------
   permx  k   10   10   10   10   10   10   10   10   10   10
   permy  k   10   10   10   10   10   10   10   10   10   10
   permz  k   10   10   10   10   10   10   10   10   10   10

#  Porosity
#  --------
   por  const  0.11

#           compr  reference_pressure
   rock_compr 0  0



#  swc  sor  sgr
   0   0.1  0

#  $GUI krwoc=1 nw=2
   krw
   0   0
   0.05  0.00308641975308642
   0.1  0.0123456790123457
   0.15  0.0277777777777778
   0.2  0.0493827160493827
   0.25  0.0771604938271605
   0.3  0.111111111111111
   0.35  0.151234567901235
   0.4  0.197530864197531
   0.45  0.25
```

```
    0.5  0.308641975308642
    0.55  0.373456790123457
    0.6  0.444444444444444
    0.65  0.521604938271605
    0.7  0.604938271604938
    0.75  0.694444444444445
    0.8  0.790123456790124
    0.85  0.891975308641976
    0.9  1
    1   1   /

    kro
    0.1  0
    0.11  0.003
    0.12  0.005
    0.15  0.013
    0.2  0.025
    0.25  0.038
    0.3  0.05
    0.35  0.082
    0.4  0.114
    0.45  0.145
    0.5  0.177
    0.55  0.233
    0.6  0.289
    0.65  0.344
    0.7  0.4
    0.75  0.48
    0.8  0.56
    0.85  0.64
    0.9  0.72
    0.95  0.86
    1   1   /

#   $GUI krgom=1 ng=2
    krg
    0   0
    0.05  0.00308641975308642
    0.1  0.0123456790123457
    0.15  0.0277777777777778
    0.2  0.0493827160493827
    0.25  0.0771604938271605
    0.3  0.111111111111111
    0.35  0.151234567901235
    0.4  0.197530864197531
    0.45  0.25
    0.5  0.308641975308642
    0.55  0.373456790123457
    0.6  0.444444444444444
    0.65  0.521604938271605
    0.7  0.604938271604938
    0.75  0.694444444444445
    0.8  0.790123456790124
    0.85  0.891975308641976
    0.9  1
    1   1   /

    Pcow
    0   1
    1   0   /
```

```
   Pcgo
   0   0
   1   1   /

*BOUNDARY_CONDITIONS

manual

#  Injection flow rates
#  --------------------
#  nsource
   0

#  ix   iy   iz   ntime  time  mw   mo   mg   temp

#  Production pressures
#  --------------------
#  npres_bou
   10

#  i   j   k   idir  type  rw   name  ntime  time  skin  WIFoil  WIFgas  WIFwater
     pres_bou temp_bou Sw_bou  So_bou  Sg_bou
   1   1   10   1   well  0.05  P10   1   0   0   1   1   1   60   110   0   0   1
   1   1   9   1   well  0.05  P9   1   0   0   1   1   1   60   110   0   0   1
   1   1   8   1   well  0.05  P8   1   0   0   1   1   1   60   110   0   0   1
   1   1   7   1   well  0.05  P7   1   0   0   1   1   1   60   110   0   0   1
   1   1   6   1   well  0.05  P6   1   0   0   1   1   1   60   110   0   0   1
   1   1   5   1   well  0.05  P5   1   0   0   1   1   1   60   110   0   0   1
   1   1   4   1   well  0.05  P4   1   0   0   1   1   1   60   110   0   0   1
   1   1   3   1   well  0.05  P3   1   0   0   1   1   1   60   110   0   0   1
   1   1   2   1   well  0.05  P2   1   0   0   1   1   1   60   110   0   0   1
   1   1   1   1   well  0.05  P1   1   0   0   1   1   1   60   110   0   0   1

*INITIAL_CONDITIONS

manual

#  Saturations
#  -----------
   sw   const  0
   so   const  0
   sg   const  1

#  Pressures
#  ---------
   Pg   const  80

#  Temperatures
#  ------------
   T   const  110

*TEMPERATURE off

*INTEGRATION

#  tstart  tstop
   0   86400

#  dtmin  dtmax  dtstart  dtfac  cflfac
```

```
   0.001  100  0.001  10  1

implicit Linsolver

*WELL_COUPLING_LEVEL
   4

*OUTPUT

#  cof_time cof_rate
   1   1

#  ntplot
   10
   P10
   P9
   P8
   P7
   P6
   P5
   P4
   P3
   P2
   P1

   Dt_Trend
   0   200  /

   Dt_Prof
   0   200  /

   screen_info 0

*END
```

A.3 Code Listings

A.3.1 Gas Deviation Factor

```
import numpy as np

def ZfacStanding(p1, T1, Yg, unit):

   # ZStanding : Calculation of Z-factor based on Hall&Yarborough equation fitted
   # to Standing-Katz Chart.
   #    P : Pressure (psia/bara)
   #    T : Temperature (oF/oC)
   #    Yg : Gas Specific Gravity (air=1)
   #    Unit:
   #        1 : Field
   #        2 : Metric

   #    Calculating pseudocritical temperature and pressure
   Tpc = 169.2 + 349.5 * Yg - 74 * Yg ** 2
   Ppc = 756.8 - 131 * Yg - 3.6 * Yg ** 2
   # Unit conversion
```

```
   if unit == 2:
      T = 9 / 5 * T1 + 32
   else:
      T = T1

   if unit == 2:
      P = 14.5038 * p1
   else:
      P = p1

   Tpr = (T + 460) / Tpc
   Ppr = P / Ppc
   T = 1 / Tpr
   a = 0.06125 * T * np.exp(-1.2 * (1 - T) ** 2)
   y = 0.001
   i = 0
   ff = 1

   while abs(ff) > 0.00000001 and i < 100:
      fy = (
         -a * Ppr
         + (y + y ** 2 + y ** 3 - y ** 4) / (1 - y) ** 3
         - (14.76 * T - 9.76 * T ** 2 + 4.58 * T ** 3) * y ** 2
         + (90.7 * T - 242.2 * T ** 2 + 42.4 * T ** 3) * y ** (2.18 + 2.82 * T)
      )
      dfY = (
         (1 + 4 * y + 4 * y ** 2 - 4 * y ** 3 + y ** 4) / (1 - y) ** 4
         - (29.52 * T - 19.52 * T ** 2 + 9.16 * T ** 3) * y
         + (2.18 + 2.82 * T)
         * (90.7 * T - 242.2 * T ** 2 + 42.4 * T ** 3)
         * y ** (1.18 + 2.82 * T)
      )
      y = y - fy / dfY
      ff = fy / dfY
      i = i + 1

      Z = a * Ppr / y
   return Z
```

A.3.2 Critical Velocity

```
def vc(liquid_density, gas_density, surface_tension, model="Turner"):
   # metric units, critical velocity returned in m/s
   model = str.upper(model)
   if model == "TURNER":
      k = 6.558 # turner value
   else:
      k = 5.465 # Coleman value

   rhol = liquid_density
   rhog = gas_density

   return k * (surface_tension * (rhol - rhog) / rhog ** 2) ** (0.25)
```

```
def Qc(p1, p2, T1, T2, d, unit=2, model="Turner"):
   # Input p1, p2 in bara, T1, T2 in degC, d in m, unit=2=metric
```

```
   # p1 and T1 as arrays (to compute properties for every p and T defined)
   # rho_g, rho_l, sigma are determined using table interpolation
   A = np.pi / 4 * (d) ** 2 # m2
   Yg = tab_interp(1.01325, 20, ROG)[0]/1.205
   Z1 = np.array([gas.ZfacStanding(p1[x], T1[x], Yg, unit) for x in
        range(len(p1))])
   Z2 = gas.ZfacStanding(p2, T2, Yg, 2)
   rho_g = np.array([tab_interp(p1[x], T1[x], ROG)[0] for x in range(len(p1))]) #
        kg/m3
   rho_l = np.array([tab_interp(p1[x], T1[x], ROHL)[0] for x in range(len(p1))]) #
        kg/m3
   sigma = np.array([tab_interp(p1[x], T1[x], SIGGHL)[0] for x in range(len(p1))])
        # N/m

   v_c = vc(rho_l, rho_g, sigma, model) # m/s
   Qc = [((p1[x] * v_c[x] * A * Z2 * (T2 + 273.15)) / (Z1[x] * p2 * (T1[x] +
        273.15)) * 86400) for x in range(len(p1))] # Sm3/d
   return Qc, v_c
```

A.3.3 Reservoir Profile Data

```
def prf(filename):
   # Get pressure or saturation data, returns time array, property array
   # x, y, z, pw, po, pg (.pprf)
   # x, y, z, sw, so, sg (.sprf)

   time = []
   data = []

   with open(filename, "r") as f:
      id_list, x_list, y_list, z_list, prop1_list, prop2_list, prop3_list = (
         [],
         [],
         [],
         [],
         [],
         [],
         [],
      )
      for idx, line in enumerate(f):
         if line.strip():
            if line.startswith("##"):
               time.append(float(line[7:-1]))
               if idx > 1:
                  data.append(
                     [
                        id_list,
                        x_list,
                        y_list,
                        z_list,
                        prop1_list,
                        prop2_list,
                        prop3_list,
                     ]
                  )
                  (
                     id_list,
```

```
                x_list,
                y_list,
                z_list,
                prop1_list,
                prop2_list,
                prop3_list,
             ) = ([], [], [], [], [], [], [])

         elif not line.startswith("#%"):
            id, x, y, z, prop1, prop2, prop3 = map(float, line.split())
            id_list.append(id)
            x_list.append(x)
            y_list.append(y)
            z_list.append(z)
            prop1_list.append(prop1)
            prop2_list.append(prop2)
            prop3_list.append(prop3)

      data.append(
         [id_list, x_list, y_list, z_list, prop1_list, prop2_list, prop3_list]
      )
   return np.array(time), np.array(data)
```

A.3.4 Reservoir Production Data

```
def prd(filename, nrows=1000):
   # Production data at defined boundaries in ROCX.
   # Returns dataframe
   # Time, waterprod-p5, oilprod-p5, gasprod-p5, waterprod-p4, oilprod-p4,
       gasprod-p4, ..., totwater, totoil, totgas, timestep
   df = pd.read_fwf(filename, infer_nrows=nrows)
   return df
```

A.3.5 Indexes of Transient Events and Related Production Information

```
#%% liquid loading identifier indexes
try:
   rate_gradient_search_idx = (
      # np.where(abs(np.gradient(QGST[50:])) > 0.00088)[0][0] + 50
      np.where(abs(np.gradient(QGST[50:], time[50:])) > 0.00001)[0][0]
      + 50
   )
   rate_gradient_search_rate = QGST[rate_gradient_search_idx]
   rate_gradient_search_pressure = PT[rate_gradient_search_idx]
   print(
      f"Rate gradient search index={rate_gradient_search_idx},
          rate={rate_gradient_search_rate*86400},
          pressure={rate_gradient_search_pressure/1e5},
          time={time[rate_gradient_search_idx]/3600}"
   )
except:
   rate_gradient_search_idx = 0
   rate_gradient_search_rate = QGST[rate_gradient_search_idx] * 86400
```

```
   rate_gradient_search_pressure = PT[rate_gradient_search_idx] * 1e-5
   print("dq/dt < 0 does not exist")

slug_identifier_idx = find_slug(ID[1], 3)[0]
slug_identifier_rate = QGST[slug_identifier_idx]
slug_identifier_pressure = PT[slug_identifier_idx]
if slug_identifier_idx == 0:
   print("Slug does not exist")
else:
   print(
      f"Slug identifier index={slug_identifier_idx},
           rate={slug_identifier_rate*86400},
           pressure={slug_identifier_pressure/1e5},
           time={time[slug_identifier_idx]/3600}"
   )

try:
   # liquidfilm_reversal_idx = np.where(np.asarray(UL[1]) < 0)[0][0]
   liste = []
   for i in range(len(UL[1])):
      try:
         liste.append(np.where(np.asarray(UL[1][i][1:]) < 0)[0][0])
      except:
         liste.append(0)
   liquidfilm_reversal_idx = np.where(np.asarray(liste) != 0)[0][0]
   liquidfilm_reversal_rate = QGST[liquidfilm_reversal_idx]
   liquidfilm_reversal_pressure = PT[liquidfilm_reversal_idx]
   print(
      f"Liquid film reversal index={liquidfilm_reversal_idx},
           rate={liquidfilm_reversal_rate*86400},
           pressure={liquidfilm_reversal_pressure/1e5},
           time={time[liquidfilm_reversal_idx]/3600}"
   )
   cr1 = Qc(
      PT_branch[1][liquidfilm_reversal_idx - 10] * 1e-5,
      1.01325,
      TM_branch[1][liquidfilm_reversal_idx - 10],
      15.556,
      0.05715,
   )[0]
   cr2 = Qc(
      PT_branch[1][liquidfilm_reversal_idx + 10] * 1e-5,
      1.01325,
      TM_branch[1][liquidfilm_reversal_idx + 10],
      15.556,
      0.05715,
   )[0]
   print(
      f"Turner critical rate pre/post liquid film reversal = {np.max(cr1),
           np.max(cr2)}"
   )
except:
   print("UL > 0")
   liquidfilm_reversal_idx = 0

try:
   # droplet_reversal_idx = np.where(np.asarray(UD[1]) < 0)[0][0]
   liste = []
   for i in range(len(UL[1])):
      try:
```

```
         liste.append(np.where(np.asarray(UD[1][i][1:]) < 0)[0][0])
      except:
         liste.append(0)
   droplet_reversal_idx = np.where(np.asarray(liste) != 0)[0][0]
   droplet_reversal_rate = QGST[droplet_reversal_idx]
   droplet_reversal_pressure = PT[droplet_reversal_idx]
   print(
      f"Droplet reversal index={droplet_reversal_idx},
           rate={droplet_reversal_rate*86400},
           pressure={droplet_reversal_pressure/1e5},
           time={time[droplet_reversal_idx]/3600}"
   )
   cr1 = Qc(
      PT_branch[1][droplet_reversal_idx - 10] * 1e-5,
      1.01325,
      TM_branch[1][droplet_reversal_idx - 10],
      15.556,
      0.05715,
   )[0]
   cr2 = Qc(
      PT_branch[1][droplet_reversal_idx + 10] * 1e-5,
      1.01325,
      TM_branch[1][droplet_reversal_idx + 10],
      15.556,
      0.05715,
   )[0]
   print(
      f"Turner critical rate pre/post droplet reversal = {np.max(cr1),
           np.max(cr2)}"
   )

except:
   droplet_reversal_idx = 0
   print("UL > 0")

oil_backflow_index = []
for (i, Q) in
     enumerate(Q_sandface.columns[Q_sandface.columns.str.startswith("Oil")]):
   try:
      idx = np.where(Q_sandface[Q] < 0)[0][0]
      oil_backflow_index.append(idx)
      print(f"Layer {z_grid-i} has oil backflow @ index={idx},
           time={time3[idx]/3600} hr")
   except:
      # print(f"Layer {z_grid-i} does not have oil backflow")
      pass
oil_backflow_index = min(oil_backflow_index)

for (i, Q) in
     enumerate(Q_sandface.columns[Q_sandface.columns.str.startswith("Wat")]):
   try:
      idx = np.where(Q_sandface[Q] < 0)[0][0]
      print(f"Layer {z_grid-i} has water backflow @ index={idx},
           time={time3[idx]/3600} hr")
   except:
      # print(f"Layer {z_grid-i} does not have water backflow")
      pass

for (i, Q) in
     enumerate(Q_sandface.columns[Q_sandface.columns.str.startswith("Gas")]):
```

```
   try:
      idx = np.where(Q_sandface[Q] < 0)[0][0]
      print(f"Layer {z_grid-i} has gas backflow @ index={idx},
           time={time3[idx]/3600} hr")
   except:
      # print(f"Layer {z_grid-i} does not have gas backflow")
      pass

try:
   # post_transient_idx = []
   # for (i, Q) in
        enumerate(Q_sandface.columns[Q_sandface.columns.str.startswith("Gas")]):
   #    try:
   #       post_transient_idx.append(np.where(
   #             abs(np.gradient(Q_sandface[Q][oil_backflow_index:],
        time3[oil_backflow_index:]))
   #             <= 0.000000003
   #          )[0][0])
   #    except:
   #       pass

   # post_transient_idx = (max(post_transient_idx) + oil_backflow_index)
   post_transient_idx = np.where(abs(np.gradient(QGST[oil_backflow_index:],
        time[oil_backflow_index:])) < 0.000000001)[0][0] + oil_backflow_index
   pre_transient_idx = (rate_gradient_search_idx)-3

   for (i, Q) in
        enumerate(Q_sandface.columns[Q_sandface.columns.str.startswith("Gas")]):
      try:
         print(f"Gas mass rate layer {z_grid-i} pre/post/change =
              {Q_sandface[Q][pre_transient_idx],
              Q_sandface[Q][post_transient_idx],
              Q_sandface[Q][post_transient_idx]/Q_sandface[Q][pre_transient_idx]}")
      except:
         # print(f"error layer {z_grid-i}")
         pass
   for (i, Q) in
        enumerate(Q_sandface.columns[Q_sandface.columns.str.startswith("Oil")]):
      try:
         if np.sum(Q_sandface[Q]) != 0:
            print(f"Oil mass rate layer {z_grid-i} pre/post =
                 {Q_sandface[Q][pre_transient_idx],
                 Q_sandface[Q][post_transient_idx]}")
      except:
         # print(f"error layer {z_grid-i}")
         pass
   for (i, Q) in
        enumerate(Q_sandface.columns[Q_sandface.columns.str.startswith("Wat")]):
      try:
         if np.sum(Q_sandface[Q]) != 0:
            print(f"Water mass rate layer {z_grid-i} pre/post =
                 {Q_sandface[Q][pre_transient_idx],
                 Q_sandface[Q][post_transient_idx]}")
      except:
         # print(f"error layer {z_grid-i}")
         pass
except:
   print("error")
```

```
depth_index =
    [np.where(satdata[post_transient_idx][5][i*x_grid:(i+1)*x_grid]==0)[0][0] for
    i in range(z_grid)]

oil_depth = [satdata[post_transient_idx][1][L] for i,L in enumerate(depth_index)]
try:
   avg_sat = [np.average(satdata[post_transient_idx][5][i*x_grid:(i)*x_grid +
       min(depth_index)],
       weights=np.diff(satdata[post_transient_idx][1][0:min(depth_index)+1])) for
       i, L in enumerate(depth_index)]

   print(f"penetration index {depth_index} \npenetration depth{oil_depth}
       \naverage saturation in lowest depth {avg_sat}")
except:
   print("error")
```

A.4 Additional plots

A.4.1 Case 1.1 - ROCX

Figure A.2 shows that the oil rate is below zero for the remaining duration of the simulation. This is not as expected, since the gas rate is normally above the critical rate in some sections (typically near the surface) of the well.

Phase velocities and liquid holdup are shown in Figures A.3, A.4, A.5, and A.6. The time series shows that the velocity of the liquid film drops below zero first (initial indication of liquid loading). The liquid holdup is increasing towards the surface before loading starts because of the fluid composition which is highly dependent on temperature. After loading starts, the holdup moves down the well.

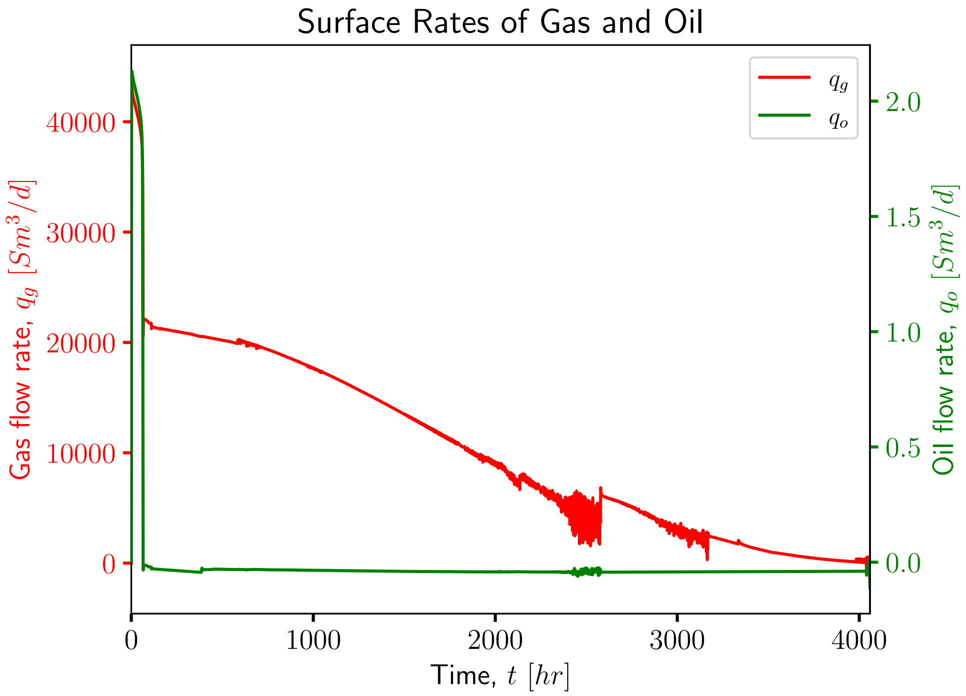

Figure A.2: Case 1.1 - ROCX: Surface rates of oil and gas during 4000 *hrs* of production.

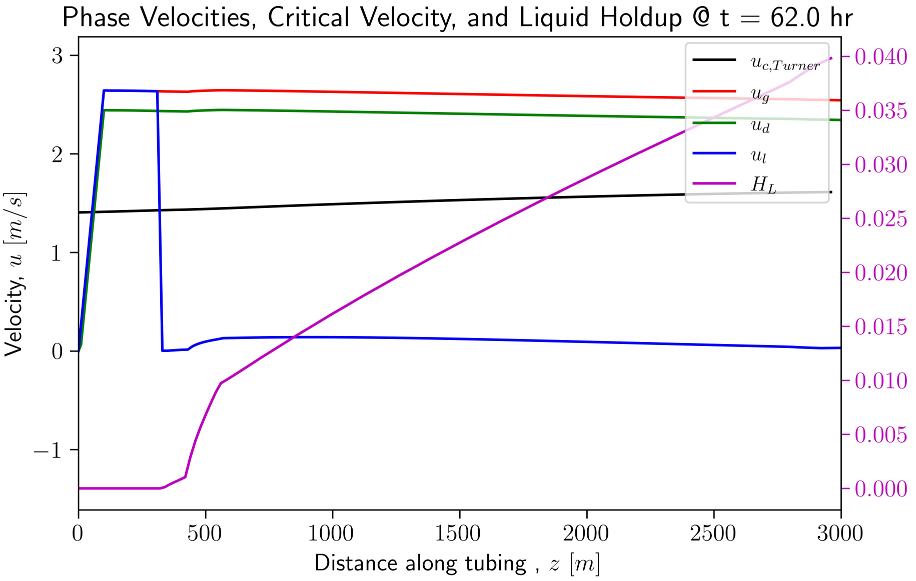

Figure A.3: Gas, liquid film, droplet, and critical velocity along the branch before liquid loading. In addition, the liquid holdup shows the area of the oil along the wellbore at the given phase velocities.

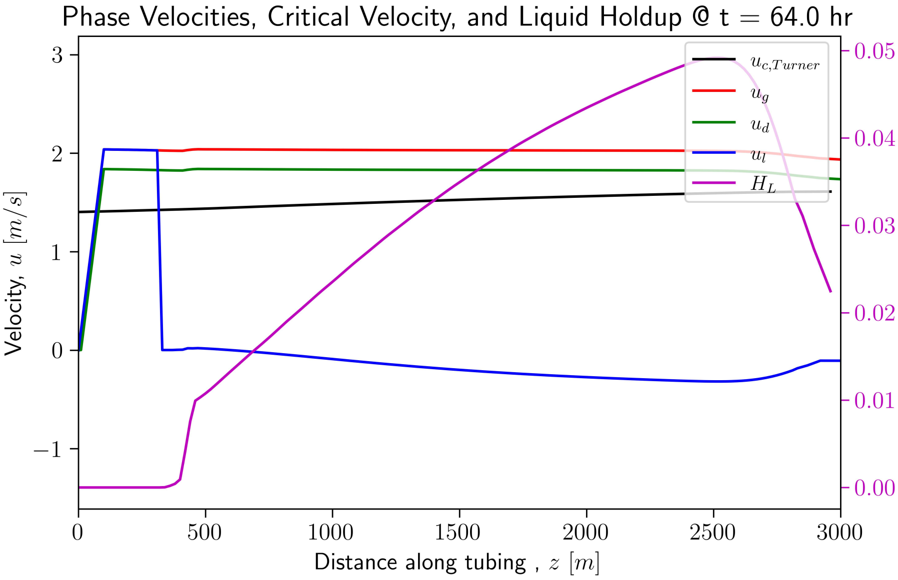

Figure A.4: Gas, liquid film, droplet, and critical velocity along the branch during liquid loading. In addition, the liquid holdup shows the area of the oil along the wellbore at the given phase velocities.

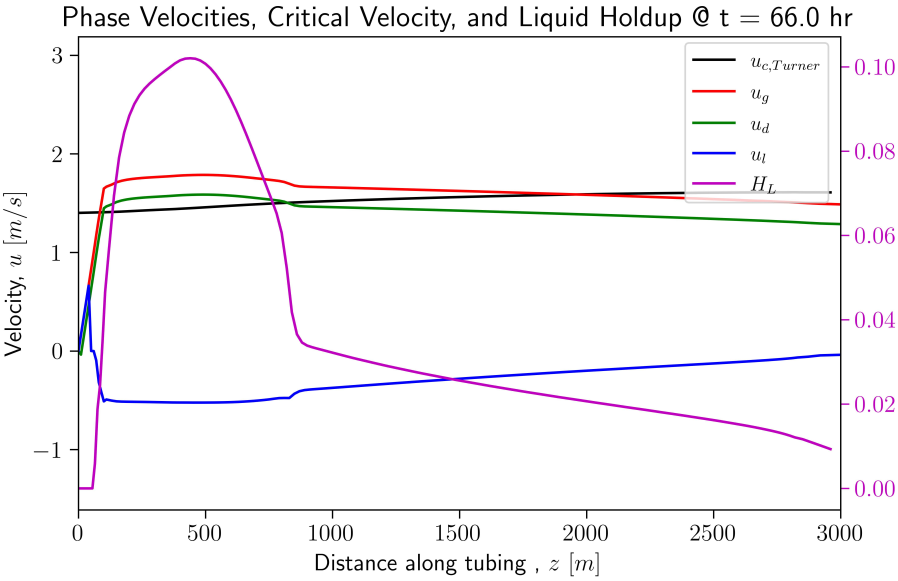

Figure A.5: Gas, liquid film, droplet, and critical velocity along the 2 *hours* after the onset of liquid loading. In addition, the liquid holdup shows the area of the oil along the wellbore at the given phase velocities.

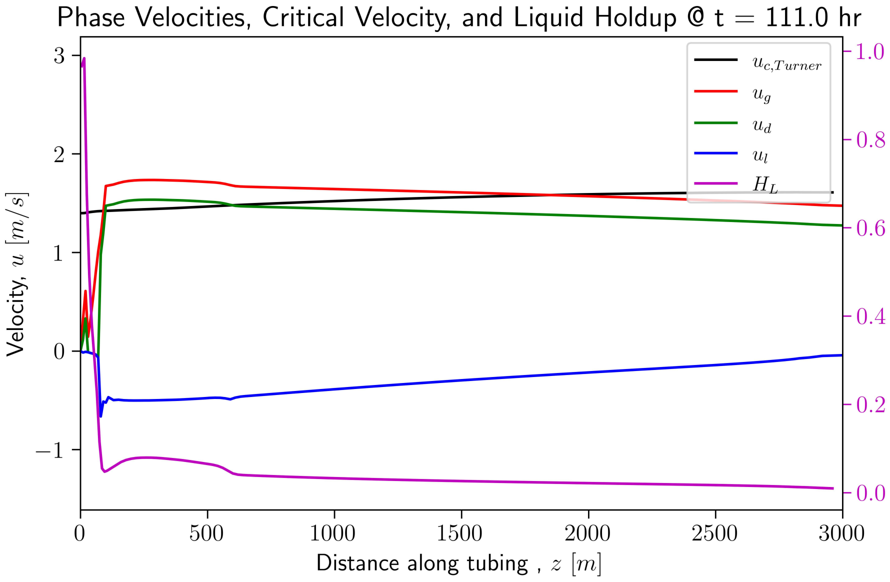

Figure A.6: Gas, liquid film, droplet, and critical velocity along the branch after stabilization. In addition, the liquid holdup shows the area of the oil along the wellbore at the given phase velocities.

A.4.2 Case 1.2a

Figure A.7 shows the surface rates of oil and gas. The initial surface gas and oil production rates are 44,037 and 2.13 Sm^3/d, respectively. Liquid loading is initiated at a rate of 35,173 Sm^3/d, as seen in Table A.1. The stabilized gas rate after the onset of liquid loading is 21,382 Sm^3/d. The oil rate is subzero since the condensate that forms in the wellbore flows back into the reservoir.

Figure A.8 shows the liquid fraction, bottomhole pressure, and length of the slug flow regime. The liquid fraction starts to increase rapidly after 67 $hours$, which marks the beginning of the liquid loading. The drop in liquid fraction and bottomhole pressure is caused by liquid backflow into the reservoir. After 92 $hours$, the liquid fraction and bottomhole pressure increase again until a steady level is reached as gas production is stabilized. The slug flow begins after 92.7 $hours$ and builds to a maximum length of 40 $meters$ in 88 $hours$. The slug flow is located near the bottom of the well, starting at 10 $meters$ from the bottom and expanding to 50 $meters$ from the bottom.

Figures A.9, A.10, A.11,A.12, and A.12 show the phase velocity and liquid holdup in periods of interest. As they provide conclusions similar to those of previous findings, they are not discussed in detail. In summary, the liquid film velocity turns negative when the gas rate drops below the critical rate, which makes the liquid content increase.

Table A.1: Case 1.2a: Comparison of rates.

Method	q_g $[Sm^3/d]$	p_{wf} $[bara]$	**time** $[hr]$
Rate gradient search	33,897	78.8	67.5
Slug index	22,048	78.8	92.7
Droplet reversal	21,624	79.1	106.5
Liquid film reversal	35,173	78.77	67.0
Turner critical rate	23,579		

A.4.3 Case 1.2b

The initial production rate is slightly higher than 50,000 Sm^3/d, with an oil rate of 2.5 Sm^3/d, and the produced oil-to-gas ratio (OGR) remains the same as in Case 1.2a. The production rate at which liquid loading begins is slightly lower than in Case 1.1 - ROCX, occurring at around 33,000 Sm^3/d. Figure 4.20 illustrates the oil and gas surface rates, while Figure 4.21 shows the bottomhole pressure, the length of the slug flow regime and the liquid fraction.

During the initial 150 hrs of production, production rates gradually decrease as the reservoir depletes before liquid loading is initiated. The surface gas production rate stabilizes quickly after the transient period, settling at a rate of approximately 11,700 Sm^3/d, while the surface oil rate reduces to less than 0. The liquid

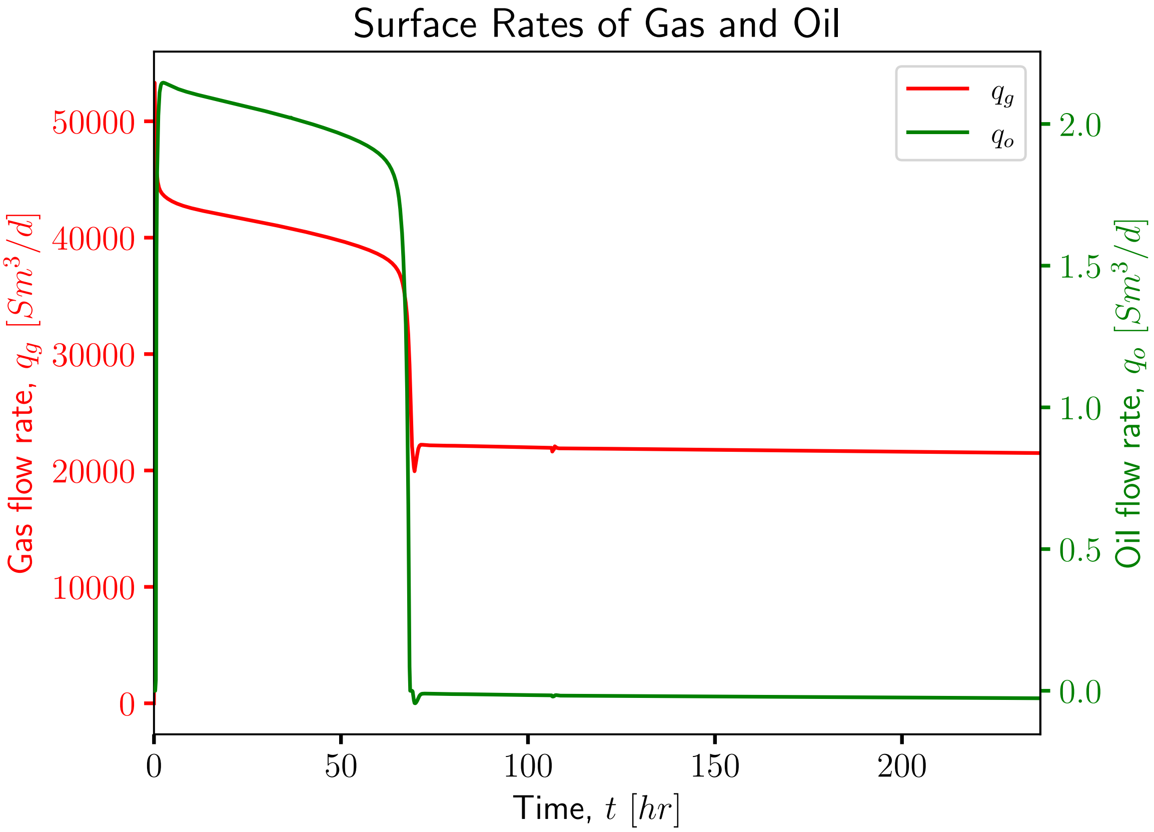

Figure A.7: Case 1.2a: Surface rates of oil and gas.

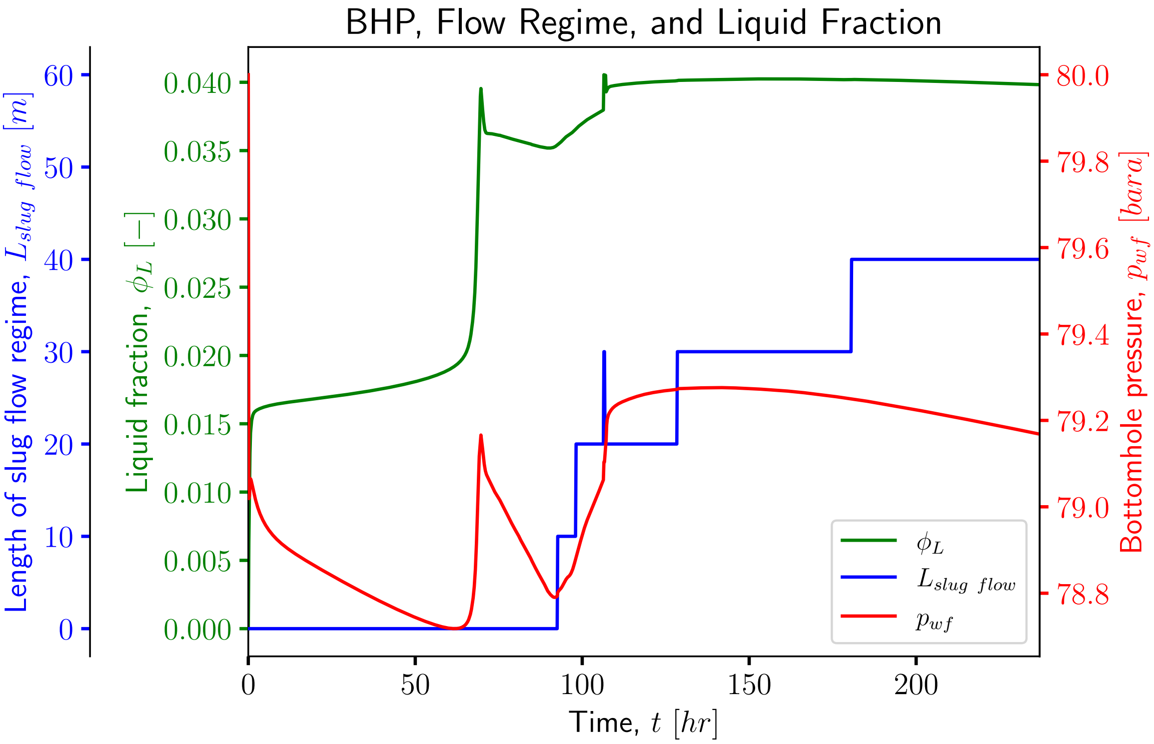

Figure A.8: Case 1.2a: Bottomhole pressure, liquid fraction, and length of slug flow regime.

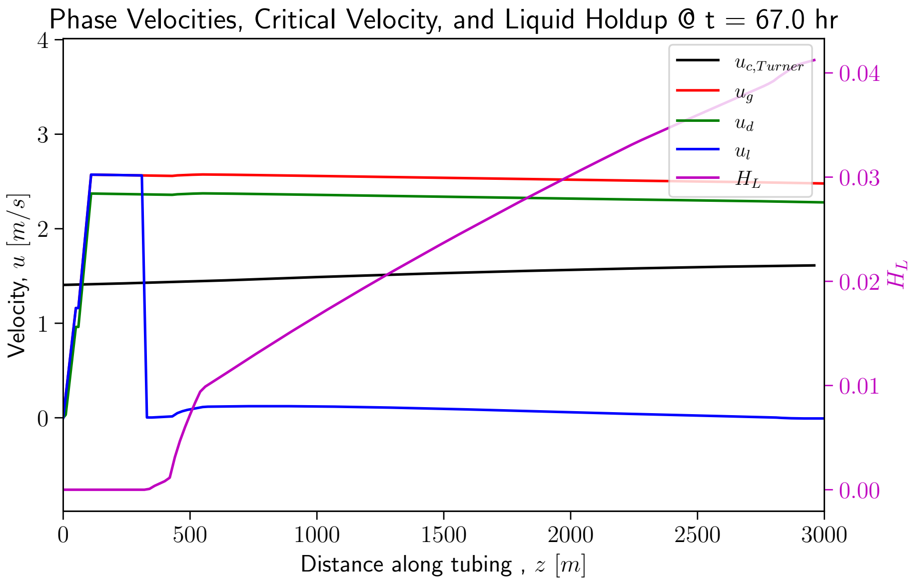

Figure A.9: Case 1.2a: Gas, liquid film, droplet, and critical velocity along the branch before liquid loading. In addition, the liquid holdup shows the area of the oil along the wellbore at the given phase velocities.

fraction and bottomhole pressure increase as a result of the liquid film reversal, which depends on the gas rate. Consequently, the gas production rate is further reduced.

Table A.4 presents the critical rates and corresponding bottomhole pressures obtained from the gradient search, liquid film and droplet reversal methods, slug identification, and Turner's critical rate. Both the gradient search and the liquid film reversal method yield identical rates of around 33,000 Sm^3/d, with a corresponding bottomhole pressure of 78.71 $bara$. This is similar to the results of Case 1.1, where a gas rate of 34,555 Sm^3/d was found using both methods. The reason for this similarity is likely due to the comparable flow conditions in the well and identical fluid properties in both cases.

Slug flow and droplet reversal are observed approximately 2 hrs after the onset of liquid loading, occurring at a rate of 16,489 Sm^3/d with a corresponding bottomhole pressure of 78.79 $bara$. The calculated Turner critical rate is 23,668 Sm^3/d, similar to the previous case, as the pressures and temperatures are nearly identical. However, this calculation fails to generate a rate similar to the slug initiation rate, likely due to the intervals at which data are stored (every 600 seconds). Some of the liquid droplets entrained in the gas are deposited at the tubing wall before reaching the surface, and then transported down the well and back into the reservoir. However, the backflow into the reservoir is initiated at the same time as the droplet reversal, probably because of the liquid front traveling down the well after the liquid film reversal, which restricts the gas flow and causes droplet

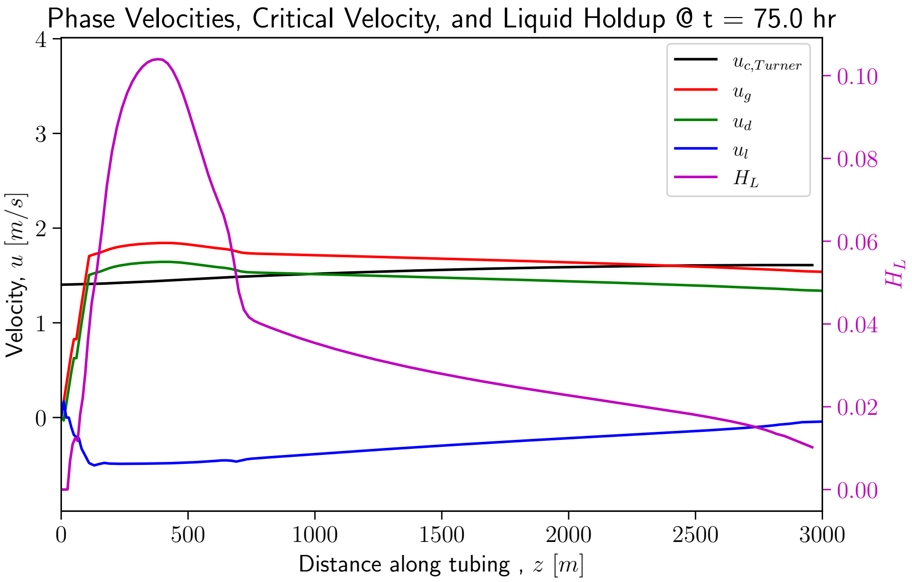

Figure A.10: Case 1.2a: Gas, liquid film, droplet, and critical velocity along the branch 2 hrs after the onset of liquid loading. In addition, the liquid holdup shows the area of the oil along the wellbore at the given phase velocities.

reversal.

The surface production rate stabilizes after approximately 15 hrs after the onset of liquid loading. The high permeability in layers 7 to 11 likely contributes to fast restabilization, as there is less liquid buildup in the well with a maximum fraction of 0.040 and more liquid reinjection during the transient event. Slug flow during liquid loading is characterized by alternating slugs of gas and liquid, appearing quite chaotic, especially close to where it happens. Slugs are not seen on the surface in this case. However, the mass rates of oil and gas moving through the sandface are greatly affected by slugging.

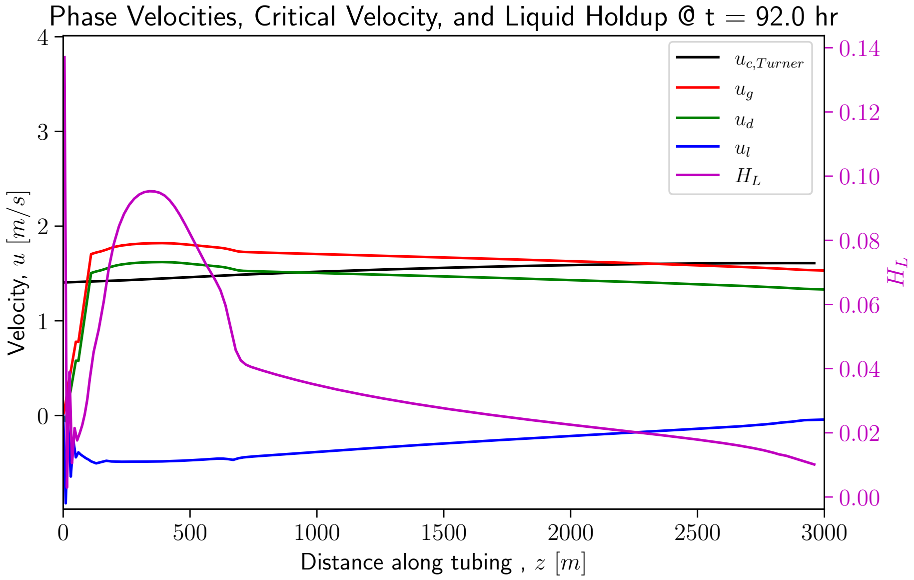

Figure A.11: Case 1.2a: Gas, liquid film, droplet, and critical velocity along the branch 25 *hours* after the onset of liquid loading. In addition, the liquid holdup shows the area of the oil along the wellbore at the given phase velocities.

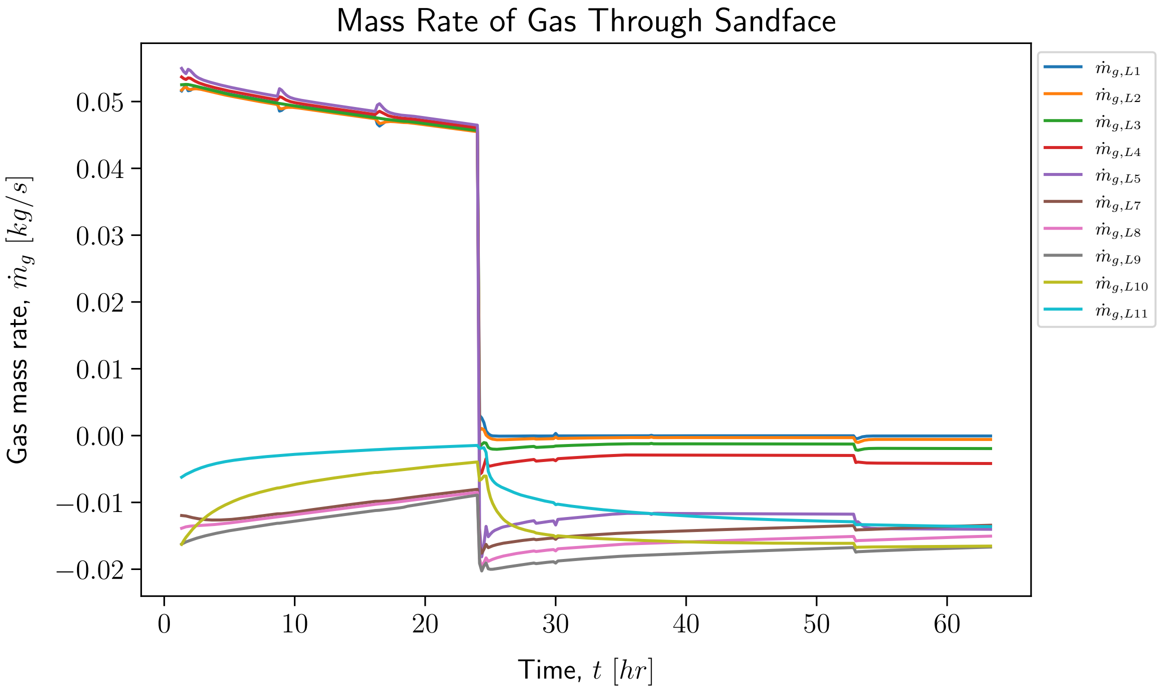

Figure A.13: Case 1.2b: Mass rates of gas through the sandface at the loading point.

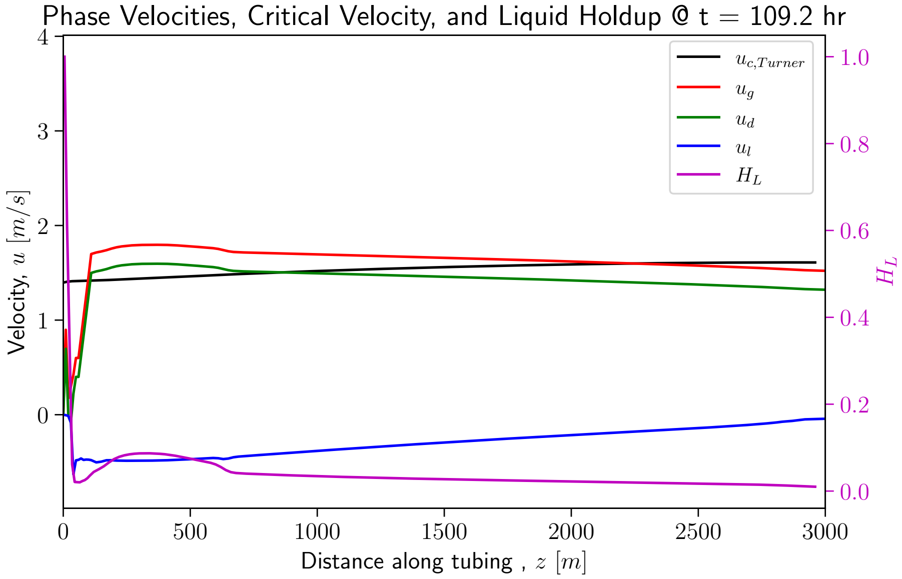

Figure A.12: Case 1.2a: Gas, liquid film, droplet, and critical velocity along the branch, late during liquid loading. In addition, the liquid holdup shows the area of the oil along the wellbore at the given phase velocities.

Table A.2: Case 1.2a: Mass rates of gas through the sandface.

Mass rate of gas through the sandface, [m_g]			
	Pre Loading [kg/s]	Post Fluid Redistribution [kg/s]	Ratio (Post/Pre) [%]
Layer 1	0.02914	0.0001930	0.66
Layer 2	0.02915	0.004485	15.4
Layer 3	0.02916	0.01263	43.3
Layer 4	0.02917	0.02019	69.2
Layer 5	0.02916	0.02671	91.6
Layer 7	0.03514	0.002499	71.1
Layer 8	0.03517	0.002711	77.1
Layer 9	0.03527	0.002753	78.1
Layer 10	0.03539	0.02774	78.4
Layer 11	0.03549	0.02797	78.8

Table A.3: Case 1.2a: Mass rates of oil through the sandface.

Mass rate of oil through the sandface, $[m_o]$		
	Pre Loading $[kg/s]$	Post Fluid Redistribution $[kg/s]$
Layer 1	0	-0.00841
Layer 2	0	-0.00281
Layer 3	0	-0.00104
Layer 4	0	-0.000419
Layer 5	0	-0.000167
Layer 7	0	-0.000159
Layer 8	0	-0.000158
Layer 9	0	-0.000136
Layer 10	0	-0.000120
Layer 11	0	-0.000101

Table A.4: Case 1.2b: Comparison of potential critical rates.

Method	q_g $[Sm^3/d]$	p_{wf} $[bara]$	**time** $[hr]$
Rate gradient search	34,764	78.70	151.5
Slug index	18,579	78.77	153.7
Droplet reversal	19,692	79.77	153.6
Liquid film reversal	35,256	78.70	151.4
Turner critical rate	23,642		

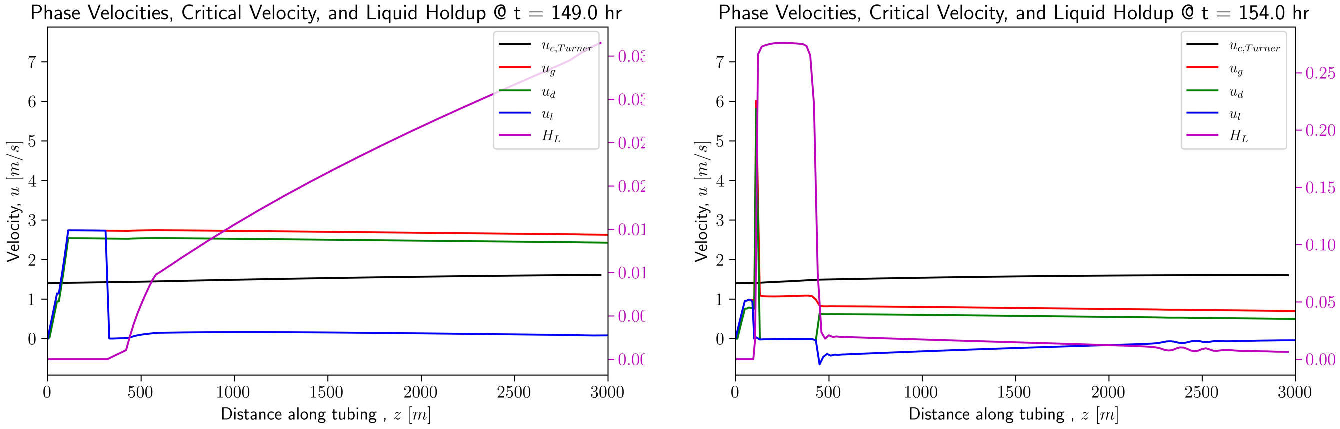

(a) Before loading

(b) During loading

Figure A.14: Case 1.2b: Phase velocities and liquid holdup.

Table A.5: Case 1.2b: Mass rates of gas through the sandface.

Mass rate of gas through the sandface, $[m_g]$			
	Pre Loading $[kg/s]$	Post Fluid Redistribution $[kg/s]$	Ratio (Post/Pre) [%]
Layer 1	0.02846	0.02113	74.2
Layer 2	0.02843	0.02108	74.1
Layer 3	0.02846	0.02106	74.0
Layer 4	0.02849	0.02105	73.9
Layer 5	0.02849	0.02101	73.8
Layer 7	0.03555	0.005120	14.4
Layer 8	0.03610	0.005434	15.1
Layer 9	0.03712	0.005879	15.8
Layer 10	0.03847	0.006667	17.3
Layer 11	0.04001	-0.0004342	-1.1

Table A.6: Case 1.2b: Mass rates of oil through the sandface.

Mass rate of oil through the sandface, $[m_o]$		
	Pre Loading $[kg/s]$	Post Fluid Redistribution $[kg/s]$
Layer 1	0	0
Layer 2	0	0
Layer 3	0	0
Layer 4	0	0
Layer 5	0	0
Layer 7	0	0
Layer 8	0	0
Layer 9	0	0
Layer 10	0	-3.28E-06
Layer 11	0	-0.0267

A.4.4 Case 1.2c

Table A.7 shows the critical rates. The liquid film reversal is again the first indication of liquid loading. Gas and oil mass rates through the sandface right before liquid loading begins and after the rates stabilize are shown in Tables A.8 and A.9. They both show that the bottom zone is mostly affected by the liquid loading.

Table A.7: Case 1.2c: Comparison of potential critical rates.

Method	q_g $[Sm^3/d]$	p_{wf} $[bara]$	**time** $[hr]$
Rate gradient search	34,542	78.71	147.5
Slug index	20,169	78.24	297.0
Droplet reversal	20,169	78.24	297.0
Liquid film reversal	35,203	78.71	147.0
Turner critical rate	23,602		

Table A.8: Case 1.2c: Mass rates of gas through the sandface.

Mass rates of gas through the sandface, m_g			
	Pre Loading $[kg/s]$	Post Fluid Redistribution $[kg/s]$	Ratio (Post/Pre) [%]
Layer 1	0.03759	0.02186	58.1
Layer 2	0.03738	0.02191	58.6
Layer 3	0.03749	0.02242	59.8
Layer 4	0.03778	0.02071	54.8
Layer 5	0.03795	0.003881	10.2
Layer 7	0.03176	0.01777	55.9
Layer 8	0.03175	0.02187	68.9
Layer 9	0.03183	0.02544	79.9
Layer 10	0.03196	0.02874	90.0
Layer 11	0.03205	0.03203	99.9

Table A.9: Case 1.2c: Mass rates of oil through the sandface.

Mass rate of oil through the sandface, m_o		
	Pre Loading $[kg/s]$	Post Fluid Redistribution $[kg/s]$
Layer 1	0	0
Layer 2	0	0
Layer 3	0	0
Layer 4	0	-1.31E-05
Layer 5	0	-0.0395
Layer 7	0	-0.000504
Layer 8	0	-0.000206
Layer 9	0	-3.20E-05
Layer 10	0	4.79E-05
Layer 11	0	9.26E-05

A.5 Additional Tests

A.5.1 1.2b - Increased Porosity

Increasing the porosity from 0.11 to 0.22 causes liquid loading to occur later in production as the gas volume doubles. Figures A.15 and A.16 show that liquid loading starts after 326 *hrs* where the mass rates suddenly drop. Except for the delayed onset of liquid loading, the post-loading fluid movement and production rates are almost identical to those of the base case in Section 4.2.2.

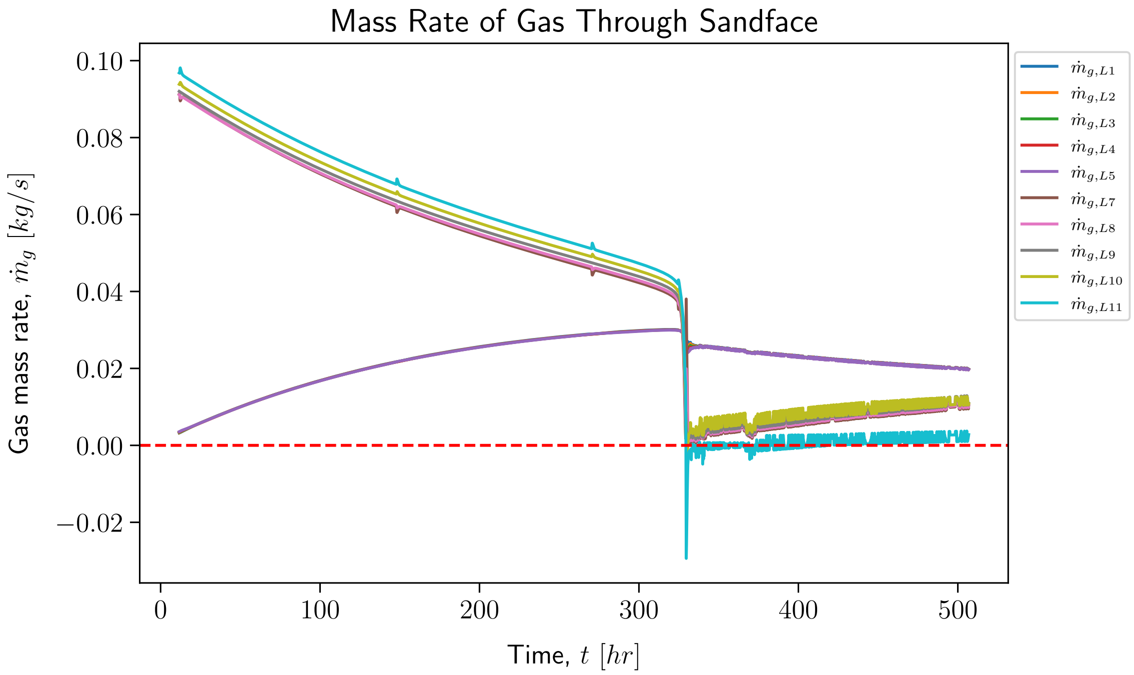

Figure A.15: Case 1.2b Increased Porosity: Mass rate of gas through each numeric layer.

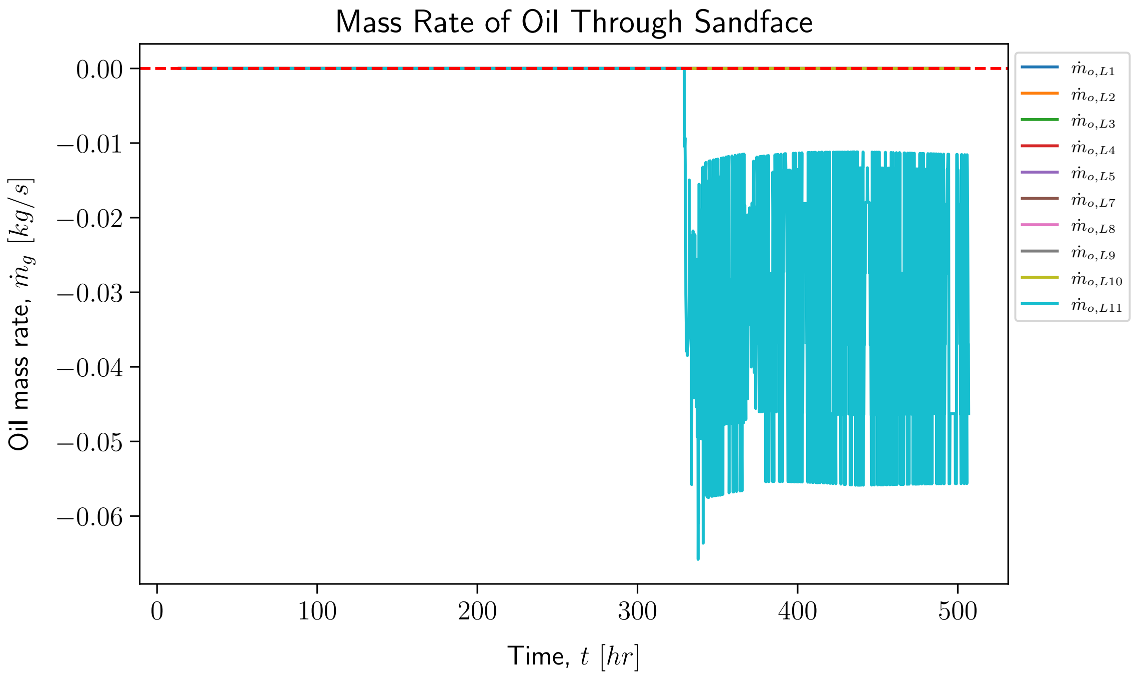

Figure A.16: Case 1.2b Increased Porosity: Mass rate of oil through each numeric layer.

A.5.2 1.2b - Increased Reservoir Radius

Increasing the radius from 100 to 500 m increases the volume of the reservoir 25 times. As a consequence, the liquid loading begins after 3760 hrs which is roughly 25 times later than in the base case in Section 4.2.2. Figure A.17 shows the mass rates of gas. This case, similar to the base case, does not have crossflow. In addition, oil flows into layer 11 instead of accumulating at the bottom of the well.

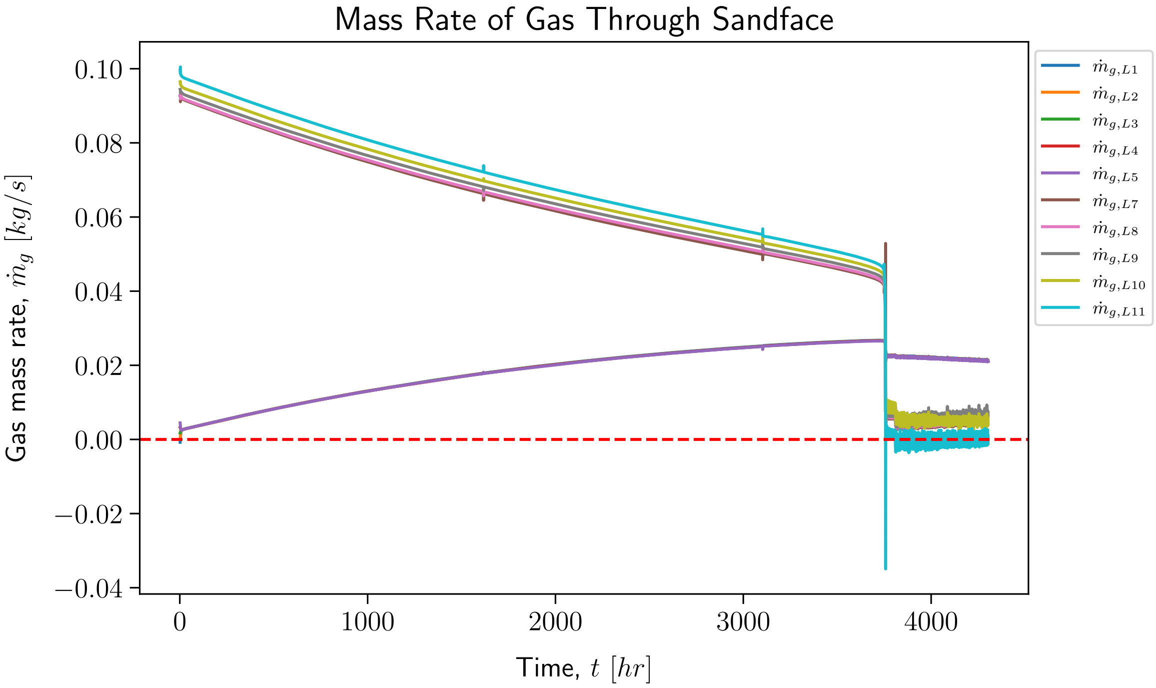

Figure A.17: Case 1.2b Increased Porosity: Mass rate of gas through each numeric layer.

A.5.3 1.2c - Increased Porosity

Increasing the porosity from 0.11 to 0.22 causes liquid loading to occur later in production as the gas volume doubles. Figure A.18 shows that liquid loading starts after 320 hrs where the mass rates suddenly drop. Except for the delayed onset of liquid loading, the post-loading fluid movement and production rates are almost identical to those of the base case in Section 4.2.3.

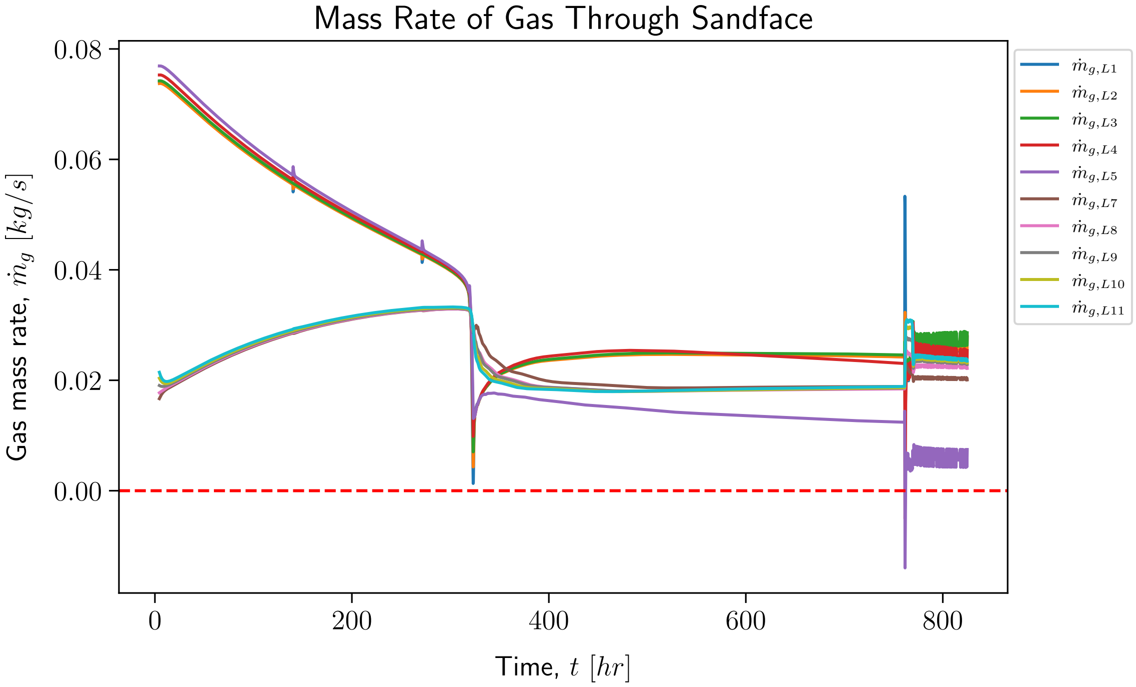

Figure A.18: Case 1.2c Increased Porosity: Mass rate of gas through each numeric layer.

A.5.4 1.2c - Increased Reservoir Radius

Increasing the radius from 100 to 500 m increases the volume of the reservoir 25 times. As a consequence, the liquid loading begins after 3625 hrs which is roughly 25 times later than in the base case in Section 4.2.3. Figure A.19 shows the mass rates of gas.

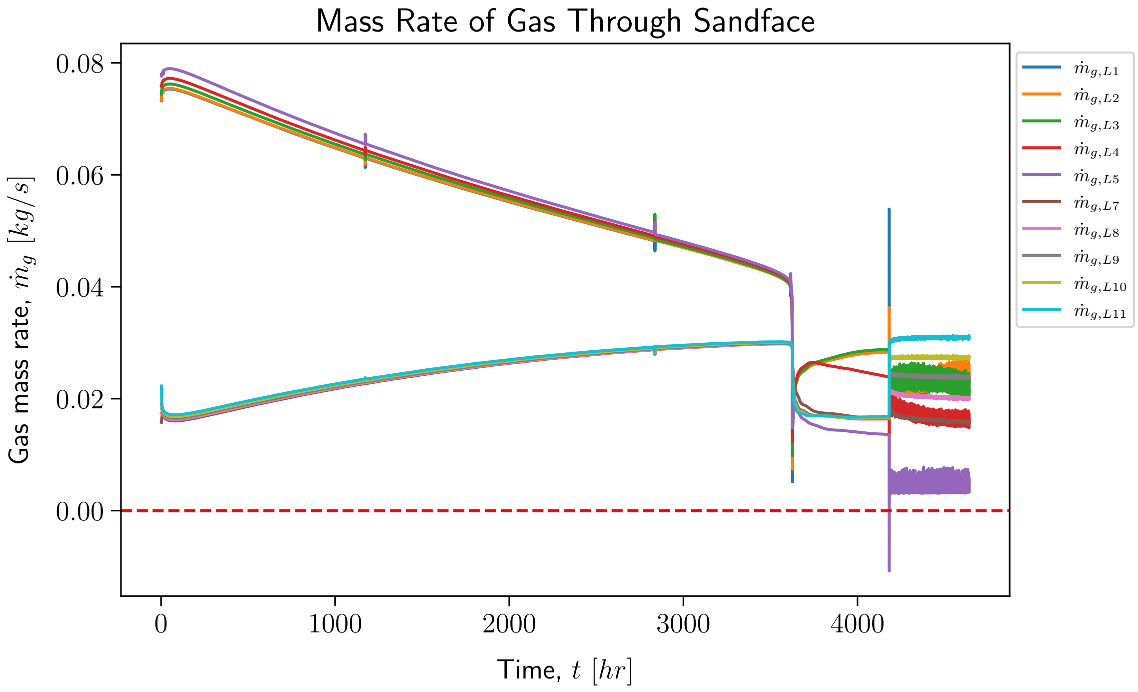

Figure A.19: Case 1.2c Increased Porosity: Mass rate of gas through each numeric layer.

NTNU

Norwegian University of
Science and Technology